HOLOCENE EVOLUTION OF LOW-ORDER WATERSHED HILLSLOPES AND SOILS IN THE SE PIEDMONT, NC USA

by

Nora Vaughan

A thesis submitted to the faculty of
The University of North Carolina at Charlotte
in partial fulfillment of the requirements
for the degree of Master of Science in
Earth Sciences

Charlotte

2023

Approved by:

_____
Dr. Martha Cary Eppes

_____
Dr. David Vinson

_____
Dr. Patricia Fall

_____
Dr. Andy R. Bobyarchick

©2023
Nora Vaughan
ALL RIGHTS RESERVED

ABSTRACT

NORA VAUGHAN. Holocene Evolution of Low-Order Watershed Hillslopes and Soils in the southeastern Piedmont, NC USA. (Under the direction of DR. MARTHA CARY EPPES)

This study characterizes four toposequences in two first-order watersheds (4.5 and 6.2 ha) of the SE Piedmont where the entire Holocene source-to-sink system is presumably still intact. Despite a long history of soil and geomorphic research in the southeastern Piedmont focused on sediment accumulation in valley bottoms, there are few investigations into of the nature and dynamics of Holocene hillslope soils and hillslope sediments in low-order watersheds that make up most of the region.

Soil profiles and sediment sequences were described for 5 soil pits (~1.5 m deep) per hillslope toposequence. The watersheds are underlain with similar lithologies (felsic metavolcanics) but vary in aspect (N & S) and near a major, high-order river. Samples (n=146) from all 21 soil pits were analyzed for particle size, bulk elemental content, carbon content, pedogenic iron content, and radiocarbon age where available.

North-facing hillslopes exhibit more mature soils with higher clay content, less sand, lower pedogenic iron ratios, and higher organic content than their south-facing counterparts. Watersheds more distal from major rivers also exhibit mature soils forming in deeper sediment with higher clay content, lower pedogenic iron ratios, less sand, and higher organic content than their river-proximal counterparts. River proximal hillslopes exhibit more and thicker buried soils with higher values of chemical enrichment for Si/Al than their south-facing counterparts. Clay and silt content are also highest in summit and shoulders of interfluves, and sand and gravel content increase towards the valley bottoms as hillslope sediments thicken. Thus, soil development and sediment mobilization on Piedmont hillslopes vary by aspect and position within Piedmont watersheds, even for hillslopes adjacent to streams of similar orders. The

implications of these observations prompt a reevaluation of Piedmont soils, suggesting their formation histories are polygenic.

ACKNOWLEDGEMENTS

I extend my heartfelt gratitude to all those who contributed to the completion of this thesis. First, I would like to thank Dr. Martha Cary Eppes for the opportunity to pursue a Master's under her guidance and for her support, encouragement, and commitment to my academic and professional growth. I would also like to thank Dr. Terry Ferguson for his dedication to my academic project and growth as a geomorphologist. Thank you to my committee members, Dr. Vinson, Dr. Fall, and Dr. Bobyarchick for their feedback and willingness to help me explore new avenues in my research. Thank you to Jon Watkins for providing training with the Laser Diffraction Particle Counter and Atomic Absorption Spectrometer, and to Jon Merkert, Adam Fessler, and Dr. Craig Allan for assistance fixing the Atomic Absorption Spectrometer. Thank you to Michelle Nelson for her assistance with luminescence sampling and dating, Dr. Daniel Richter for his theoretical contributions on paper and in the field, Dr. Debra Willard for her guidance with paleoclimate literature, and Dr. Steven Falconer for his generosity with the XRF in the field and lab. Thank you to Patrick Mitchell, Dalton Buchanan, Rick McSwain, Erin Hines, and Kristine Ryan of the NC Department of Agriculture Division of Soil and Water Conservation, and USDA for field assistance describing soils and in coordination of the Soils Training at Redlair. Thank you to all of those who helped dig soil pits, including Dr. Eppes' Soil Science class '22. Special thanks to Alec Wells, Mac Bouzigard, Robert Griffin, Stephen Porson, David Crews, Morgan Rinehart, Matthew Yankech, Kayla Eury, Mai Vang, Nate Jones, Ali Van Ormer, Stephen Rachide, and Harrison Hill for their time in the field and in the lab with me. Finally, I would like to thank Haywood and Sabine Rankin and the Redlair Observatory for access to field sites and for their encouragement with and interest in my project.

TABLE OF CONTENTS

LIST OF TABLES **XI**

LIST OF FIGURES **XII**

LIST OF ABBREVIATIONS **XIV**

CHAPTER 1: INTRODUCTION **1**

1.1 Introduction 1

CHAPTER 2: BACKGROUND **3**

2.1 Geomorphic concepts 3

2.1.1 Soil development 3

2.1.2 Soil development as a function of time (chronosequences) 4

2.1.3 Soil development as a function of hillslope position (toposequences) 5

2.1.4 Aspect dependence of hillslope processes 6

2.1.5 Landscape evolution and dynamic equilibrium 7

2.1.6 Conceptual model of landscape evolution 8

2.1.7 Hillslope soils and sediments 11

2.1.8 Mobile and immobile regolith 13

2.1.9 Knickpoint propagation 14

2.1.10 Major global climate controls 15

2.2 Geomorphic concepts at work in the Piedmont 15

2.2.1 The Piedmont's distinctive immobile regolith: saprolite 15

2.2.2 Rediscovered history of mobile regolith in the Piedmont 16

2.2.3 New progress in distinguishing colluvium from saprolite in the Piedmont 18

2.2.4 Interfluve and hillshed order 19

2.2.5 Aspect dependence of Piedmont hillslope processes 20

2.2.6 Piedmont valley bottom sediments and alluvial fans 21

2.2.7 Terraces 22

2.2.8 Tectonics 23

2.2.9 Anthropogenic erosion 23

2.2.10 Geomorphological and palynological evidence of Pleistocene to Holocene climate change 25

CHAPTER 3: FIELD AREA BACKGROUND 30

3.1 Field area: Redlair Observatory Property - Gaston County, NC 30

3.2 Modern climate and vegetation 30

3.3 Geologic setting 31

3.4 Soil survey 32

3.5 Topography 33

3.6 North Rhyne, Duffey, and Deep Creek watersheds 33

3.7 Previous work in the Redlair Observatory 34

CHAPTER 4: METHODS 45

4.1 Field methods 45

4.1.1 Distinguishing residual material from transported sediment 46

4.2 Soil laboratory analyses 46

4.2.1 Particle size distribution 47

4.2.2 Loss on ignition 47

4.2.3 Soil hue 48

4.2.4 Bulk density 48

4.2.6 Radiocarbon dating 48

4.2.7 Pedogenic iron content 48

4.2.8 Bulk elemental analysis 49

4.2.9 Geochemistry 50

CHAPTER 5: RESULTS 52

5.1 Soil morphology 52

5.2 Particle size 53

5.3 Organic content 55

5.4 Radiocarbon dating of charcoal samples 55

5.5 Pedogenic iron analysis 56

5.6 Geochemistry 56

5.7 Soil stratigraphy 57

CHAPTER 6: DISCUSSION / INTERPRETATIONS 84

6.1 Weathering differences as a function of hillshed 84

6.2 Weathering differences as a function of aspect 86

6.3 Weathering differences as a function of hillslope position 86

6.4 Mobile sediment variability between hillsheds, aspects, and hillslope position 87

6.5 Sediment mobilization and climate change 89

6.6 Particle size and organic content comparisons with Deep Creek 92

6.7 Implications 93

CHAPTER 8: CONCLUSIONS 95

REFERENCES 98

APPENDIX A: Field Methods from North Rhyne and Duffey Watersheds, Redlair Observatory, NC 113

APPENDIX B: Soil Pit Locations and Photographs from North Rhyne and Duffey Watersheds, Redlair Observatory, NC 115

APPENDIX C: Soil Pit Sketches from North Rhyne and Duffey Watersheds, Redlair Observatory, NC 165

APPENDIX D: Soil Pit Descriptions from North Rhyne and Duffey Watersheds, Redlair Observatory, NC 165

APPENDIX E: Gravel Weight Percent Methods and Raw Data 165

APPENDIX F: Particle Size Analysis Methods and Raw Data 165

APPENDIX G: Loss on Ignition Methods and Raw Data 165

APPENDIX H: Bulk Density Methods and Raw Data 165

APPENDIX I: Radiocarbon Dating 165

APPENDIX J: Fed and Feh Methods and Raw Data 165

APPENDIX K: Bulk Elemental Data Methods and Raw Data Using Olympus Vanta XRF 165

APPENDIX L: XRF Sample Locations From NR-S10 In North Rhyne Watershed, Redlair Observatory, NC 165

APPENDIX M: Protolith Determination 165

APPENDIX N: Soil Geochemistry and Mass Balance Calculations 165

APPENDIX O: OSL Sample Locations from North Rhyne and Duffey Watersheds, Redlair Observatory, NC 165

LIST OF TABLES

TABLE 3.1: NORTH RHYNE, DUFFEY, AND DEEP CREEK SOIL PIT HILLSLOPE POSITION AND ASPECT 40

TABLE 5.1: AVERAGE AND STANDARD DEVIATION VALUES FOR SAND, SILT, CLAY, GRAVEL, AND LOSS-ON-IGNITION CONTENT FOR DUFFEY, NORTH RHYNE, AND DEEP CREEK 67

TABLE 5.2: TWO SAMPLE T-TEST COMPARING NORTH RHYNE AND DUFFEY 68

TABLE 5.3: AVERAGE AND STANDARD DEVIATION VALUES FOR SAND, SILT, CLAY, GRAVEL, AND LOSS-ON-IGNITION CONTENT FOR UNITS 1, 2, 3, 4. 69

TABLE 5.4: RADIOCARBON SAMPLES AND AGES FROM NORTH RHYNE AND DUFFEY 74

TABLE 5.5: AVERAGE AND STANDARD DEVIATION VALUES FOR AL, SI, FE, SR, ZR, MG, K, CA, AND MN FROM XRF 78

LIST OF FIGURES

FIGURE 2.1: THREE-DIMENSIONAL HILLSLOPE SAMPLING SCHEMATIC 28

FIGURE 2.2: “CONVEYOR BELT” MODEL OF TOPOSEQUENCE EVOLUTION 29

FIGURE 3.1: LITHOLOGY MAP OF CHARLOTTE AREA 36

FIGURE 3.2: LITHOLOGY MAP OF REDLAIR OBSERVATORY 37

FIGURE 3.3: MAPPED SOILS IN REDLAIR OBSERVATORY BY WSS 38

FIGURE 3.4: RELATIONSHIP BETWEEN SOIL ORDERS IN GASTON COUNTY 38

FIGURE 3.5: MAP OF SOIL PIT LOCATIONS IN NORTH RHYNE, DUFFEY, AND DEEP CREEK 39

FIGURE 3.6: SOIL PIT LOCATIONS IN NORTH RHYNE AND DUFFEY 41

FIGURE 3.7: ORDERED INTERFLUVE NETWORK 42

FIGURE 3.8: IDEALIZED SOIL PIT LOCATIONS ALONG TOPOSEQUENCES 43

FIGURE 3.9: WELL BORING PROFILE LOG 44

FIGURE 5.1: SOIL PROFILE LOGS ALONG EACH TOPOSEQUENCE 61

FIGURE 5.2: REPRESENTATIVE FIELD DESCRPITIONS FROM SOIL PITS IN NORTH RHYNE AND DUFFEY 63

FIGURE 5.3A: RADIOCARBON AGES AND PALEOCLIMATE RECORDS FROM THE SE US 64

FIGURE 5.3B: LOCATION OF OTHER PALEOENVIRONMENTAL STUDY SITES IN THE SE US 64

FIGURE 5.4: TERNARY PLOTS OF SAND, SILT, AND CLAY FRACTION 66

FIGURE 5.5: ANOVA TESTS FOR NORTH RHYNE, DUFFEY, AND DEEP CREEK 70

FIGURE 5.6: CLAY, SAND, SILT, GRAVEL AND CARBON CONTENT (X-AXIS) PLOTTED AGAINST SAMPLE DEPTH BELOW SURFACE (Y-AXIS) 71

FIGURE 5.7: IRON ACTIVITY RATIO AS A FUNCTION FO THE CLAY FRACTION FOR NORTH RHYNE AND DUFFEY 75

FIGURE 5.8: CHRONOFUNCTIONS OF THE IRON ACTIVITY RATIO AND CLAY CONTENT 76

FIGURE 5.9: TERNARY DIAGRAM OF FE2O3, SIO2, AND AL2O3 CONTENT OF SAMPLES FROM DUFFEY AND NORTH RHYNE 77

FIGURE 5.10: CHEMICAL ENRICHMENT AND DEPLETION RATIOS FOR NORTH RHYNE AND DUFFEY SOIL PITS 79

FIGURE 5.11: RADIOCARBON AGES FROM NORTH RHYNE AND DUFFEY WATERSHEDS GROUPED BY SEDIMENTARY UNIT 83

LIST OF ABBREVIATIONS

DE	Deep Creek watershed, Redlair Observatory, Gastonia NC, USA
DU	Duffey watershed, Redlair Observatory, Gastonia NC, USA
Mvf	Felsic metavolcanic rocks
NR	North Rhyne watershed, Redlair Observatory, Gastonia NC, USA
Zbs	Quartz sericite schist

CHAPTER 1: INTRODUCTION

1.1 Introduction

Long-held paradigms of landscapes in the southeastern United States (hereafter 'Piedmont') emphasize their gentle slopes and temperate climate, which have been interpreted to both promote and to result from steady-state weathering of bedrock into deep, in-situ soil profiles (Stephens 1977, Holbrook et al. 2019). However, a reevaluation of soils and stratigraphy of sites first described in historical literature (Eargle 1940) suggests that the Piedmont is a dynamic landscape characterized by: 1) discrete periods of episodic erosion, transportation, and deposition from ~40ka to ~150ka (Richter et al. 2020, Ferguson 2022); 2) a notable lack of late-Glacial-aged deposits; and 3) common early- and late- Holocene deposits with a consistent lack of middle-Holocene-aged deposits (Opalka et al. 2022). To date, most of this research has focused on valley bottom deposits, and there are few records of hillslope soils and sediments that would help elucidate these overall Piedmont landscape evolution processes. This study aims to examine spatial and temporal variations in hillslope soils and sediments in two first order watersheds in the SE Piedmont during the Holocene.

Recent studies of low-order watersheds in the Piedmont suggest periods of alternating hillslope processes, from widespread hillslope erosion (inferred from alluvial fan and valley bottom aggradation) to inferred hillslope stability (no evidence of valley bottom accumulation) throughout the late Holocene (Opalka et al. 2022) and the late Pleistocene back to ~130ka (Richter, Eppes et al. 2020). It is understood that hillslope processes comprise interactions between weathering (soil development) and erosion, moderated by the interplay of factors such as climate and aspect (e.g. Pelletier, Barron-Gafford et al. 2018). Unlike in the semiarid southwestern and western United States (e.g. West et al. 2013), few studies have examined

hillslope processes or the factors that influence them in humid temperate climates, such as the Piedmont.

Dual objectives drive this study: 1) to understand weathering as a function of landscape position, and 2) to elucidate the variability of surface processes based on landscape position. To examine both of these, I will investigate four slopes that comprise contrasting aspects (N vs. S) and contrasting proximities to major rivers (i.e. high versus low interfluve order (Brecheisen 2012). To this end, I characterize the field and laboratory characteristics of soils, sedimentology, and stratigraphy of four toposequences— including adjacent valley deposits— in two first-order watersheds of the SE Piedmont where the entire Holocene source-to-sink system has the highest likelihood of still being intact. In doing so, I show that hillslope soils exhibit weathering differences as a function of soil excavation location on the hillslope (including aspect) and the watershed location within the broader landscape, and that soil properties not only influence but are also dependent upon landscape evolution differences within each watershed.

CHAPTER 2: BACKGROUND

In this chapter, I provide background information for geomorphic and pedological concepts and prior research that informs the interpretation of soils and sediments on Piedmont hillslopes.

2.1 Geomorphic concepts

The following sections contain an overview of concepts related to landscape change, sediment, and soils which form the foundation of this thesis.

2.1.1 Soil development

Soils are *in situ* weathering profiles that differ from their parent material morphologically, physically, chemically, mineralogically, and biologically (Birkeland 1999). Soils and their horizons (the natural surface-parallel zones of different weathering intensity) are created by soil-forming mechanisms as organic material and water facilitate the disintegration of the parent material (rock or sediment). This sum of all such changes due to weathering is known as 'soil development' or 'soil genesis.' The term 'soil production' was coined by Heimsath (1997) and refers to the subsurface incorporation of material from weathered bedrock into the disrupted, overlying soil horizons. It comprises a portion of overall soil development.

Soil profiles (vertical arrangement of horizontal layers extending to unaltered parent material) deepen over time as the probability of a higher magnitude rainfall event increases, which serves to saturate previously unsaturated material and advance the weathering front. Time, precipitation, soil moisture, and infiltration capacity control soil profile thickness.

Vertical movement is an essential part of the pedogenic processes. Pedogenesis occurs through vertical movement of materials by water action, biological action, and horizontal movement. Climate and hydrology also promote movement via freeze-thaw cycles, changing

temperature, and saturating and drying of soil (expanding and shrinking). Movement is proportional to the slope on which the soil is developing.

The prevailing model of soil genesis states that soil development is a function of climate, organisms, relief, parent material, and time. This classic “five factors” approach was initially conceived by Dokuchaev and subsequently communicated in English by Byers et al. (1938), Jenny (1941), Kellogg (1936), and Neustruev (1927) (Johnson and Watson-Stegner 1987). Joffe (1936) divided the five factors into two groups: active (climate, organisms) and passive (relief, parent material, time).

2.1.2 Soil development as a function of time (chronosequences)

Soil chronosequences, a series of soils that have formed under the same conditions but differ in time since deposition, can be used to determine the relative ages of landscape surfaces (Birkeland 1999). Rock and sediment weathering and associated soil profile development are time-dependent. Soil development begins virtually instantaneously after a landform or landscape position stabilizes and can continue for 1,000-100,000 years. Thus, geomorphologists are interested in understanding soil properties at different ages to help estimate the age of soils and the deposits and landforms they are forming in and on. Soil chronosequences provide information about how weathering characteristics of soils change with time when climate, parent material, vegetation, and relief are held constant (Jenny 1941).

By conceptualizing soils in this way, it is possible to use certain field sites to develop ‘sequences ’whereby all but one of these ‘state factors’ are held constant allowing an investigation of the impact of the one factor on soil development. All factors of soil genesis will be explored in this project, emphasizing the impact of topography on soil formation.

Certain soil properties are known to change with age systematically. For example, particle size distribution and pedogenic iron content are both known to vary with soil age (Birkeland 1999). In soils with no known age control, the relative degree of soil development can be used to indicate age. Furthermore, radiocarbon dating of charcoal samples from known soil horizons helps calibrate the soils in the field area. Chronosequence studies in the Piedmont exist for terraces (Layzell et al. 2012), upland surfaces (Markewich, Pavich et al. 1990), and alluvial fans (Opalka et al. 2022). Much of this past work leads to the conclusion that the inheritance of soil properties such as color and clay content from the reworking of older upland soils in the landscape frequently impacts the characteristics of soils in the Piedmont. There has, to date, been little exploration of how this reworking operates on hillslopes.

2.1.3 Soil development as a function of hillslope position (toposequences)

Soil properties are related not only to slope gradient but also to position on a slope. The term toposequence is used to describe a sequence of soils along a slope (Schaetzl 2013). Jenny (1941) argues that topography is the primary factor leading to soil variation in the field. Soil development along a toposequence can be used to understand landscape dynamics during periods of climate change and tectonic deformation (e.g. Eppes et al. 2002). The term catena is also used to describe soils along a slope but necessitates a consistent lithology (Schaetzl 2013).

Hillslope positions include the summit (upper portion of hillslope), shoulder (convex, upper portion of hillslope), backslope (planar, middle portion of hillslope), footslope (convex, lower portion of hillslope), and toeslope (valley bottom). Horizon thickness and depth to residuum is known to vary with landscape position (McCracken et al. 1989). For example, soils are expected to be thickest in concave hollows and thinnest on convex ridges (Patton et al. 2018).

To my knowledge, however, there have been no explicit studies of toposequences published for the Piedmont.

2.1.4 Aspect dependence of hillslope processes

Hillslope stability is impacted by soil moisture, temperature and vegetation growth, and slope gradient. Soil moisture is related to changes in microclimates, which are known to vary with solar radiation intensity. In the Northern Hemisphere, north-facing hillslopes receive less sunlight, are cooler, experience slower rates of evaporation, and have higher soil moisture content than their south-facing counterparts. At low latitudes, north-facing hillslopes are steeper, and conversely, south-facing hillslopes are steeper at high latitudes. Moreover, Pelletier et al. (2018) found that in a water-limited hillslope, the equator-facing hillslope is poorly developed, has less vegetation, and receives more direct sunlight, which increases potential evapotranspiration and limits water storage potential. On the other hand, in temperature-limited hillslopes, equator-facing hillslopes tend to be more well-developed with more vegetation and direct sunlight, which still increases potential evapotranspiration, leading to less water storage (Pelletier et al. 2018). West et al. (2013) found deeper weathering profiles on south-facing hillslopes in central Pennsylvania. Generally, more well-developed soils are expected on south-facing hillslopes in the temperate United States (south of 50°N) because they are likely to remain more stable.

Studies in arid environments exemplify aspect-dependent soil formation and erosion during the Pleistocene-Holocene transition (Persico et al. 2021). The Pleistocene-Holocene transition diminished hillslope vegetation in their field area (Nevada), increasing runoff, erosion, and sediment load in streams. North aspects maintained minimal erosion during the transition and remain stable even now, whereas a substantial amount of sediment was eroded off of south

aspects. Burnett et al. (2008) studied the dependence of hillslope processes on microclimate in Arizona and found that south-facing hillslopes are consistently slightly steeper, warmer, drier, and have less deeply weathered bedrock than their north-facing counterparts. These studies provide evidence for the importance of climate change-induced vegetation changes in the erodibility of arid landscapes, but there have been minimal studies of aspect dependence of hillslope processes in humid environments, especially away from areas impacted by periglacial processes during the last ice age, and none to my knowledge in the Piedmont.

2.1.5 Landscape evolution and dynamic equilibrium

Landscape evolution comprises the changing topography of the Earth's surface. Two end-member hypotheses have been proposed to explain landscape evolution in the Eastern U.S. landscapes; particularly mountain terrane: one suggests that topography persists in a dynamic equilibrium (a state of balance between the processes of erosion and erosion resistance of any earthy material) (Hack 1975), and the other suggests that topography is a result of modern rejuvenation driven by climate change, epeirogenic uplift (e.g. Gallen et al. 2013), and/or periodic watershed reorganization (Gallen 2018). Gilbert's law of erosion (Field 1877) introduced the idea that landscapes persist in a dynamic equilibrium. Still, it was overshadowed by William Morris Davis's idea of time-dependent erosional stages (Davis 1899). Davis introduced the idea of the "cycle of erosion" in which a landscape cycles through three stages: 1) youth (characterized by narrow, V-shaped valleys and vertical erosion exceeding lateral erosion; 2) maturity (when lateral erosion begins to compete with vertical erosion); and 3) old age (lateral erosion dominates, minimal vertical erosion) (Davis 1899, Bryan 1940, Garner, 1947). Davis's theory of slope retreat was in opposition and response to Penck's view that steep slopes retreat without a loss in inclination: two slopes with the same base level (which he thought of as largely

stable) will retreat until the original highland has been consumed, the drainage divide lowered, and the relief of the area reduced to a gently undulating plain (Meyerhoff 1980). The conceptual framework embedded in this paper aligns closely with Davis's view of slope retreat: that erosion, transportation, and deposition are the processes through which particulate matter is moved throughout the landscape, and these processes occur simultaneously and continually, although not constantly (Davis 1899).

In 1960, John Hack reintroduced the time-independent concept of dynamic equilibrium to the field of geomorphology, arguing that landforms are controlled by lithology and geomorphic processes rather than by regional erosional history (Hack 1960). This new concept carried ideas from Penck's previous erosional model assuming that the system had been downcutting for so long that it can be analyzed as though it is in a steady state (Hack 1975). Pavich (1985, 1986) posited that the uplift, weathering, and erosion rates in the Piedmont can be considered roughly equal. Others have called for non-steady state landscape evolution or the lack of an endpoint (i.e. Richter et al. 2020). Erosion, transportation, and deposition are considered as processes responding to dynamic equilibrium. Furthermore, in natural environments, environmental perturbations such as thermal cycles, bioturbation, and wetting and drying make hillslopes perpetually fragile (Deshpande et al. 2021). Natural systems under study in this paper may provide insights into if the Piedmont landscape is operating under steady-state conditions.

2.1.6 Conceptual model of landscape evolution

The Piedmont is a polymorphic landscape that has been altered and written over repeatedly (Bloom 2001). Thus most soil and regolith (including unconsolidated sediment and soil weathered to some degree (Richter et al. 2020)) have polygenetic histories to their formation. Understanding how hillslope processes in the Piedmont respond to climate, aspect, slope,

landscape position, and lithology applies not only to the current landscape but also to relict landscapes. “Relict” landscapes are inherited landscapes shaped by processes no longer active on that region (Bloom 2001). For example, in some places, high points in the topography represent the oldest geomorphic (depositional) surfaces and form a ‘peneplain’ (Davis 1889), or gently undulating, almost featureless plains formed by the lowering of an entire region containing more than one watershed to a common base level. It is essential to consider how the processes operating on a current landscape may not always be operative in that system.

Hillslope evolution is a prime example of where this complexity may come into play. Conventional ideas regarding soils on hillslopes (Stephens 1977, Holbrook et al. 2019) expect that all hillslope soils in the Piedmont are derived directly from bedrock, but in some ancient hillslopes, upper portions of the soil profile form from sediment (e.g. colluvium, alluvium).

In Figure 2.2, I developed a conceptual model that melds the idea of a toposequence and a chronosequence to think about past toposurfaces. This is a look at a landform at a mesoscale, or the scale of hillslope, to help understand what is happening at the scale of the landscape as a whole. As the initial hillslope erodes (T0 -T3 of Figure 2.2), the valley fills in with sediment once part of the hillslope. The resulting filled valley records the characteristics of the hillslope horizons in reverse order; the last unit to erode, for example the brightest red color, will be the last to be deposited in the valley. The resulting landscape around T3 is relatively flat. The channel shifts to the right in the model, and the recently deposited sediment begins to erode and be transported in the direction of the channel (T4-T6). As the channel moves, material erodes, transports, and deposits into the newly formed valley. Notice that as the hillslope forming in a paleo valley encounters an erosion-resistant layer (similar to a Bt) comprised of colluvium from the paleo hillslope, it erodes much slower than before. Bt-horizons contain a minimum of 13%

clay, and around the 28% clay content threshold, deposits are resistant to erosion by fluid flow (Layzell and Mandel 2014). The erosion-resistant layers are also responsible for the slight change in the inflection point. As the channel shifts away from the paleo valley, the drainage divide also shifts in the opposite direction. The valley is now the highest point in the landscape (the concept of inverted topography). The order of these processes is perfectly sequential for the convenience of the model (Figure 2.2), but hillslopes in nature would not necessarily behave in this way. Erosion, transportation, and deposition are distinct processes, but they may occur continuously and simultaneously and/or at different rates at any given point and time in the model. This study will begin to test this conceptual model of hillslope evolution in the Piedmont.

The process of episodic erosion depicted in Figure 2.2 aligns with Bryan's (1940) concept of 'gully gravure' which describes the process in which abandoned drainage ways were filled with erosion-resistant colluvium, and subsequently, channels developed in softer materials of the old slopes. Bryan's theoretical framework is also related to that of Davis, who served as his mentor.

Because hillslopes in low-order drainages are not overly channelized, the primary sediment source from the conceptual model of Figure 2.2 is hillslope creek (a.k.a. diffusion; sediment mobilization) and possibly hortonian overland flow. Here I focus on the former. Hillslope creep is classically related to soil diffusion (Jenny 1941). Mechanical disturbance incites soil creep through freeze-thaw cycles and thermal agitation (e.g. Berut et al. 2019), acoustic disturbances or mechanical noise (e.g. Nowak et al. 2001), and burrowing agents (e.g. Viles et al. 2021). Soil creeps persistently and "viscously" (Culling 1963) downhill to achieve a lower energy state. Since grains at the surface are not confined by the weight of those above them, the rate of weathering decreases with depth along hillslopes. Surface cover depth also

depends on the rate of material transport on the slope. Even in undisturbed landscape models, creep decays as a power law in time, and it occurs in every landscape position over all observed timescales (Deshpande et al. 2021).

2.1.7 Hillslope soils and sediments

Under the dynamic equilibrium paradigm, hillslope soils and hillslope sediments are fundamentally different. Whereas a hillslope soil has formed in situ due to primarily vertical weathering processes, hillslope sediment (or mobile regolith), as defined by Kleiss (1970) comprises reworked material transported from upslope. In some geomorphology literature, this hillslope sediment is sometimes referred to using the term 'soil' (e.g. Heimsath et al, 1997). To avoid confusion, I employ the term 'sediment' when referring to any previously transported material. Hillslope sediment is typically considered thinnest on the summit and shoulder hillslope positions and thickest on the foot and toe slopes (McCracken et al. 1989). Sometimes, the base of the hillslope sediment is bounded by a planar concentration of gravel called a stone line, which marks the boundary between immobile and mobile regolith (Sharpe 1941). Stone lines suggest that lateral migration has taken place above them. Transported sediment, or colluvium, is identified based on a higher percentage of gravel.

While sediments provide information on depositional processes and the specific environments present, hillslope soils preserve evidence of landscape stability and degree of in situ weathering. Hillslope soil comprises the weathering profile that occurs when hillslopes are sufficiently stable. The in-situ chemical transformation process can proceed, such as hydrolysis, or physical transportation within the vertical profile (e.g. illuviation of clays along pores). Hillslope soils can be formed within sediment or residuum, but the parent material (be it

sediment or bedrock, the parent material is the material in which the weathering progresses) must be made clear in their description.

Distinguishing parent materials in well-developed soils is sometimes difficult (e.g. Nelson et al. 2022), but there are also tell-tale signs. For example, compared to residuum, colluvium is expected to be poorly sorted, have higher total organic content, and be coarser overall. Relative concentrations of immobile and mobile elements from bulk elemental analysis also help identify soils derived from different parent materials. Residual soils and saprolite (*in situ* weathered rock) may retain primary geologic structures such as veins, bedding, or foliation; or can have platy structures inherited from the foliation of the bedrock. In soils forming in legacy sediments (meaning those related to anthropogenic activities), poorly sorted particulate matter/ varied particle size distribution is expected throughout the profile, like the homogeneous urban conditions Herrmann et al. (2020) compared to heterogeneous pre-urban soil conditions.

The presence of buried soils indicates past periods of landscape stability and soil formation that have been covered with sediment. Buried soils often have a darker color and higher organic content than the horizons immediately above them. Buried soils can be formed from residual soil or sediment, but they always represent an unconformity separating discrete allostratigraphic units.

With time, all soil properties – regardless of parent material—are known to progress predictably with respect to several soil characteristics. For example, despite climate, clay accumulates in soil profiles over time as primary minerals weather through hydrolysis to clay minerals (Birkeland 1999). In well-developed, older soils, the clay content is expected to also increase with the horizon (i.e. a higher percentage of clay in the B-horizon than in the A-horizon) (e.g. Layzell et al. 2012) as finer particles are translocated down the profile by water infiltrating

through the weathering profile. The iron activity ratio (FeH/FeD) is also expected to decrease with time as FeH converts to FeD (more stable). This ratio emphasizes the formation of crystalline iron oxides from weathering and deemphasizes the parent material's initial content (FeH). Residuum is expected to have the lowest iron activity ratio, followed by soil of colluvial origin and then by legacy sediment/ soils due to the progressive accumulation of iron oxides in the soil. Residual soils have the longest residence time, and therefore a greater potential for FeH to convert into FeD. Legacy soils, on the other hand, have lived shorter lives and this ratio is likely to be greater.

2.1.8 Mobile and immobile regolith

Protolith (bedrock) weathers to regolith (material that has been weathered to any degree from a range of substrata and includes weathered rock, saprolite, sediment, and soil) with access to reactive waters through increasing porosity, exposure to surficial processes, and time (Bazilevskaya et al. 2012). Regolith is traditionally split into two major categories: mobile regolith (A-, E-, B- horizons) and immobile regolith (saprolite; C- and R- horizons). The entire weathered mantle profile is potentially movable in the case of deep-seated mass movement and gully incision, wherein gravity-induced deep-seated failure can exceed the depth of the saprolite. The magnitude of horizontal movement (regolith) and vertical movement (vertical growth of weathering profile to depth) generally decreases with depth. The thickness of the soil profile is understood as the balance between regolith production (via weathering) and mass loss (via dissolution, erosion, and transport) (West et al. 2013).

Oxidizing fluids percolate through the critical zone via fractures and pores in the protolith of two types (Holbrook et al. 2019): fractures can form through stresses related to tectonics, environment – including chemical weathering—or gravity. Chemical weathering is expected to

decrease with depth because material closer to the surface has more potential for contact with reactive fluids during exhumation and because the number and magnitude of environmental stresses that cause fracturing decreases with depth.

2.1.9 Knickpoint propagation

Stream channels grow in length through headward erosion, a foundational concept in fluvial geomorphology describing how stream erosion occurs at the stream head resulting from undercutting at its base. Subsurface water flow moistens soil, causing the material to be more easily removed at the head (Morisawa 1968). Once the head is undercut, more resistant overlying layers begin to collapse into the stream and wash away. This advancement begins at the knickpoint, which is the most active point of stream erosion (Sharpe 1941). Causes for knickpoint propagation include excessive rainfall, flooding, loss of topsoil, or clearing of vegetation by way of agriculture or forest fires.

Knickpoints in low-order streams are generally associated with soil (saprolite), but in high-order streams they can be associated with bedrock outcrops. Appalachian knickpoints evolve through parallel repeat and vertical channel incision, forming upstream-dipping strath terraces (Frankel et al. 2007). Base level fall causes a complex series of responses of the alluvial channel involving burying and uncovering the bedrock substrate. The rate at which streams incise into bedrock is the main determining factor of local hillslope erosion and regional landscape evolution (Gallen et al. 2011). Here we are operating under the conceptual model that low-order watersheds (Figure 3.6, 3.7) have experienced more and more recent landscape modification related to knickpoint retreat from the incision of major drainages than those further away from the large-order rivers of the region. As such, hillslopes on low-and high-order hillsheds may represent end members of soil and erosion processes in the Piedmont.

2.1.10 Major global climate controls

Here, I will provide a general overview of the global climates of the late Pleistocene, a factor that has long been documented to influence soil and geomorphology (e.g. Bull, 1991).

For the last 21,000 years, the critical climatic controls and boundary conditions for eastern North America include the large increase in CO2 and other greenhouse gases associated with the deglaciation, retreat of the Laurentide ice sheet, changing sea-surface temperatures, and fluctuating intensity of seasonal insolation (Webb et al. 1993).

Earth's orbital, or Milankovitch cycles, including precession (drives tropical convection), obliquity (drives ice ages), and eccentricity (drives both tropical convection and ice ages), are responsible for the climate changes that characterize the Quaternary. The first major cold events substantial enough to produce glaciation occurred during MIS 22 (Ehlers et al. 2018). Geomorphic evidence of early glaciations during the Pleistocene is difficult to identify because they have largely been removed by later, more extensive ice sheets.

The last deglaciation in North America spanned about 21 to 11 ka BP covering the Pleistocene-Holocene boundary and is punctuated by several abrupt climate changes: Heinrich event 1 (~17ka BP), the onset of the Bølling-Allerød warming (~14.5 ka BP), accompanied by and related to heat transport associated with the Atlantic meridional overturning circulation (Liu et al. 2009). The Younger Dryas period imminently preceded the Holocene and is characterized by a reversal in the trend of global warming since the LGM. Climate, vegetation, and geomorphic process response dramatically changed at the Pleistocene-Holocene boundary.

2.2 Geomorphic concepts at work in the Piedmont

2.2.1 The Piedmont's distinctive immobile regolith: saprolite

The Piedmont's most distinctive regolith, saprolite, is more ubiquitous and deeply weathered in the Piedmont compared to surrounding areas (Clark and Kite 2000). Holbrook et al. (2019) examined physical and chemical weathering in a 65-meter deep borehole that surpassed the depth-extent of the critical zone (i.e. weathered bedrock) into unweathered bedrock at the Calhoun Critical Zone Observatory (CZO) in the South Carolina Piedmont. They mapped a complete Appalachian granitoid profile and found that the regolith at the Calhoun CZO is about 38 meters thick with saprolite comprising the first 18 meters below the surface and soil for less than a meter below the surface. Around 38 meters (transition from regolith to bedrock), plagioclase and biotite begin to weather, oxidation is first detected, and fractures dramatically decrease (Holbrook et al. 2019). This study illustrates the likely vertical extent of in situ, stable regolith throughout the Piedmont.

2.2.2 Rediscovered history of mobile regolith in the Piedmont

Although saprolite is the most distinctive overall type of regolith, transported regolith (sediment) is abundant yet often overlooked in the Piedmont. Geological surveys in North Carolina and South Carolina began in 1875 when the North Carolina State Geologist William Kerr drew the first comprehensive geologic map of North Carolina. Kerr (1875) was also the first to document organic deposits buried beneath Piedmont soils made visible primarily by road and railroad cuts. He hypothesized that the rapid accumulation of sediment happened too quickly to have been alluvial in origin, so he attributed these deposits to periglacial phenomena which are documented extensively throughout Western NC (Soller and Mills 1991).

In a modern context since European settlement, the southern Piedmont is considered one of the most severely eroded areas in the US (Trimble 1974, Costa 1975, Daniels 1987). In 1936, the Soil Conservation Service (SCS) began a study of anthropogenic erosion caused by intensive

agricultural practices following European settlement using Spartanburg County, South Carolina as a case study. In this area, the nature of the topography, land use, soils, weathering, and climate lead to severe and detrimental historic gullying (Ireland et al. 1939). The gullies range from 20 to 50 feet deep and can widen up to 12 feet during a single rain (Cain 1944).

In turn, however, this anthropogenic gullying exposed paleo-valleys containing organic soil and colluvial deposits first described by Kerr (1875). Buried organic matter was found in drainage basins and dales in all 25 sites around Spartanburg (Eargle 1977). This stratigraphy also has broader regional significance; reconnaissance of the Piedmont in surrounding states has revealed similar deposits (pers. comm. T. Ferguson).

In one of the only published papers in any major journal about this ancient erosional history of the Carolinas that was exhumed by modern gully gravure, Eargle (1940) describes buried transported organic material containing pollen and macrofossils in Spartanburg, SC. From the eight hundred boreholes dug for this publication, Eargle found that half of the study areas had these transported sediments. This 80-year-old publication challenges the existing paradigm regarding soil formation and landscape change in the Piedmont, which still holds today.

The presence of filled paleo-valleys in the Piedmont directly opposes the traditional thinking that Piedmont soils are formed *in situ* only from the weathering of bedrock. The preceding evidence indicates soils can form in hillslope sediment as well. Additionally, accelerated erosion is still largely thought to only be of anthropogenic origin, but this interpretation is inconsistent with sediment filled paleo-valleys described by Eargle (1940): organic deposits that grade upslope into distinct paleosols within the colluvium indicate multiple episodes or stages of accelerated colluvial deposition. This is further supported by observation of preserved macro fossils by Overstreet and White (1968). Because the soil thickness increases

drastically downslope during the Pleistocene, valleys must have been deeper, divides must have been higher, and slopes must have been steeper to allow for sediment accumulation (Figure 2.2).

Despite the 17th and 18th-century research, the current paradigm of Piedmont landscapes emphasizes long-term landscape stability. For example, an important implication of these observations of drastic paleo-features is that their in-filling is part of why the Piedmont landscape is gentle and rolling. Traditionally, this topography has been attributed to the stability and old age of the landscape (as described by Davis, 1899).

Furthermore, around 90% of the Piedmont is mapped as a Cecil soil by the NRCS, which is considered to develop in a stately, residual, and slow process (USDA-NRCS 2014), but numerous filled valleys with buried organic deposits were mapped and described by Ireland (1939), Eargle (1940), and Sharpe (1941) are antithetical to this thinking. This study will continue this work by examining the nature and extent of sediment found on hillslopes in the Piedmont.

2.2.3 New progress in distinguishing colluvium from saprolite in the Piedmont

One reason soils forming in sediments have not been identified in the Piedmont is that overall soil development proceeds quickly in this warm, temperate climate, thus likely quickly masking the nature of the parent material from which the soils have formed. In addition, long-term (Cenozoic) landscape stability has promoted well-developed soils and deep saprolite in upland landscape positions. In the Piedmont, any obvious boundary between immobile and mobile regolith has been masked by thousands (or hundreds of thousands) of years of soil development, so a worker might easily overlook the distinction. Nevertheless, prior work in the Piedmont at Redlair Observatory and elsewhere (Eppes, unpublished) has enabled the identification of key identifiers of sediment versus saprolite (see section 2.1.8 above).

Recent advances in optically stimulated luminescence (OSL) allow a possibility to better distinguish sediment from saprolite (e.g. Bateman et al. 2007, Gliganic et al. 2015, Reimann et al. 2017, Bartz et al. 2022) and to confirm Eppes' otherwise untested criteria for the distinguishment. Nelson et al. (2022) used the intensity of fast-decay luminescence component in quartz grains to distinguish transported versus *in situ* material from Deep Creek watershed in the field site (Redlair Observatory, Gaston Co., NC). Quartz grains from transported sediment are expected to have more dominant fast-decay components than bedrock-derived saprolite, which is not dominated by a fast-decay luminescence component. The 'brightness' of the light-sensitive signal in quartz grains reflects the sediment's transportation history or lack thereof. Specifically, for soils where there were unambiguous sediment/saprolite boundaries (e.g. stone lines, rock structures visible in the saprolite), material identified as sediment was distinctly 'brighter' than that of the saprolite. Thus, in pits where the distinction was less clear from sedimentary or rock features, the OSL allowed identification of the boundary. This published research thus confirms the presence of mobile sediment on hillslopes in the Redlair Observatory field area. Here, I build on that work by describing the characteristics of that sediment – and the soils forming in it – along four entire hillslopes.

2.2.4 Interfluve and hillshed order

Following Brecheisen et al. (2021), interfluves were ordered according to the Strahler ordering system to find the order of the overall hillshed, whereby low-order hillsheds are located proximal to the primary stream of the mapped area and higher-order hillsheds are found in increasingly distal locations from the stream and increasing proximal to its overall watershed divide.

Like all stream networks in a given watershed, the majority of hillslopes in a nearby hillshed in the Piedmont are first-order (~77% in Calhoun Critical Zone Observatory in South Carolina (Brecheisen et al. 2021)), and high-order hillsheds are progressively less common with increasing order. Median hillshed elevation, slope, and curvature are thus all related to interfluve order. Furthermore, hillshed geomorphology is influenced by how hillsheds are connected to each other (first-order to second-, third-, fourth-, fifth-, or sixth-order).

First-order hillsheds are the steepest and narrowest with the lowest elevation (furthest from maturity). High-order hillsheds are those which are furthest away from major rivers. Low-order hillsheds are expected to be less stable landscape positions compared to high-order hillsheds because the latter are further from the local base level.

I hypothesize that ancient colluvium (e.g. Kerr 1875; Eargle 1977) will be most preserved at the surface of high-order interfluves (i.e. 5th, 6th, 7th order), as these are the longest-lived and most stable portions of the landscape. This stability likely preserved the previously observed (Kerr 1875; Eargle 1939; Ireland 1939) deposited Pleistocene material through the Holocene (Figure 2.2). On the other hand, saprolite and residual soils are expected to be at low-order interfluves since these are more transient landscape positions.

2.2.5 Aspect dependence of Piedmont hillslope processes

Unlike in the semiarid southwestern and western United States (e.g. West et al. 2013) or the northeast and possibly mountain areas that were subject to periglacial conditions during glacial conditions (West, 2013 and Desta et al. 2004) to date, few if any studies have examined hillslope processes or the factors that influence them in warmer humid temperate climates, such as the Piedmont. Previous work by Opalka et al. (2022) found qualitatively no vegetation differences between north- and south-facing hillslopes on alluvial deposits in the Piedmont.

Based on my preliminary field observations of no major differences in plant type and cover, this trend also seems to extend to hillslopes at Redlair Observatory, with no significant difference in soil moisture or vegetation based on hillslope aspect. However, I acknowledge that this was a cursory examination that would require a full study to characterize more minor differences.

2.2.6 Piedmont valley bottom sediments and alluvial fans

Prior work on the terraces of the Catawba River (Arey, 2018 and Layzell 2012) as well as studies of alluvial fans (Opalka et al. 2022) suggest that the Piedmont is characterized by distinct periods of sediment mobilization likely correlated to periods of climate change. Mobile regolith is continually moving, and climatic excursions are known to incite prolonged changes in velocity. Deposition is driven by increased sediment supply resulting from temperature and moisture changes destabilizing hillslopes wherein fine sediments are eroded gradually from hillslopes, transported down the basin, and deposited on fans. Alluvial fans are produced by climates that favor hillslope erosion without extreme or extensive runoff and have a high sediment supply-to-discharge ratio.

The Piedmont is characterized by periods of significant valley bottom sediment accumulation evidenced by alluvial fans issuing from zero- and first-order watersheds throughout the Holocene (Opalka et al. 2022), however, the origin of the sediment within the watershed is still largely unknown. Opalka et al. (2022) dated fifteen fans issuing from low-order watersheds to the early- and late-Holocene and reported radiocarbon dates of sediments to be dominantly late-Holocene, with almost 90% of fans dating to around 600 to 3000 ka BP, and the remaining 10% dating to between 7000 and 10,000 ka BP. None of the alluvial fans in the study are dated to the mid-Holocene or late Pleistocene. Low-order streams had only Holocene

material, with no Pleistocene deposits, whereas higher-order streams had a Pleistocene component.

Dotterweich et al. (2014) found evidence of landscape stability during the mid-Holocene in Tennessee inferred from radiocarbon dating and the degree of soil formation in gully fan sediments. It is possible that there was also geomorphic stability around the same period in North Carolina. Alternatively, if climate change during the mid-Holocene caused the die-off of many plants, triggering fires, high runoff, and soil erosion, the missing alluvial fan sediments could be a result of widespread erosion with subsequent deposition that bypassed alluvial fans through increased discharge.

2.2.7 Terraces

Fluvial terraces are reminiscent of past depositional surfaces and can provide insight into the Quaternary landscape evolution of incision (e.g. Leigh et al. 2004). Terrace formation is attributed to periods of increased sediment supply or decreased discharge, which are climate-related factors (e.g. Eppes et al., 2008). Tectonic uplift, base level fall, or an uplift in the headwaters are all factors that produce a relief in a landscape that preserves terraces. Playfair's Law describes the principle that all streams join at accordant levels: when one stream lowers itself, all tributaries tend to lower themselves accordingly (Eargle 1937).

Layzell et al. (2012) explored alluvial terraces of the Catawba River and found that soil color, pedogenic iron, and clay content showed a positive trend with increasing age. Mills (2000) found that terrace ages correlate to their relative height above the stream level; the age of terraces increases by the square of the height above the modern river level. This regional incision rate curve can be applied by location and used to approximate terrace age.

Arey (2018) found that the Catawba River's terrace straths are carved during interglacial periods with warmer temperatures, rising sea levels and regional base levels, and reduced discharge. This study proposed that tectonic-induced base level change is a possible cause of incision, and increased discharge during glacial periods can cause of terrace abandonment on the Catawba River (Arey 2018).

2.2.8 Tectonics

Geologic, geomorphic, and hydrologic systems determine hillslope erosion and landscape evolution. The southern Appalachians have not experienced a period of significant tectonic forcing for the last 200 Ma (e.g. Gallen et al. 2011). However, this area is still subject to frequent mass-wasting events and other forces that maintain steep and unstable slopes. Faulting is the most definitive evidence of regional tectonism in the SE Piedmont. Uplift, subsidence, faulting, and geomorphic and earthquake-induced features suggest continuous tectonic deformation of the Carolinas from the Late Cretaceous to the Holocene (Soller and Mills 1991). Reverse faults throughout the Piedmont indicate regional compression from the Early Cretaceous through the Pleistocene. Cretaceous and younger faults parallel existing NE trending rock fabric. Long-term compression since the Early Cretaceous has led to uniform fault movement for the last 100 million years.

2.2.9 Anthropogenic erosion

Anthropogenic activity in prehistoric times made a relatively smaller difference in ecosystem and landscape evolution compared to historic anthropogenic activity in the Eastern US (Dotterweich et al. 2014). Only after colonization did wide-scale and intensive agriculture and deforestation significantly alter the landscape (Dotterweich et al. 2014). Even still, prehistoric anthropogenic sediment deposits in valley bottoms have been identified as separate

from historic anthropogenic sediments in southwestern Tennessee by Dotterweich et al. (2014), so soil erosion due to prehistoric land use by Native Americans should not be overlooked.

In these regions' more recent geomorphological history, European cultivation of relatively flat upland and hillslope valley areas, terraces, and floodplains resulted in the removal of a significant portion of the A-horizon, such that most continued agricultural activity takes place on the B-horizon or mixed A- and B-horizons (Kerr 1881), and in some cases today even the C-horizon. Headward gullying through drainage ways destroyed much of the viable agricultural land, which was the initial call to action for the onset of soil geomorphology research in the Carolinas. Today, stream bank erosion is the leading contributor to suspended sediment. This problem worsens in areas affected by intensive agriculture practices. Erosion rates are highest in the legacy sediment zones (Lyons et al. 2015).

The natural history of the Piedmont has always included periods of time with significant gullying (Eargle et al. 1938, Ireland et al. 1939, Eargle 1977). Agricultural denudation mimicked natural erosional processes from the Pleistocene, perhaps pointing to potential triggers of hillslope erosion in the past. During the late Pleistocene, sheet and gully erosion acted on the surface (Eargle 1946). Natural forces like freeze-thaw cycles, torrential rains, or extensive burning (loss of vegetation cover holding soil in place) that caused gullying in the past are replicated through intensive agriculture recently (Eargle 1946). Studies in the SE Piedmont support that 18th – 21st-century anthropogenic modification alone was enough to trigger alluvial fan aggradation (Spell and Johnson 2019). Together, natural, prehistoric, and historic erosion have all caused erosion to the subsoil. Even though the drivers of erosion, transportation, and deposition have changed over time, these processes observed in the present have been operating in the past.

2.2.10 Geomorphological and palynological evidence of Pleistocene to Holocene climate change

Paleochannel morphology and pollen assemblages can be used as a proxy to understand past climates. Biomes are defined as assemblages of plant functional types (consistent around the world) as opposed to species assemblages (vary with region) (Williams et al. 2000). Paleo assemblages can be compared to groupings found on earth today. Still, the climate and conditions of the Pleistocene were so different that they are not reproduced together anywhere today. Therefore, pollen assemblages can be used to help support geomorphological and climatic data.

Leigh (2008) used paleochannel morphology to identify major climatic episodes for the Southeast US over the last 30ka BP. Scars of braided stream systems in the Coastal Plain dating to the late Pleistocene (30–16 ka) indicate increased sediment load due to a climate that produced high runoff (Leigh 2004). Deep sea and ice core records that this region's distinct phases of paleochannel patterns correspond to global cooling events of the Marine Isotope Stage (MIS) 5e/5d boundary (~115 ka BP) and MIS 5/4 boundary (~80-70 ka BP) (Leigh 2008). The climate that produced braided streams in the Coastal Plain was likely similar to the climate in the Piedmont at the time.

Stadial-interstadial transitions in the Pleistocene (i.e. MIS 5e / 5c) were much greater than anything in the Holocene, but climate change throughout the Holocene still affected the landscape. Pollen assemblages from White Pond, SC, and Clear Pond, SC show that during 30-16ka BP, pine-savanna biomes were present in the Southeast (Leigh 2008). Snowfall and snowpack would have been common in colder months during this time period, so periglacial processes could have operated in the headwaters of the Catawba (Leigh, 2008). Relatively small

climatic fluctuations from 16-11ka were followed by the early Holocene warming (~11-5.5 ka) which is a planet-wide trend reflected in deep sea and ice core data.

There is evidence of mid-Holocene warming that affected different parts of North America (Webb et al. 1993). During the mid-Holocene, the northern limit of cool mixed forest extended farther north than it does today, whereas the southern limit of cool mixed forest was farther north around the Great Lakes but farther south along the eastern seaboard, suggesting the SE was cooler during this period (Williams et al. 2000). Biomes in the Mid-Holocene were structurally similar to those of today. However, the importance of individual plant functional types shifted as a response to precipitation and temperature changes during the Holocene, suggesting that albedo, canopy conductance, and surface roughness have also varied throughout the Holocene.

During the last 5.5ka, temperature, precipitation, and vegetation established humid subtropical conditions with warm, wet summers and cool, dry winters— similar to conditions today (Leigh 2008). During the late-Holocene time interval (4.2ka BP to 0ka BP), conditions were such that regolith that had previously been stabilized throughout the span of the Holocene in certain locations was remobilized. Increased erosion, transportation, and deposition are evident in sediment accumulation on North and South Carolina floodplains in multiple episodes of intensified aggradation, predating European settlement (Clark 1993). Summers during the late Holocene are considered as cooler than summers in the early Holocene. Climate is presumably responsible in part for periods of geomorphic change in the Piedmont during the Pleistocene and Holocene, but no research has documented this effect.

In the 1930s, the Division of Physiographic and Climatic Research of the Soil Conservation Service (SCS) initiated multiple studies on the causes of gullying and identify

processes contributing to gully erosion. Palynological evidence from buried organic soils in sediment-filled gully in Spartanburg, SC showed an abundance of fir and spruce species, indicating that the climate before the time that these sediments were deposited was considerably colder than the prevailing climate (Cain 1944). The spruce-fir climax fossils occur substantially enough in the lower levels of the buried soils to dismiss the hypothesis that the pollen was blown into the area from somewhere else, and are absent to sporadic from the upper half of the soil (Cain 1944). Species distribution in these deposits suggests a gradually warming climate. Cain (1944) and Eargle (1977) conclude that these buried organic deposits are Pleistocene in age, suggesting climatic conditions since the Pleistocene have resulted in considerable geomorphic activity in the Piedmont that is still underappreciated today.

\

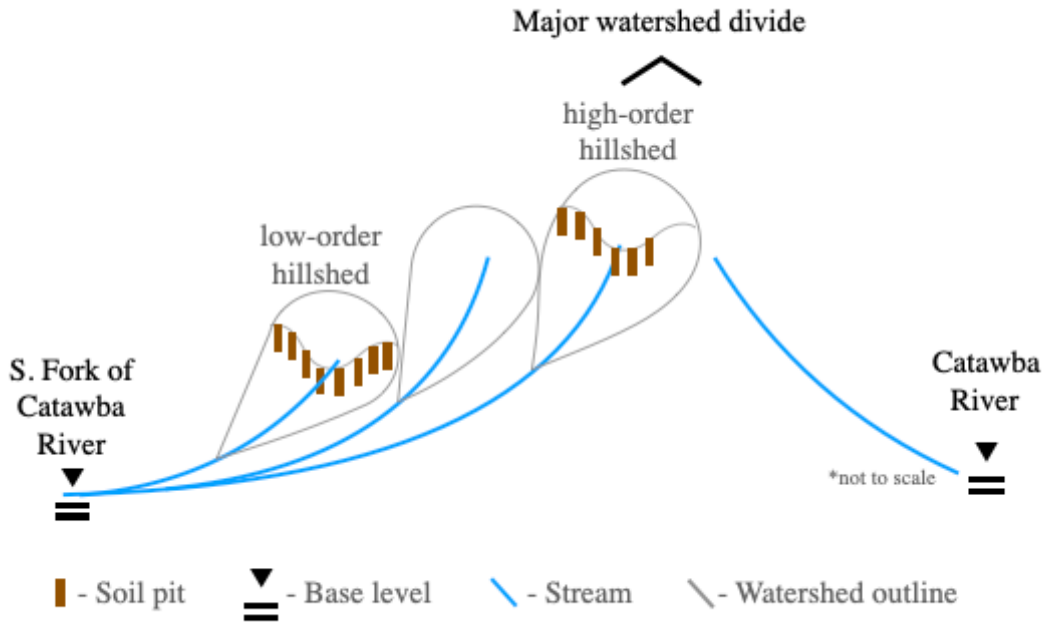

Figure 2.1: Three-dimensional hillslope sampling schematic of toposequence placement. Low-order hillsheds are expected to be less stable landscape positions compared to high-order hillsheds (following Brecheisen et al. 2021).

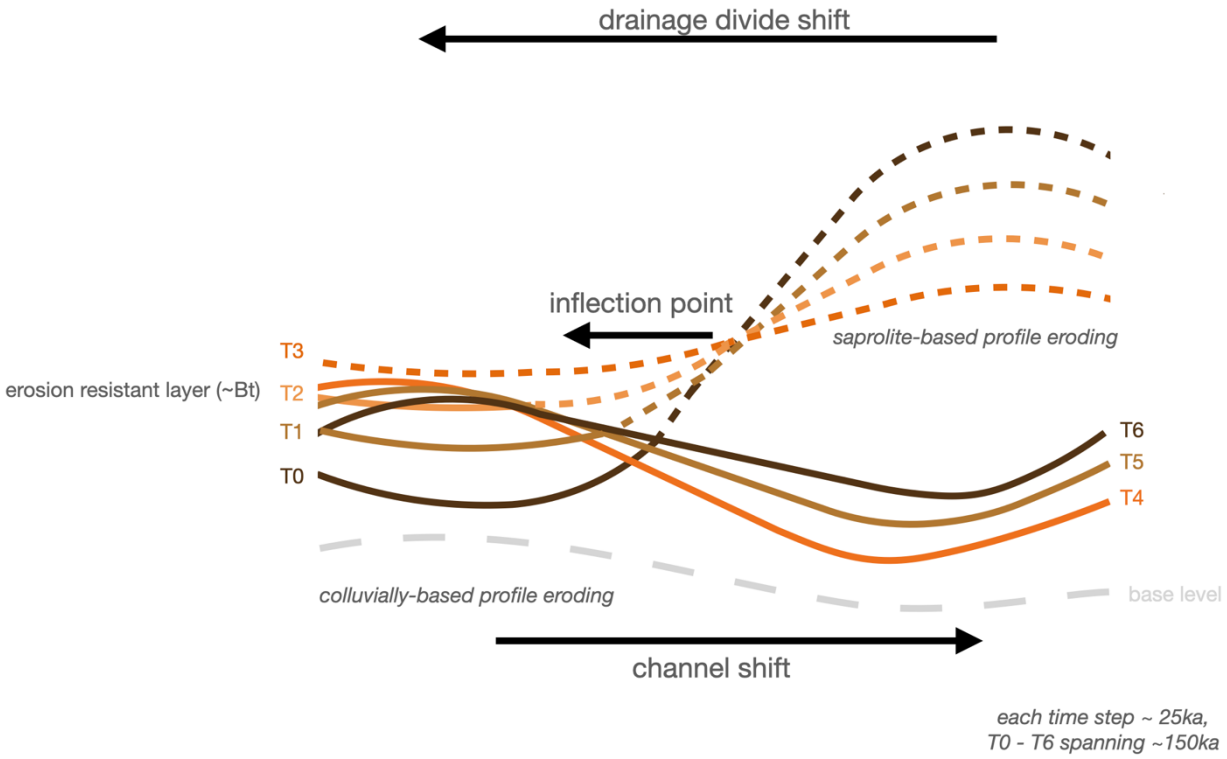

Figure 2.2: “Conveyor belt” model of toposequence evolution driven by channel (not pictured) over ~150 ka time scale. Dashed lines represent paleo surfaces not present in the current landscape. Each time step represents about 25ka, so T0 - T6 spans roughly 150 ka. Time step 0 (T0) represents some initial hillslope that gets eroded over T0 to T6, representing the current topography. A stream channel (not pictured in the figure) is the driver of incision at every step in the model.

CHAPTER 3: FIELD AREA BACKGROUND

This chapter overviews the climate, geology, soils, topography, and previous work conducted in the Redlair Observatory.

3.1 Field area: Redlair Observatory Property - Gaston County, NC

The Redlair Observatory comprises a 1,200-acre project area on Spencer Mountain Conservation Area protected by the Catawba Lands Conservancy. A 750-acre portion of the property is currently owned by Charles, Haywood, and Katherine Rankin and the North Carolina Plant Conservation Preserve, who are concerned with the protection and documentation of the big-leaf magnolia, a regionally rare tree, and the Schweinitz sunflower, which is federally endangered. This property represents one of the last intact forests adjacent to the South Fork of the Catawba River. The bottomlands of this area have been farmed by Native Americans and European settlers for centuries, as evident by terraced hillslopes on parts of the property. There is also a history of gold mining spanning the last century. The land use history is partially reflected in the vegetation.

3.2 Modern climate and vegetation

Charlotte is characterized as a humid subtropical climate. Summers are characteristically hot and humid, while winters are moderate and short. Annual precipitation is approximately 1060 mm, and average temperatures range from about 5°C in January to 25°C in July (NOAA 1895-2022). In the winter months, baroclinicity leads to mid-latitude cyclonic precipitation. Still, in the summer, convection occurs due to moist static energy (MSE) advection by flow around North American subtropical highs, or the Bermuda High. Increased precipitation, a potential mass-wasting trigger, is common in the late summer months. Precipitation events in this region are influenced by the El Nino Southern Oscillation (Thompson and Wallace 2001) whereby

overall dryer and warmer years occur during La Nina events, and cooler and wetter years occur during El Nino.

Current local vegetation is primarily mixed hardwood and pine-hardwood forests and grasslands. From around 5ka BP until European settlement, longleaf pine dominated the area, and prior to that, forests consisted of mixed oak and pine (Carroll et al. 2002). Basic vegetation surveys have been conducted on each hillslope at Redlair Observatory (www.redlair.org). The species represented on each hillslope reflect recent land use history more than hillslope aspect. The north-aspect hillslope in Duffey watershed contains sweet-gum, tulip poplar, hickory, walnut, shortleaf pine, red maple, and cherry trees, as well as muscadine, green briar, rattlesnake fern, wing stem sunflower, trumpet vine flower, Virginia creeper, blackberry, and Christmas fern. These species are typical of recently cleared/ disturbed areas and areas with poor nutrient availability. The north-aspect hillslope in North Rhyne contains planted loblolly pines on the summit, American holly, sourwood, red maple, Virginia pine, tulip poplar, and big leaf magnolia. If there are aspect-dependent vegetation differences, these have been masked by recent land use history.

3.3 Geologic setting

The Redlair Observatory sits on the boundary between two major litho-tectonic terranes (sometimes referred to as belts) in North Carolina: the Charlotte terrane and the Carolina terrane. The lithology in the Charlotte belt is mapped as felsic metavolcanics (Map symbol: Mvf) by Goldsmith et. al (1988) (Figure 3.1), which includes fine- to coarse-grained felsic metarhyolites, metatuffs, and hydrothermal fracture-fill vein quartz. The Kings Mountain belt is mapped as quartz sericite schist (Map symbol: Zbs) in the field area, including very fine to medium-grained quartz-sericite schist and phyllite (Figure 3.1).

Price (2009) worked to identify the location of the Boogertown Shear Zone (Figure 3.2) and other rock units already mapped at a larger scale (1:250,000) by Goldsmith et al. (1988) at Redlair Observatory based on outcroppings on the property--of which there are few. The shear zone is an important landscape feature that not only separates different lithologies, but it is also the contact between different metamorphic facies: it separates the felsic metavolcanics (Mvf) on the east from the quartz-sericite schist (Zbs) of the Battleground formation to the west (Late Proterozoic), which is part of the Kings Mountain Belt. The shear zone is mapped to bisect Redlair Observatory from north to south roughly, but evidence of the sericite schist in the bedrock of a soil pit on the Eastern side of the shear zone suggests further investigation is needed to find its exact location. Many Piedmont shear zones have multiple phases of deformation: early ductile deformation followed by a later semi-ductile to brittle deformation.

Fieldwork at an outcrop near Belmont, NC with 5 meters (vertically) of exposed sediment and saprolite reveals the complex geologic history of the area (Figure 3.1) The area is mapped as metamorphosed quartz diorite and tonalite and is on the boundary with one of the larger plutonic bodies (described above) in the area, but multiple additional lithologies were present and distinguishable based on saprolite color, foliation, and grain size. This site exemplified the diversity of lithologies possibly present in the field area over shorter distances.

3.4 Soil survey

Mapped soil units by the NRCS (1969) found at Redlair Observatory include Cecil sandy clay loam, Pacolet sandy clay loam, and Pacolet sandy loam (Figure 3.3). Cecil and Pacolet soils are defined as Typic Kanhapludults formed in residuum (i.e. saprolite). Cecil soils are commonly mapped at the summit and shoulder positions along areas with a 2 to 8 percent slope, while Pacolet soils are typically mapped along the backslope and toeslope positions with 8 to 15

percent slope (Figure 3.4). Ultisols in the region are clay-rich through chemical alteration of feldspar and mica minerals.

3.5 Topography

The highest elevation points (~875 m) of Redlair Observatory occur on the northeastern sides of the property, farthest from the South Fork of the Catawba River (Figure 3.5). These high points have been hypothesized as a peneplain, supported by optically stimulated luminescence (OSL) signals that suggest transport (Nelson et al. 2022) Stream channels headwardly retreating from the South Fork of the Catawba River represent the youngest geomorphic surfaces. Hillslopes at the southwestern portions of the property have responded to this base-level incision, and regolith has presumably eroded off the former peneplain accordingly. The relative immaturity of hillslopes in the south and west of the property is evident from higher slope angles and thinner regolith with bedrock outcrops in stream valleys. Conversely, hillslopes on the north and east sides of the property have lower slope angles and thicker regolith with no observed bedrock outcrops (Nelson et al. 2022).

3.6 North Rhyne, Duffey, and Deep Creek watersheds

In this thesis, I primarily focus on the North Rhyne and Duffy watersheds. There has been extensive description of hillslope soils conducted in the Deep Creek watershed (e.g. Eppes et al., unpublished, and Nelson et al., 2022). Because I incorporate this information into my data analysis from North Ryne and Duffey, I also include a description of Deep Creek here.

North Rhyne and Duffey watersheds are first-order watersheds that drain into the 7th-order South Fork of the Catawba River. They share similar lithology, relief (~30 and 20 m, respectively), upslope contributing areas (4.5 and 6.2 hectares, respectively), and hillslopes with comparable north and south aspects (four toposequences total) (Figure 3.6, Table 3.1). They vary

in their relative proximity to major rivers, that is in their hillshed order (Brecheisen et al. 2021) (Figures 3.7, 3.8). North Rhyne hillslopes comprise primarily 1st and 2nd hillshed orders and Duffey hillslopes comprise 5th order hillsheds. Deep Creek watershed has a larger upslope contributing area (11.9 hectares) and sits in between NR and DC (Figure 3.7) with hillslopes ranging from 3rd to 4th hillshed orders.

Hillsheds were ordered (Figure 3.7) following Brecheisen et al. (2021). A minimum stream length threshold was defined (see key in Figure 3.7). High-order hillsheds are those which are furthest away from major rivers. Duffey watershed is a 5th-order hillshed that sits immediately adjacent to the watershed divide between the 7th-order Yadkin Pee Dee and Catawba Rivers, while North Rhyne (closer to the South Fork of the Catawba) is a 2nd-order hillshed (Figures 3.6, 3.7). Deep Creek watershed is a primarily 3rd-order hillshed.

Hillslopes comprising North Rhyne and Duffey watersheds are in first-order watersheds <0.02km^2 in size, with the hillslopes spanning 8.27m and 15.20m in relief across 141m and 244m in distance, respectively. This latter data is from measurements taken with a level traverse across the four major hillslopes.

3.7 Previous work in the Redlair Observatory

Nelson (2022) identified thick packages of colluvium across multiple backslope and shoulder positions in Deep Creek watershed in Redlair Observatory. However, full toposequences have not been examined in Redlair Observatory, so the full picture of soil development from the summit to the toeslope of any given hillslope is missing from the story.

At the Redlair Observatory, a previous well boring was taken and described by Geologic Explorations, Inc. at the summit of Duffey watershed reports regolith down to ~24 meters

(Figure 3.9). Around 22 meters below the surface begins the transition to partially weathered bedrock (felsic metavolcanics).

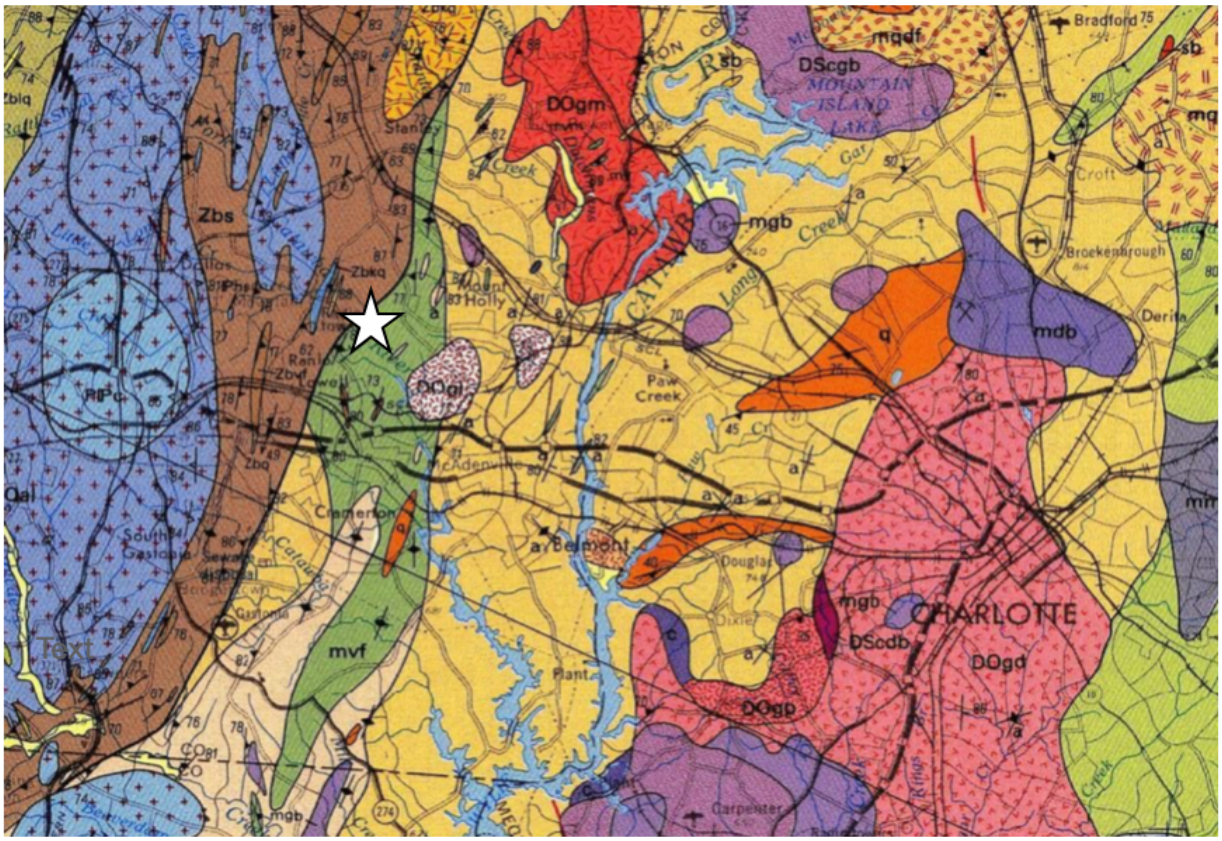

mvf — Felsic Metavolcanic Rocks—Fine- to medium-grained, locally coarse-grained or agglomeratic rhyolitic and rhyodacitic metatuffs. May include some hypabyssal intrusives. Contains minor intermediate and mafic metavolcanic rocks. Probably correlative, at least in part, with felsic metavolcanic rocks of the Battleground Formation (Zbvf)

Battleground Formation (Late Proterozoic)

Zbs — Quartz-sericite schist—Very fine to medium-grained quartz-sericite schist and phyllite. Very light gray, light-bluish-gray, light-brown, or yellowish-gray. Composed largely of quartz (typically >50%) and sericitic white mica (muscovite and paragonite). Accessory minerals may include chloritoid, biotite, pyrite, hematite, kyanite, andalusite, sillmanite, staurolite, garnet, oligoclase or albite, chlorite, tourmaline, zircon, and graphite

DOgl — **Biotite monzogranite and leucogranite**—Very light to light- to yellowish-gray, medium- to coarse-grained, massive-to very weakly foliated biotite monzogranite and leucogranite southwest of Mt. Holly, N.C. Plagioclase variably saussuritized; grains fractured and strained. May be related to Salisbury Plutonic Suite

Figure 3.1: Lithology map with relevant lithology descriptions (Goldsmith et al. 1988) Redlair Observatory (☆) in the area mapped as felsic metavolcanics.

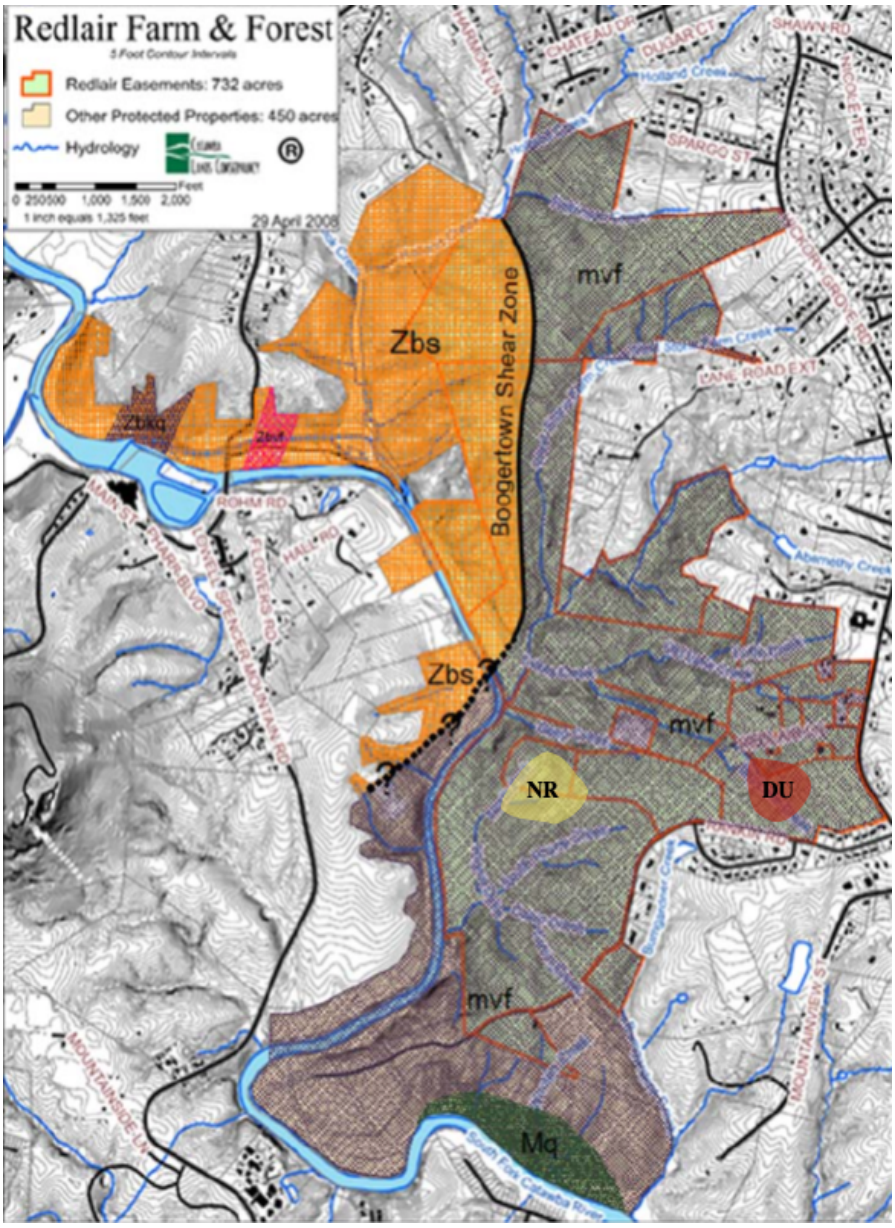

Figure 3.2: Lithology map of Redlair Observatory highlighting the approximate location of Boogertown Shear Zone as mapped by Price (2009). Both watersheds (North Rhyne in yellow and Duffey in red) are inside the mapped felsic metavolcanics (mvf).

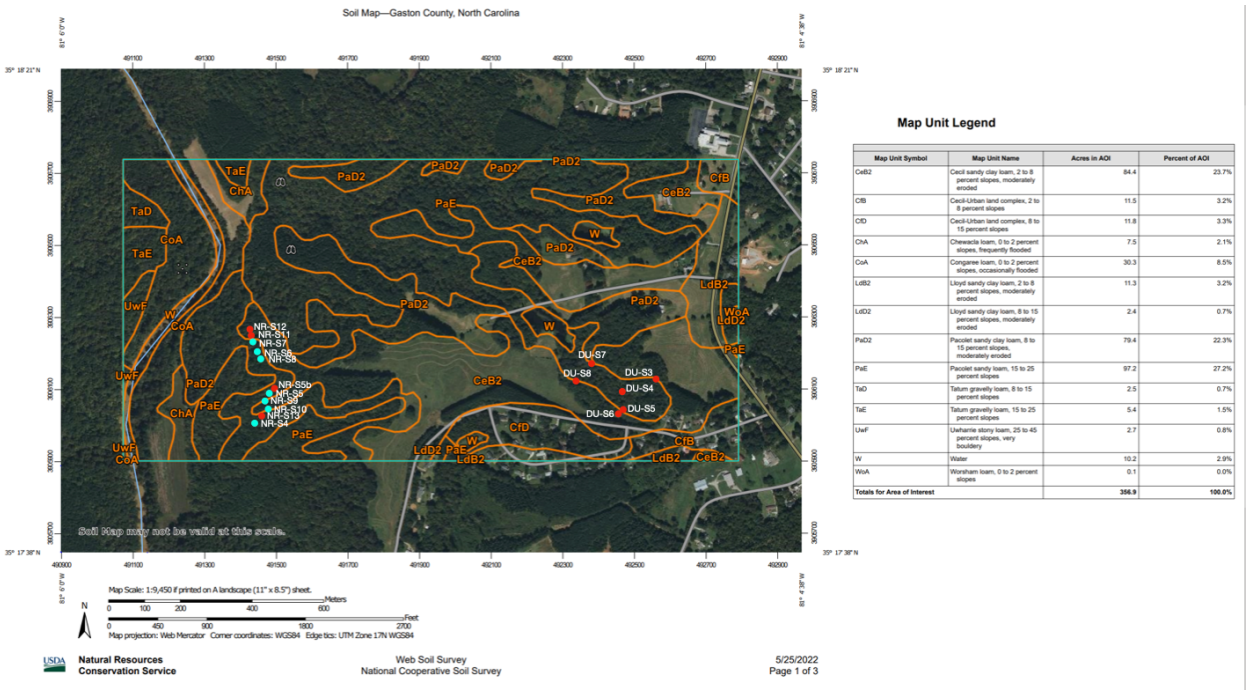

Figure 3.3: Soil pits in the context of mapped soils (Web Soil Survey, accessed 2022).

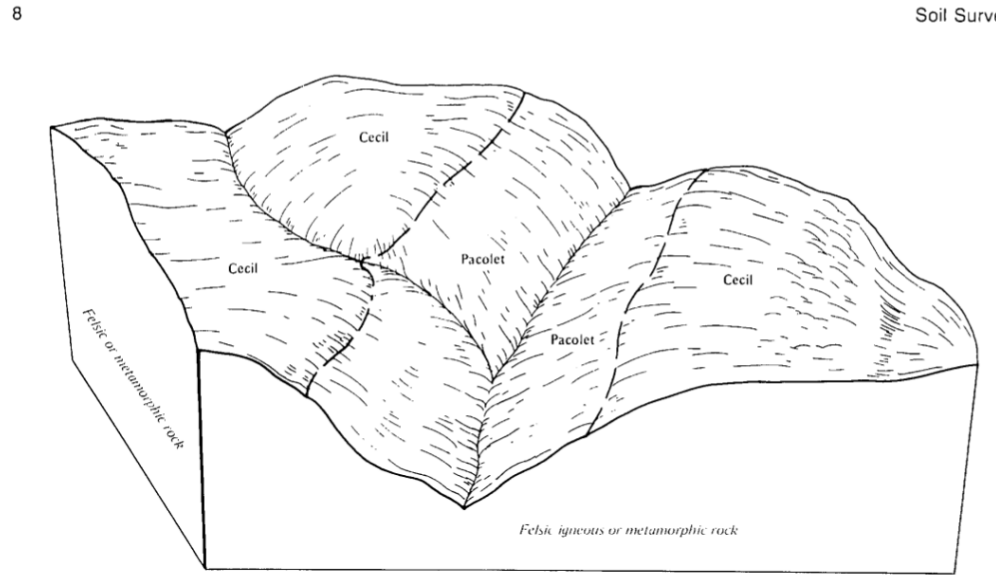

Figure 2.—The relationship of soils and landscape in the Cecil-Pacolet map unit.

Figure 3.4: The expected relationship between soil orders in Gaston County (Soil Conservation Service 1969).

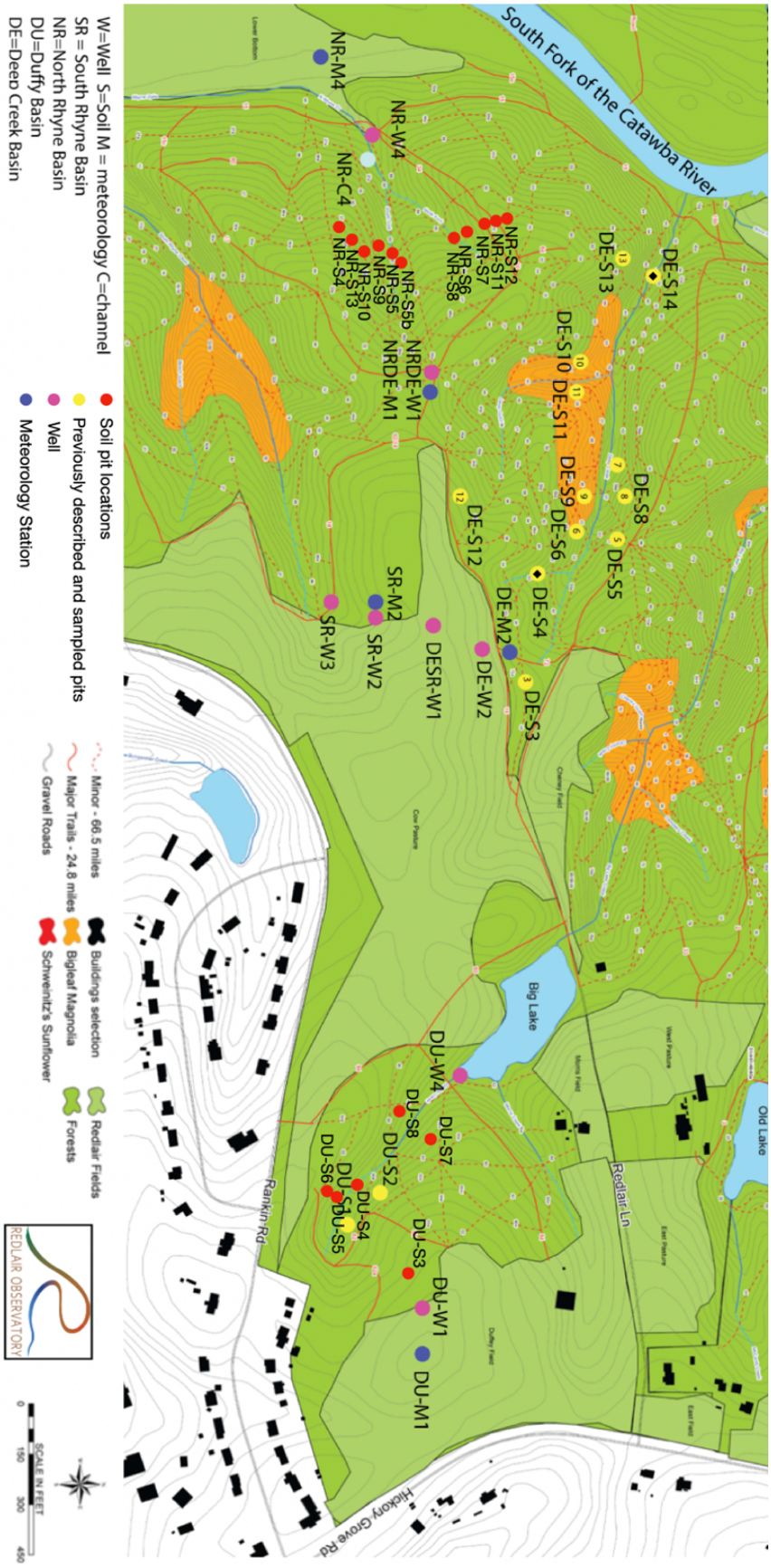

Figure 3.5: Map of North Rhyne (NR), Duffey (DU), and Deep Creek (DE) soil pit locations with meteorology station and well locations for reference.

Aspect	Summit	Shoulder	Backslope	Footslope	Toeslope
N-facing		DE-S6 DE-W2 NR-S13 DU-S6	DE-S12 DE-S9 NR-S10 NR-S9 DU-S5 DU-S8		
S-facing		DU-S3 DE-S5 SR-W2 NR-S11	DU-S7 DU-S2 NR-S7 NR-S6 DE-S8		
E-facing		DE-S10			
W-facing		DE-S11			
No aspect	DESR-W1 DU-W1 NR-S4 NR-S12 NRDE-W1				NR-S8 NR-S5 DU-S4 DE-S14 SR-W3
Fan					DU-S1 NR-S1

Table 3.1: Table of North Rhyne (NR), Duffey (DU), and Deep Creek (DE) soil pits organized by position on hillslope and aspect.

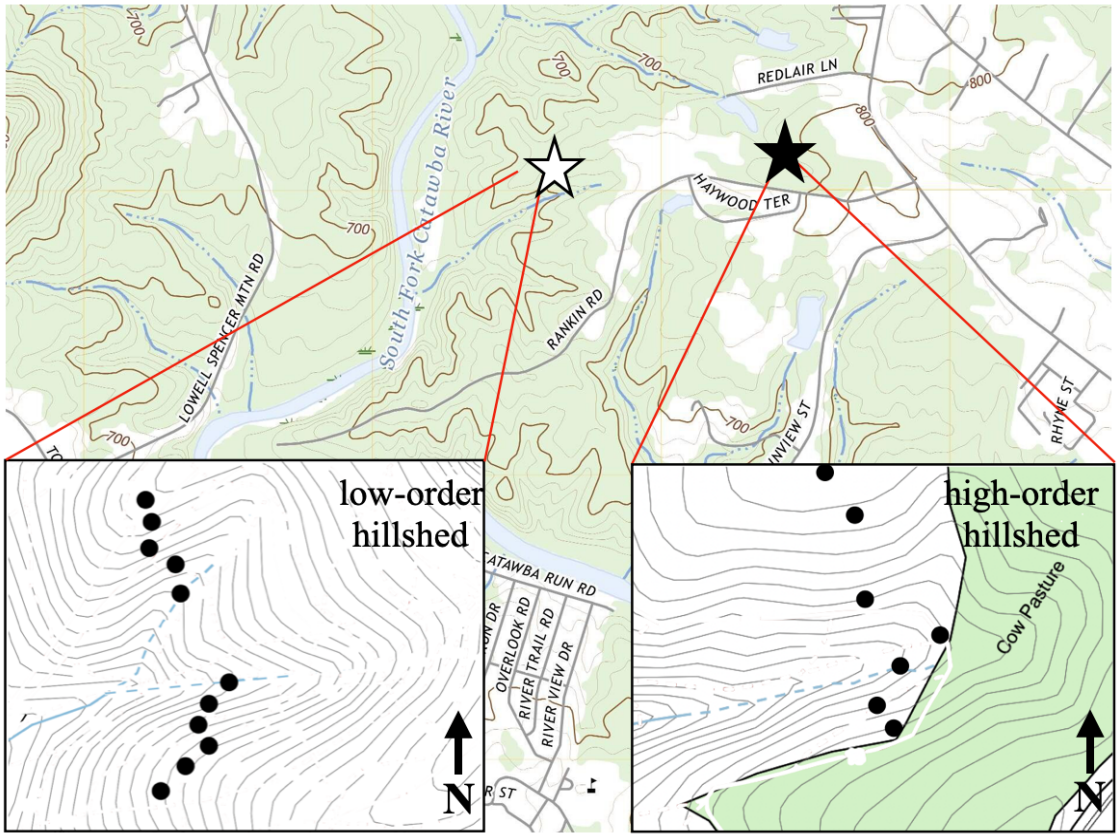

Figure 3.6: Soil pit locations (●) in low-order (North Rhyne) and high-order (Duffey) hillsheds.

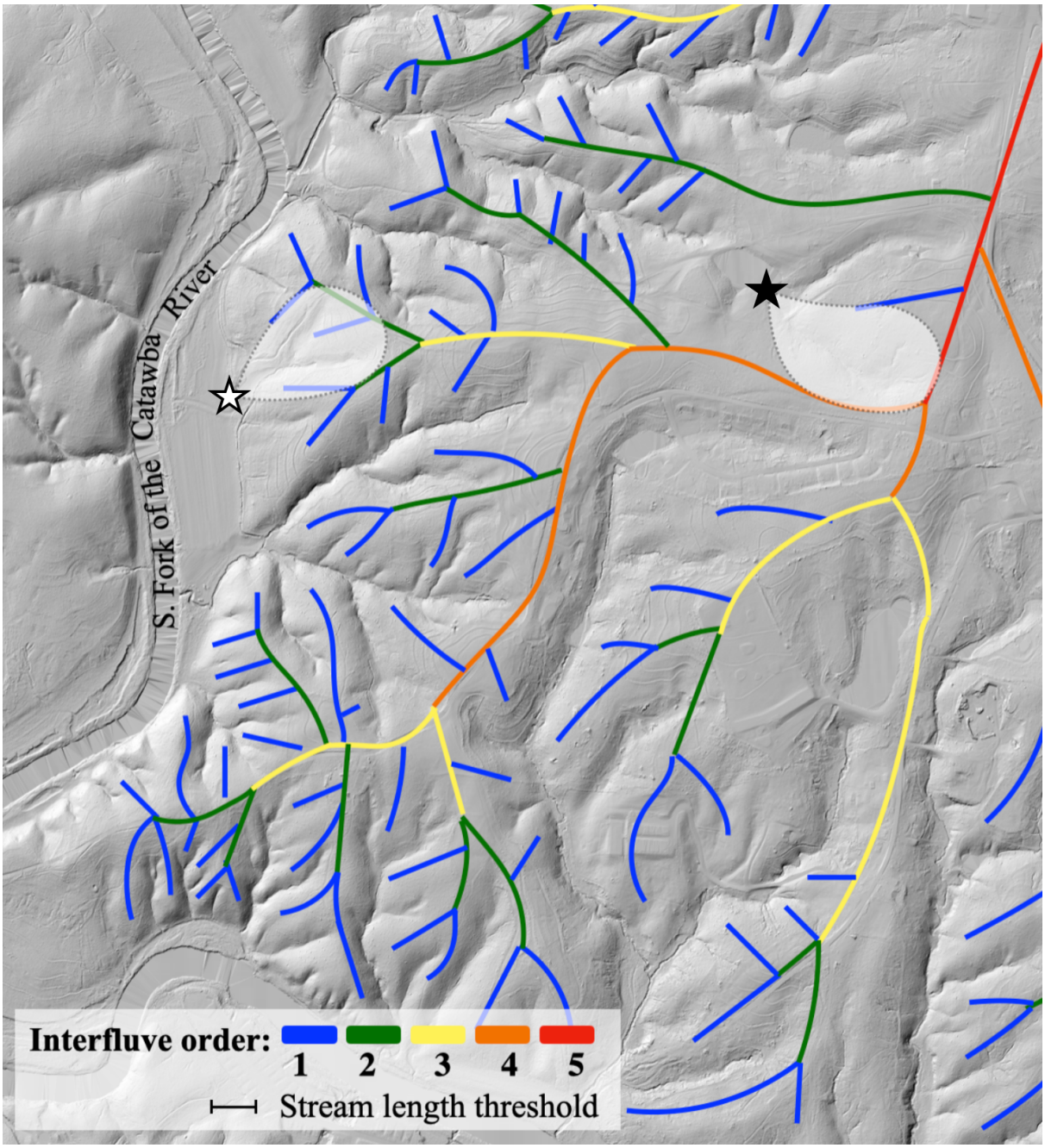

Figure 3.7: Ordered interfluve network (following Brecheisen et al., 2021) in field site. Low-order hillsheds (☆) are close to major streams. High-order hillsheds (★) are close to major watershed divides. Interfluves are numbered using Strahler ordering.

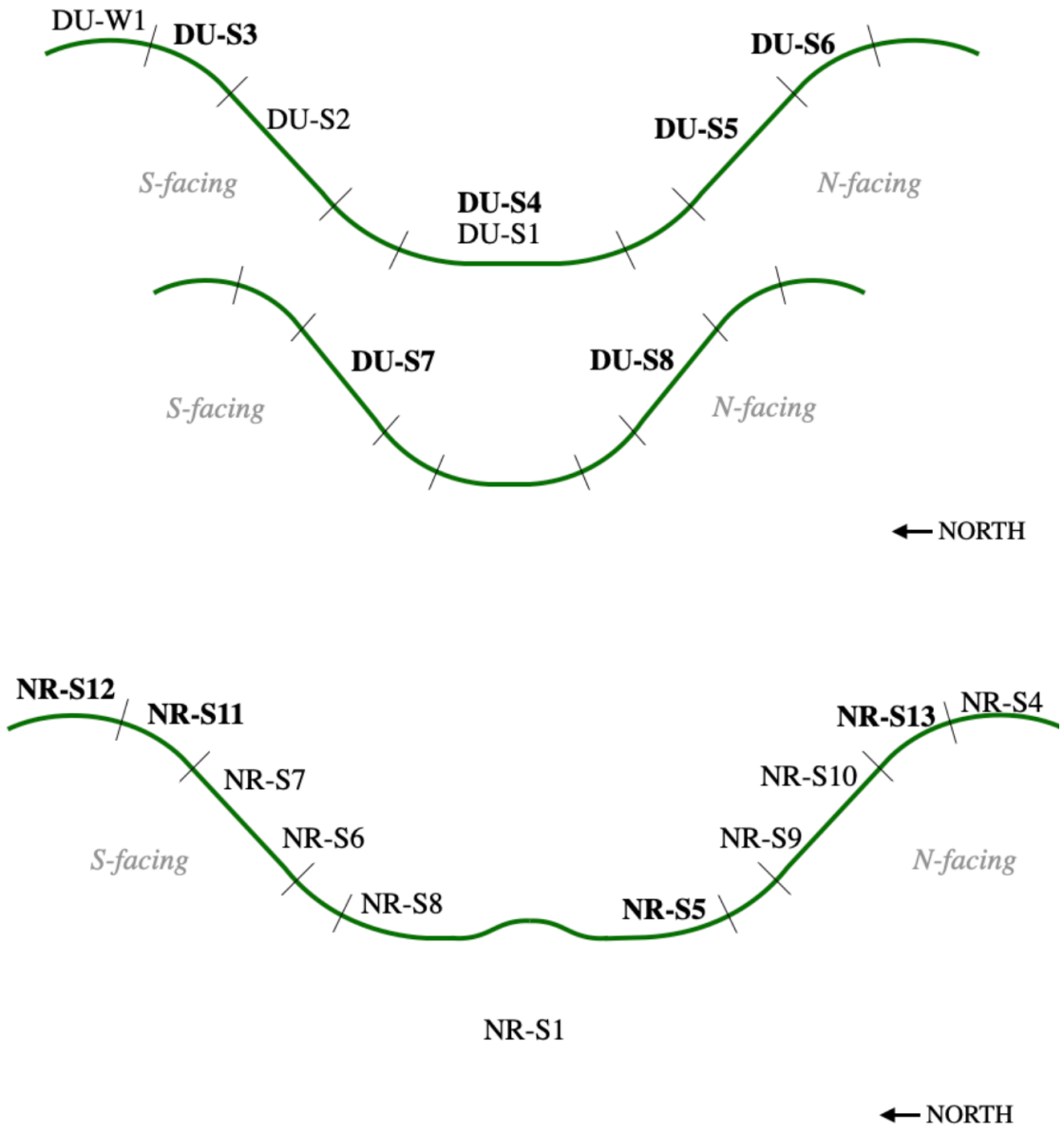

Figure 3.8: Pit locations (facing east) along idealized hillslope positions, with pits opened for this project in bold type (other pits dug with the help of Dr. Eppes Applied Soil Science class).

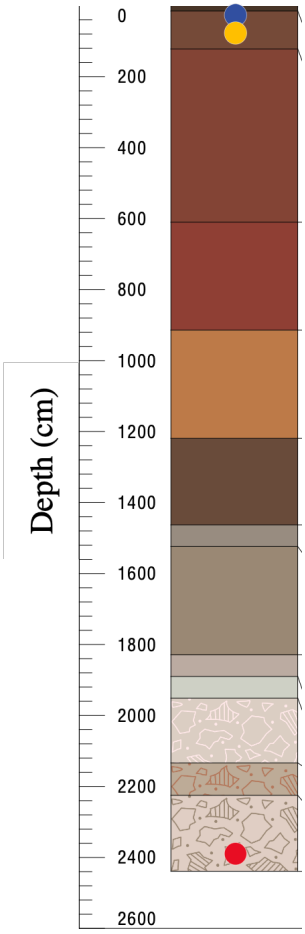

Figure 3.9: Well boring profile log reports Regolith (unconsolidated sediment or soil) to ~22m below which is partially weathered and hard bedrock. Circles are locations of OSL samples (Nelson et al. 2022).

CHAPTER 4: METHODS

4.1 Field methods

I chose two North and South-facing hillslopes in the Duffey and North Rhyne watersheds for this research in the SE Piedmont. A total of 21 soil pits (Figures 3.8, 3.9) were excavated in Duffey and North Rhyne watersheds. My team hand dug and described (Appendix A, B) a total of five soil pits per toposequence (~1.5 m deep) on the summit, shoulder, upper and lower backslope, and toeslope positions. Nowhere in the field area did we indicate footslope positions based on the hillslope morphology. Instead, the lower backslope position is defined as the planar portion of a hillslope within 2.5 vertical meters of the valley bottom. Photographs and sketches of each soil pit can be seen in Appendices B and C, respectively. Hillslope position was identified using methods described in (Schaetzl 2013). The soil pits were placed along representative hillslope positions. In addition, in Duffey watershed, two additional soil pits were dug on the backslope position of the same north- and south-facing hillslopes as the main toposequences, but downstream on a steeper location where it appears an incisional knickpoint has already propagated through. These latter two pits will allow for an examination of the impact of slope on the hillslope soils and sediments in the same watershed.

Soils were described in detail following Birkeland (1999) and Eppes and Johnson (2021) (Appendix D). Soil descriptions included quantifying observables such as horizons, boundaries, soil structure, roots, pores, color, texture, clay films, and sedimentary descriptions including sedimentary structures, grain size, rounding, and sorting. Soil pits were sampled by horizon and multiple samples were taken when horizon thickness exceeded 20 cm, as outlined in Birkeland (1999). This averages to about 9 samples per pit, for a total of 150 samples. Within each pit,

unconformities were identified both between different packages of hillslope colluvium and between underlying saprolite by identifying buried soils that indicate past periods of hillslope stability (Birkeland 1999). Buried soils were recognized from characteristics such as abrupt changes in weathering characteristics, stone lines, changes in sedimentology, and/or increases in carbon content. Charcoal was collected from soil pits and submitted for dating. Data from this study was compared and contrasted with data from 15 pits dug in the Deep Creek watershed that were excavated in prior work following identical procedures as described above (Nelson et al. 2022) (Figure 3.5).

4.1.1 Distinguishing residual material from transported sediment

In both North Rhyne and Duffey watersheds, a platy structure of soil peds is inherited from foliation of the bedrock/saprolite, which aids in differentiating soil derived from colluvium (not platy in structure) from soil derived from the saprolite (platy in structure). Further, as the bedrock was igneous in nature, the presence of poorly sorted, random pebbles and clasts is also consistent with sediment rather than saprolite (Nelson et al. 2022).

The presence of visible foliation, intrusive dykes, and veins in some cases provides unambiguous evidence that the bedrock is *in situ*, because such structures would be destroyed during transportation. The Salisbury Plutonic Suite is mapped to the east of the shear zone, but evidence of magmatic veins containing the same mineralogical assemblage suggests it is also present at Redlair Observatory, though this has not been confirmed with petrology. This rock is medium- to coarse-grained, massive to weakly foliated biotite monzogranite and leucogranite. This lithology appears in some of the pits as small (1-3 cm) dykes (Figure 3.1, Appendix B).

4.2 Soil laboratory analyses

All field soil samples (n= 145 unless otherwise specified) were hand sieved to the fine fraction, <2 mm, for the following analyses: 1) total organic carbon (measured as loss-on-ignition); 2) particle size distribution; 3) pedogenic iron content (n=53); 4) XRF with an Olympus pXRF to conduct bulk-elemental analysis; 5) radiocarbon dating of charcoal samples (n=10).

4.2.1 Particle size distribution

All soil samples were hand sieved to the fine fraction (<2mm), and the remaining gravel sized particles were weighed and recorded (Appendix E).

Soil samples were analyzed for particle size (Appendix F) using a Beckman Coulter LS 13 320 Laser Diffraction System equipped with an auto-prep station and Aqueous Liquid Module (ALM) (Eppes 2019). This system measures particles from 2000um (coarse sand) to .017um (very fine clays). Before analysis, samples were prepared with a dispersing agent that contains deionized water and sodium pyrophosphate. Organic matter was removed from samples taken from every A-horizon with a hydrogen peroxide solution. Graphic mean grain size, inclusive graphic standard deviation, inclusive skewness, and inclusive graphic kurtosis were calculated for each sample. Soil texture was reported based on the NRCS Soil Triangle, and estimations of texture in the field were adjusted using particle size data from the Laser Diffraction System.

4.2.2 Loss on ignition

The organic content was calculated for each sample as loss-on-ignition (Eppes 2019) (Appendix G). Spikes in organic content below the surficial A-horizon will help identify buried soils observed in the field. Organic content increases as landscapes are stable for long enough

periods of time to accumulate organic matter (given that the accumulation of organic material outpaces carbon decay).

4.2.3 Soil hue

Soil color is determined using a Munsell Soil Color Chart both under saturated conditions in the field–- termed 'moist', and on air-dried, sieved, and homogenized samples in the laboratory— termed 'dry.' Foss and Wagner (1981) demonstrated that soil hue at or deeper red than a value of 2.5YR on the Munsell color chart is likely older than 100,000 years. Soil color is included in the soil description sheets in Appendix D.

4.2.4 Bulk density

The paraffin clod method (Singer and Janitzky 1986, Eppes 2019) was used to calculate bulk density on twenty representative soil samples from multiple A horizons, upper B horizons in the colluvium, lower Bt horizons in presumably residual material, and C horizons/ saprolite (Appendix H). Bulk density is calculated as weight per unit volume on oven-dried samples and is an indicator of soil compaction.

4.2.6 Radiocarbon dating

Nine charcoal samples were collected from seven different soil pits and submitted for dating by Direct AMS (Appendix I). Radiocarbon ages were calibrated using the University of Oxford's OxCal online tool with the IntCal20 calibration curve (Reimer et al., 2020). Radiocarbon dates will act as an age control for a chronofunction of iron activity ratios and particle size, which also vary with age (e.g. Layzell et al. 2012). Weathering is used as a proxy for age when no material is viable to date.

4.2.7 Pedogenic iron content

The most well-developed horizons (2-3 samples per profile, total n=61) were identified based on consistence, structure, color, and clay content to be analyzed on the Atomic Absorption Spectrometer. Samples were first crushed using a SampleTek vial rotator Model 200 to pass through a 100 mesh sieve. Iron was analyzed using two processes: citrate-dithionite extraction (Mehra and Jackson 1960), and hydroxylamine extraction (McDonald 2015). Hydroxylamine extractable iron, crystalline or 'background'iron, is measured as Fe_H, and citrate-dithionite extractable iron, or pedogenic iron, is measured as FeD (Eppes 2019) by the flame atomic absorption spectrometer in the UNC Charlotte Hydrology and Geochemistry lab (Appendix J). The iron activity ratio (FeH/FeD) indicates the relative intensity of in situ weathering. Iron activity rations in weathering profiles (soils) has been shown to decrease as surface age increases (e.g.Eppes and McFadden 2008).

4.2.8 Bulk elemental analysis

Bulk elemental analysis was conducted on each sample with a handheld pXRF (Olympus Delta Premium 50kV GeoChem Analyzer) (Appendix K). This analysis helps construct a depletion/enrichment profile that can be used to determine the relative degree of weathering (where pedogenesis has translocated elements into or out of each horizon), and to identify soils forming from colluvium as distinctly different from soils forming from residuum. Soil formed in saprolite (immobile regolith) should have low luminescence sensitivity and relatively higher concentrations of mobile elements (K, Mg, Ca), while soil formed in colluvium or alluvium (mobile regolith) should have high luminescence sensitivity and low concentrations of mobile elements. Further work by Nelson et al. (2019) suggests that OSL data correlates with detailed geochemistry of the luminescence samples– meaning the Redlair soils have been shown to follow this general trend for sediment versus saprolite. In addition to distinguishing saprolite

from sediment, total element analysis may help to confirm parent material similarities. The original bedrock parent material controls the concentration of immobile elements (e.g. Ti, Zr). Thus, these concentrations will help confirm similar and consistent rock types across hillslopes and between watersheds.

One soil pit (NR-S10) in North Rhyne watershed revealed the contact between the two lithologies that bound either side of the Boogertown shear zone (based on saprolite structure, color, and presence of mica), suggesting the location of the shear zone is more disseminated than suggested on the map. All soil-forming factors are unambiguously the same in this pit except the parent material. The pXRF was used *in situ* in all four pit walls (Appendix L) to get a sense of the spatial variability of the geochemical results within a single horizon, and in the laboratory on sieved, homogenized samples.

4.2.9 Geochemistry

To estimate chemical enrichment and depletion (tau) values, we compare changes in the concentrations of 9 major elements (Al, Si, Fe, Sr, Zr, Mg, K, Ca, Mn) in the soil to the concentrations of that of the protolith. Tau values for soils were calculated using zirconium and aluminum as the immobile elements, following Brimhall and Dietrich (1987), Chadwick et al. (1990), and Holbrook (2019) in equation 1:

$$\tau_{i,j} = \frac{C_{j,w}C_{i,p}}{C_{j,p}C_{i,w}} - 1$$

Equation 1 is used to calculate the mass transfer coefficient ($t_{i,j,}$), which is the fractional loss or gain of an element (subscript *j*) with respect to the immobile element (subscript *i*) in the protolith (subscript *p)*. *C* is concentration, and subscript *w* denotes the weathered material,

respectively. If an element is neither lost nor gained with respect to the immobile element then $t_{i,j}$ = 0. Negative and positive $t_{i,j}$ values imply loss and gain, respectively.

Here, we are using Al and Zr as our immobile reference elements, assuming they are relatively insoluble in felsic metavolcanic rocks. Hodson (2002) found that in granitic podzol soils, Zr and Al showed the lowest percent loss (0.0002% and 0.008%, respectively) compared to all other trace and major elements. Differences in the tau value between Zr and Al are expected because Zr is slightly less mobile than Al.

The protolith was defined based on the averaged compositions of three hard rock samples (DU-W1, DE-SR W1, and SR-W2) from 66, 70, and 50 feet below the surface at Redlair Observatory (Appendix M). If the parent material was chosen correctly, and there are no additional inputs to the system (i.e. aeolian sediment), tau values comparing Zr/Al would be 0. In Duffey watershed, the tau values are often enriched greater than 100%, suggesting there are likely minor differences in the underlying geology—or additions of dust-- within and between watersheds. This result aligns with findings from geologic maps of the area from Goldsmith et al. (1988) and Price (2009).

CHAPTER 5: RESULTS

Overall, soils examined in North Rhyne and Duffey watersheds varied both between the two watersheds and to a lesser extent within each watershed by aspect and slope position. Here I present the overall results of various analyses organized by watershed. In the discussion, I highlight variations in soil and stratigraphic features as a function of hillslope characteristics.

5.1 Soil morphology

Overall, Duffey soil exposures (ranging from 90-183 cm deep) exhibit limited variability between exposures and are generally characterized by A/AB/Bt/2Bt/2BC horizonation (Figures 5.1, 5.2; Appendix D). Saprolite with clear primary structures was identifiable in only one exposure (Appendix A Figure 6). In the well boring at the summit of the south-facing hillslope, primary structures became visible at 152 cm (Figure 3.9). Dry soil hues of the most developed B horizons range from 5YR to 2.5YR, values from 4 to 5, and chromas from 6 to 8. Soil textures of the same horizons are primarily silty clay or clay. The most developed B horizons have prominent clay films on pores and all ped faces. Structure is primarily medium subangular blocky above the most developed B horizon, grading to medium platy structure below. Dry consistence ranges from hard in the A and AB horizons to very or extremely hard in the B and Bt horizons, and finally decreases to hard or slightly hard in the BC or Cr horizons. Wet consistence measurements reveal that soils from the A/AB/B horizons are slightly sticky to sticky and slightly plastic to plastic; soils from Bt/2Bt horizons are very sticky and very plastic; and soils from the BC/Cr horizons are commonly sticky and very plastic.

North Rhyne soil exposures (ranging from 101-166 cm deep) are characterized by horizonation ranging from A/AB/Bt/2Bt/2CB to Ap/Bp/2Eb/2Bb/3Btb/3Cr (Figures 5.1, 5.2; Appendix D). Almost all soil exposures identified saprolite with clear primary structures

(Appendix A Figure 6). Dry soil hues of the most developed B horizons range from 10YR to 5YR, values range from 6 to 7, and chromas range from 6 to 8. Soil textures of the same horizons are primarily silty clay loam to clay loam. The most developed B horizons have prominent clay films on all ped faces. Structure is always medium to course subangular blocky or angular blocky, and size generally increases with depth from fine or medium to course. Dry consistence ranges from soft to slightly hard or hard in the A/AB/Bt and Ap/Bp/2Eb/2Bb horizons to hard or very hard in the Bt horizons. The lower most horizons (CB, BC, or Cr) are generally slightly hard or soft. Wet consistence measurements reveal that soils from the A/AB and Ap/Bp/2Eb horizons are friable and slightly sticky to sticky and nonplastic to slightly plastic; soils from Bt/2Bt or 3Btb horizons are firm, very sticky, and slightly plastic; and soils from CB/BC/Cr horizons are commonly sticky to slightly sticky and slightly plastic to nonplastic.

5.2 Particle size

Sand, silt, and clay fractions were compared between Duffey and North Rhyne datasets aligned by depth. Percent sand, silt, and clay fraction for each watershed is reported on a ternary diagram (Figure 5.3).

Duffey soils exhibit overall relatively high clay content (average of 23.77% +/- 8.12% in all horizons Table 5.1; average of 31.00% +/- 6.35% in most developed B horizons, Figure 5.4) and low sand content (average of 15.92%, Table 5.1; Figures 5.4, 5.5). Depth profiles (Figure 5.6) indicate that clay content remains relatively consistent with depth in these soils after the upper 20 cm of the soil excavation. Depth profiles of sand content show a trend of higher sand content in the upper ~25cm of the soil profile, followed by lower sand content in the midsection, and increasing sand content in the bottom 20cm of the soil excavation (Figure 5.6). Duffey soils have an average of 60.32% +/- 7.77% silt in all horizons (Table 5.1). Silt content generally is

lowest in the upper 20cm of the soil excavation and is consistent with depth after that point (Figure 5.6). Soils have an average of 5.26 % +/- 9.07% gravel content by weight (Table 5.2). Gravel content is greatest in the upper 50 cm except the toeslope pits, and subsequently decreases to 0-5% (Figure 5.6).

North Rhyne exhibits soils with lower overall clay content compared to Duffey (average of 14.7% +/- 4.8% in all horizons (Table 5.1; average of 18.0% +/- 2.6% in most developed B horizons, Figures 5.4, 5.5). Depth profiles in Figure 5.6 show that clay content is also generally consistent with depth but shows a slight decrease with depth after the first 20cm of the soil excavation. Soils have an average of 27.96% +/- 14.65% sand in all horizons (Table 5.1), and sand content is generally highest in the upper 30cm of the profile and the lower 10 cm of the profile. Generally, soil pits with higher average sand content tend to be in lower hillslope positions (Figure 5.6). North Rhyne soils have an average of 57.37% +/- 10.80% silt in all horizons (Table 5.2). Silt content generally is lowest in the upper 20cm of the soil excavation and is consistent with depth after that point (Figure 5.6). Soils have an average of 3.76% +/- 6.11% gravel content by weight in all horizons (Table 5.2). Gravel content is greatest in the upper 30 cm in every pit except the toeslope pits, and subsequently decreases to 0-10% (Figure 5.6).

One-way analyses of variances (ANOVA) tests were used to understand differences between North Rhyne and Duffey (Figure 5.5). Two sample t-tests were used to compare any of the two watersheds to each other. Relationships are considered statistically significant when the p-value is less than 0.05. The strongest observed relationships between North Rhyne and Duffey are for clay content. Duffey has significantly more clay than North Rhyne and Duffey ($p = 3.10e-19$). No significant difference is observed between the gravel content of North Rhyne and Duffey (averages of 3.76% and 5.26%, respectively; $p = 0.234$). Differences in sand content follow the

opposite trend as that which was observed between clay content and watershed order. Duffey has significantly less sand than North Rhyne watershed (averages of 15.92% and 27.96%, respectively; p = 2.23E-7) (Table 5.2). No difference was observed between the silt content (p = 0.07) of North Rhyne and Duffey.

5.3 Organic content

Duffey soils contain significantly more organic matter compared to North Rhyne (average of 8.78% +/- 3.52% and 5.47% +/- 2.82%, respectively, Table 5.1). The results from the two sample t-test and anova test support that high-order watershed positions store significantly more carbon than their low-order counterparts (p = 3.42E-11, Table 5.2, Figure 5.5).

5.4 Radiocarbon dating of charcoal samples

Radiocarbon dating of charcoal from hillslope sediments give numeric ages and provide a test for correlation of sedimentary units in low-order watersheds. Ten radiocarbon dates from ten unique soil horizons in seven different soil pits across North Rhyne and Duffey watersheds yield ages ranging from the modern period until 6050±31 calibrated years before present (cal YBP) (Table 5.4). Most of the results (five from North Rhyne and Duffey) are modern, or from the last 175 years. Another group of dates (three from North Rhyne and Duffey) appears in the late Holocene from 1587 ±29 through 1786±22 cal YBP. The last two radiocarbon ages come from the mid-Holocene (4313±27 and 6050±31 cal YBP). Each of the three pits with two samples taken from them report dates in the correct stratigraphic order.

Five samples from the Piedmont were added to the probability plot, adding one point to the modern cluster (137±21 cal YBP) from Deep Creek watershed. Two dates formed a new cluster between 915±22 cal YBP and 955±15 cal YBP, the former from Deep Creek. Another

date fell into the late Holocene category at 2930±15 cal YBP. The last date, from UNC Charlotte campus, was from 9709±40 cal YBP.

5.5 Pedogenic iron analysis

The absolute concentration of iron (g/cm^2) was measured for the most weathered B horizons (n=61). Bulk density results were utilized to assess total iron. Bulk density values ranged from 1.28 g/ml to 2.25 g/ml with an average bulk density of 1.56 g/ml (Appendix E).

Iron content (weight %) for samples from North Rhyne watershed averaged 1.24% +/- 0.82% for FeD and 0.41% +/- 0.17% for FeH (Figure 5.7, Table 5.1). The average iron activity ratio was 0.55 +/- 0.47 (Figure 5.7, Table 5.1). In Duffey watershed, the iron content (weight %) for the most weathered B averaged 4.75% +/- 1.51% for FeD and 0.62% +/- 0.22% for FeH (Figure 5.7, Table 5.1). The average iron activity ratio was 0.15 +/- 0.09 (Figure 5.7, Table 5.1). Duffey watershed has overall higher FeD (p= 1.4386E-14), lower FeH (p= 5.2469E-04), and lower iron activity ratios (p= 7.7575E-04, Table 5.2).

If iron activity ratios are considered for pits from which there is age control, the ratios for the most weathered horizons in this study show an overall decline with age (Figure 5.8). Overall, the lowest iron activity ratios for most weathered B horizons were found in the oldest soils (Figure 5.7). In soils without age control, the relative degree of soil development (e.g. clay fraction) can indicate age. Duffey soils have consistently lower iron activity ratios (p-value 7.7575E-04, Table 5.2) of the most developed B horizons, all containing more clay than North Rhyne (Figure 5.7, Tables 5.1). In addition to age trends evident in the chronofunction, there is also a pattern in the iron activity ratio variability relative to their landscape position.

5.6 Geochemistry

In general, geochemical analysis using single-element XRF data can assist with identifying the provenance of sediment or rock in which soils are developed, as well as the overall degree of weathering. Single-element data for Al, Fe, and Si was converted to their respective oxide equivalents to facilitate a comprehensive understanding of the compositional variations between and within the two watersheds of this study that could point to lithological variations or differential weathering effects (Figure 5.9). Similarly, chemical enrichment and depletion ratios are plotted for each soil pit in Figure 5.10. Overall, North Rhyne soil pits show greater depletion signals than the Duffey watershed (Figure 5.10).

North Rhyne watershed contains an average of 76,265 ppm Al; 175,221 ppm Si; 34,529 ppm Fe; 33 ppm Sr; 195 ppm Zr; 56702 ppm Mg; 18,202 ppm K; 9,163 ppm Ca; and 497 ppm Mn (standard deviations found for each element in Table 5.5). When samples from North Rhyne are plotted on the ternary diagram, there is a trend of overall low Fe2O3 content, low Al2O3 content, and high SiO2 (Figure 5.9).

Duffey watershed contains an average of 37,128 ppm Al; 77,418 ppm Si; 63,400 ppm Fe; 13 ppm Sr; 176 ppm Zr; 31,516 ppm Mg; 22,937 ppm K; 949 ppm Ca; and 761 ppm Mn (standard deviations found for each element in Table 5.5). When samples are plotted on a ternary diagram, samples from Duffey watershed overall have high Fe2O3 content, low Al2O3 content, and moderate SiO2 (Figure 5.9).

The ternary diagram of Fe2O3, SiO2, and Al2O3 content of samples from Duffey and North Rhyne shows that samples from Duffey watershed have the highest Fe2O3 content. In contrast, samples from North Rhyne are almost always dominant in SiO2, with both watersheds displaying comparable Al2O3 content (Figure 5.9).

5.7 Soil stratigraphy

Across the field area, three distinct sedimentary units (Units 4, 3, 2) overlying residual soil and saprolite (Unit 1) were identified based on stratigraphic relationships and their degree of weathering (Figure 5.1).

Unit 4 is always located on the ground surface, typically comprising A/B, Ap/Bp or A/AB horizonation. Radiocarbon dates from this unit range from 294 +/- 156 calibrated YBP to modern (n=5) (Figure 5.11). Dry soil colors are consistently 7.5YR or yellower Munsell hues. Soils are generally silt loam or loam with the highest average sand content (28.76% +/- 15.20%, Table 5.3) and moderate gravel content relative to the other units (average of 3.75% +/- 4.29%, Table 5.3), high organic matter (average of 6.34% +/- 4.44%), and the lowest average clay content (15.44% +/- 6.40%, Table 5.3). Overall, ped structure is the weakest (1-2 very fine/fine/medium subangular blocky). In North Rhyne, Unit 4 thickens towards the valley bottom, and in Duffey, Unit 4 is only present in the valley bottom. Overall, Unit 4 exhibits enrichment of of Si/Al throughout the unit (Figure 5.10, Si column).

Unit 3 is present across all four hillslopes of the study area and is also commonly present at the ground surface, particularly in the Duffey watershed (Figure 5.1). It is distinct from Unit 4 from its overall more developed soil characteristics, with common A/B/Bt, and Eb/Btb horizonation. Radiocarbon dates from this unit average 1556 +/- 90 calibrated YBP, n=3 (Figure 5.11). Soils are characterized by dry colors 10YR or redder. Soils are silt loam with high average sand content (24.03% +/- 15.56%, Table 5.3) and the highest average gravel content (7.55% +/- 10.15%, Table 5.3), second highest clay content (average of 18.78% +/- 9.39%, Table 5.3), and average silt content of 57.19% +/- 9.39% (Table 5.3). Organic matter is the second highest of all units (average of 6.63% +/- 2.93%, Table 5.3), and weak ped structure (2 medium/course

subangular/angular blocky). If Unit 4 is present, Unit 3 is consistently found as a buried horizon separated from Unit 4 by an unconformity.

Unit 2, where present, occurs in the lower backslope and toeslope positions, and is always between Units 1 and 3. This unit is present along the lower backslope positions in Duffey, and the backslope and toeslope positions on the North-facing hillslope in North Rhyne. Compared to Unit 3, Unit 2 has soil characteristics similar to those of residuum, but also show clear evidence of movement in their sedimentary structure (no primary features). Horizonation is Ab/Bb/BCb, or Bb/Cr. Radiocarbon dates from this unit average 5888 +/- 72 calibrated YBP, n=2, Figure 5.11). This unit has soils characterized by 5YR or redder Munsell hues, lower clay content than surrounding horizons (average of 16.20% +/- 2.77%, Table 5.3), high gravel and sand content (averages of 5.50% +/- 4.02% and 16.20% +/- 2.77% respectively, Table 5.3). Silt content is the second highest (average of 59.10% +/- 11.45%, Table 5.3) of all the units, second to Unit 1. Organic matter is the lowest in Unit 2 (average of 4.02% +/- 1.23%, Table 5.3). This unit exhibits moderate to well-developed ped structure (2/3 medium/course angular/subangular blocky).

Unit 1 is residual soil, or the top of the bedrock parent material. It is always located at the bottom of the soil excavation pits, and never extends to the ground surface. All 21 soil pits were excavated to saprolite except the alluvial fan pit in North Rhyne. Soils are generally silty clay loam with common Bt/Btr/Cr or Bt/BCt/BCr/Cr horizonation. No charcoal was found in this unit to submit for radiocarbon dating. Unit 1 has soils characterized by 5YR or often redder Munsell hues, higher clay content than overlying horizons (average of 11.24% +/- 7.66%, Table 5.3), and the highest silt content for every unit (average of 63.26% +/- 6.60%, Table 5.3). Unit 1 has the lowest gravel content of all units except for unambiguously *in situ* material (average of 0.74%

+/- 1.87%, Table 5.3), and the lowest sand content (average of 11.24% +/- 7.67%, Table 5.3). Organic matter is the highest in Unit 1 of any unit (9.0%, Table 5.3). Ped structure is the strongest in this unit (2-3 course to medium platy/subangular blocky), and clay films are minimal.

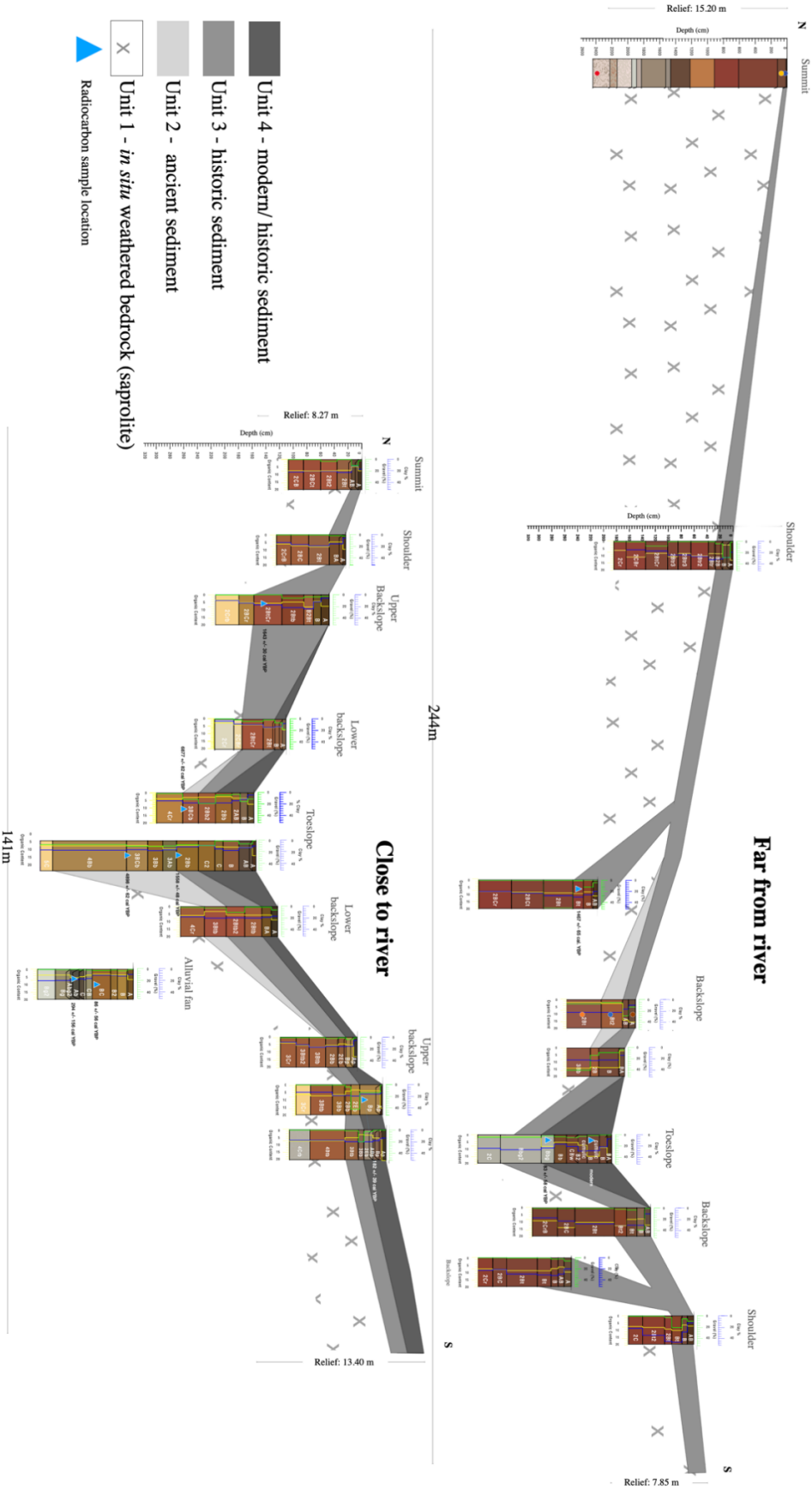
Far from river
Close to river
Summit
Shoulder
Backslope
Toeslope
Upper backslope
Lower backslope
Alluvial fan
N
S
Relief: 15.20 m
Relief: 7.85 m
Relief: 8.27 m
Relief: 13.40 m
244m
141m
Depth (cm)
Unit 4 - modern/ historic sediment
Unit 3 - historic sediment
Unit 2 - ancient sediment
Unit 1 - *in situ* weathered bedrock (saprolite)
Radiocarbon sample location

Figure 5.1: Soil profile logs along each toposequence. Vertical exaggerated 2x. Clay content analyzed with the laser diffraction system (%) in blue, organic carbon content measured as loss-on-ignition (%) in yellow, and gravel content (% >2mm) in green. Background soil colors were obtained from moist soil samples using the Munsell color chart. Shaded boxes represent discrete allostratigraphic units (defined by unconformities) in each hillslope sediment between soil pits. Circles are locations of OSL samples. Blue triangles are radiocarbon sample locations.

Locality	Horizon	Depth (cm)	Color Moist	Color Dry	Gravel (%)	Organic Content	Texture	%clay	%sand	%silt	Structure	Clay Films	Consistence Dry	Consistence Wet	Boundary	Roots	Pores	Mottling	Samples	Other Notes	Toeslope (S-F-ase)
Pit #	A	0-9	10YR 4/4	7.5YR5/3	11.40%	7.53%	CL	4.64	53.4	41.96	2 f sbk	/	so	vfi	a s	3vc 3c 3m 3f 3vf	3c 3m 3f 3vf	/	NR-S8-1		Geomorphic Surface:
NR-S8	B	9-20	7.5YR 5/4	7.5YR6/3	11.80%	3.66%	SL	11.8	37.6	50.6	2 m sbk	2 f pf	vh	vfi	c s	3vc 3c 3m 3f 3vf	3c 3m 3f 3vf	/	NR-S8-2	General Notes: Clay films not as well developed. Rhyne homestead at top of divide here.	
Latitude	2AB	20-32	7.5YR 5/6	7.5YR6/3	9.50%	3.46%	SL	14.6	27.2	82.5	2 m sbk	2 f pf	vh	fr	c s	0vc 3c 3m 3f 3vf	3c 3m 3f 3vf	/	NR-S8-3	Vegetation Types: Maple, Beech, Sweetgum Holly	
Latitude	2Bt	32-56	7.5YR 5/8	7.5YR7/4	4.80%	2.41%	SC	18.2	34.6	50.1	2 c abk	2 f pf/po	eh	fr	c s	0vc 0c 2m 2f 2vf	0c 2m 3f 3vf	7.5YR 5/6	NR-S8-4	% Bare Ground:	
N 35.2969682	2Bt2	56-81	5YR 5/8	5YR7/4	19.20%	2.79%	SC	18.7	35.9	47.2	2 c abk	3 f pf	h	fr	c s	0vc 0c 0m 0f 1vf	0c 0m 2f 3vf	NR-S8-5	Lots of Quartz ~85cm	% Canopy Cover:	80
Longitude	3BCb	81-109	5YR 5/8	5YR7/4	12.10%	2.98%	SC	18.2	34.7	45.4	2 c abk	3 f pf	vh	vfr/fr	c s	0vc 0c 0m 0f 0vf	0c 0m 1f 2vf	5 YR 4/6 (Clay films), 7.5YR 4/3	NR-S8-6	modling color describes clay films	Parent Material 1)	legacy colluvium
W 81.0944457	4Cr	104-142	7.5YR 6/8	5YR7/4	2.30%	3.87%	L	14.7	43	47.1	2 m abk	3 f pf	eh	vfr	/	0vc 0c 0m 0f 0vf	0c 0m 0f 0vf	/	NR-S8-7		Parent Material 2)	colluvium
Projection																					Parent Material 3)	colluvium
WGS84																					Parent Material 4)	Saprolite-MVF

Locality	Horizon	Depth (cm)	Color Moist	Color Dry	Gravel (%)	Organic Content	Sand %	Silt %	Clay %	Texture	Structure	Clay Films	Consistence Dry	Consistence Wet	Boundary	Roots	Pores	Samples	Other Notes	Geomorphic Surface:	Backslope
Pit #	AB	0-7	7.5YR3/4	7.5 YR 4/6	4.20%	10.97%	32.0	59.5	8.5	1 gr	vf f pf po	h	so po	c s	t vc 2c 3m 3f 3vf	0c 0m 0f 0vf	DU-S7-1		General Notes:	Slope ~17 degrees
DU-S7	B	7-22	2.5YR4/8	2.5 YR 5/6	12.10%	8.13%	8.31	65.49	26.2	silt loam	2 m sbk	2 d pf po	eh	so ps	c s	t vc 1c 2m 3m 3vf	0c 0m 2f 3vf	DU-S7-2	higher gravel	Vegetation Types:	
	Bt	22-38	10R4/8	2.5 YR 5/8	0.60%	9.30%	6.3	63.4	30.3		2 m abk sbk	3 p f po	eh	s p	c s	0vc 0c 1m 3f 3vf	0c 1m 2f 2vf	DU-S7-3	color mottled, black MnO, super prominent clay films:	% Bare Ground:	85
Latitude	2Bt	38-83	10R4/6	2.5 YR 4/8	0.00%	8.82%	11.5	60.6	27.9	silty clay loam	2 m pl abk	3 p f pf	vh	s p	c s	0vc 0c 1m 1f 1vf	0c 1m 1f 2vf	DU-S7-4			
N 35.2983054	2BCt	83-132	10R4/6	2.5 YR 5/8	0.00%	8.39%	15.2	61.8	23		2 m pl	3 p pf	eh	ss p	c s	0vc 0c 1m 0f 1vf	0c 0m 1f 1vf	DU-S7-5	50/50 pH-abk	QTZ ~ 80-93 combo; very prominent clay films	50
W 81.0831859	2BCr	132-182	10R4/8	2.5 YR 4/8	0.00%	7.63%	23.6	62.2	14.2		2 m pl	vf f pf	ah	ss p	—	0vc 0c 0m 2f 1vf	0c 0m 1f 1vf	DU-S7-6	well defined platy structure	Parent Material 2)	Saprolite-MVF
Projection	2BCr	132-182	10R4/8	2.5 YR 5/8	0.00%	7.63%	23.6	62.2	14.2		2 m pl	vf f pf	ah	ss p	—	0vc 0c 0m 2f 1vf	0c 0m 1f 1vf	DU-S7-8	vf roots throughout; Foliations (following platy structure) ~vertical		
WGS84																					

Locality	Horizon	Depth (cm)	Color Moist	Color Dry	Gravel (%)	Organic Content	Sand %	Silt %	Clay %	Texture	Structure	Clay Films	Consistence Dry	Consistence Wet	Boundary	Roots	Pores	Samples	Other Notes	Geomorphic Surface:	Shoulder
Pit #	A	0-4	7.5YR2.5/3	5YR3/2	0.80%	13.21%	59.3	36.1	4.6	2 f gr sbk	---	so	so po	a s	3vc 3c 3m 3f 3vf	0c 3m 3f 3vf	DU-S3-1		General Notes:	
DU-S3	B	4-16	5YR4/4	5YR5/4	29.10%	2.36%	18	62.8	19.2	2 f sbk	---	sh	so ps	a w	3vc 3c 3m 3f 3vf	0c 3m 3f 3vf	DU-S3-2	Vegetation Types:			
	B2B	16-27	2.5YR4/6	2.5YR5/6	3.70%	8.56%	11.6	59.5	28.9	2 f sbk	2 f pf po	vh	ss ps	c s	2vc 2c 3m 3f 3vf	0c 2m 3f 3vf	DU-S3-3	Color not as homogenious as above	Vegetation Types:	
Latitude	2Bt	27-38	2.5YR4/6	2.5YR5/6	0.00%	8.46%	5.9	62.3	31.8	2 f sbk	2 d pf po	eh	s p	a s	0vc 0c 1m 2f 3vf	0c 0m 2f 3vf	DU-S3-4	intrusion widest (.4cm) at this point	% Bare Ground:	70
N 35.2985561	2Bt2	38-65	10R4/8	2.5YR4/8	0.30%	10.04%	4.5	62.5	33	2 f pl / abk	2 f pf po	eh	vs p	g s	0vc 0c 1m 3f 3vf	0c 0m 2f 2vf	DU-S3-5		% Canopy Cover:	50
	2Bt3	65-85	10R4/6	2.5YR4/8	0.00%	8.37%	9.09	63.71	27.2	2 f	2 f pf po	vh	s p	g s	0vc 0c 0m 3f 3vf	0c 0m 0f 0vf	DU-S3-6		Parent Material 1)	Colluvium
Longitude	2Bt3	85-101	10R4/6	2.5YR4/8	0.00%	10.64%	13.5	62.3	24.2	2 f	2 f pf po	h	s p	g s	0vc 0c 0m 3f 3vf	0c 0m 0f 0vf	DU-S3-7	Increasing yellow mottling towards bottom	Parent Material 2)	Saprolite-MVF
W 81.0821942	2BtCr	101-135	10R4/6	2.5YR5/6	7.90%	8.27%	10.8	64.7	24.5	2 m pl	1 f pf	sh	ss p	g s	0vc 0c 1f 2vf	0c 0m 0f 2vf	DU-S3-8			
	2CBr	135-165	10R4/8	5YR6/6	0.30%	10.93%	11.5	71.7	16.8	---	---	sh	ss p	c s	0vc 0c 1f 2vf	0c 0m 0f 2vf	DU-S3-9			
Projection	2Cr	165-184	10R4/8	5YR6/6	0.00%	6.15%	15.2	70.1	14.7	---	---	so	ss p	—	0vc 0c 1f 0vf	0c 0m 1f 1vf	DU-S3-10			
WGS84																					

Figure 5.2: Representative field descriptions from four soil pits in North Rhyne and Duffey (NR-S4, NR-S8, DU-S7, DU-S3).

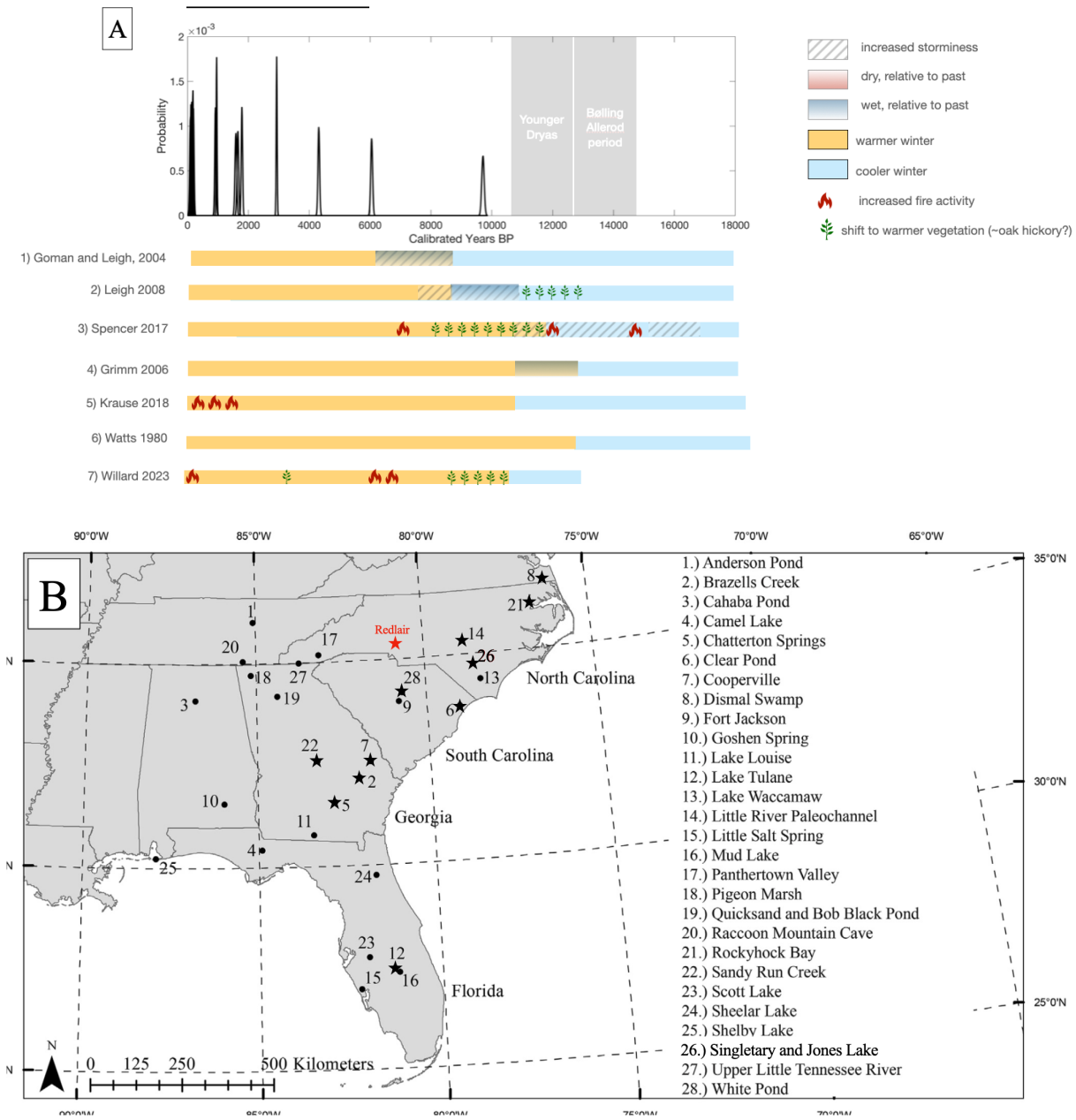

Figure 5.3a: Comparison of sedimentation events on hillslopes from Redlair Observatory and UNC Charlotte campus represented as a probability curve, or a sum of normal distributions of median calibrated individual radiocarbon ages (top) with paleoclimate records from the southeast US (bottom): 1) Little River, Coastal Plain, NC, 2) Atlantic Coastal Plain, NC, SC, and GA, 3) Jones and Singletary Lakes, NC, 4) Lake Tulane, FL, 5) and 6) White Pond, SC. Warm periods represented in yellow; cool periods represented in light blue; periods with increased storminess

represented by diagonal grey lines; dry periods represented by red gradient; wet periods represented by dark blue gradient; increased fire activity represented by fire symbols; and increased terrestrial production represented by plant symbols.

Figure 5.3b: *Modified from Spencer et al., 2017*. Location of other paleoenvironmental study sites in the SE US. The red star shows the location of Redlair Observatory, Gastonia NC. Black stars on the map represent locations of sites accounted for in this studies paleoclimate record. Black dots represent a comprehensive list of all the paleoclimate studies that have been conducted in the SE US (compiled by Spencer et al., 2017). Other SE US paleoenvironmental studies on the map include: 1: Delcourt, 1979; Liu et al., 2013; 2: LaMoreaux, 1999; 3: Delcourt et al., 1983; 4: Watts et al., 1992; 5: Seielstad, 1994; LaMoreaux, 1999; 6: Hussey, 1993; 7: Brook, 1996; 8: Lewis and Cocke, 1929; Whitehead, 1973; 9: Taylor et al., 2011; 10: Delcourt, 1980; 11: Watts, 1971; Tepper and Hyatt, 2011; 12: Grimm et al., 1993, 2006; Donders et al., 2011; Donders, 2014; 13: Stager and Cahoon, 1987; 14: Goman and Leigh, 2004; 15: Clausen et al., 1979; Zarikian et al., 2005; 16: Watts, 1969; Filley et al., 2001; 17: Tanner et al., 2015; 18: Watts, 1975; 19: Watts, 1970; 20: Driese et al., 2012; Li et al., 2012; 21: Whitehead, 1981; 22: LaMoreaux, 1999; LaMoreaux et al., 2009; 23: Watts, 1971; 24: Watts, 1980b; 25: Fearn and Liu, 1995; Liu et al., 2008; 26: Frey, 1951, 1953; 27: Wang and Leigh, 2012; 28: Watts, 1980a.

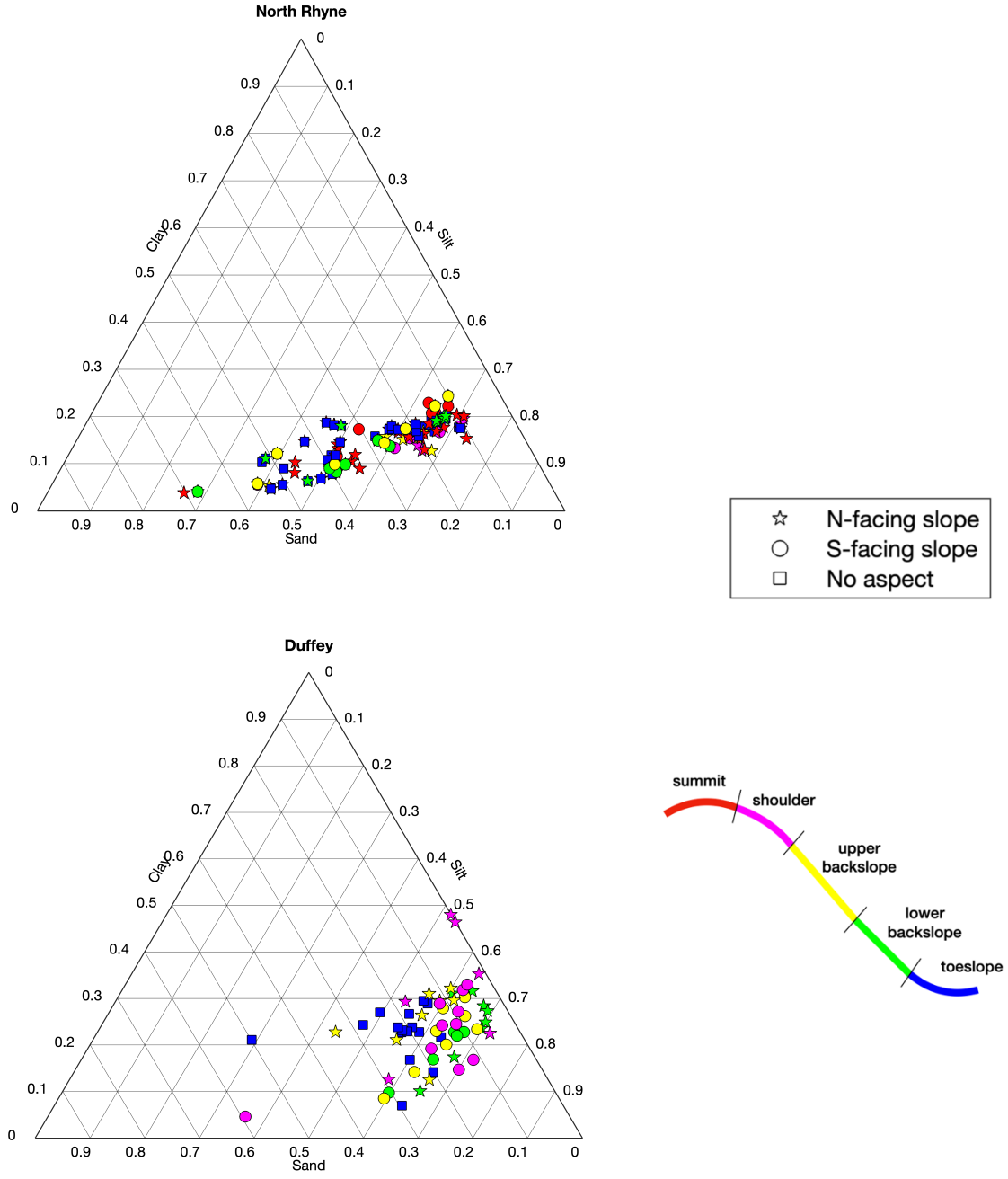

Figure 5.4: Ternary plots of sand, silt, and clay fraction (measured as volume % of total <2mm sample) in North Rhyne (top) and Duffey (bottom) watersheds. Summit hillslope positions are in red, shoulder positions in magenta, upper backslope in yellow, lower backslope in green, and

toeslope in blue. North-facing hillslopes are represented by stars, south-facing hillslopes are represented by circles, and toeslope positions, or squares represent those with no aspect.

	Sand	Silt	Clay	Gravel	LOI	FeD	FeH	FeH/FeD
Duffey	AV: 15.92% STDEV: 10.91%	AV: 60.32% STDEV: 7.77%	AV: 23.77% STDEV: 8.12%	AV: 5.26% STDEV: 9.07%	AV: 8.78% STDEV: 3.52%	AV: 4.75% STDEV: 1.51%	AV: 0.62% STDEV: 0.22%	AV: 0.15% STDEV: 0.09%
North Rhyne	AV: 27.96% STDEV: 14.65%	AV: 57.37% STDEV: 10.80%	AV: 14.67% STDEV: 4.76%	AV: 3.76% STDEV: 6.11%	AV: 5.47% STDEV: 2.85%	AV: 1.24% STDEV: 0.82%	AV: 0.41% STDEV: 0.17%	AV: 0.55% STDEV: 0.47%
Deep Creek	AV: 38.324% STDEV: 15.744%	AV: 49.179% STDEV: 11.071%	AV: 12.497% STDEV: 5.8972%	AV: 13.615% STDEV: 16.215%	AV: 1.5468% STDEV: 1.0357%	—	—	—

Table 5.1: Average (AV) and standard deviation (STDEV) values for sand, silt, clay, gravel, loss-on-ignition, FeD, FeH, and FeH/FeD (iron activity ratio) for all three watersheds: Duffey, North Rhyne, and Deep Creek.

DU vs NR	**gravel**	**clay**	**sand**	**silt**	**LOI**	**FeD**	**FeH**	**FeH/FeD**	**depth**
h	0	1	1	0	1	1	1	1	0
p-value	0.2344	3.0488 E-14	2.2389 E-07	0.0706	3.4294 E-11	1.4386 E-14	5.2469 E-04	7.7575 E-04	0.4466

Table 5.2: Two sample t-test comparing North Rhyne and Duffey. The result h is 1 if the test rejects the null hypothesis at the 5% significance level, and 0 otherwise. When $p < 0.05$ the null hypothesis can be rejected at the 5% significance level.

	Sand	Silt	Clay	Gravel	LOI
Unit 4	AV: 28.76% STDEV: 15.20%	AV: 55.80% STDEV: 11.41%	AV: 15.44% STDEV: 6.40%	AV: 3.75% STDEV: 4.29%	AV: 6.34% STDEV: 4.44%
Unit 3	AV: 24.03% STDEV: 15.56%	AV: 57.19% STDEV: 9.39%	AV: 18.78% STDEV:9.39%	AV: 7.55% STDEV: 10.15%	AV: 6.63% STDEV: 2.93%
Unit 2	AV: 24.70% STDEV: 13.39%	AV: 59.10% STDEV: 11.45%	AV: 16.20% STDEV: 2.77%	AV: 5.50% STDEV: 4.02%	AV: 4.02% STDEV: 1.23%
Unit 1	AV: 11.24% STDEV: 7.67%	AV: 63.26% STDEV: 6.60%	AV: 25.49% STDEV: 6.97%	AV: 0.74% STDEV: 1.87%	AV: 9.00% STDEV: 1.66%

Table 5.3: Average (AV) and standard deviation (STDEV) values for sand, silt, clay, gravel, and loss-on-ignition content for all four units.

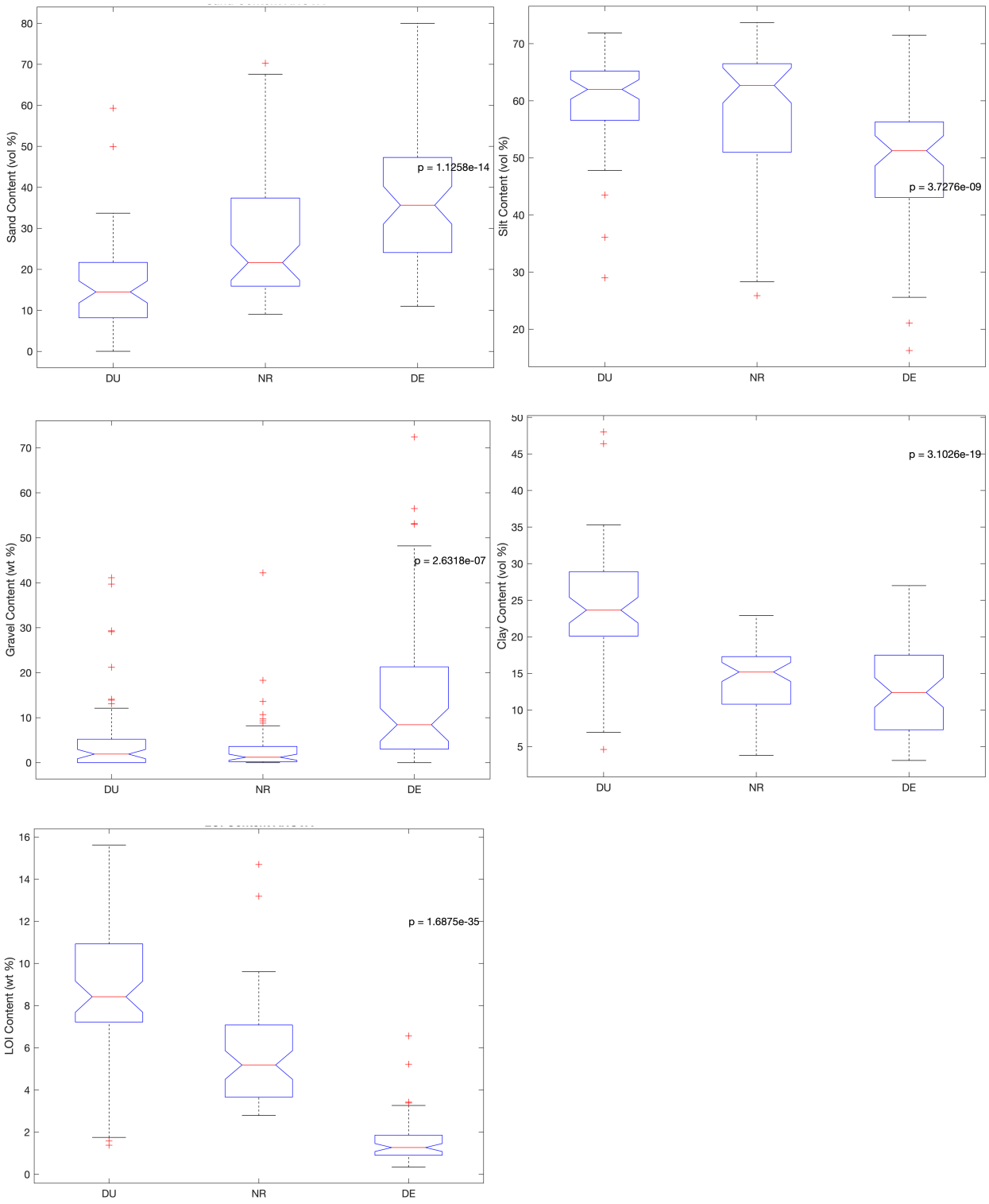

Figure 5.5: One-way analyses of variances (ANOVA) tests were used to understand the variance between North Rhyne, Duffey, and Deep Creek. P-values displayed on each plot.

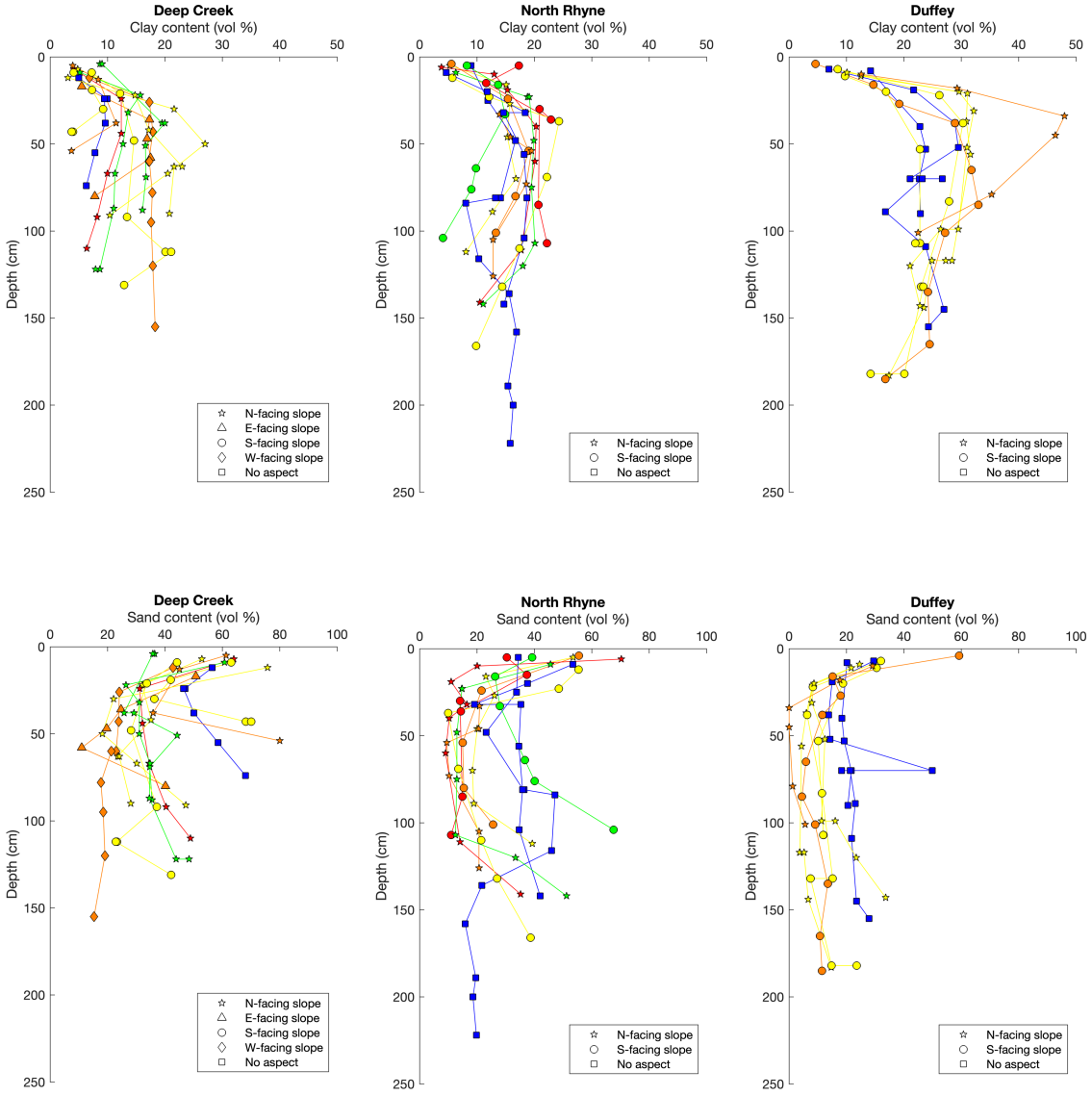
Deep Creek
Clay content (vol %)
North Rhyne
Clay content (vol %)
Duffey
Clay content (vol %)
Deep Creek
Sand content (vol %)
North Rhyne
Sand content (vol %)
Duffey
Sand content (vol %)
Depth (cm)
N-facing slope
E-facing slope
S-facing slope
W-facing slope
No aspect

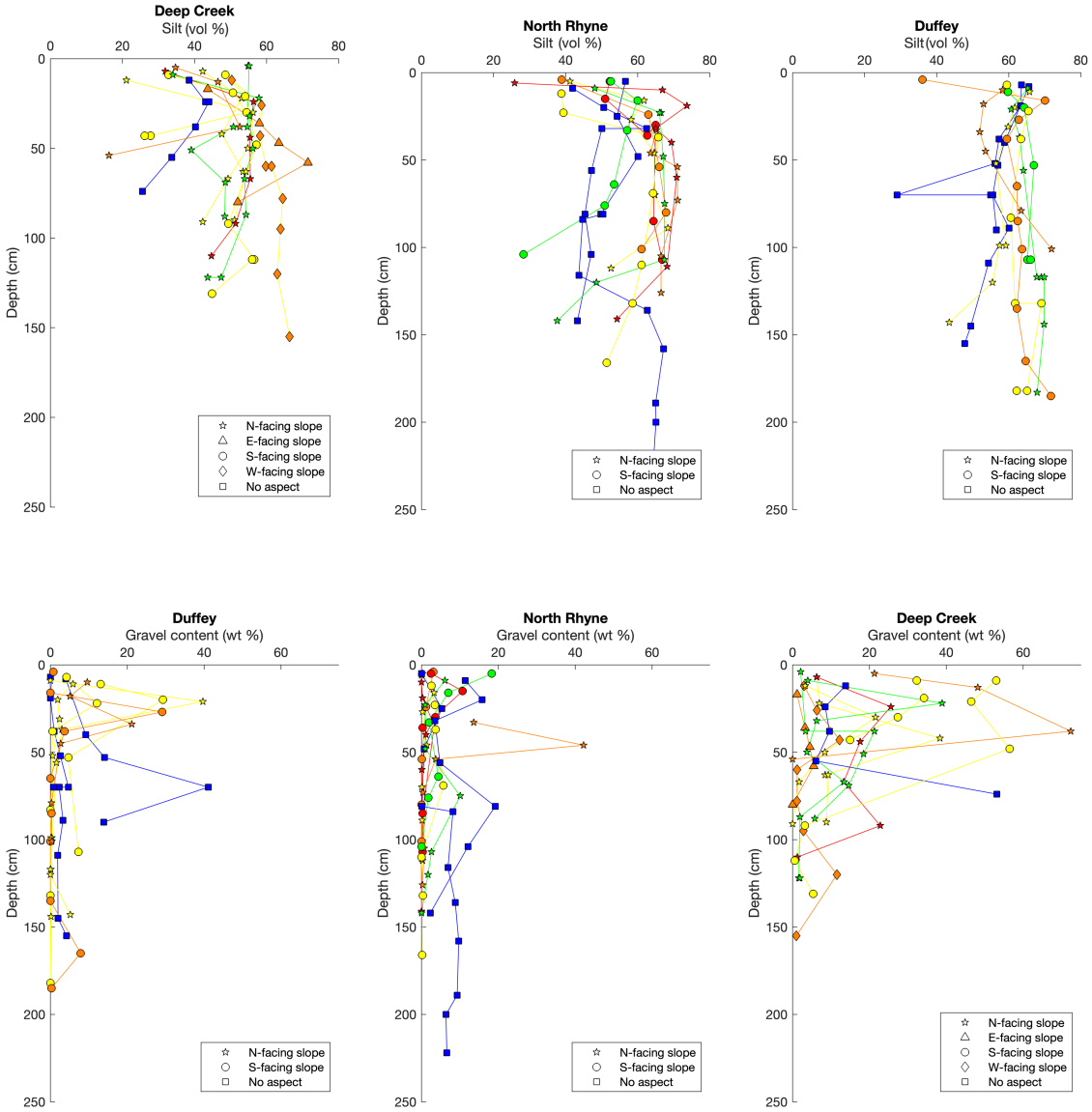
Deep Creek
Silt (vol %)
Depth (cm)
N-facing slope
E-facing slope
S-facing slope
W-facing slope
No aspect
North Rhyne
Silt (vol %)
Depth (cm)
N-facing slope
S-facing slope
No aspect
Duffey
Silt (vol %)
Depth (cm)
N-facing slope
S-facing slope
No aspect
Duffey
Gravel content (wt %)
Depth (cm)
N-facing slope
S-facing slope
No aspect
North Rhyne
Gravel content (wt %)
Depth (cm)
N-facing slope
S-facing slope
No aspect
Deep Creek
Gravel content (wt %)
Depth (cm)
N-facing slope
E-facing slope
S-facing slope
W-facing slope
No aspect

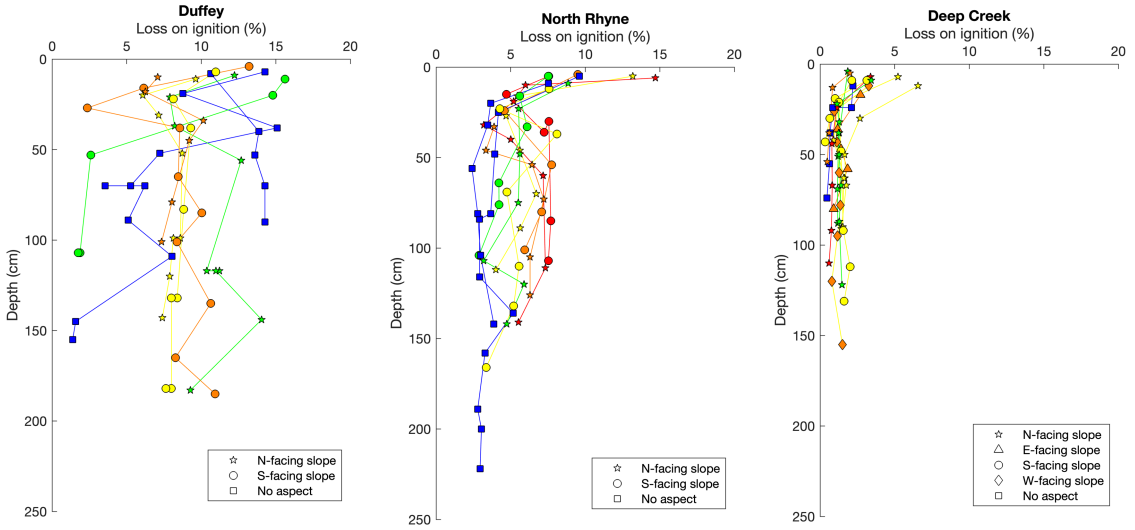

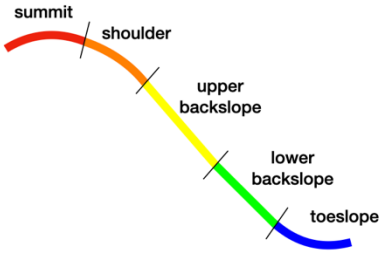

Figure 5.6: Clay, sand, silt, gravel and carbon content (x-axis) plotted against sample depth below surface (y-axis). Samples from north-facing hillslopes are plotted as stars, samples from south-facing hillslopes are plotted as circles, east-facing hillslope samples plotted as triangles, west-facing hillslopes plotted as diamonds, and samples from toeslope positions with no hillslope aspect are plotted as squares. The hillslope position of each sample is represented by the color of each marker. Summit hillslope positions are in red, shoulder positions in orange, upper backslope in yellow, lower backslope in green, and toeslope in blue. Lines trace samples from the same pit down the profile.

Hillshed order	Aspect	Hillslope position	Depth (cm)	14C age	Calibrated age (YBP)	Lat; Long
high	—	toeslope	57	modern	modern	N 35.2978101; W 81.0826572
high	—	toeslope	82	112 +/- 21	140-25 (70.8%)	N 35.2978641; W 81.0829493
low	N	toeslope	195	4313 +/- 27	4960-4836 (95.4%)	N 35.2978641; W 81.0829493
low	N	shoulder	43	193 +/- 22	220-143 (58.5%)	N 35.2976776; W 81.0941992
low	N	toeslope	82	175 +/- 19	225-138 (55.8%)	N 35.2978641; W 81.0829493
high	S	backslope	32	1587 +/- 29	1531-1402 (95.4%)	N 35.2983054; W 81.0831859
low	S	toeslope	105	6050 +/- 31	6985-6795 (95%)	N 35.2986882; W 81.0944457
low	—	alluvial fan	62	95 +/- 24	142-30(69.7%)	N 35.2978641; W 81.0829493

low	N	toeslope	120	1653 +/- 28	1605-1510 (71.2%)	N 35.2978641; W 81.0829493

Table 5.4: Radiocarbon samples and ages from DirectAMS. 14C ages calibrated using OxCal v4.4.4 with the IntCal20 calibration curve (Reimer et al., 2020). High order hillshed samples are from Duffey watershed, and low order samples are from North Rhyne watershed.

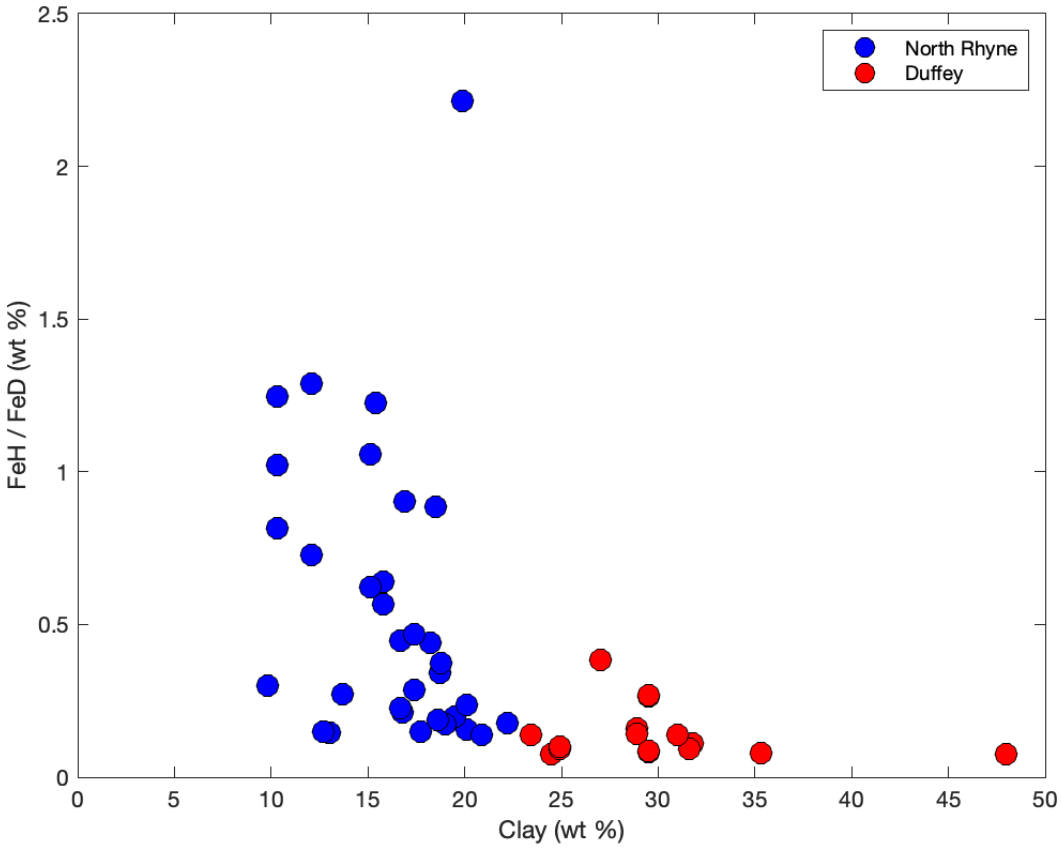

Figure 5.7: Iron activity ratio as a function of the clay fraction of all soil samples from North Rhyne (blue) and Duffey (red) watersheds analyzed for pedogenic iron. North Rhyne samples are represented as blue circles, and samples from Duffey watershed are represented by red circles.

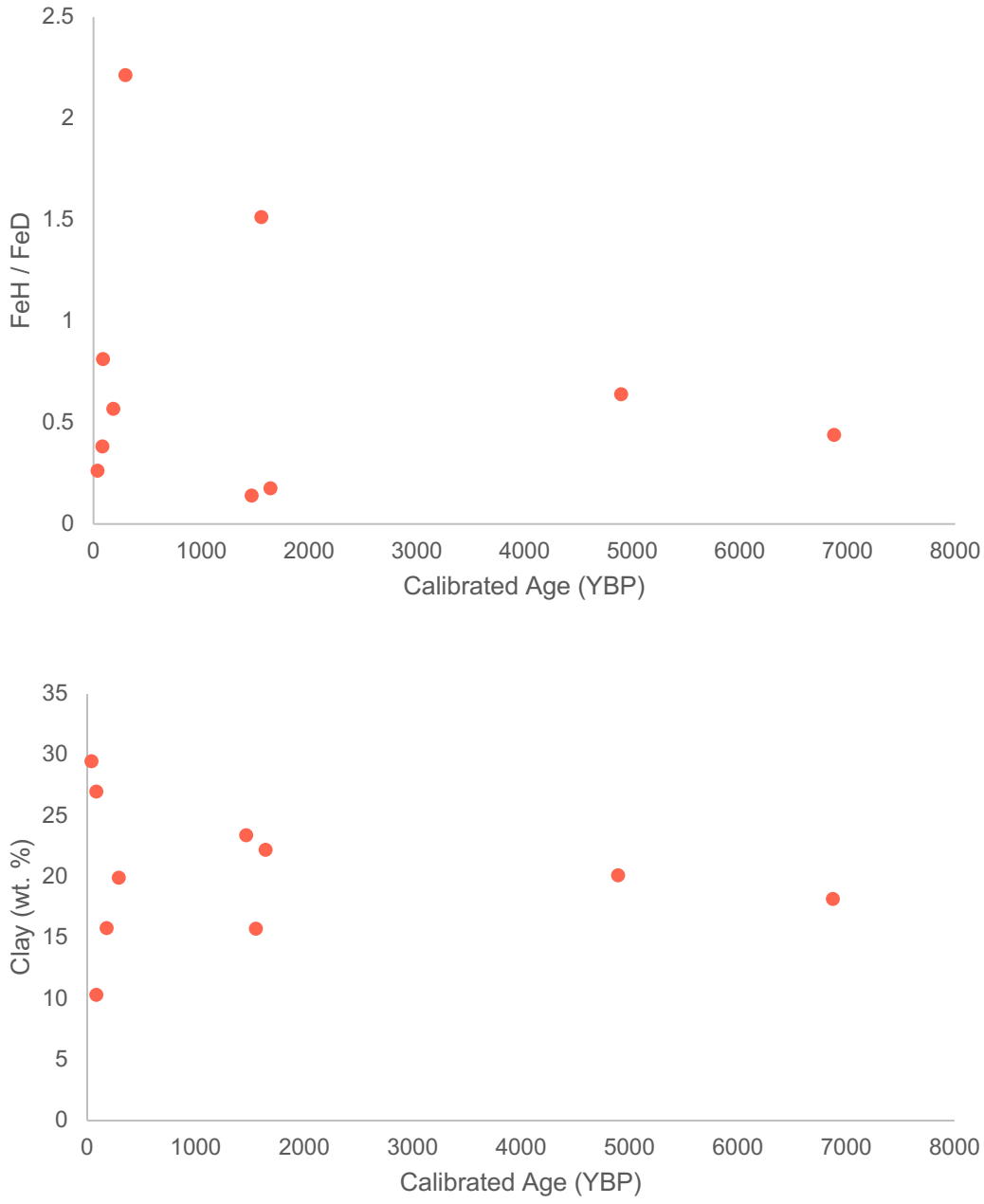

Figure 5.8: Chronofunctions of the iron activity ratio (top) and clay content (bottom) generated from 10 calibrated radiocarbon ages from North Rhyne and Duffey watersheds.

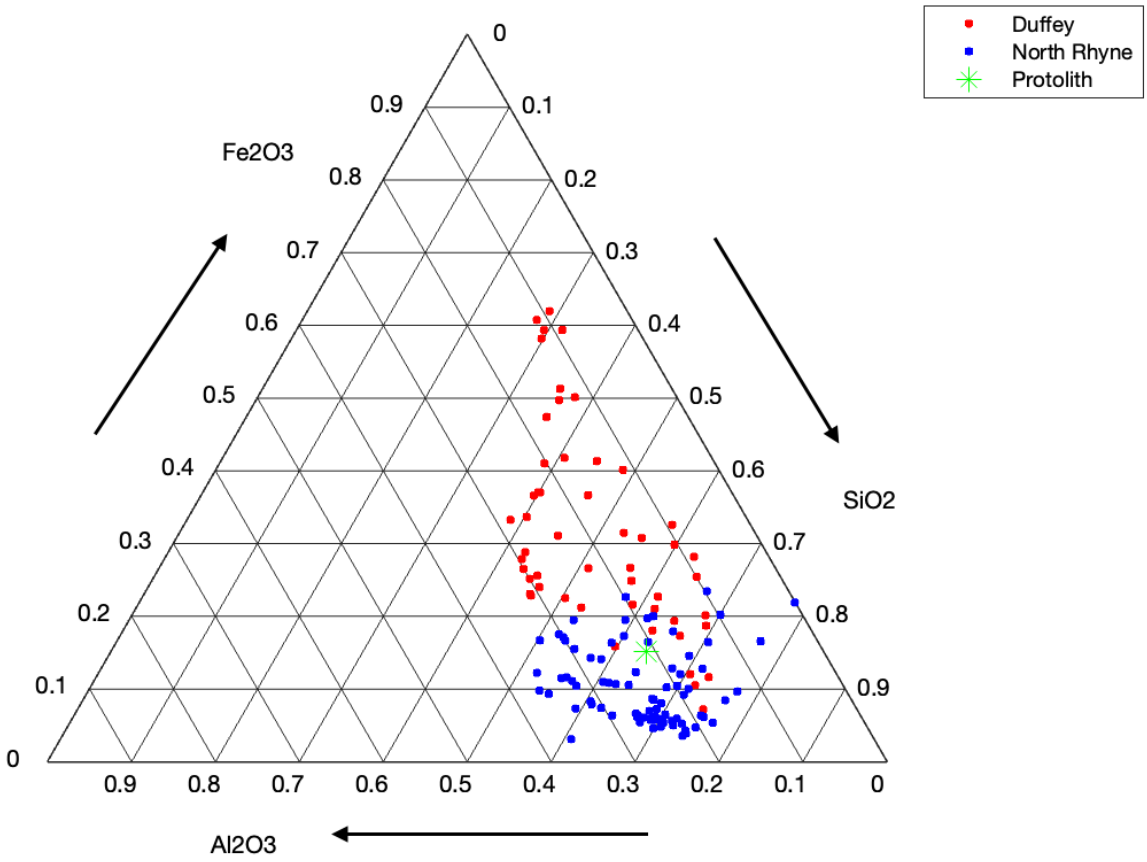

Figure 5.9: Ternary diagram of Fe2O3, SiO2, and Al2O3 content of samples from Duffey (red circles) and North Rhyne (blue circles) watersheds and the protolith (green star).

	Al	Si	Fe	Sr	Zr	Mg	K	Ca	Mn
North Rhyne averages	76265.0	175221.0	34528.7	32.5	194.9	56701.7	18202.4	9162.6	497.2
North Rhyne standard deviation:	38933.7	82977.4	10822.2	15.2	59.8	20757.2	10023.1	19813.0	143.3
North Rhyne # samples	80	80	81	81	81	54	36	17	9
Duffey averages	37128.4	77418.0	63400.2	12.9	175.6	31516.2	22936.5	948.5	761.2
Duffey standard deviation	29322.2	44004.5	26172.6	11.7	94.8	12991.1	10914.7	1170.5	344.7
Duffey # samples	52	52	52	43	52	14	3	23	16

Table 5.5: Average and standard deviation values for Al, Si, Fe, Sr, Zr, Mg, K, Ca, and Mn in ppm collected by the Olympus delta XRF, and the total number of samples that reported values per each element.

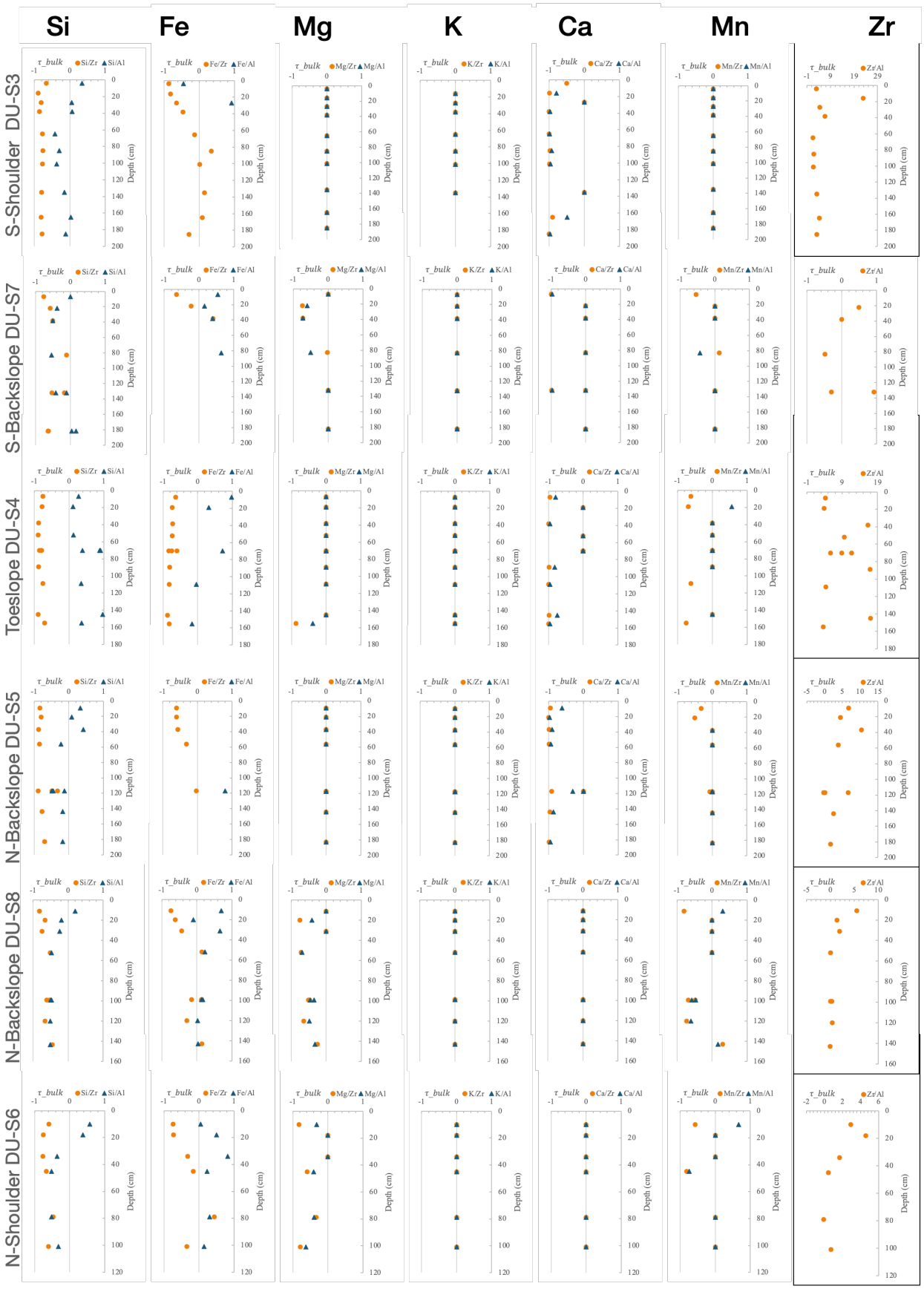
Si
Fe
Mg
K
Ca
Mn
Zr
S-Shoulder DU-S3
S-Backslope DU-S7
Toeslope DU-S4
N-Backslope DU-S5
N-Backslope DU-S8
N-Shoulder DU-S6
τ_bulk
Si/Zr
Si/Al
Fe/Zr
Fe/Al
Mg/Zr
Mg/Al
K/Zr
K/Al
Ca/Zr
Ca/Al
Mn/Zr
Mn/Al
Zr/Al
Depth (cm)

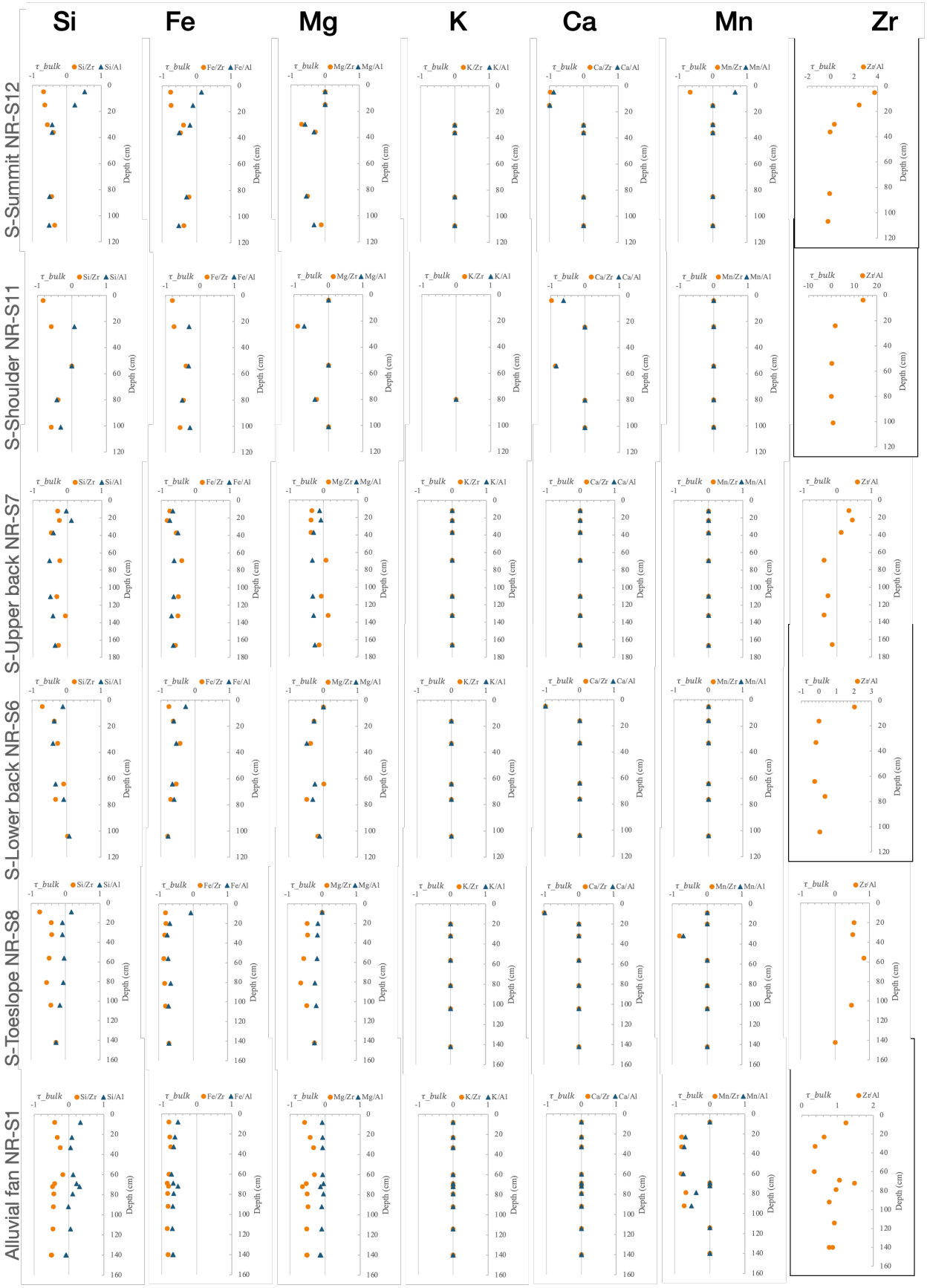
Si
Fe
Mg
K
Ca
Mn
Zr
S-Summit NR-S12
S-Shoulder NR-S11
S-Upper back NR-S7
S-Lower back NR-S6
S-Toeslope NR-S8
Alluvial fan NR-S1
τ_bulk
Si/Zr
Si/Al
Fe/Zr
Fe/Al
Mg/Zr
Mg/Al
K/Zr
K/Al
Ca/Zr
Ca/Al
Mn/Zr
Mn/Al
Zr/Al
Depth (cm)

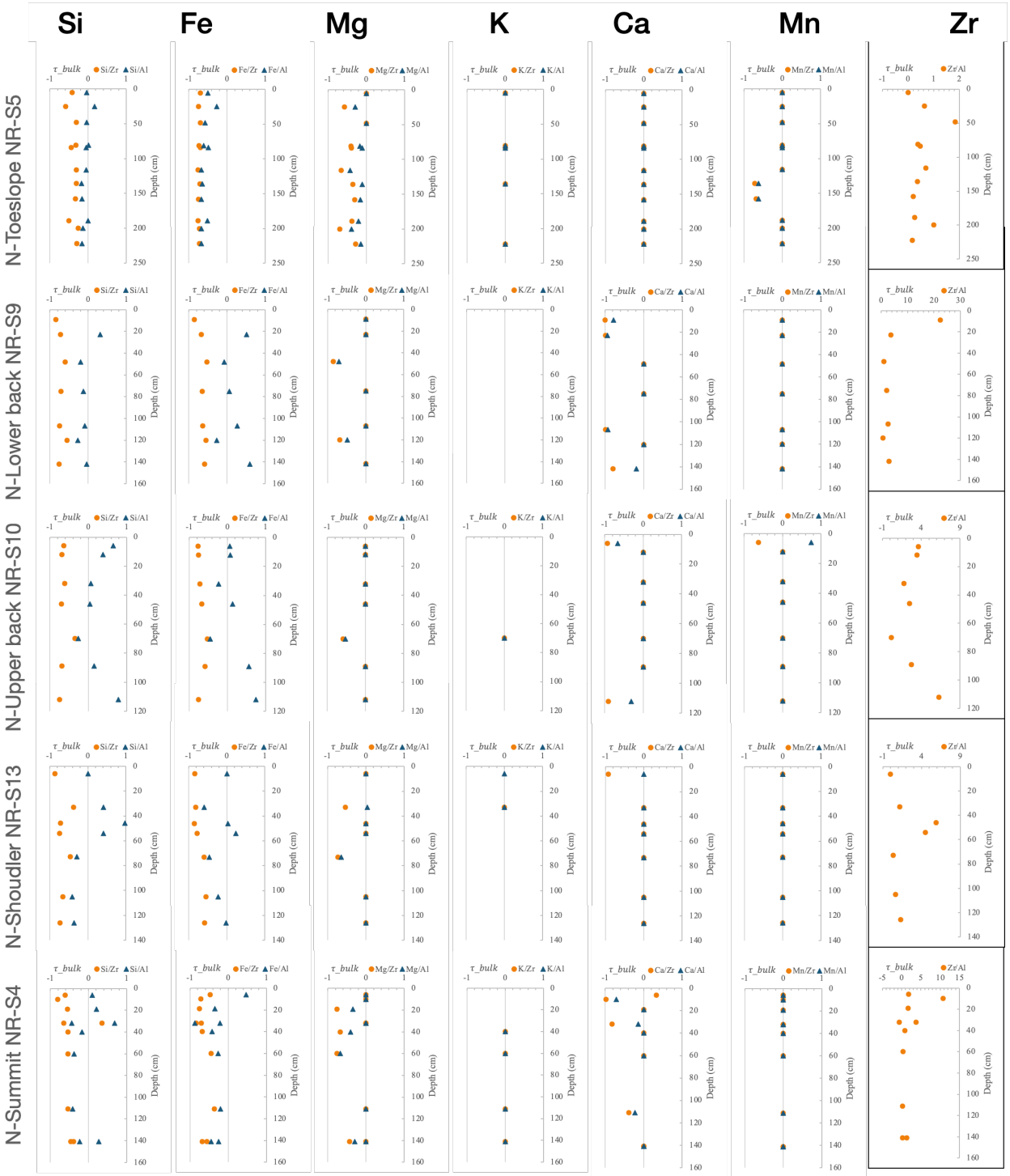

Figure 5.10: Chemical enrichment and depletion (tau) values plotted by sample depth organized by watershed (page), by element (column), and by toposequence from N to S (row). Plots with

black solid outlines have X axes scaled differently to fit the data. All zeroes on the plots represent missing data.

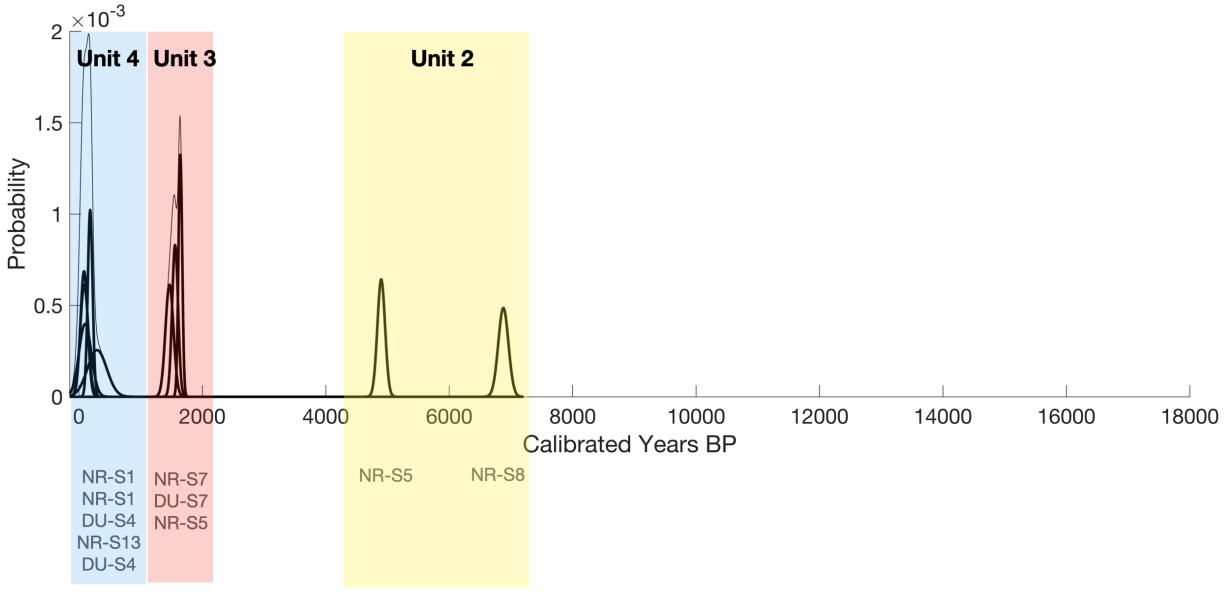

Figure 5.11: Radiocarbon ages from North Rhyne and Duffey watershed represented as a probability curve, or a summation of normal distributions of median calibrated individual 14C ages. Calibrated ages and corresponding soil pit IDs for Unit 4 are highlighted in blue, Unit 3 highlighted in red, and Unit 2 highlighted in yellow.

CHAPTER 6: DISCUSSION / INTERPRETATIONS

On hillslopes there are two main processes: in situ weathering and downslope movement of sediment. These processes are discussed separately as they are influenced differently by the hillslope position, hillslope aspect, and the watershed's location within the broader landscape.

6.1 Weathering differences as a function of hillshed

The results of this study indicate that weathering profile characteristics at Redlair Observatory are dependent upon the distance (horizontal and vertical) of a watershed from a major river (local base level inciting erosion) and the hillshed order (high-order hillshed is distal from the S. Fork of the Catawba). Average clay content is highest at Duffey watershed (Table 5.1, Figures 5.4, 5.5, 5.6), which suggests that high-order hillsheds, or distal hillslopes, are more deeply weathered, reflecting a longer period of landscape stability. Overall, Duffey soils are much more homogenous than those from North Rhyne, with deeper red values, lower iron activity ratios, higher organic content, and more frequent Bt horizons (Figures 5.1, 5.6, 5.7, Tables 5.1, 5.2). Each of these characteristics develops with the advancement of the weathering front into saprolite. These results indicate that Duffey has a relatively more stable landscape position. It also suggests that any disturbance to these slopes caused by incision of the South Fork of the Catawba River and subsequent knickpoint migration has reached the low-order hillsheds to a greater extent that high-order hillsheds.

Hillslope steepness is not the only factor that accounts for differences between Duffey and North Rhyne since the alternate pits in Duffey are on hillslopes just as sleep as those in North Rhyne. For example, two soil pits (DU-S7 and DU-S8) positioned along the steep, incised backslope positions in Duffey exhibit similar weathering characteristics to the rest of the soils in Duffey. The main transect differs from the additional transect in slope steepness and in transition

from an ephemeral stream (bisecting the main transect) to a perennial stream. The soils in Duffey watershed below this small knickpoint have similar clay content, prominent clay films on the pores and ped faces, and slightly lower organic content when compared to the backslope positions on the main transect in Duffey. The similarity between the two sets of backslope pits enforces the idea that base-level incision from the South Fork of the Catawba River is not felt as significantly in higher-order hillsheds despite differences in slope. The steeper hillslope in Duffey suggests an older passing knickpoint in between the two soil pit transects in the watershed.

Overall, a discernible trend of depletion is evident in both watersheds, with notably higher depletion ratios from Duffey when compared to those in North Rhyne. The enrichment of Si/Al seems to be a distinct marker of colluvium across both watersheds, albeit this is a predominantly detectable signal in younger soils (as seen in NR-S8).

Iron and Mn indicate secondary weathering because they are sensitive to redox conditions. Mn can become leached out more easily than Fe under reducing conditions, which could explain why there were so many undetected Mn values by XRF. Piedmont soils are well known for being well-oxidized and Fe-rich. However, the XRF cannot distinguish between different iron species in its readings. Still, the most prominent trend in Fe/Al is between watersheds. Duffey watershed is largely enriched in Fe (especially in the upper horizons), while North Rhyne is largely depleted in Fe.

Magnesium, K, and Ca are susceptible to hydrolysis and become depleted with in situ chemical weathering. In all the soil pits, Mg, K, and Ca are depleted regardless of the immobile element in the tau ratio. This suggests that soils in both watersheds have been subject to significant chemical weathering over time.

Future work could account for geologic complexity by using the bottommost soil horizon (saprolite) to estimate the local parent material for each pit following McIntosh (2017). However, using the saprolite from each pit as a reference would provide a conservative estimate of the chemical depletion since regolith in the Piedmont is so deeply weathered. Alternatively, the composition of the protolith could be redefined from hard rock samples in each watershed instead of using a single averaged indicator of composition for both watersheds.

6.2 Weathering differences as a function of aspect

North-facing hillslopes in the Northern Hemisphere receive less sunlight and maintain higher soil moisture content than south-facing hillslopes, facilitating more weathering on north-facing slopes (Jenny 1941). At Redlair, soils on north-facing hillslopes—regardless of watershed-- have lower pedogenic iron ratios and higher organic content than their south-facing counterparts in all watersheds (Figures 5.1, 5.6, 5.7, Tables 5.1, 5.2). Higher moisture content in soils can promote chemical weathering through dissolution and hydrolysis of minerals, accelerating the breakdown of minerals. Bulk tau ratios show that north-facing hillslopes show greater enrichment of Si/Al in the upper, colluvial portions of the slope (Unit 4 and 3) than their south-facing counterparts, but there are no significant differences in chemical enrichment/ depletion at greater depths (Figure 5.10). Low pedogenic iron and high organic content, regardless of hillshed order, suggest more available moisture promotes a higher degree of weathering on north-facing hillslopes.

6.3 Weathering differences as a function of hillslope position

Weathering/soil profiles share common characteristics common between watersheds but depend on hillslope position. Clay and silt content are highest on the summits and shoulders of interfluves, while sand and gravel content increases towards the valley bottoms as hillslope

sediments thicken. Sand content also increases in the colluvial and alluvial (backslope and toeslope) hillslope sediments (Figure 5.6). Organic content is also highest in samples from hillslope summits and shoulders, as seen in North Rhyne (Figure 5.6). Downslope, sediment has been significantly reworked and no contrast in organic content is identifiable between lower backslope and toeslope positions.

Although hillshed position has a greater effect on chemical enrichment/depletion than landscape position, it is apparent that toeslope positions have less variable tau values with depth compared to the upper sections of the hillslopes. In general, toeslope pits seem to be depleted in Fe, which could be because hillslope sediments are more likely to be saturated. Furthermore, the most enriched Fe values are in the sediment in the upper horizons of the soil profiles (Units 4 and 3) (Appendix N). Because iron accumulates via secondary weathering and redox conditions, the enrichment signals of Fe seen in the summit, shoulder, and backslope positions of Units 4 and 3 indicate sufficient moisture available to facilitate oxidation in these landscape positions, whereas toeslope positions often have conditions that favor reduction and mobilization of iron out of the soil profile.

6.4 Mobile sediment variability between hillsheds, aspects, and hillslope position

The presence of different sedimentary units throughout the study area suggests that 1) sedimentary deposits are ubiquitous across Piedmont upland soils and 2) sediment mobilization varies as a function of location within the landscape.

With respect to the latter, it appears sediment moves across the landscape at different rates based on watershed proximity to a major river. Distal hillslopes are more gently undulating than proximal hillslopes, which have steep slopes and more frequent small gullies (Slope steepness ~ 7-10% vs. 15-20%, respectively; Figure 5.1). Soils on distal hillslopes have thinner

sedimentary packages and no buried soils except in toeslope positions. Overall, the hillslope sediments exhibit more weathering than surface soils in North Rhyne, with Unit 2 exposed at the surface most frequently (Figure 5.1, 5.9).

The data on the ternary plot clusters by watershed based on SiO2—Fe2O3 content indicatesthe possibility of lithological or weathering differences between the watersheds (Figure 5.9). Duffey watershed samples displayed consistently higher Fe2O3 content, which could be attributed to its stability and deeper weathering profiles than in North Rhyne (Figure 5.8). In contrast, higher silica content (likely in quartz sand) in colluvium compared to residuum could indicate that North Rhyne is comparatively less stable (Figure 5.8). Sand content in North Rhyne is significantly higher than in Duffey ($p = 2.24E-07$), which supports this hypothesis. The protolith chemical values fall in between Duffey and North Rhyne indicating an intermediate Al2O3 content, lower Fe2O3 compared to Duffey, and higher SiO2 compared to most of North Rhyne (Figure 5.9).

Hillslope aspect contributes to weathering differences that affect hillslope stability and erosion. North-facing hillslopes have soils forming in deeper sediment that is more weathered - as evidenced by higher clay and gravel content throughout the profile than south-facing hillslopes (Figures 5.4, 5.6). North-facing hillslopes also exhibit more frequent and thicker buried soils with higher values of Si/Al chemical enrichment than their south-facing counterparts, which indicates increased sediment production on north-facing hillslopes. In North Rhyne and Duffey, north-facing hillslopes are slightly steeper than south-facing hillslopes (Figure 5.1). Excessive moisture reduces the cohesion of soil particles, inciting slope failures even at a small scale. Greater insolation on south-facing hillslopes is associated with more frequent wetting-drying events, a process associated with gravitational collapse of regolith and

downslope creep (e.g., Anderson et al., 2013). Gravity-driven erosion on south-facing slopes has likely removed material off south-facing hillslopes, resulting in shallower sediment and hillslopes with lower relief on south-facing slopes. The topographic asymmetry suggests that microclimatic differences have been sustained over the Holocene.

Hillslope position also impacts variability in sediment mobility. Overall, more sediment accumulates, as expected, in footslope and toeslope positions with up to ~2 m of Holocene sediment overlying saprolite (Figure 3.9). Toeslope sediments are comprised primarily of colluvial and alluvial sediment (Units 4 and 3), show enrichment of Si/Al throughout their entire profiles (Figure 5.10), and have sandier compositions than their upslope counterparts (Figure 5.4, 5.5, 5.6). Gravel content is consistently higher in footslope and toeslope positions in both watersheds (Figure 5.6). These characteristics are supportive of downslope sediment transport by water action.

6.5 Sediment mobilization and climate change

Comparisons of 14C charcoal ages from the hillslope sediments with regional paleoclimatic records (figure 5.2) help understand Holocene climate and landscape change in the SE Piedmont. These comparisons show that Holocene episodes of sediment erosion, transportation, and deposition of sediment are likely influenced by the following climate-related perturbations: 1) increased fire activity, 2) shifts to warmer vegetation types, and 3) increases in the frequency and intensity of large rainfall events. Changes in the frequency and intensity of rainfall seem to have the greatest influence on Piedmont soils and sediments. Each of these climatic changes likely increase sediment discharge and preservation on hillslopes and valley bottoms. Most radiocarbon ages are concentrated in the late Holocene (Figure 5.11). The burial of these samples under variable amounts of sediment suggests that after the deposition of these

samples in the late Holocene, there has been significant hillslope erosion and valley bottom deposition across hillslopes at Redlair.

While field evidence supports that hillslope sediment transportation and deposition is preserved during the late Holocene (Figure 5.11), there is insufficient detail in the climate record in the last 6,000 years to attribute the aggradation to any climate event (Figure 5.3). Studies in the southwestern US (Johnson et al. 2011, Bacon et al. 2017) show evidence that Holocene landforms respond to climate fluctuations driven, in part, by El Niño Southern Oscillation events in the late Holocene. Johnson (2011) proposed that stronger climate switching and variable precipitation associated with an increase in intensity of El Niño drives late Holocene sedimentation off small watershed hillslopes in the San Juan Mountains. In the Piedmont, warm phase El Niño Southern Oscillation events are known to result in increased storminess, precipitation, and flooding (Cahoon 2012). Independent records of late Holocene hillslope sedimentation reconstructed from alluvial fans in the SE Piedmont attribute periods of fan aggradation to higher precipitation intensity (Opalka 2022). Still, a more detailed climate record from the SE Piedmont is needed to definitively attribute aggradation to regional climate.

The most notable climatic change evident in the compilation of data (Figure 5.3) occurs around the Pleistocene to Holocene transition. However, at Redlair and in other places in the Piedmont (e.g. Opalka et. Al 2022) there are few if any records of the preservation of deposited sediment from this time. Some studies suggest Late Pleistocene and Early Holocene sediment is stored offshore (e.g. Carver 1971).

The timing of deposition of the sedimentary units across Redlair Observatory toposequences may be correlated based on radiocarbon ages, sedimentology, and stratigraphy.

The ages of the stratigraphic units coincide with periods of known sediment mobilization caused by climate change and anthropogenic activity in the Piedmont (Figure 5.1, Figure 5.3).

In general, we find Units 4 and 3 to be enriched in silica, which is a residual element that likely indicates the presence of quartz sand and is likely to have been incorporated into regolith by sediment mobilization. Thus, associated Si/Al values indicate of colluvium. Toeslope pits (like NR-S1 and DU-S4), which are comprised primarily of colluvial and alluvial sediment in Units 4 and 3, show enrichment of Si/Al throughout their entire profiles. However, another toeslope pit (NR-S8) which has much older radiocarbon ages than the rest of the toeslope pits, NR-S8, does not follow this trend, suggesting that the enrichment signal might be time dependent. Units 4 and 3 date to the late Holocene and have valley bottom alluvial features like cumulic horizons, graded bedding, and overall sandier and poorly sorted compositions which all suggest down slope sediment erosion.

It is clear from the burial of radiocarbon dated charcoal at variable depths across all hillslope positions, however, that not all sediment is trapped in the valley bottoms. Most of the dates cluster to the mid and late Holocene, postdating 1786 cal YBP with two exceptions; a finding consistent with local sediment studies done in the Uwharrie (Opalka et al. 2022). There is a lack of Pleistocene charcoal dates from Redlair Observatory and other locations in the Piedmont, suggesting conditions were such that sediment was not being produced, or that material has since been flushed out of the system.

Radiocarbon dates from Unit 2 average 5888 +/- 72 calibrated YBP, (n=2, Table 5.3). Paleoclimate records indicate that before this date the Piedmont had a climate with cooler winters, increased storminess, and was likely wetter relative to the past. Some climate records (Spencer, 2017; Willard 2023) indicate that the climate from about 10000 to 8000 calibrated

YBP also supported a shift to warmer vegetation types, similar to oak / hickory assemblages. These records also indicate brief periods of increased fire activity after establishing new warmer vegetation types around 7000 to 6500 calibrated YBP (Spencer, 2017; Willard 2023) (Figure 5.3). Studies in semi-arid landscapes show evidence supporting fire-driven hillslope sedimentation on Holocene fluvial terraces (Pierce 2011), but nowhere in the field area was there evidence of significant wildfire activity (e.g. charcoal beds, abundant charcoal). Climate records from the Coastal Plain (Krause 2018; Willard 2023) indicate increased fire activity in White Pond, SC and the Great Dismal Swamp, VA in the last 1000 calibrated YBP, pointing to anthropogenic influence (Figure 5.3).

The oldest unit observed in the field area shows no evidence of sediment mobilization. Unit 1 is present on the most stable portions of the landscape, showing evidence of in situ weathering, including primary structures in the saprolite, few to no clay films, and no gravel content. In Unit 1, organic content (9% in Unit 1) is significantly higher than in the overlying units, including Unit 4 (Table 5.3). Organic content accumulates in weathering profiles over time as landscapes are sufficiently stable to accumulate organic matter. Therefore, the high organic content in Unit 1 supports the soil's stability.

Overall, we recognize that soils are perpetually creeping towards lower energy states, and this movement decreases exponentially with depth (Deshpande et al. 2021), but this movement is punctuated by more extreme erosional and depositional events caused by climatic changes (Figure 5.3). Sedimentary Units 4, 3, and 2 represent discrete allostratigraphic units with radiocarbon ages corresponding to different periods of climatic activity (Figures 5.1, 5.11, Table 5.4) By understanding the source of sediment on hillslopes and the drivers of deposition in the

Holocene, this study can contribute to interpreting hillslope behavior in the Piedmont during the Pleistocene.

6.6 Particle size and organic content comparisons with Deep Creek

Soil characteristics of North Rhyne (2nd order hillshed) and Duffey watersheds (5th order hillshed) were compared to those of the previously excavated Deep Creek watershed (3rd order hillshed). Previous work by Nelson (2022) identified thick packages of colluvium across multiple backslope and shoulder positions in Deep Creek watershed in Redlair Observatory. Here, particle size and organic content is compared between all three watersheds.

Although no significant difference is observed between the gravel content of Duffey and North Rhyne ($p = 0.234$), Deep Creek has the highest gravel content at a significance level of $p= 2.63e-7$. Deep Creek has much higher gravel content (average of 13.6%) compared to North Rhyne and Duffey (averages of 3.76% and 5.26%, respectively) (Table 5.1). Deep Creek has significantly higher sand content than either North Rhyne or Duffey ($p=1.13e-14$). No difference was observed between the silt content of North Rhyne and Duffey ($p= 0.07$), but Deep Creek has lower silt than the other two watersheds ($p= 3.73e-9$) (Table 5.2). No trends in particle size were observed between the east- and west-facing hillslopes of Deep Creek watershed. Because the bedrock parent material in Deep Creek is similar to quartz sericite schist (Zbs, Figures 3.1, 3.2) (pers. comm. M.C. Eppes), we conclude that the differences in particle size exhibited by Deep Creek are likely a result of a change in protolith instead of differential weathering between the watersheds.

Duffey contains significantly more organic matter than North Rhyne or Deep Creek ($p= 1.68e-35$), suggesting that distal hillslopes are more stable landscape positions. Following the same line of thinking, Deep Creek has much lower organic content across every hillslope

position and aspect, reflecting its instability. Deep Creek has steeper slopes and more frequent small landslides than either North Rhyne or Duffey, which support this claim.

6.7 Implications

The findings of this study stand in direct contrast to long-held paradigms of in situ residual soil formation on Piedmont landscapes. This study shows that hillslope sediments illuminate processes of landscape evolution based on soil variability and moisture regimes (e.g. Butleretal., 1986). In particular, this research will contribute to understanding two important environmental problems: carbon storage and stream sediment supply.

Hillslope erosion and deposition in low-order watersheds is a key contributing factor in global carbon storage (e.g. Berhe et al. 2007), and sediment is the leading pollutant of east coast streams (e.g. Lyons et al. 2015). Soil carbon sequestration is expected to peak in the next ~50 years in the Southeast (Albani et al. 2006). This timing holds important implications for the management and protection of a previously under-appreciated carbon reservoir in the Piedmont since paleosols and buried soils are known to contain soil organic carbon pools that cycle at slower rates than surface soils (e.g. Longbottom et al. 2022). For example, the study presented here suggests that high-order hillsheds have higher organic content thank lower-order hillsheds, and therefore high-order hillsheds should be accorded greater recognition as substantial carbon reservoirs. Additionally, studies of zero-order watersheds need to identify the hillshed order; evidence from North Rhyne and Duffey watersheds elucidate different weathering characteristics between zero order watersheds. Critical zone studies that seek to characterize regional soil and sediment patterns should take hillshed order into account. Developing a better understanding of the timing and spatial patterns of sediment transport can also help archaeologists working on hillslopes understand where cultural sites of varying ages are likely to be preserved or eroded

from the landscape. This research can contribute to developing management strategies and best practices for future urban development and erosion control in this rapidly growing region by identifying factors that control sediment transport and stability.

CHAPTER 8: CONCLUSIONS

The analysis of soil and sedimentary profiles at Redlair Observatory illuminates landscape evolution in the Piedmont during the Holocene, based especially on processes of episodic deposition from uplands to lowlands. The amount of sediment and the extent to which it is weathered depends on geomorphic variables, such as proximity to major rivers, hillslope position, and aspect. Discrete allostratigraphic units can be defined within each watershed based on unconformities.

The analysis of evidence from soil excavations at Redlair Observatory presented in this study refutes the assumption that Piedmont soils are uniformly the result of *in situ weathering of bedrock*. Instead, they are often developed in transported materials that have been moved and deposited by colluvial or alluvial action (or a combination of the two). In addition, either one (whether developed from crystalline bedrock or from sediment) may have migrated downslope due to gravity (soil creep or slump), water (sheet or rill wash), freeze/thaw cycles, anthropogenic or natural erosion (resulting in sudden vegetation loss and/or removal of the B horizon) during or after the development of a mature soil profile.

The major soil series of the Piedmont (Ultisols) are defined by residual profiles, but the evidence presented in this thesis combined with historic investigations of Piedmont sediments, shows that few soils do not show evidence of migration.

The sedimentary units defined in each toposequence loosely correlate with climatic and vegetation change, the onset of fire activity resulting in rapid vegetation loss, and increased storminess. This combination of variables suggests a climatically induced sediment mobilization. Chronofunctions demonstrate that soils have different spatial and temporal evolutionary histories, which depend on both hillslope position (including aspect) and watershed position

within broader landscapes. In conclusion, there is abundant evidence of hillslope sediment erosion, transportation, and deposition in the SE Piedmont. This activity depends on geomorphic factors like aspect (N & S) and proximity to the major, high-order rivers.

REFERENCES

Albani, M., et al. (2006). "The contributions of land-use change, CO2 fertilization, and climate variability to the Eastern US carbon sink." Global Change Biology 12(12): 2370-2390.

Anderson, R.S., Anderson, S.P., and Tucker, G.E., 2013, Rock damage and regolith transport by frost: An example of climate modulation of the geomorphology of the critical zone: Earth Surface Processes and Landforms, v. 38, p. 299– 316, doi:10.1002/esp.3330.

Arey, J. V. (2018). "STRATIGRAPHY AND SOILS OF FLUVIAL TERRACES ON THE CATAWBA RIVER, NC AND SC: LANDSCAPE EVOLUTION OF THE SOUTHEASTERN US."

Bacon, S. N., et al. (2017). "Timing and distribution of alluvial fan sedimentation in response to strengthening of late Holocene ENSO variability in the Sonoran Desert, Southwestern Arizona, USA." Quaternary Research 73(3): 425-438.

Bartz, M., et al. (2022). "Potential impacts of chemical weathering on feldspar luminescence dating properties." Geochronology.

Bateman, M. D., et al. (2007). "Detecting post-depositional sediment disturbance in sandy deposits using optical luminescence." Quaternary Geochronology 2(1-4): 57-64.

Bazilevskaya, E., et al. (2012). "Where fast weathering creates thin regolith and slow weathering creates thick regolith." Earth Surface Processes and Landforms 38(8): 847-858.

Berut, A., et al. (2019). "Brownian Granular Flows Down Heaps." Phys Rev Lett 123(24): 248005.

Birkeland, P. (1999). "Soils and Geomorphology." Oxford University Press(3rd Edition).

Bloom, A. L. (2001). "Teaching about relict, no-analog landscapes." Geomorphology.

Brecheisen, Z. S., et al. (2021). "Quantitative analysis of hillshed geomorphology and critical zone function: Raising the hillshed to watershed status." GSA Bulletin.

Brimhall, G. H. and W. E. Dietrich (1987). "Constitutive mass balance relations between chemical composition, volume, density, porosity, and strain in metasomatic hydrochemkai systems: Results on weathering and pedogenesis." Geochimico et Cosmhimicn Acta 51.

Bryan, K. (1940). "Gully Gravure — A Method of Sloe Retreat." Journal of Geomorphology III: 89 to 107.

Bryan, K. (1940). "The Retreat of Slopes." Annals of the Association of American Geographers 30: 254-268.

Bull, W. B. (1991) *Geomorphic responses to Climatic Change*, New York, NY (United States); Oxford University Press.

Burnett, B. N., et al. (2008). "Aspect-related microclimatic influences on slope forms and processes, northeastern Arizona." Journal of Geophysical Research 113(F3).

Byers, H. G., et al. (1938). "Formation of Soil." USDA publications.

Cahoon, L.B. (2012) El Niño–Southern Oscillation Effects on River Flows in the Lower Cape Fear River Watershed, North Carolina. *Journal of North Carolina Academy of Science*, 128(3), pp.74-80.

Cain, S. A. (1944). "Pollen Analysis of Some Buried Soils, Spartanburg County, South Carolina." Bulletin of the Torrey Botanical Club 71: 11-22.

Carroll, W. D., et al. (2002). "Ch 24: Historical overview of the southern forest landscape and associated resources." Southern Forest Resource Assessment: 583-605.

Carver, R. E. (1971). "HOLOCENE AND LATE PLEISTOCENE SEDIMENT SOURCES, CONTINENTAL SHELF OFF BRUNSWICK, GEORGIA." Journal of Sedimentary Petrology **41**: 517-525.

Chadwick, O. A., et al. (1990). "From a black to a gray box: A mass balance interpretation of pedogenesis." Geomorphology 3: 369-390.

Clark, M. (1993). "Quaternary Geology and Geomorphology of part of the inner Piedmont of the Southern Appalachians in the Columbus Promontory Upland Area, Southwestern North Carolina and Northwestern South Carolina." Carolinas Geological Society.

Clark, M. and S. Kite (2000). "An Introduction to some recent advances in regolith research in the Appalachians beyond the late Wisconsonian glacial borders." Southeastern Geology 39.

Costa, J. E. (1975). "Effects of agriculture on erosion and sedimentation in the Piedmont Province, Maryland." Geological Society of America Bulletin 86: 1281-1286.

Culling, W. E. H. (1963). "Soil Creep and the Development of Hillside Slopes." The Journal of Geology 71: 127-161.

Daniels, R. B. (1987). "Soil erosion and degradation in the southern Piedmont of the USA." Land Transformation in Agriculture: 407-428.

Davis, W. M. (1889). "Topographic Development of the Triassic Formation of the Triassic Formation of the Conneticut Valley." American Journal of Science Art. XLIII.

Davis, W. M. (1899). "The Geographical Cycle." The Geographical Journal **14**: 481-505.

Deshpande, N. S., et al. (2021). "The perpetual fragility of creeping hillslopes." Nat Commun 12(1): 3909.

Desta, F., et al. (2004). "Aspect Induced Differences in Vegetation, Soil, and Microclimatic Characteristics of an Appalachian Watershed." Castanea **69**.

Dotterweich, M., et al. (2014). "Natural and human-induced prehistoric and historical soil erosion and landscape development in Southwestern Tennessee, USA." Anthropocene 8: 6-24.

Eargle, D. H. (1937). "Physiographic Factors Affecting Stable Gullies in the S.C. Piedmont."

Eargle, D. H. (1940). "New Light on the Origin and History of Piedmont Soils and Surface."

Eargle, D. H. (1946). Pleistocene soils of the Piedmont of South Carolina, University of South Carolina.

Eargle, D. H. (1977). "PIEDMONT PLEISTOCENE SOILS OF THE SPARTANBURG AREA, SOUTH CAROLINA."

Eargle, D. H. and C. F. S. Sharpe (1938). "Report on Geomorphic Studies in the Southern Piedmont."

Ehlers, J., et al. (2018). Quaternary Glaciations and Chronology. Past Glacial Environments: 77-101.

Eppes, M. C. (2019). "Laboratory Instruction Manual." Department of Geography & Earth Sciences Soil Laboratory.

Eppes, M. C. and B. G. Johnson (2021). Describing Soils in the Field: A Manual for Geomorphologists. Reference Module in Earth Systems and Environmental Sciences.

Eppes, M. C. and L. McFadden (2008). "Holocene climates, San Bernardino Mountains, California, USA." The Holocene.

Eppes, M. C., et al. (2002). "Influence of soil development on the geomorphic evolution of landscapes: An example from the Transverse Ranges of California." Geology 30.

Ferguson, T. (2022).

Foss, J. E., et al. (1981). Soils of the Savannah River valley, Soil Resource Analysts.

Frankel, K. L., et al. (2007). "Knickpoint evolution in a vertically bedded substrate, upstream-dipping terraces, and Atlantic slope bedrock channels." Geological Society of America Bulletin 119(3-4): 476-486.

Gallen, S. F., et al. (2013). "Miocene rejuvenation of topographic relief in the southern Appalachians." GSA Today 23(2): 4-10.

Gallen, S. F., et al. (2011). "Hillslope response to knickpoint migration in the Southern Appalachians: implications for the evolution of post-orogenic landscapes." Earth Surface Processes and Landforms 36(9): 1254-1267.

Gallen, S. F. (2018). "Lithologic controls on landscape dynamics and aquatic species evolution in post-orogenic mountains." Earth and Planetary Science Letters **493**: 150-160.

Garner, H.F., 1974, Origin of Landscapes: Oxford University Press, p.734.

Gilbert, G. K. (1877). "Report on the Geology of the Henry Mountains." US Geographical and Geological Survey of the Rocky Mountain Region. Washington, DC: U.S. Gov. Print. Office.

Gliganic, L. A., et al. (2015). "All mixed up: Using single-grain equivalent dose distributions to identify phases of pedogenic mixing on a dryland alluvial fan." Quaternary International 362: 23-33.

Goldsmith, R., et al. (1988). "GEOLOGIC MAP OF THE CHARLOTTE l° x 2° QUADRANGLE, NORTH CAROLINA AND SOUTH CAROLINA." DEPARTMENT OF THE INTERIOR U.S. GEOLOGICAL SURVEY.

Hack, J. (1975). "Dynamic Equilibrium and Landscape Evolution."

Hack, J. T. (1960). "nterpretation of erosional topography in humid temperate regions." American Journal of Science 258-A: 80–97.

Heimsath, A. M., et al. (1997). "The soil production function and landscape equilibrium." Nature.

Holbrook, W. S., et al. (2019). "Links between physical and chemical weathering inferred from a 65-m-deep borehole through Earth's critical zone." Sci Rep 9(1): 4495.

Ireland, H. A. (1939). "“Lyell” Gully, A Record of a Century of Erosion." Journal of Geology 47: 47-63.

Ireland, H. A., et al. (1939). Principles of gully erosion in the Piedmont of South Carolina, US Department of Agriculture.

Jenny, H. (1941). "Factors of Soil Formation — A System of Quantitative Pedology."

Joffe, J. S. (1936). Pedology.

Johnson, B. G., et al. (2011). "Post-glacial landscape response to climate variability in the southeastern San Juan Mountains of Colorado, USA." Quaternary Research 76(3): 352-362.

Johnson, D. and D. Watson-Stegner (1987). "Evolution Model of Pedogenesis." Soil Science 143(5): 349-366.

Kellogg, C. E. (1936). "Development and Significance of the Great Soil Groups of the United States." USDA.

Kerr, W. C. (1875). Report of the geological survey of North Carolina. : Volume I. Physical geography, resumé, economical geology, Josiah Turner, state printer and binder.

Kerr, W. C. (1881). "On the action of frost in the arrangement of superficial earthy material." Am. Jour. Sci 21: 345.

Kleiss, J. H. (1970). "Hilllslope sedimentation and soil formation in northeastern Iowa." Soil Science Society of America 34.

Layzell, A., et al. (2012). "A Soil Chronosequence Study on Terraces of hte Catawba River Near Charlotte, NC: Insights Into The Long-Term Evolution of a Major Atlantic Piedmont Drainage Basin." Southeastern Geology 49: 13-24.

Layzell, A. L. and R. D. Mandel (2014). "An assessment of the erodibility of Holocene lithounits comprising streambanks in northeastern Kansas, USA." Geomorphology 213: 116-127.

Leigh, D., et al. (2004). "Late Pleistocene braided rivers of the Atlantic Coastal Plain, USA." Quaternary Science Reviews 23(1-2): 65-84.

Leigh, D. S. (2008). "Late Quaternary climates and river channels of the Atlantic Coastal Plain, Southeastern USA." Geomorphology 101(1-2): 90-108.

Leigh, D. S. and P. A. Webb (2006). "Holocene erosion, sedimentation, and stratigraphy at Raven Fork, Southern Blue Ridge Mountains, USA." Geomorphology 78: 161-177.

Liu, Z., et al. (2009). "Transient Simulation of Last Deglaciation with a New Mechanism for Bølling-Allerød Warming."

Longbottom, T., et al. (2022). "What's Soil Got to Do with Climate Change?" GSA Today 32(5): 4-10.

Lyons, N. J., et al. (2015). "Bank erosion of legacy sediment at the transition from vertical to lateral stream incision." Earth Surface Processes and Landforms 40(13): 1764-1778.

Markewich, H. W., et al. (1990). "Contrasting soils and landscapes of the Piedmont and Coastal Plain, eastern United States." Geomorphology 3.

McCracken, R., et al. (1989). "Undisturbed Soils, Landscapes, and Vegetation in a North Carolina Piedmont Virgin Forest."

McDonald, E. V. (2015). "Iron Extraction (Hydroxylamine Method)." The Desert Research Institute Soil Characterization and Quaternary Pedology Laboratory Methods Manual 3.3: 58-59.

Mehra, O. P. and M. L. Jackson (1960). "Iron oxide removal from soils and clays by a dithionite– citrate system buffered with sodium bicarbonate." Elsevier: 317-327.

Meyerhoff, H. A. (1980). "The Penckian Model - With Modifications."

Mills, H. H. (2000). "Apparent increasing rates of stream incision in the eastern United States during the late Cenozoic." Geology.

Morisawa, M. (1968). Streams: their dynamics and morphology, McGraw-Hill Book Company.

Nelson, M. S., et al. (2022). "Quartz luminescence sensitivity from sediment versus bedrock in highly weathered soils of the Piedmont of North Carolina, south-eastern USA." Quaternary Geochronology 72.

Neustruev, S. S. (1927). "Genesis of Soils." Russian Pedological Investigations.

NOAA (1895-2022). "Climate at a Glance: Statewide Time Series, Average Temperature, published October 2022, retrieved on November 1, 2022 from https://www.ncdc.noaa.gov/cag/." National Centers for Environmental information.

Nowak, E. R., et al. (2001). "Density-noise power fluctuations in vibrated granular media." Phys Rev E Stat Nonlin Soft Matter Phys 63(2 Pt 1): 020301.

Opalka, C. E., et al. (2022). "Alluvial fan aggradation in low relief, humid-temperate landscapes, Uwharrie National Forest, North Carolina Piedmont." Earth Surface Processes and Landforms.

Overstreet, W. C., et al. (1968). Fluvial monazite deposits in the southeastern United States, with a section on mineral analyses, US Govt. Print. Off.

Patton, N. R., et al. (2018). "Predicting soil thickness on soil mantled hillslopes." Nat Commun 9(1): 3329.

Pelletier, J. D., et al. (2018). "Which way do you lean? Using slope aspect variations to understand Critical Zone processes and feedbacks." Earth Surface Processes and Landforms 43(5): 1133-1154.

Persico, L. P., et al. (2021). "Late Quaternary geochronologic record of soil formation and erosion: Effects of climate change on Mojave Desert hillslopes (Nevada, USA)." Geology 50(1): 54-59.

Pierce, J., et al. (2011). "The relation of Holocene fluvial terraces to changes in climate and sediment supply, South Fork Payette River, Idaho." Quaternary Science Reviews(5-6): 628-645.

Price, J. (2009). "Geology of Redlair Preserve, NC."

Reimann, T., et al. (2017). "Getting a grip on soil reworking – Single-grain feldspar luminescence as a novel tool to quantify soil reworking rates." Quaternary Geochronology 42: 1-14.

Richter, D. D., et al. (2020). "Soil production and the soil geomorphology legacy of Grove Karl Gilbert." Soil Science Society of America Journal 84(1): 1-20.

Schaetzl, R. J. (2013). 4.9 Catenas and Soils. Treatise on Geomorphology: 145-158.

Service, S. C. (1969). "Soil Survey of Gaston County, North Carolina." USDA.

Sharpe, C. F. S. (1941). "Geomorphic Aspects of Normal and Accelerated Erosion."

Singer, M. J. and P. Janitzky (1986). "Field and Laboratory Procedures used in a Soil Chronosequence Study: Bulk Density-paraffin clod method." U.S. Geological Survey Bulletin: 18-19.

Soller, D. R. and H. H. Mills (1991). The Geology of the Carolinas. Knoxville, University of Tennessee PRess.

Spell, R. L. and B. G. Johnson (2019). "Anthropogenic alluvial sediments in North Carolina Piedmont gullies indicate swift geomorphic response to 18th century land-use practices." Physical Geography 40(6): 521-537.

Stephens, R. B. (1977). "Soil survey of Guilford County, N.C." USDA-SCS, Washington, DC.

Thompson, D. W. J. and J. M. Wallace (2001). "Regional Climate Impacts of the Northern Hemisphere Annular Mode." Science.

Trimble, S. W. (1974). "Man-induced soil erosion in the southern Piedmont." Soil Conservation Service. Ankey, IA.

USDA-NRCS (2014). "Keys to Soil Taxonomy." United States Department of Agriculture Natural Resources Conservation Service Twelfth Edition.

Viles, H. A., et al. (2021). "Ants as geomorphological agents: A global assessment." Earth-Science Reviews 213.

Webb, T., et al. (1993). Vegetation, Lake Levels, and Climate in Eastern North America for the Past 18,000 Years. Global Climates since the Last Glacial Maximum. H. E. W. Jr., J. E. Kutzbach, T. Webb et al., University of Minnesota Press.

West, N., et al. (2013). "Regolith production and transport at the Susquehanna Shale Hills Critical Zone Observatory, Part 2: Insights from meteoric10Be." Journal of Geophysical Research: Earth Surface 118(3): 1877-1896.

Williams, J. W., et al. (2000). "Late Quaternary biomes of Canada and the eastern United States." Journal of Biogeography 27: 585-607.

Appendix A: Field methods from North Rhyne and Duffey watersheds, Redlair Observatory, NC

The following data was collected by Alec Wells, Mac Bouzigard, Robert B. Griffin, Matt Yankech, Morgan Rinehart, Mai Vang, Kayla Eury, Matthew Tovey, Stephen Lail, Dale Strong, Nora Vaughan, and the Dr. Eppes's Applied Soil Science Class ('22) following instructions in Eppes and Johnson (2021), including their *Soil Description Sheet*, seen here:

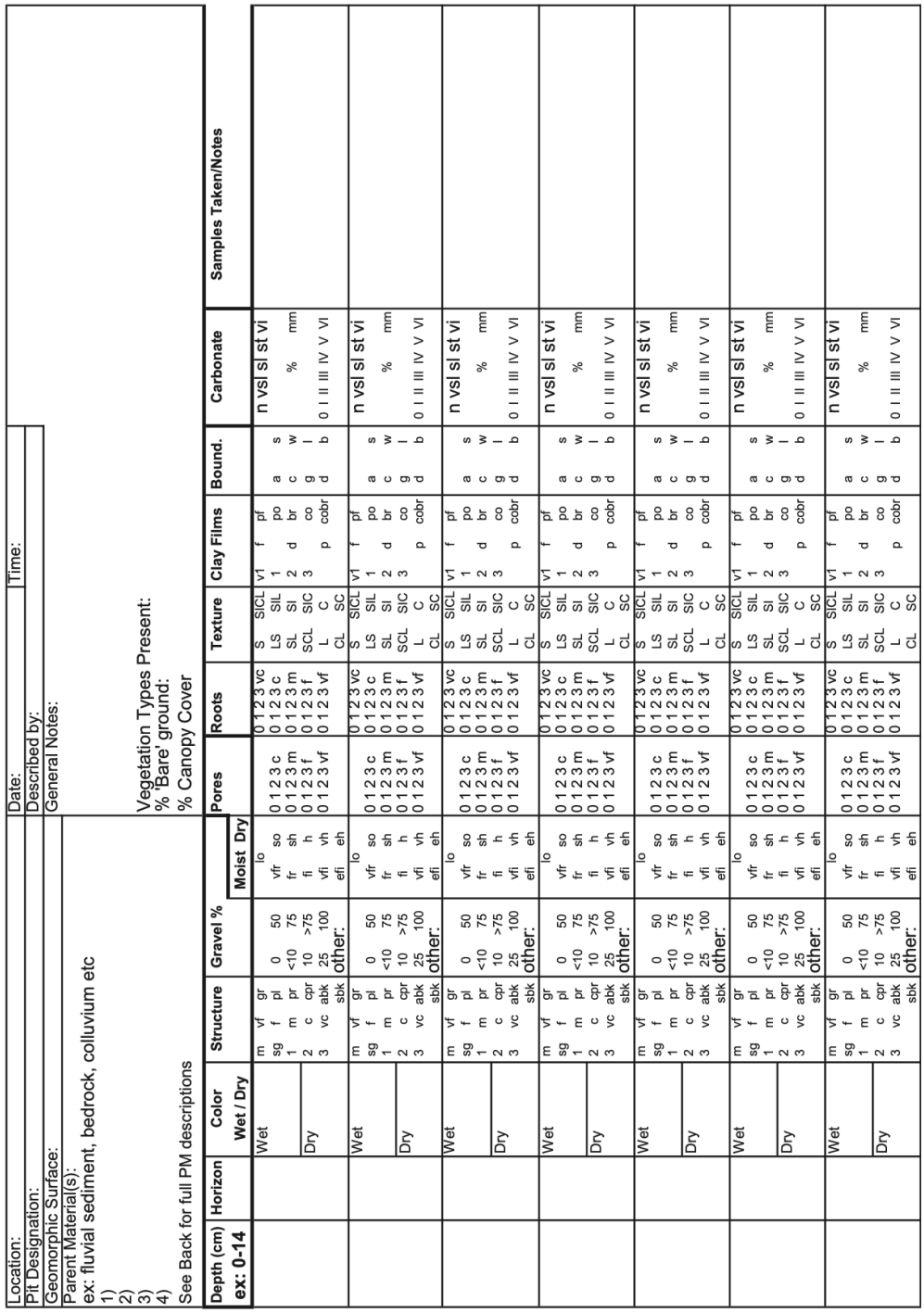

Location: Date: Time:
Pit Designation: Described by:
Geomorphic Surface: General Notes:
Parent Material(s):
ex: fluvial sediment, bedrock, colluvium etc
1)
2)
3)
4)
See Back for full PM descriptions

Vegetation Types Present:
% 'Bare' ground:
% Canopy Cover

Depth (cm) ex: 0-14	Horizon	Color Wet / Dry	Structure	Gravel %	Moist Dry	Pores	Roots	Texture	Clay Films	Bound.	Carbonate	Samples Taken/Notes
		Wet	m vf gr sg f pl 1 m pr 2 c cpr 3 vc abk sbk	0 50 <10 75 10 >75 25 100 other:	lo vfr so fr sh fi h vfi vh efi eh	0 1 2 3 c 0 1 2 3 m 0 1 2 3 f 0 1 2 3 vf	0 1 2 3 vc 0 1 2 3 c 0 1 2 3 m 0 1 2 3 f 0 1 2 3 vf	S SiCL LS SiL SL SI SCL SiC L C CL SC	v1 f pf 1 po 2 d br 3 co p cobr	a s c w g l d b	n vsl sl st vi % mm 0 I II III IV V VI	
		Dry										
		Wet	m vf gr sg f pl 1 m pr 2 c cpr 3 vc abk sbk	0 50 <10 75 10 >75 25 100 other:	lo vfr so fr sh fi h vfi vh efi eh	0 1 2 3 c 0 1 2 3 m 0 1 2 3 f 0 1 2 3 vf	0 1 2 3 vc 0 1 2 3 c 0 1 2 3 m 0 1 2 3 f 0 1 2 3 vf	S SiCL LS SiL SL SI SCL SiC L C CL SC	v1 f pf 1 po 2 d br 3 co p cobr	a s c w g l d b	n vsl sl st vi % mm 0 I II III IV V VI	
		Dry										
		Wet	m vf gr sg f pl 1 m pr 2 c cpr 3 vc abk sbk	0 50 <10 75 10 >75 25 100 other:	lo vfr so fr sh fi h vfi vh efi eh	0 1 2 3 c 0 1 2 3 m 0 1 2 3 f 0 1 2 3 vf	0 1 2 3 vc 0 1 2 3 c 0 1 2 3 m 0 1 2 3 f 0 1 2 3 vf	S SiCL LS SiL SL SI SCL SiC L C CL SC	v1 f pf 1 po 2 d br 3 co p cobr	a s c w g l d b	n vsl sl st vi % mm 0 I II III IV V VI	
		Dry										
		Wet	m vf gr sg f pl 1 m pr 2 c cpr 3 vc abk sbk	0 50 <10 75 10 >75 25 100 other:	lo vfr so fr sh fi h vfi vh efi eh	0 1 2 3 c 0 1 2 3 m 0 1 2 3 f 0 1 2 3 vf	0 1 2 3 vc 0 1 2 3 c 0 1 2 3 m 0 1 2 3 f 0 1 2 3 vf	S SiCL LS SiL SL SI SCL SiC L C CL SC	v1 f pf 1 po 2 d br 3 co p cobr	a s c w g l d b	n vsl sl st vi % mm 0 I II III IV V VI	
		Dry										
		Wet	m vf gr sg f pl 1 m pr 2 c cpr 3 vc abk sbk	0 50 <10 75 10 >75 25 100 other:	lo vfr so fr sh fi h vfi vh efi eh	0 1 2 3 c 0 1 2 3 m 0 1 2 3 f 0 1 2 3 vf	0 1 2 3 vc 0 1 2 3 c 0 1 2 3 m 0 1 2 3 f 0 1 2 3 vf	S SiCL LS SiL SL SI SCL SiC L C CL SC	v1 f pf 1 po 2 d br 3 co p cobr	a s c w g l d b	n vsl sl st vi % mm 0 I II III IV V VI	
		Dry										
		Wet	m vf gr sg f pl 1 m pr 2 c cpr 3 vc abk sbk	0 50 <10 75 10 >75 25 100 other:	lo vfr so fr sh fi h vfi vh efi eh	0 1 2 3 c 0 1 2 3 m 0 1 2 3 f 0 1 2 3 vf	0 1 2 3 vc 0 1 2 3 c 0 1 2 3 m 0 1 2 3 f 0 1 2 3 vf	S SiCL LS SiL SL SI SCL SiC L C CL SC	v1 f pf 1 po 2 d br 3 co p cobr	a s c w g l d b	n vsl sl st vi % mm 0 I II III IV V VI	
		Dry										
		Wet	m vf gr sg f pl 1 m pr 2 c cpr 3 vc abk sbk	0 50 <10 75 10 >75 25 100 other:	lo vfr so fr sh fi h vfi vh efi eh	0 1 2 3 c 0 1 2 3 m 0 1 2 3 f 0 1 2 3 vf	0 1 2 3 vc 0 1 2 3 c 0 1 2 3 m 0 1 2 3 f 0 1 2 3 vf	S SiCL LS SiL SL SI SCL SiC L C CL SC	v1 f pf 1 po 2 d br 3 co p cobr	a s c w g l d b	n vsl sl st vi % mm 0 I II III IV V VI	
		Dry										
		Wet	m vf gr sg f pl 1 m pr 2 c cpr 3 vc abk sbk	0 50 <10 75 10 >75 25 100 other:	lo vfr so fr sh fi h vfi vh efi eh	0 1 2 3 c 0 1 2 3 m 0 1 2 3 f 0 1 2 3 vf	0 1 2 3 vc 0 1 2 3 c 0 1 2 3 m 0 1 2 3 f 0 1 2 3 vf	S SiCL LS SiL SL SI SCL SiC L C CL SC	v1 f pf 1 po 2 d br 3 co p cobr	a s c w g l d b	n vsl sl st vi % mm 0 I II III IV V VI	
		Dry										

Modified from David Jorgenson (Harbor) and Birkeland, 1999.

Appendix A: Soil pit locations and photographs from North Rhyne and Duffey watersheds, Redlair Observatory, NC

Soil Pit ID	Coordinates	Watershed	Position on slope	Aspect
DU-S3	N 35.2985561 W 81.0821942	Duffey/ High-order	Shoulder	South
DU-S2	N 35.29789 W 81.08297	Duffey/ High-order	Backslope	South
DU-S4	N 35.2978101 W 81.0826572	Duffey/ High-order	Toeslope	None
DU-S1	N 35.2978641 W 81.0829493	Duffey/ High-order	Alluvial fan / toeslope	None
DU-S5	N 35.2978641 W 81.0829493	Duffey/ High-order	Backslope	North
DU-S6	N 35.2980542 W 81.0820387	Duffey/ High-order	Shoulder	North
DU-S7	N 35.2983054 W 81.0831859	Duffey/ High-order	Backslope	North
DU-S8	N 35.2981522 W 81.0833713	Duffey/ High-order	Backslope	North
NR-S12	N 35.2990396 W 81.0948178	North Rhyne/ Low-order	Summit	South
NR-S11	N 35.2989207 W 81.0948097	North Rhyne/ Low-order	Shoulder	South
NR-S7	N 35.2987352 W 81.0947244	North Rhyne/ Low-order	Upper Backslope	South
NR-S6	N 35.2988901 W 81.0944515	North Rhyne/ Low-order	Lower Backslope	South
NR-S8	N 35.2986882 W 81.0944457	North Rhyne/ Low-order	Toeslope	South
NR-S1	N 35.2978641 W 81.0829493	North Rhyne/ Low-order	Alluvial Fan	None
NR-S5	N 35.2978641 W 81.0829493	North Rhyne/ Low-order	Toeslope	North
NR-S9	N 35.2980989 W 81.0939880	North Rhyne/ Low-order	Lower Backslope	North
NR-S10	N 35.2978491 W 81.0940164	North Rhyne/ Low-order	Upper Backslope	North
NR-S13	N 35.2976776 W 81.0941992	North Rhyne/ Low-order	Shoulder	North
NR-S4	N 35.2975904 W 81.0943850	North Rhyne/ Low-order	Summit	North

Figure 1: DU-S3: Zbs vein more prominent in wall in first photo



Appendix B
Figure 1

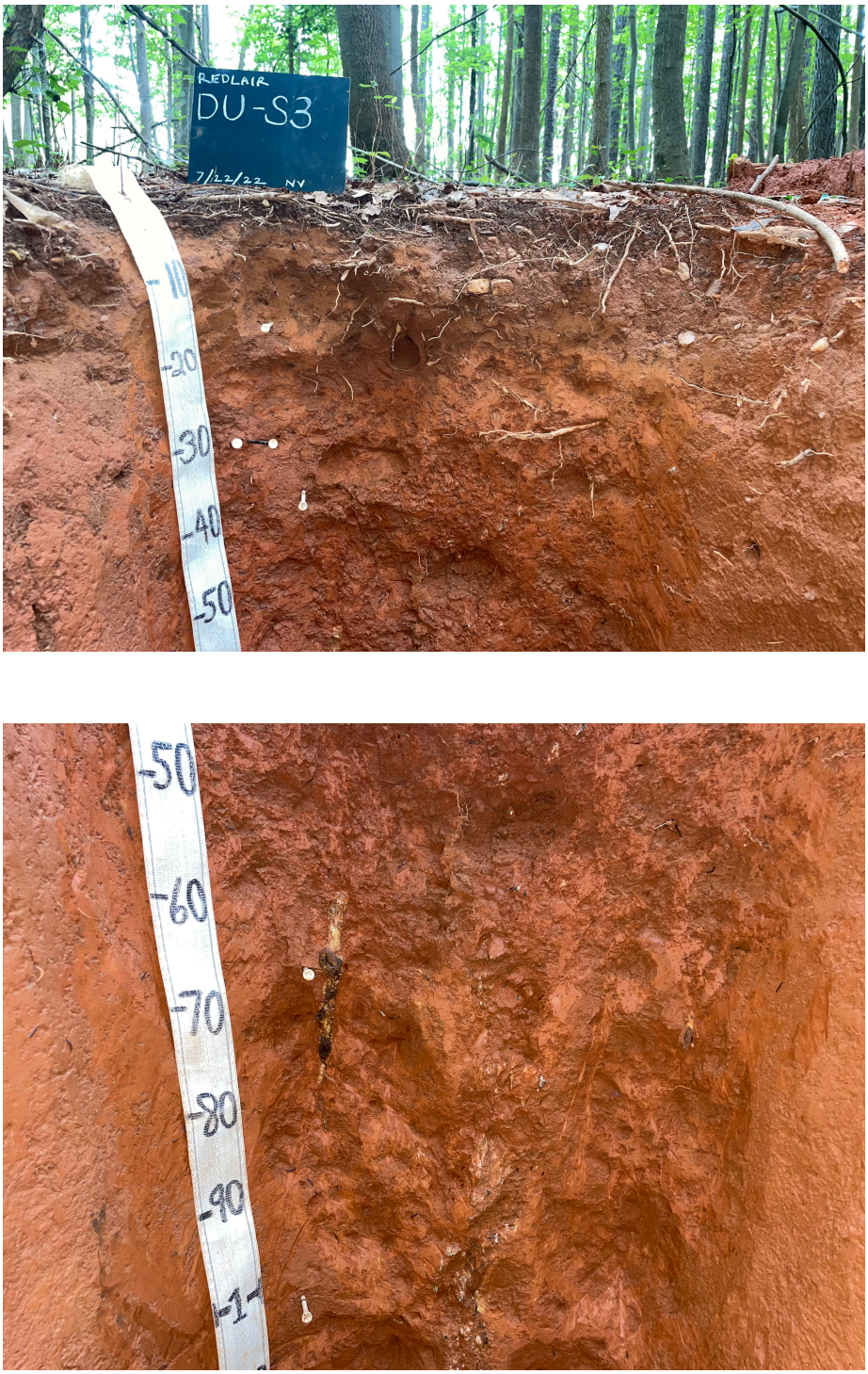

DU-S3

Appendix B
Figure 1

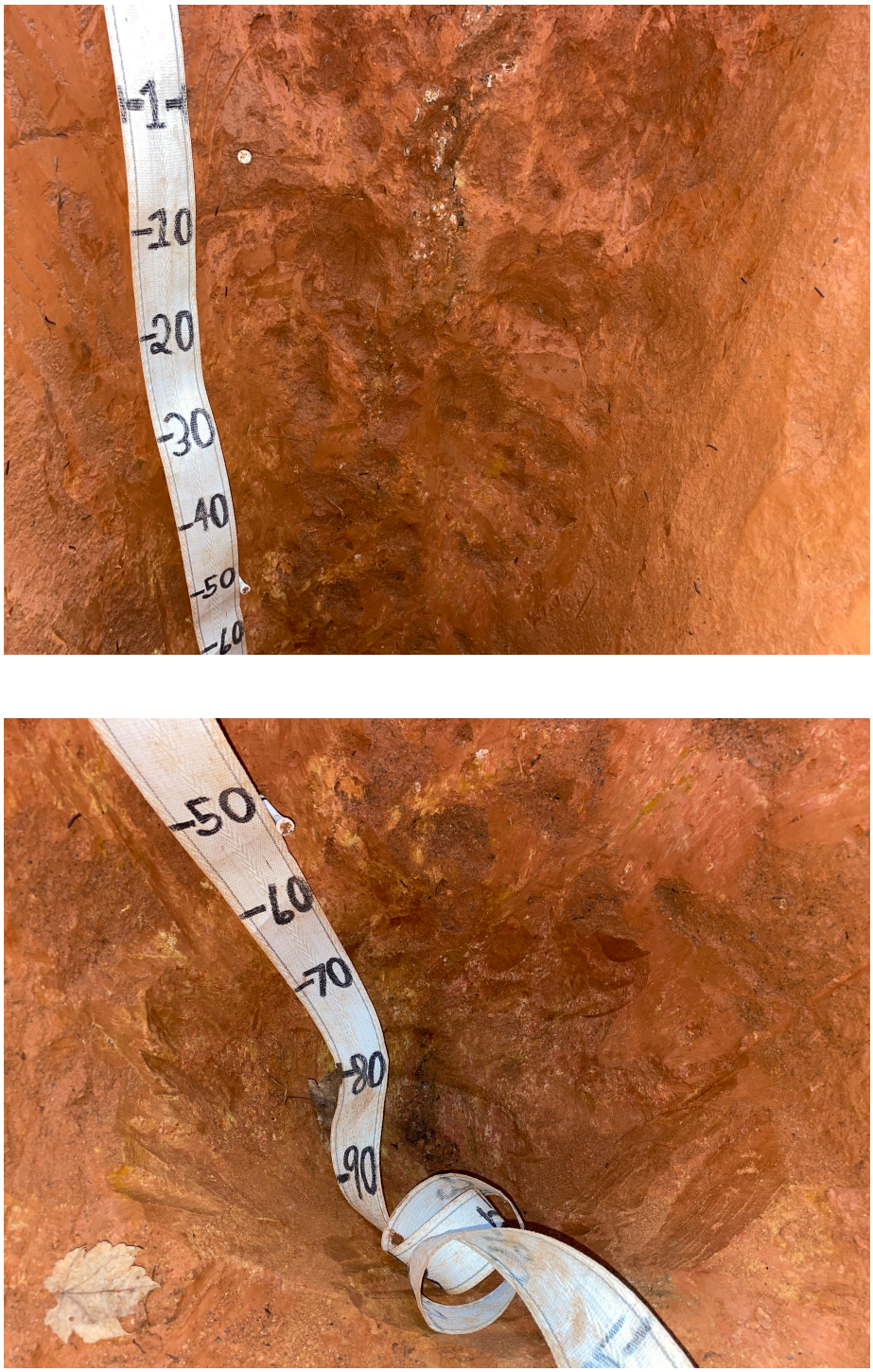

DU-S3

Appendix B
Figure 2



DU-S2

Appendix B
Figure 3



DU-S4

Appendix B
Figure 4



DU-S1

Appendix B
Figure 5



DU-S5

Appendix B
Figure 5



DU-S5

Appendix B
Figure 5

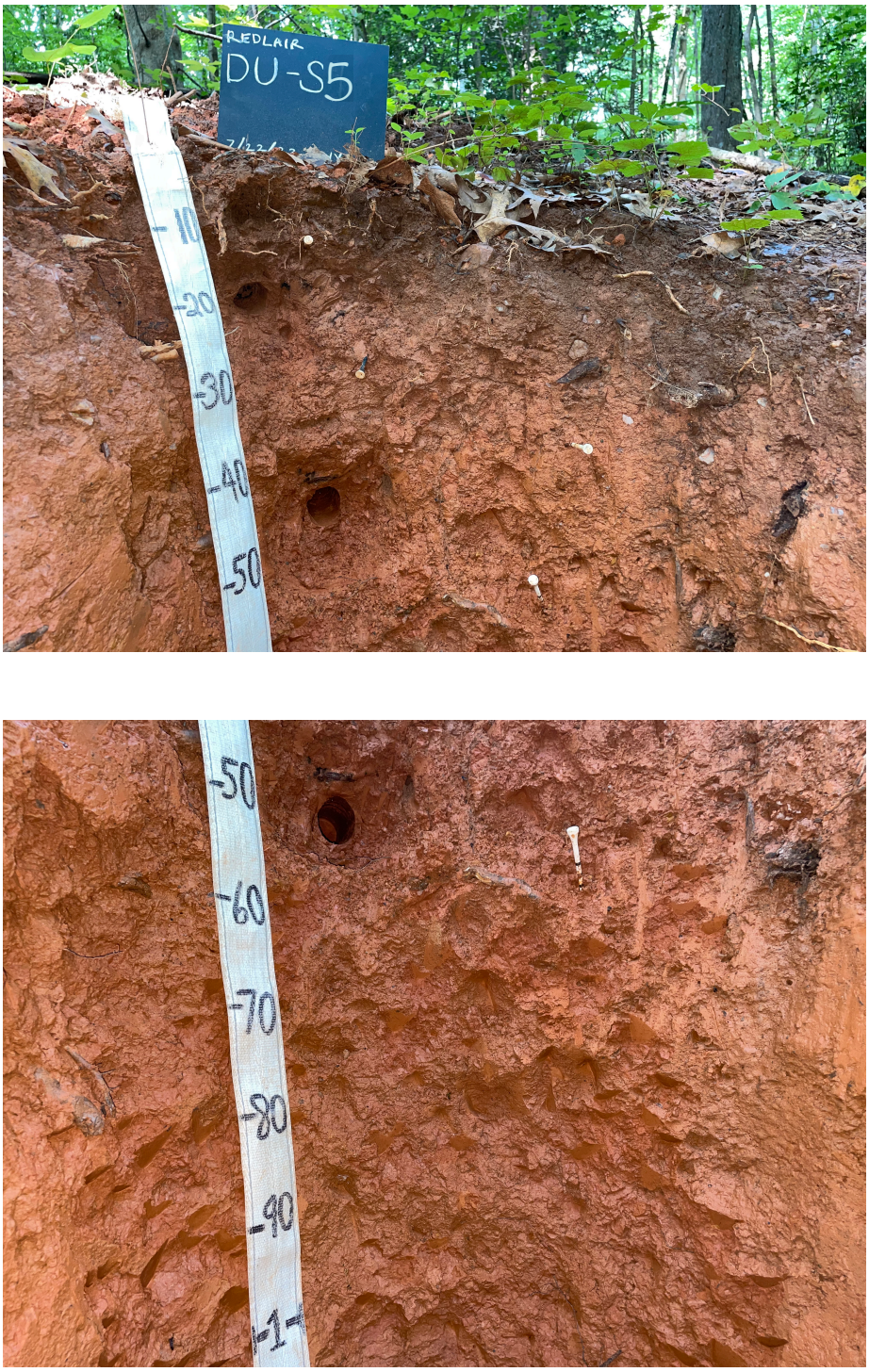

DU-S5

Appendix B
Figure 5

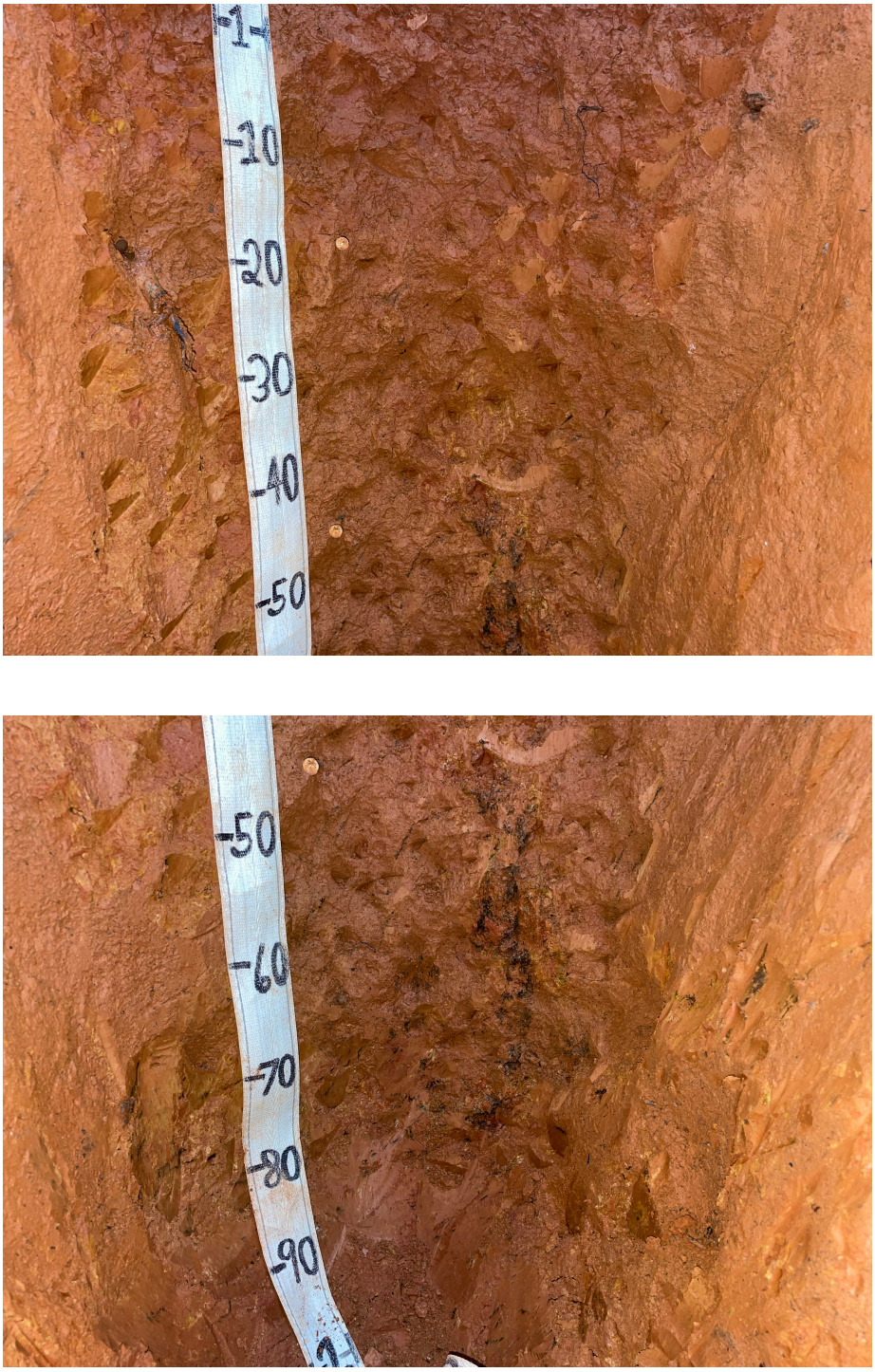

DU-S5

Appendix B
Figure 6

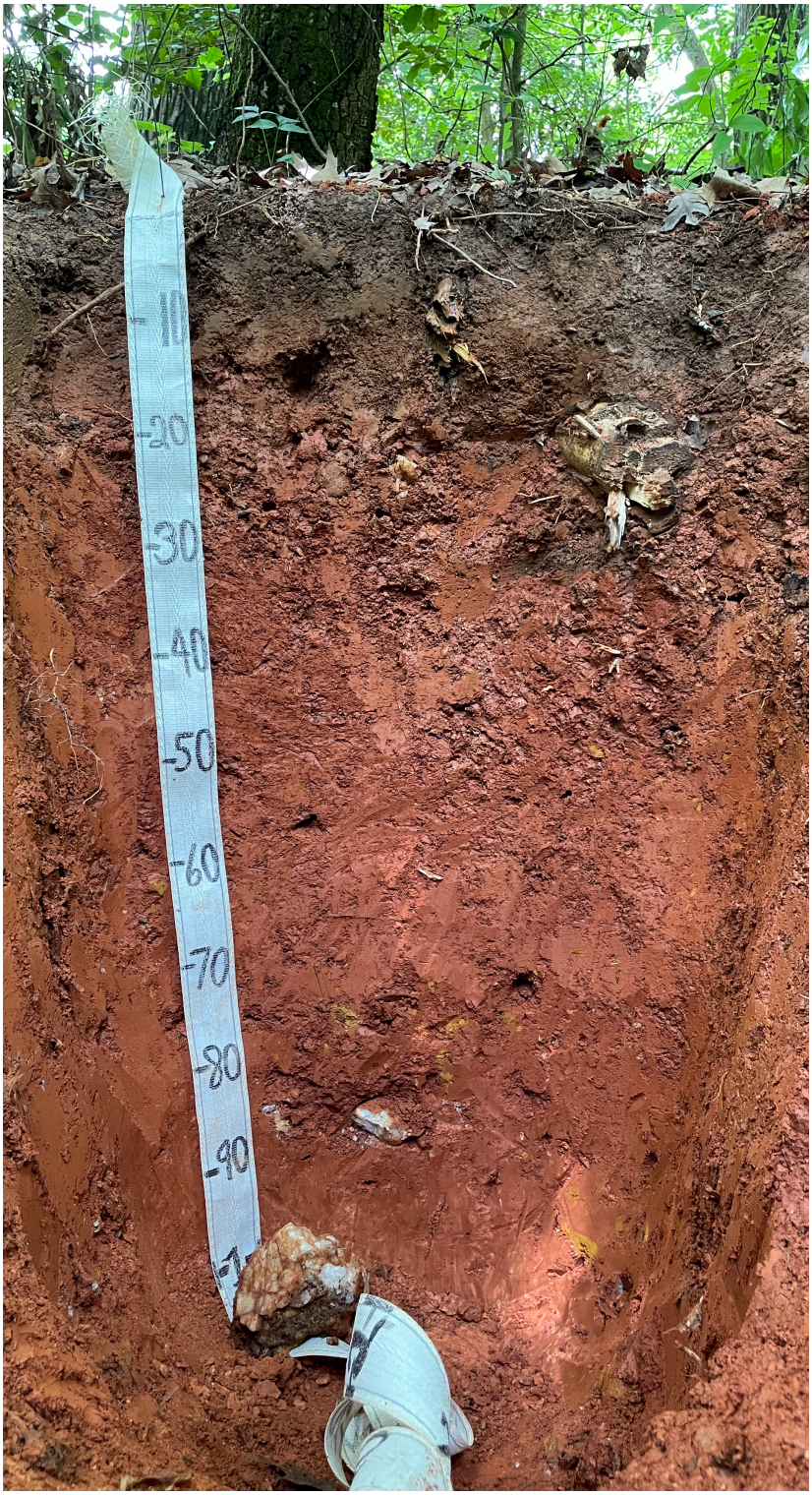

DU-S6

Appendix B
Figure 6



DU-S6

Appendix B
Figure 6

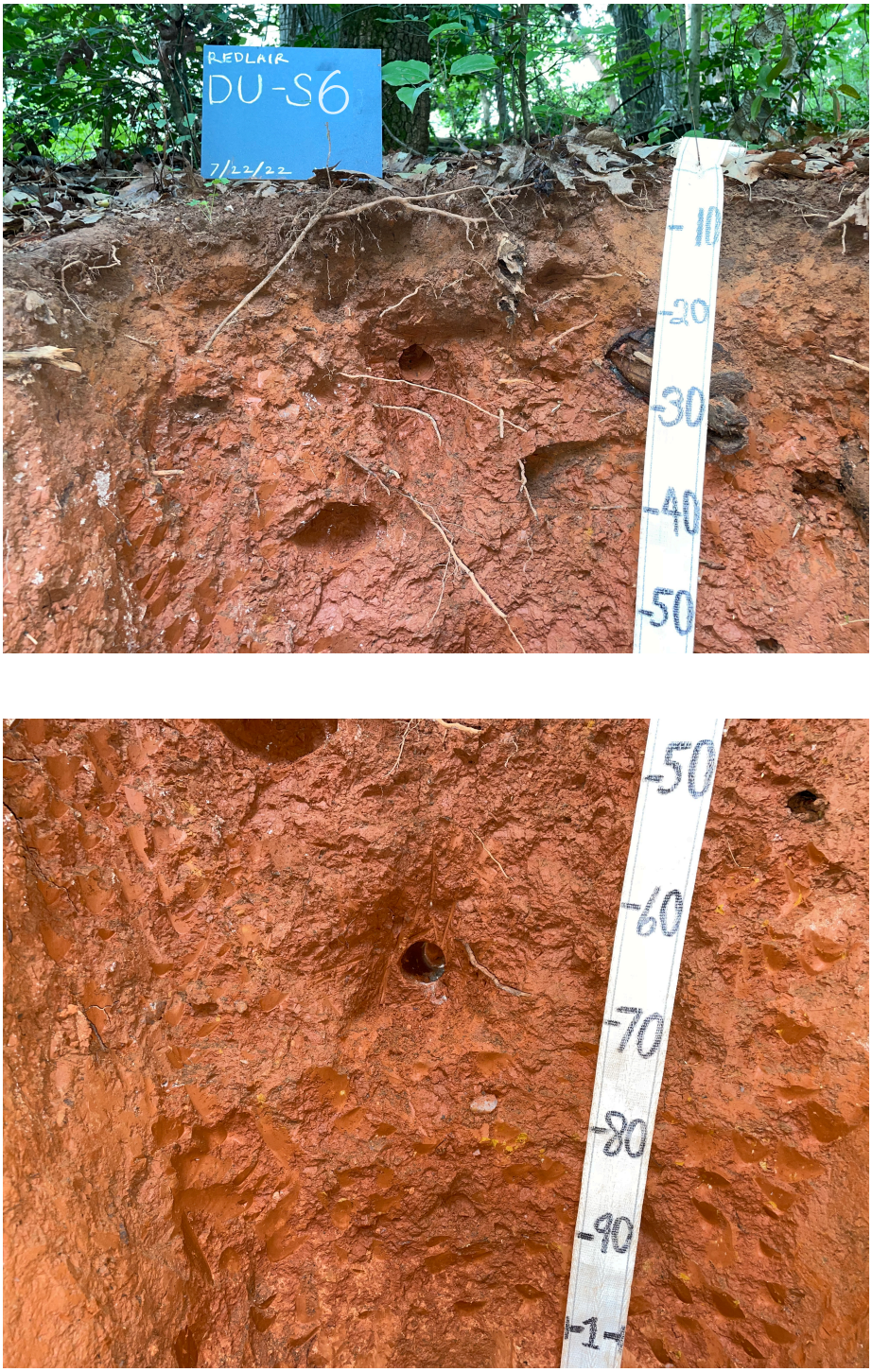

DU-S6

Appendix B
Figure 6

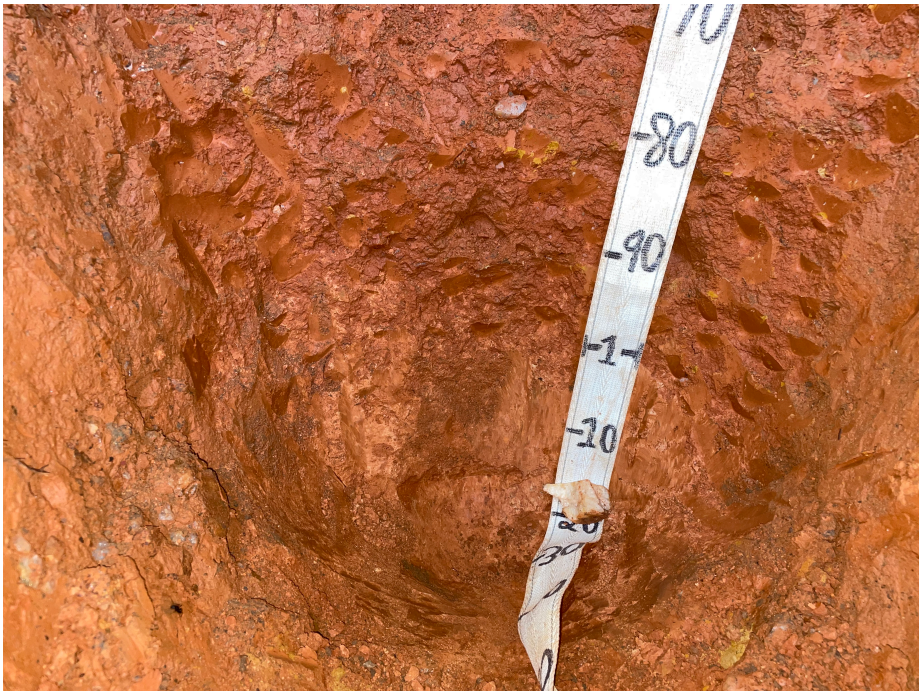

DU-S6

Appendix B
Figure 7



DU-S7

Appendix B

Figure 7

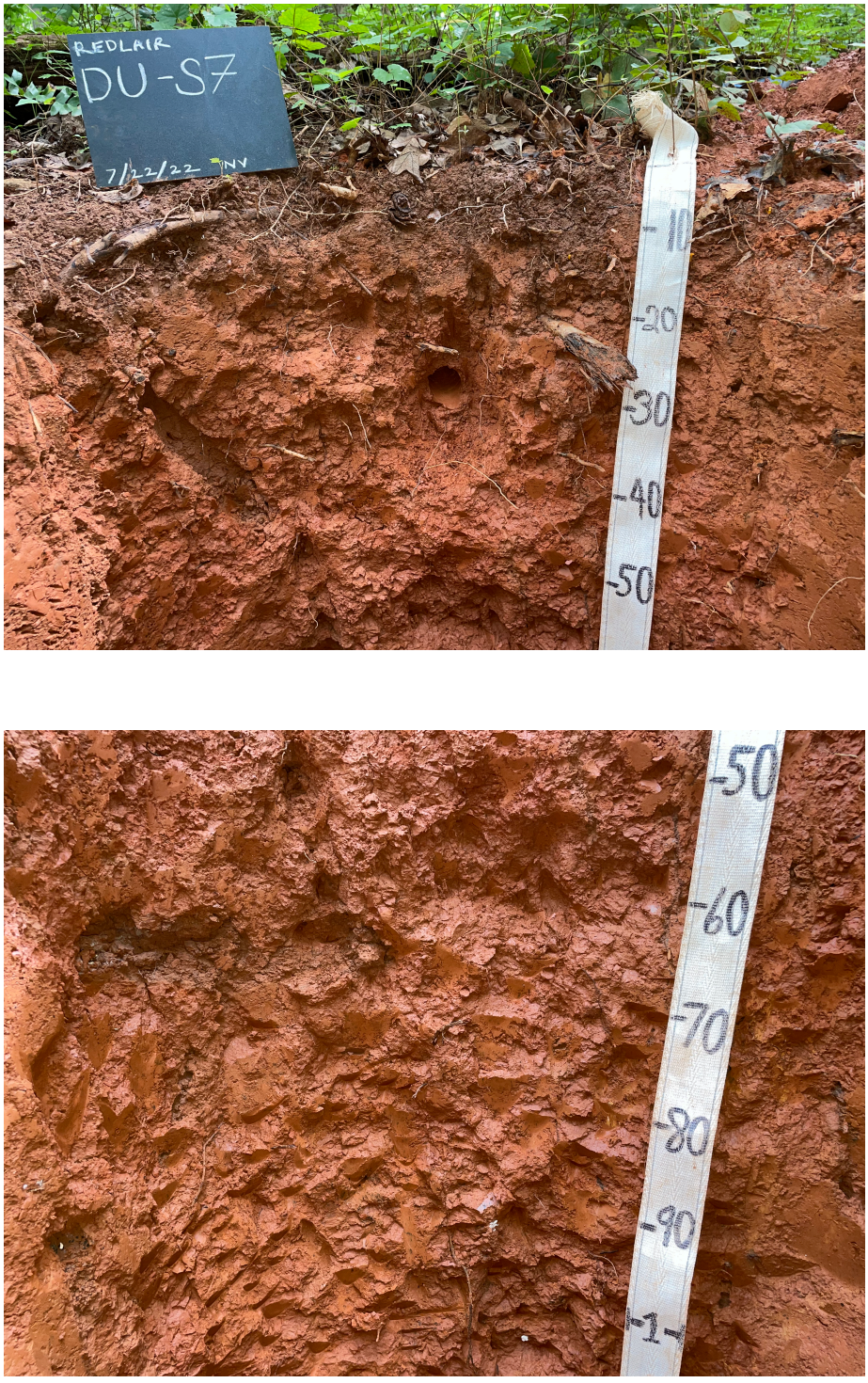

DU-S7

Appendix B

Figure 7

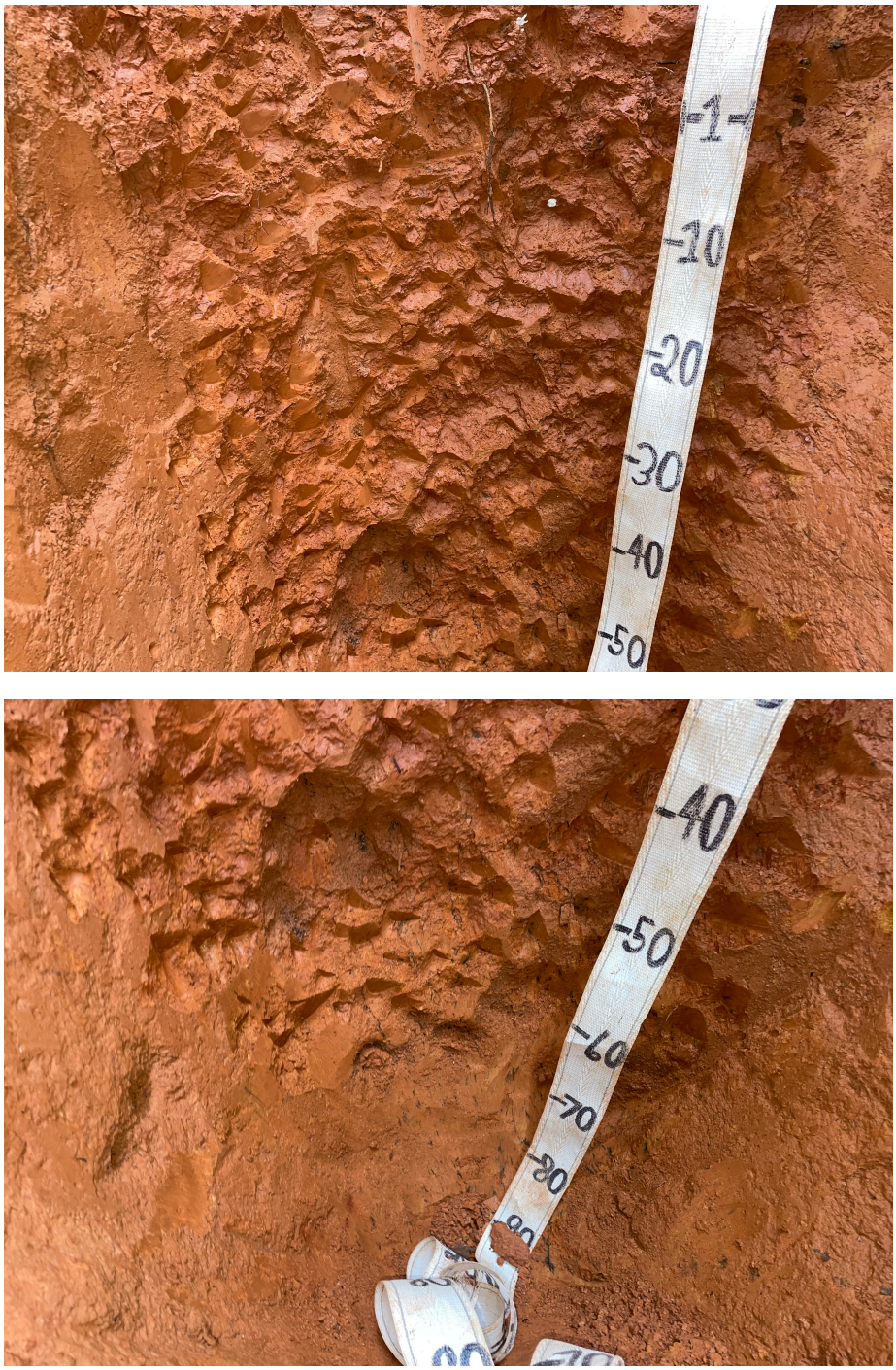

DU-S7

Appendix B
Figure 8



DU-S8

Appendix B
Figure 8



DU-S8

Appendix B
Figure 8

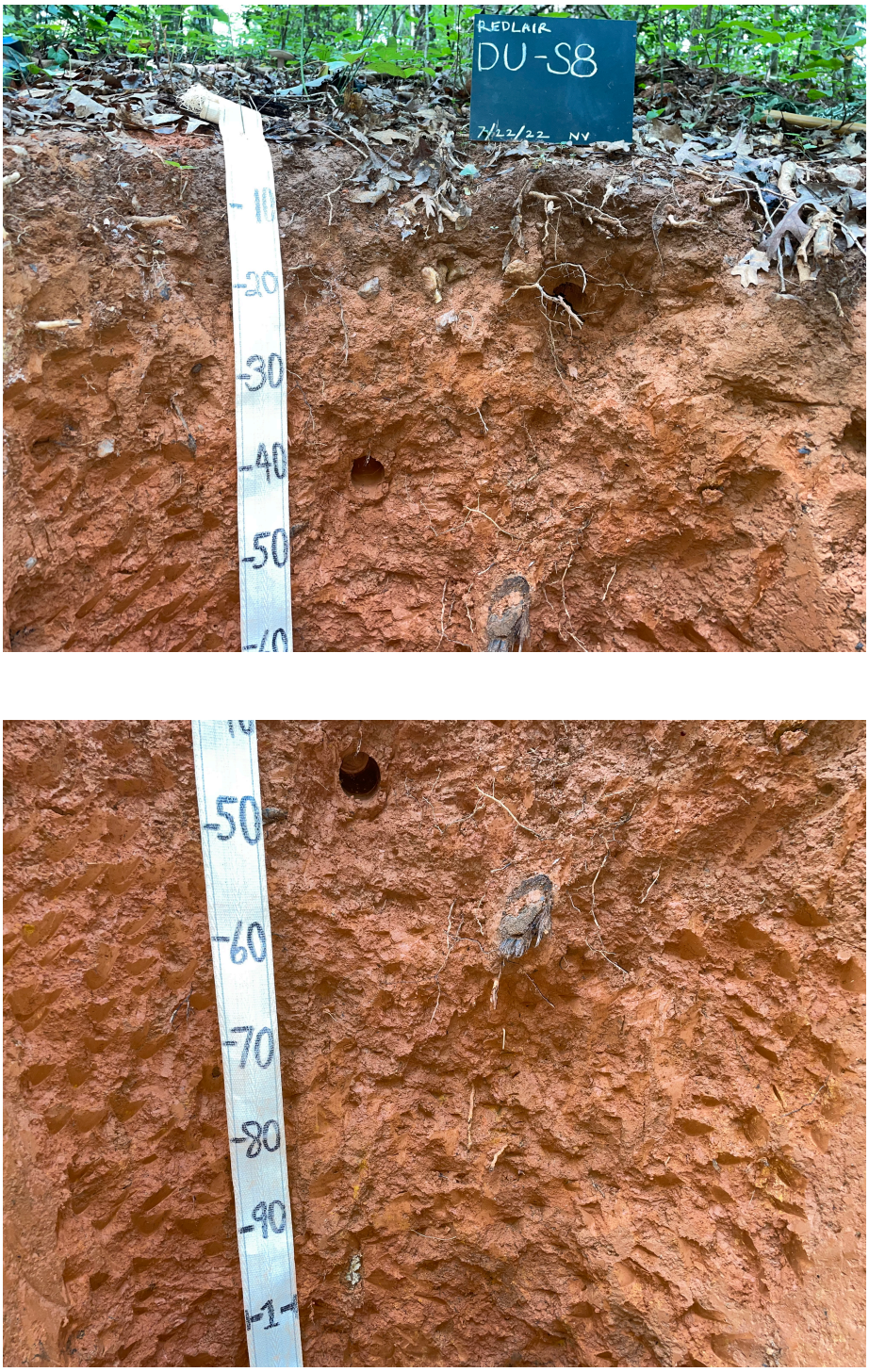

DU-S8

Appendix B
Figure 8



DU-S8

Appendix B
Figure 9

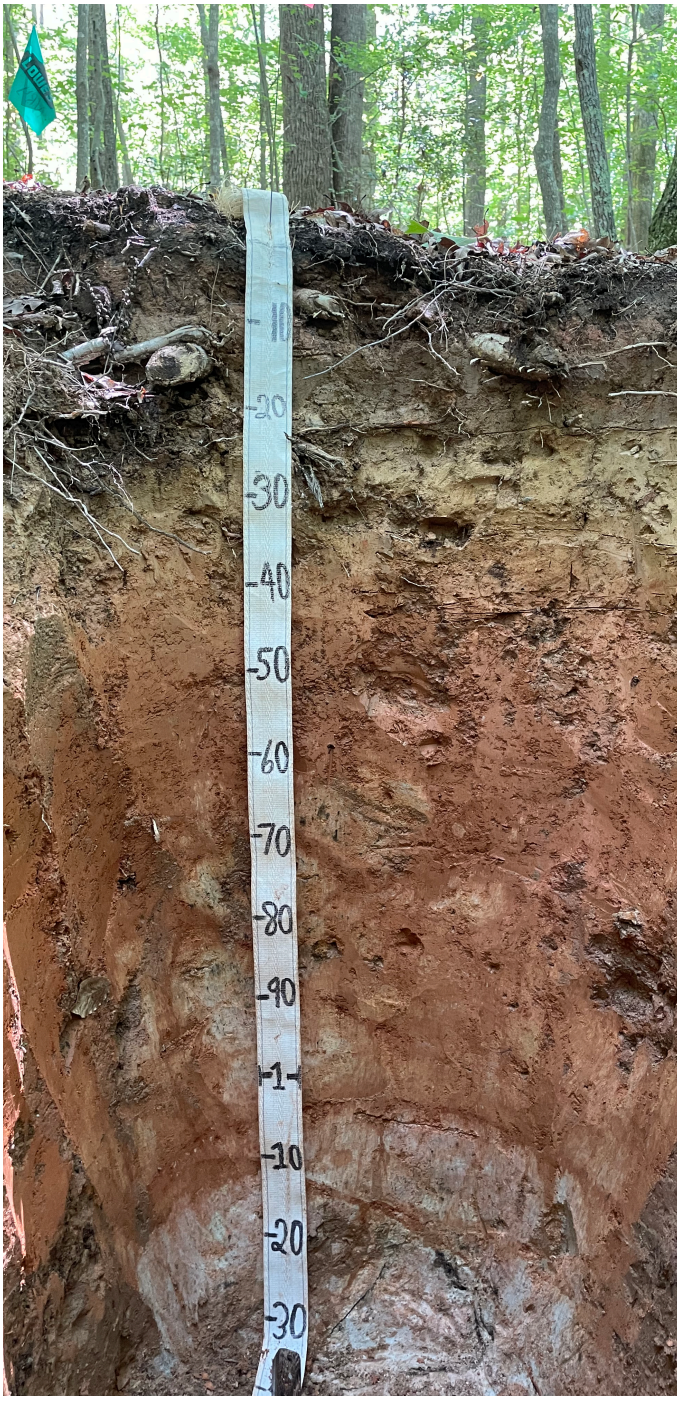

NR-S4

Appendix B
Figure 9



NR-S4

Appendix B
Figure 9

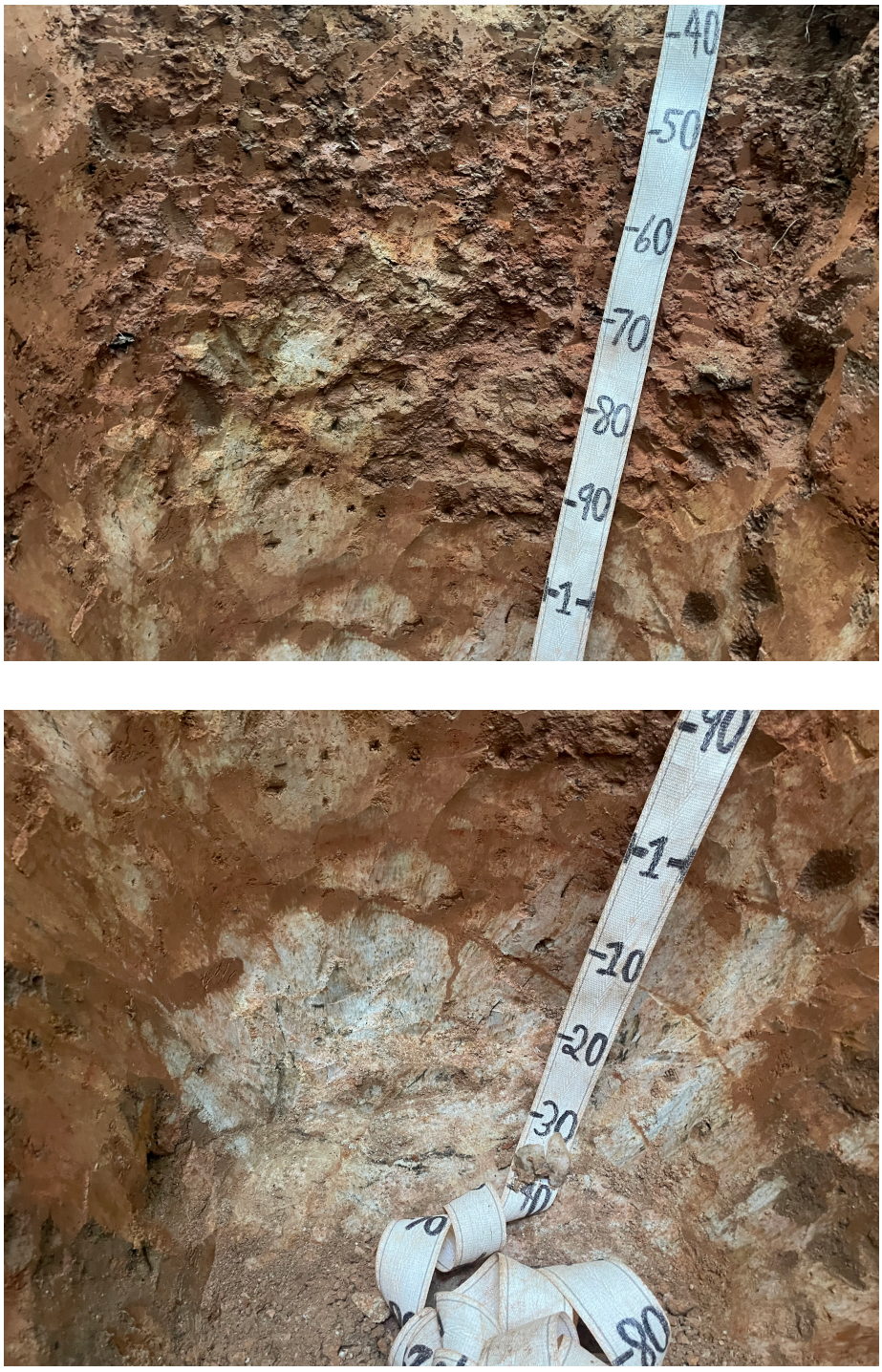

NR-S4

Appendix B
Figure 10



NR-S13

Appendix B

Figure 10



NR-S13

Appendix B
Figure 11

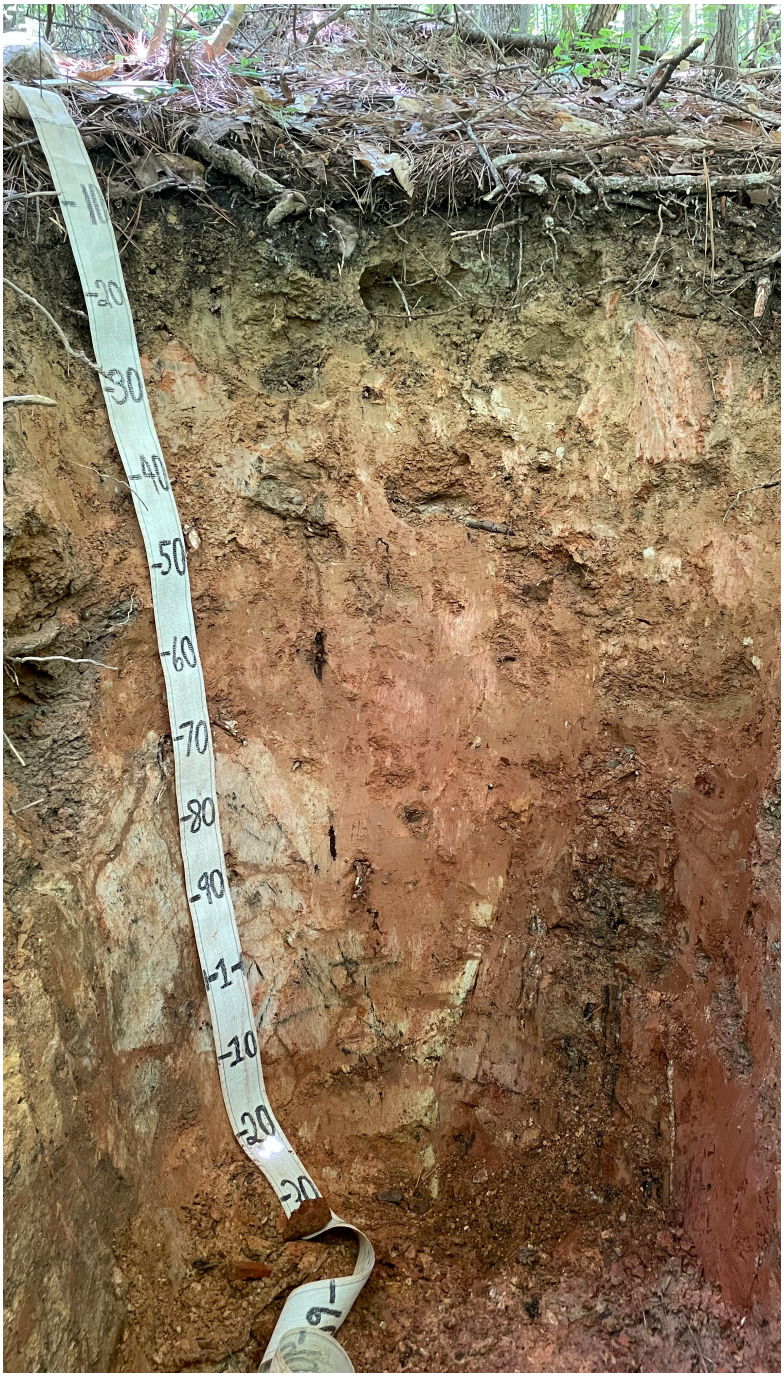

NR-S10

Appendix B
Figure 11



NR-S10

Appendix B
Figure 11

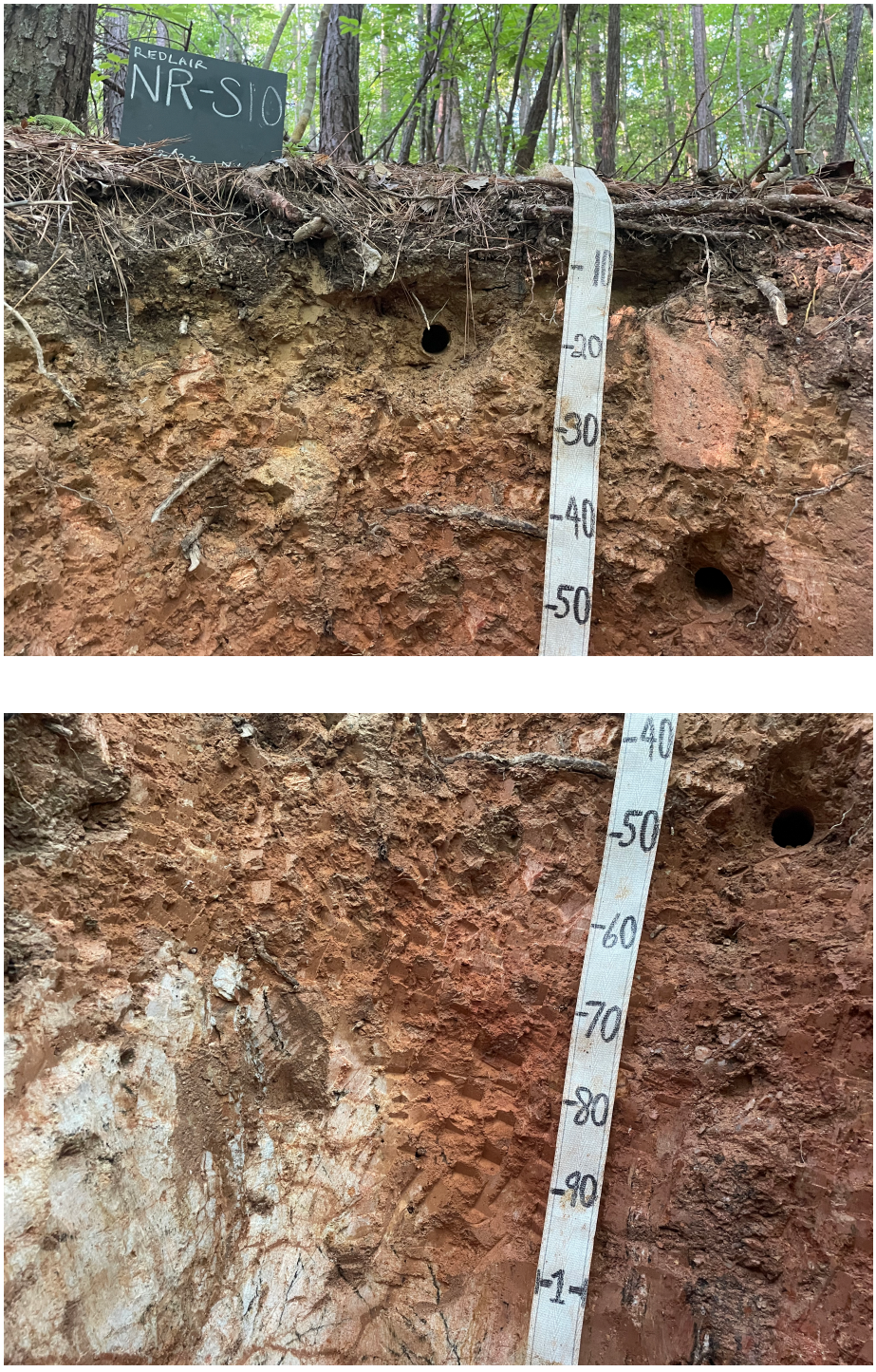

NR-S10

Appendix B
Figure 11



NR-S10

Appendix B
Figure 11





NR-S10

Appendix B
Figure 12- adjust fig#s after this



NR-S9

Appendix B
Figure 12- adjust fig#s after this

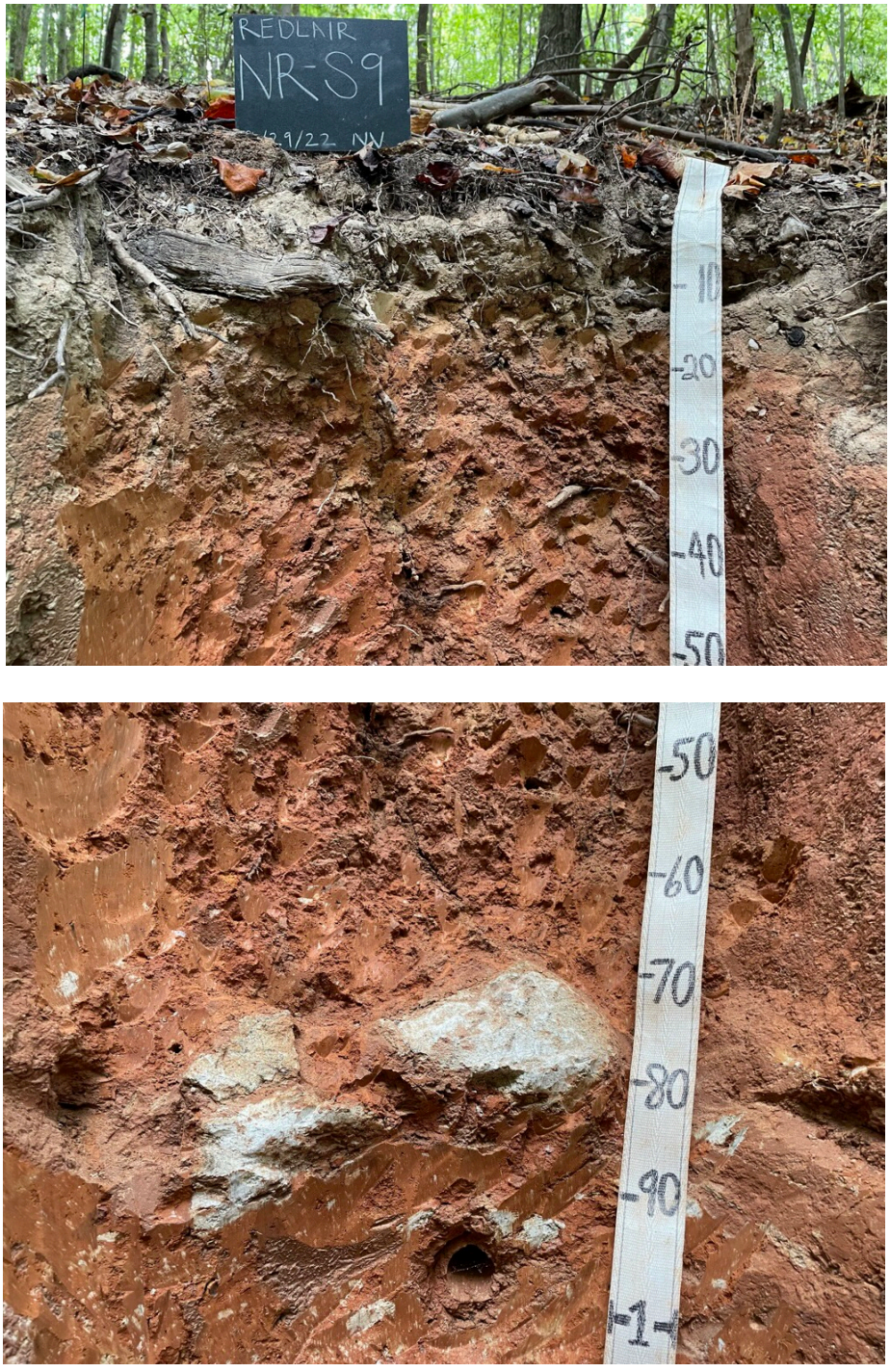

NR-S9

Appendix B
Figure 12- adjust fig#s after this

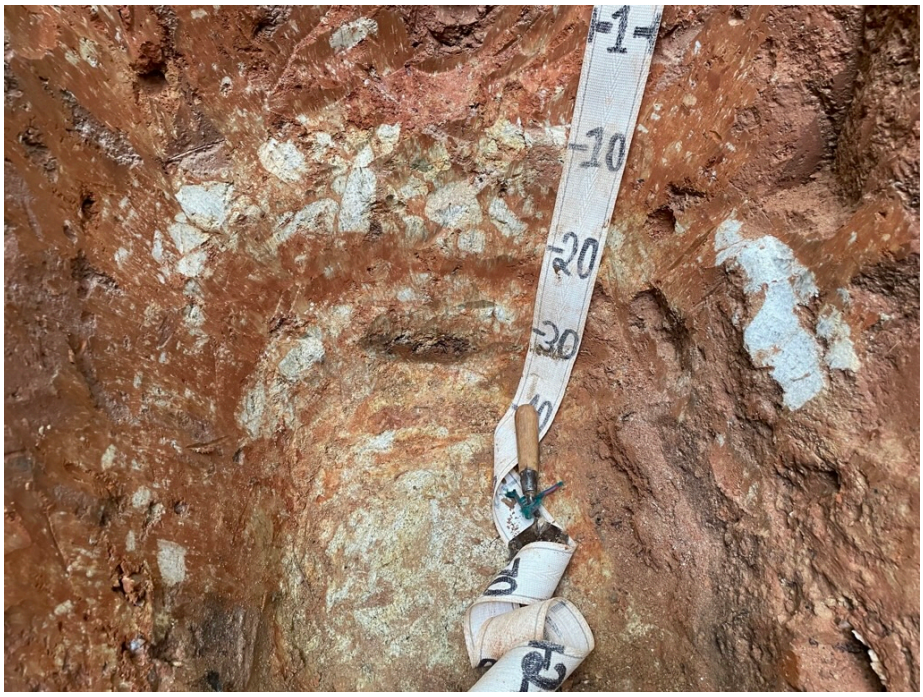

NR-S9

Appendix B
Figure 12



NR-S5b

Appendix B
Figure 12- adjust fig#s after this



NR-S1

Appendix B
Figure 12- adjust fig#s after this



NR-S1

Appendix B
Figure 12- adjust fig#s after this



NR-S8

Appendix B
Figure 13



NR-S6

Appendix B
Figure 13

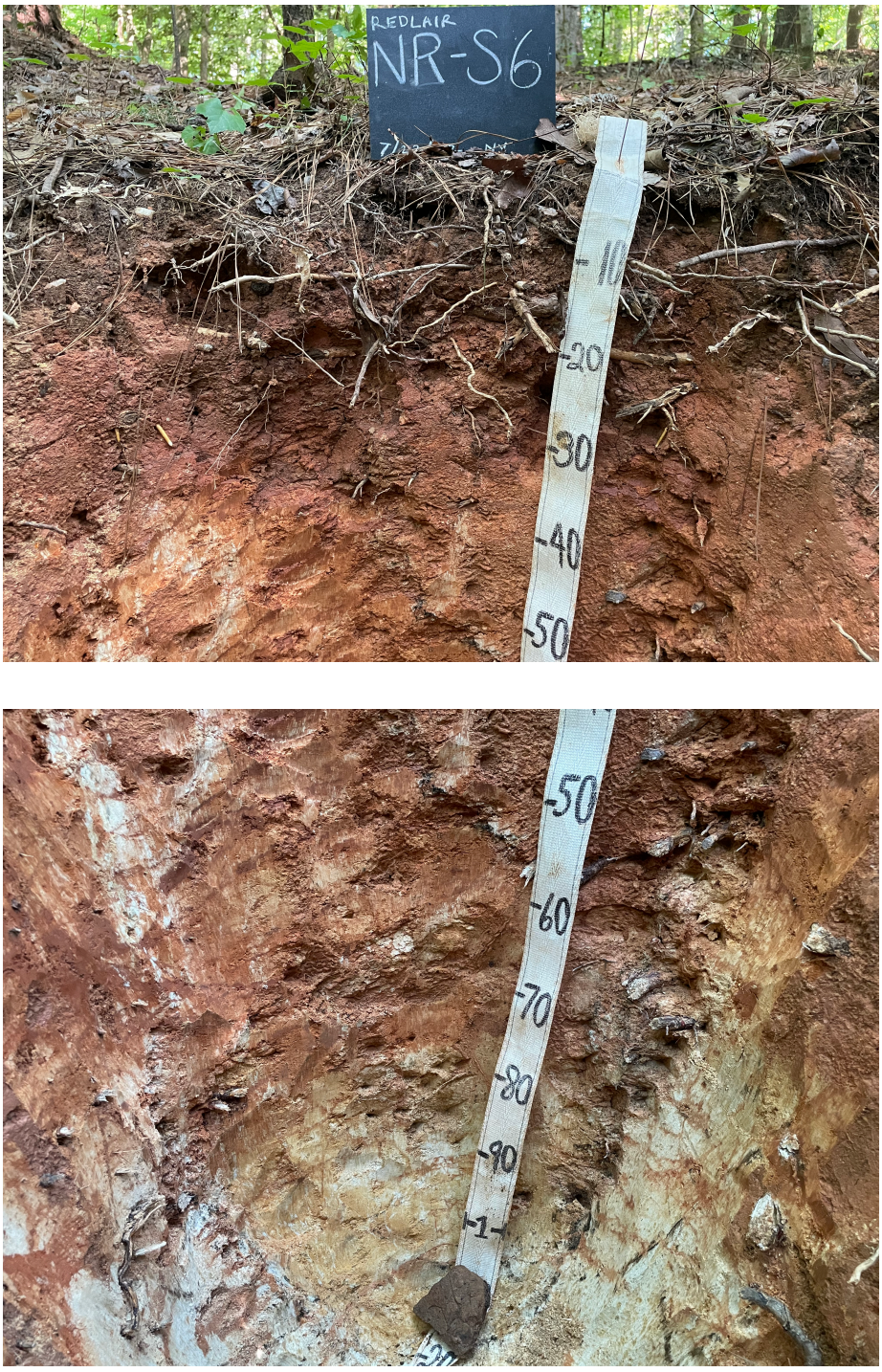

NR-S6

Appendix B
Figure 14



NR-S7

Appendix B
Figure 14

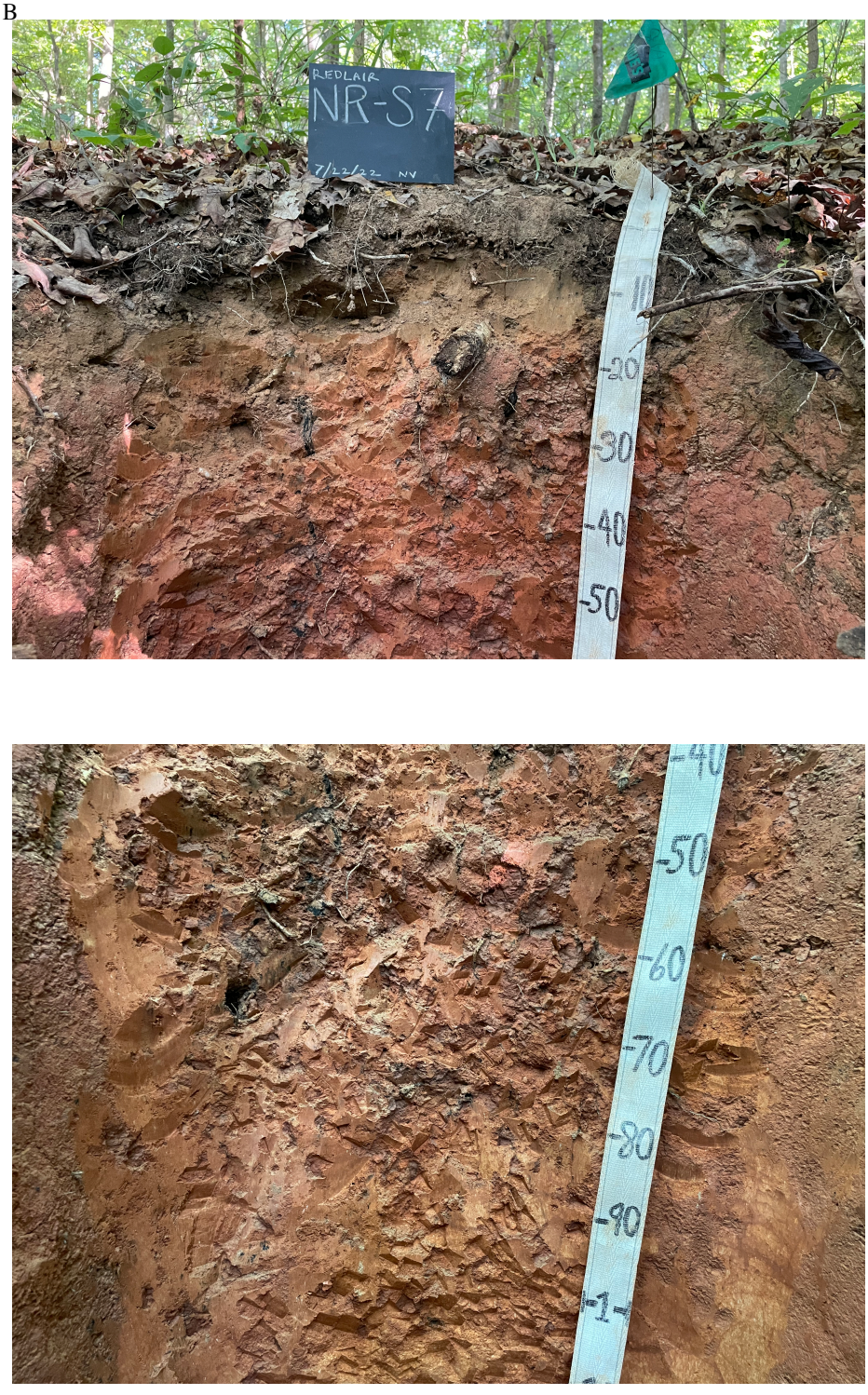

NR-S7

Appendix B

Figure 14

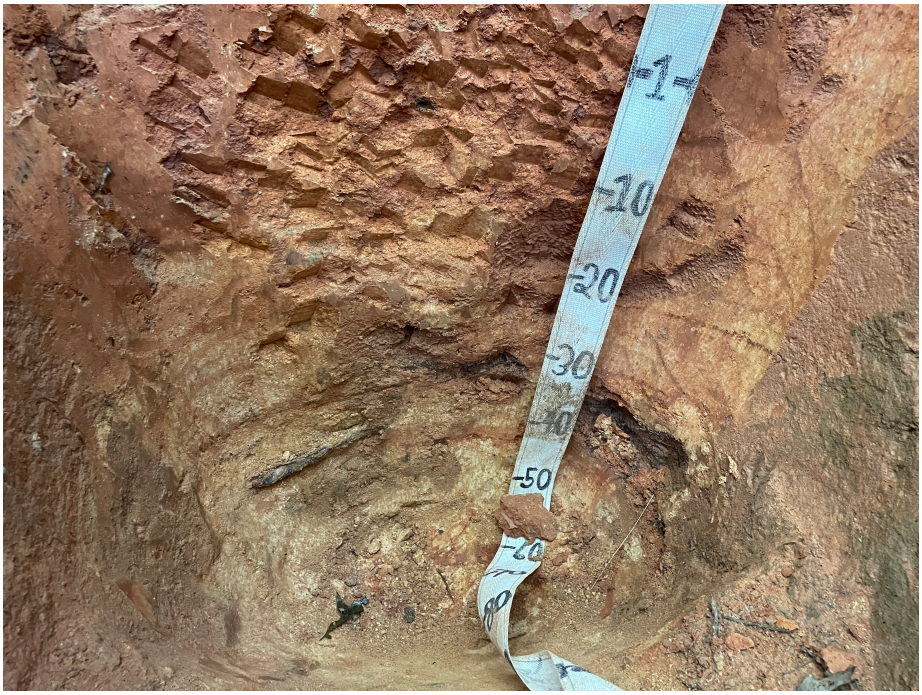

NR-S7

Appendix B
Figure 15



NR-S11

Appendix B
Figure 15

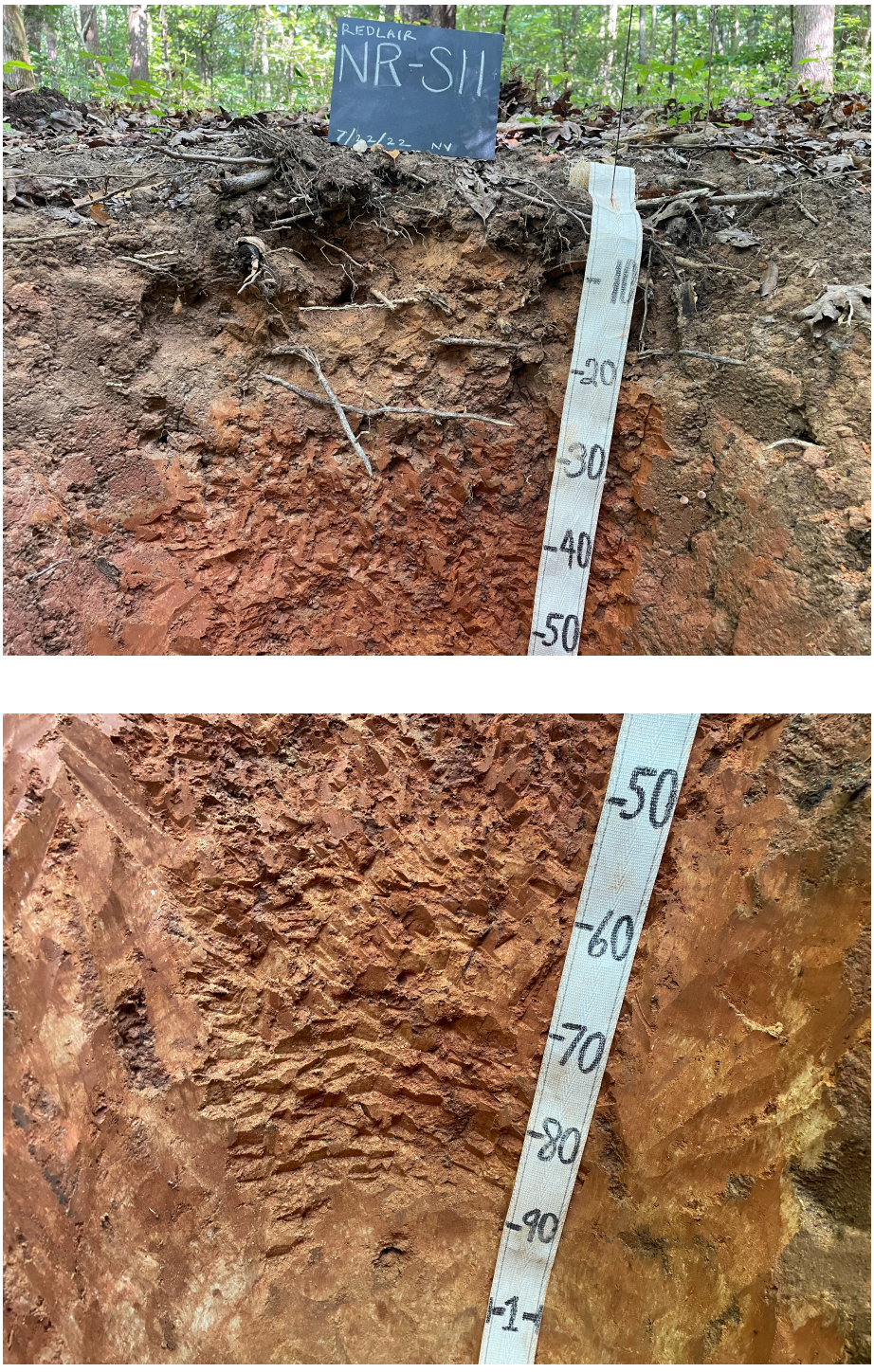

NR-S11

Appendix B

Figure 15

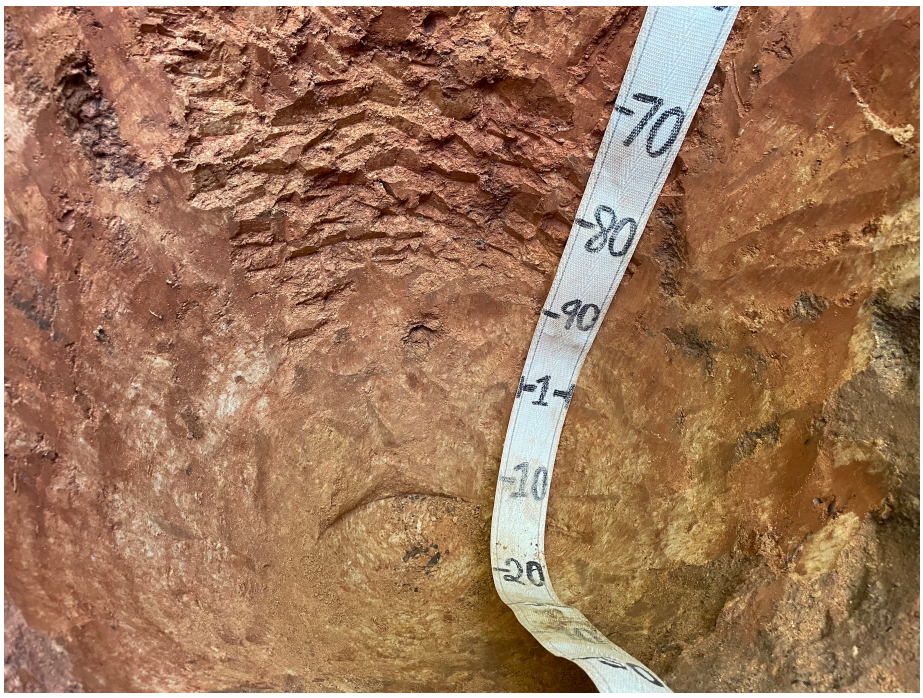

NR-S11

Appendix B
Figure 16



NR-S12

Appendix B
Figure 16

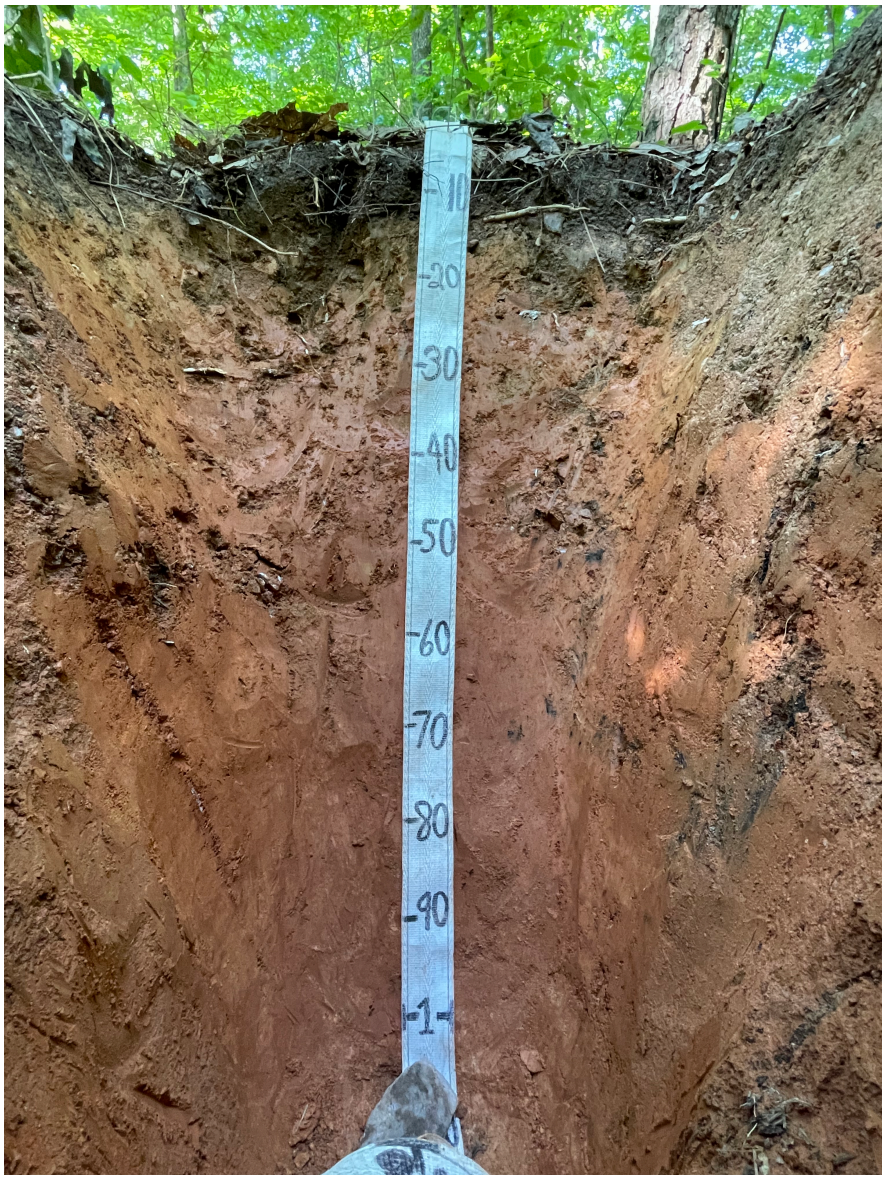

NR-S12

Appendix B
Figure 16

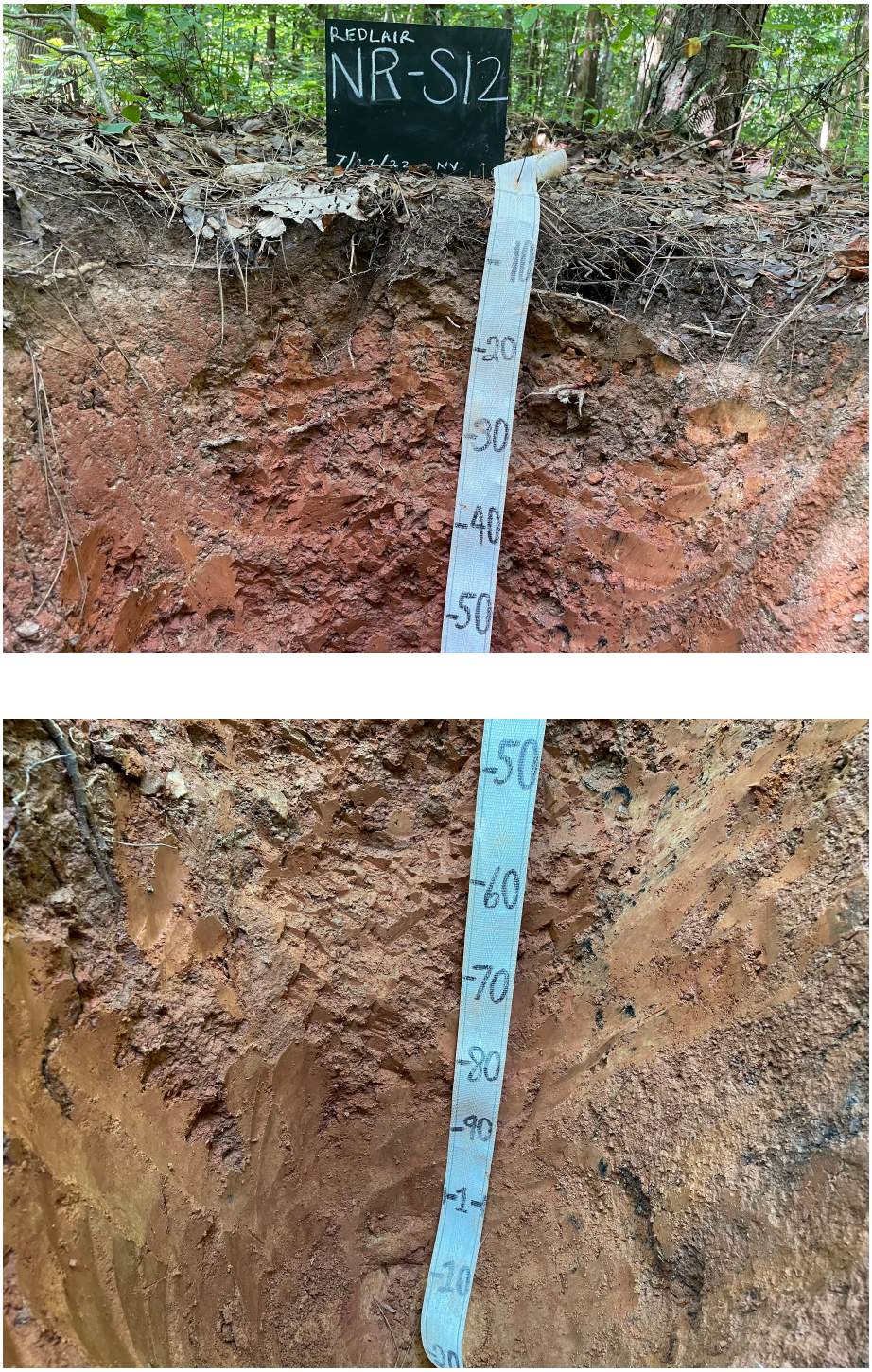

NR-S12

Appendix B
Figure 16



NR-S12

Appendix C: Soil pit sketches from North Rhyne and Duffey watersheds, Redlair Observatory, NC

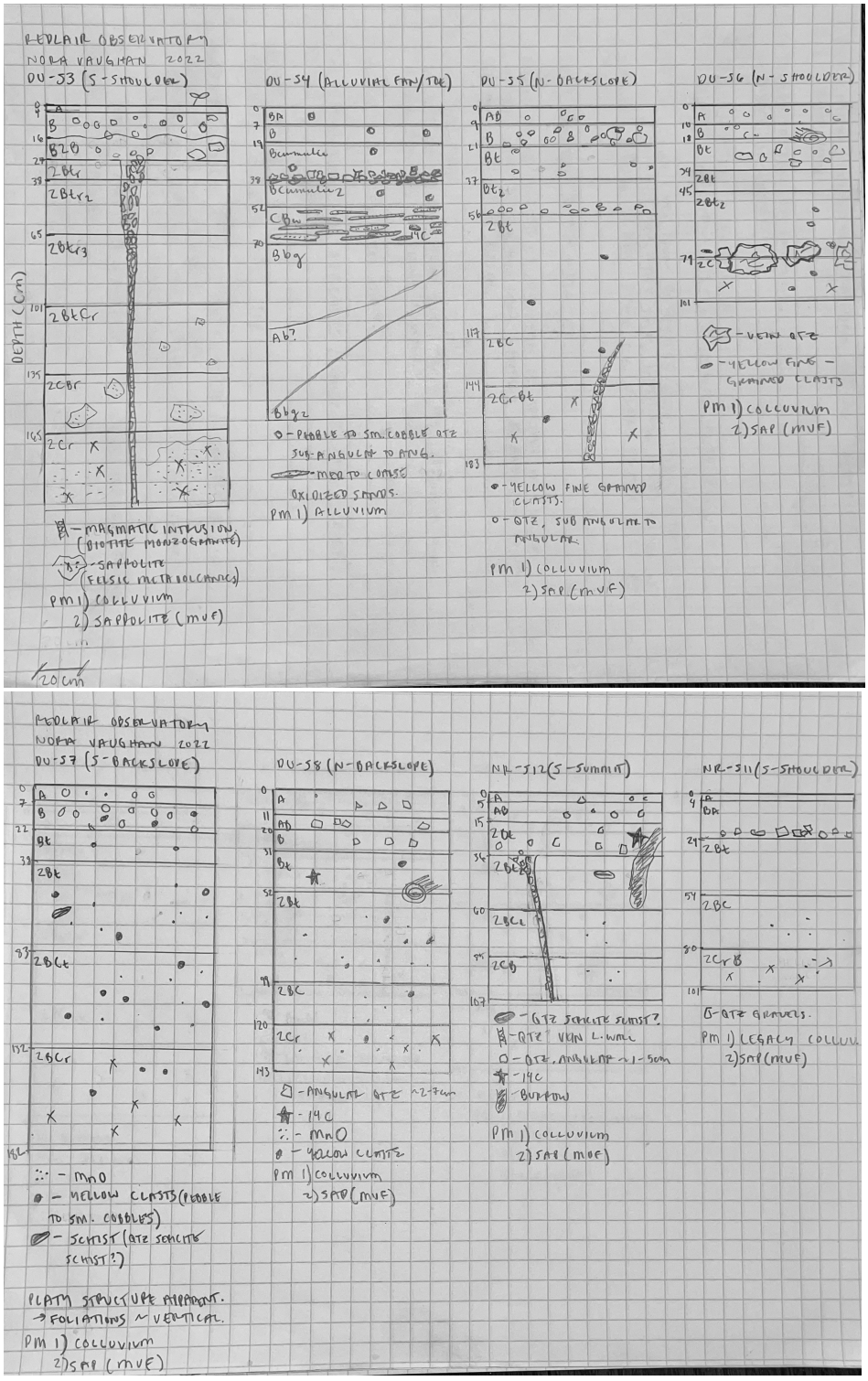

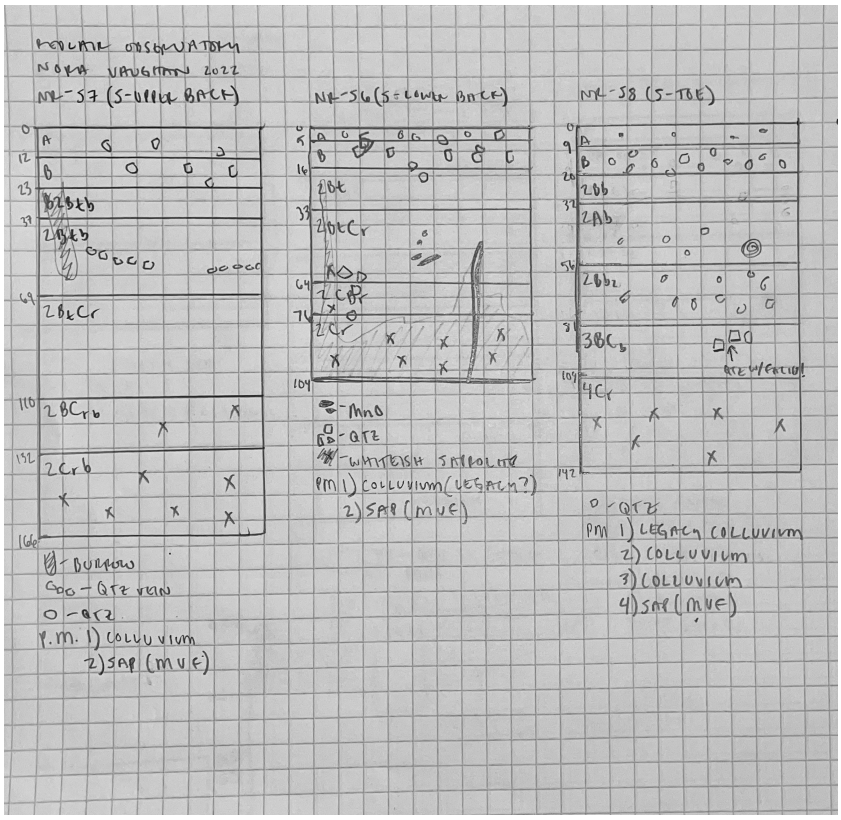
REGULAR OBSERVATORY
NORA VAUGHAN 2022
NR-57 (S-UPPER BACK)
NR-56 (S-LOWER BACK)
NR-58 (S-TOE)
- BURROW
- QTZ VEIN
- QTZ
P.M. 1) COLLUVIUM
2) SAP (MVF)
- MnO
- QTZ
- WHITEISH SAPROLITE
PM 1) COLLUVIUM (LEGACY?)
2) SAP (MVF)
- QTZ
PM 1) LEGACY COLLUVIUM
2) COLLUVIUM
3) COLLUVIUM
4) SAP (MVF)

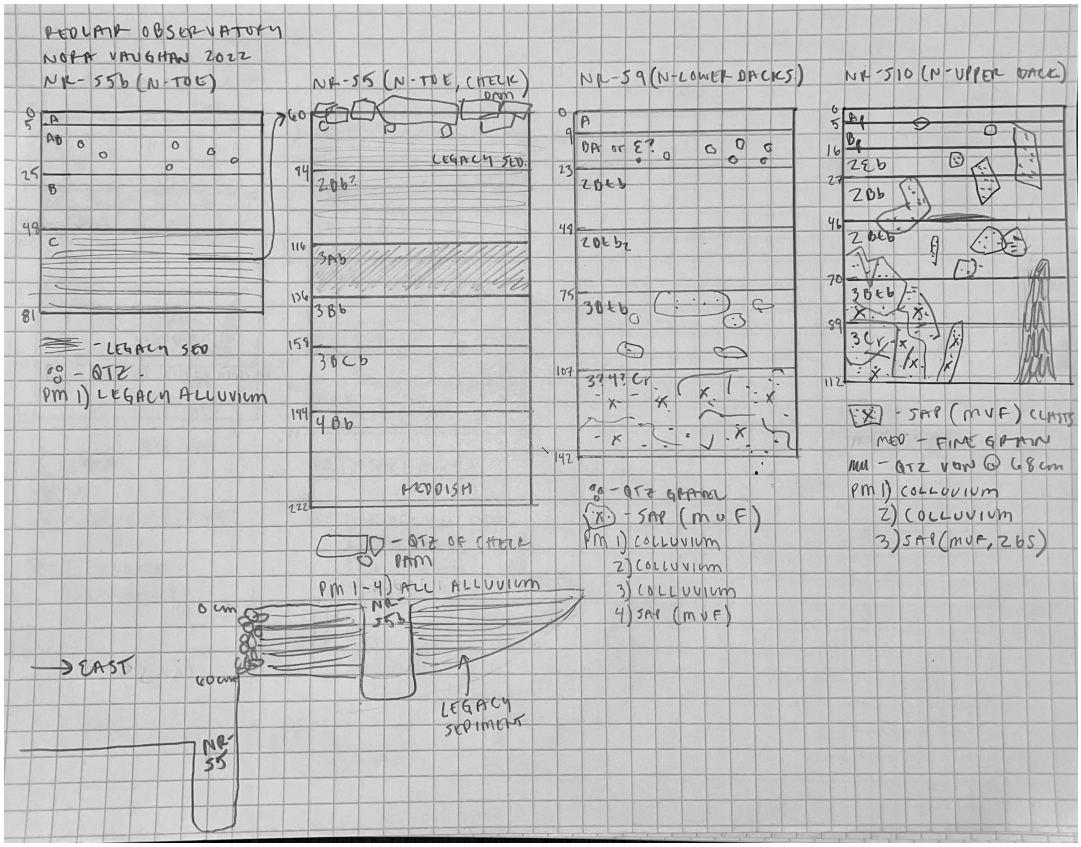
REGULAR OBSERVATORY
NORA VAUGHAN 2022
NR-55b (N-TOE)
NR-55 (N-TOE, CHECK)
NR-59 (N-LOWER BACKS)
NR-510 (N-UPPER BACK)
- LEGACY SED
- QTZ.
PM 1) LEGACY ALLUVIUM
LEGACY SED.
REDDISH
- QTZ OF CHECK
PM 1-4) ALL ALLUVIUM
- QTZ GRAVEL
- SAP (MVF)
PM 1) COLLUVIUM
2) COLLUVIUM
3) COLLUVIUM
4) SAP (MVF)
- SAP (MVF) CLAYS
MED - FINE GRAIN
- QTZ VEIN @ 68cm
PM 1) COLLUVIUM
2) COLLUVIUM
3) SAP (MVF, 2BS)
EAST
0 cm
60 cm
NR-553
NR-55
LEGACY SEDIMENT

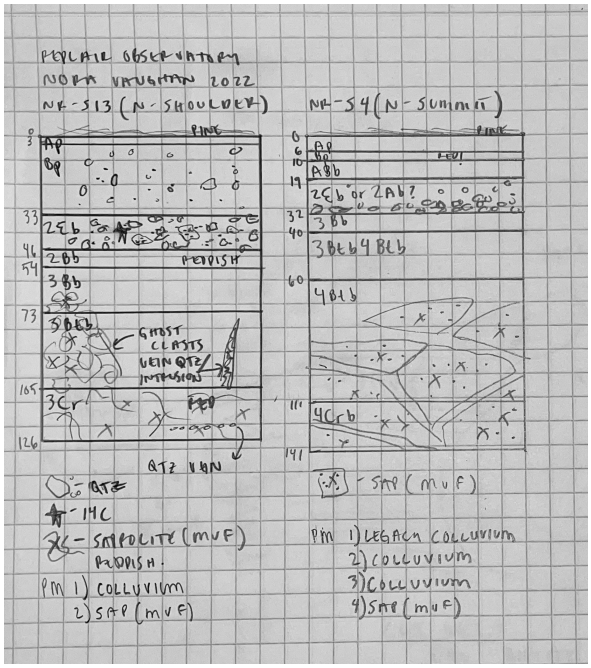
REPLAIR OBSERVATORY
NORA VAUGHAN 2022
NR-S13 (N-SHOULDER)
NR-S4 (N-SUMMIT)
PINK
Ap
Bp
2Eb
2Bb
REDDISH
3Bb
3Btb
GHOST CLASTS
VEIN QTZ/INTRUSION
3Cr
QTZ VEIN
QTZ
14C
SAPPOLITE (MVF)
REDDISH.
PM 1) COLLUVIUM
2) SAP (MVF)
RED!
2Eb or 2Ab?
3Btb 4Btb
4Btb
4Crb
SAP (MVF)
PM 1) LEGACY COLLUVIUM
2) COLLUVIUM
3) COLLUVIUM
4) SAP (MVF)

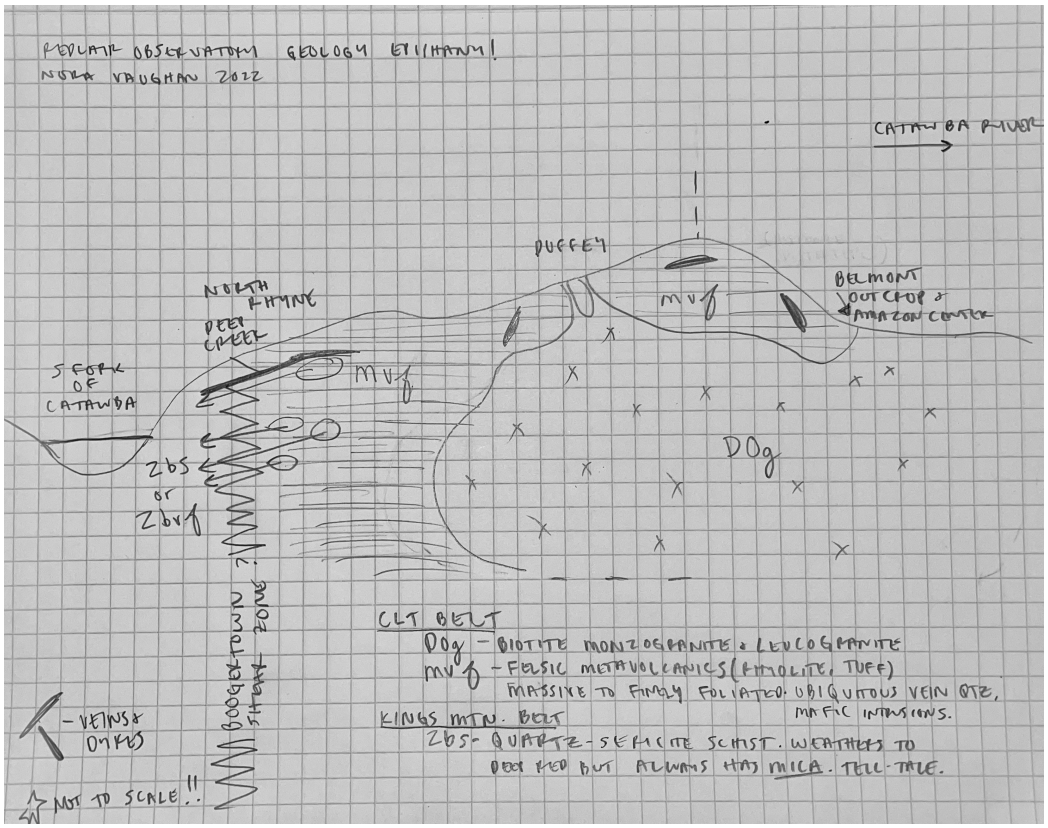
REPLAIR OBSERVATORY GEOLOGY EPIPHANY!
NORA VAUGHAN 2022
CATAWBA RIVER
DUFFEY
NORTH RHYNE
DEEP CREEK
S FORK OF CATAWBA
MVf
BELMONT OUTCROP & AMAZON CENTER
DOg
2bs or 2bvf
BOOGERTOWN SHEAR ZONE?
CLT BELT
DOg - BIOTITE MONZOGRANITE & LEUCOGRANITE
MVf - FELSIC METAVOLCANICS (RHYOLITE, TUFF)
MASSIVE TO FINELY FOLIATED. UBIQUITOUS VEIN QTZ, MAFIC INTRUSIONS.
KINGS MTN. BELT
2bs - QUARTZ-SERICITE SCHIST. WEATHERS TO DEEP RED BUT ALWAYS HAS MICA. TELL-TALE.
- VEINS & DYKES
NOT TO SCALE!!

Appendix D: Soil Pit Descriptions from North Rhyne and Duffey watersheds, Redlair Observatory, NC

See excel file “Redlair soil description sheets Vaughan”

Appendix E: Gravel weight percent methods and raw data

The following data was collected by Alec Wells, Mac Bouzigard, and Nora Vaughan following instructions in Soils Laboratory Manual Spring 2021, seen here:

SIEVING WHILE ALSO CALCULATING GRAVEL WEIGHT %

EQUIPMENT
2mm sieve (same as is in the soil bucket)
Small ziplock sample bags
Permanent marking pen
Scale
Soil log notebook

PROCEDURE

1. If you plan to analyze your sample for bulk density, remove 2-3 peds from sample and put in a separate baggie labeled with the sample designation and the words 'peds for BD'.
2. In the soil log notebook, create a table with headings as follows:

Sample ID
Weight Sample & Bag (g)
Weight Bag (g)
Weight <2mm (g)
Weight > 2mm (g)

3. Write down the name of the sample under the "Sample ID" heading. (If the sample bag has multiple lines of information ex: "penetrometer: 4.5, Shear value: 5 etc" copy all of it down.)
4. Tare the scale with nothing on it.
5. Weigh the sample in the bag to the nearest 0.00 g and record the value under the "Weight Sample and Bag (g)" heading.
6. Dump the sample into the top of the 2 mm sieve, making sure the pan is in place!
7. Put the entire sample through the 2mm sieve.
8. If you see obvious organic matter such as roots or stems, remove it as much as possible.
9. Break up all peds and 'grate' everything through that will go, with the exception of obvious organic material from above.
10. If the sample has a high clay content, it may be difficult to sieve, and wet sieving of the sample may be necessary, in which case you will have to re-air dry the sample before proceeding.
11. Tare the scale again with nothing on it.
12. Weigh the empty bag that the sample originally came from and record the weight to the nearest 0.00 g in the "Weight Bag (g)" Heading.
13. Collect a small ziplock bag and use a permanent marker to label the bag with your sample ID and the label ">2mm" This bag will hold all of the sample that is larger than 2mm.
14. Place the small, empty ziplock bag on the scale and tare it.

1) Carefully transfer the sample <2mm from the top of the sieve screen into the small ziplock baggie and weigh the sample.

PAY ATTENTION THAT YOU TRANSFER THE SAMPLE INTO A CORRECTLY LABELED BAGGIE.

15. Record the weight to the nearest 0.00 g under the "Weight >2mm (g)" heading.
16. Tare the scale again with nothing on it.
17. Carefully transfer the sample found in the bottom of the sieve to the original sample bag. This portion of sample will account for the amount less than 2mm.
18. Weigh the sample <2mm in the original bag and record the value under the "Weight <2mm (g)" heading.
19. Use the following formula to calculate Gravel Weight Percentage:

$$Gravel\ Weight\ Percentage\ = \frac{(Weight > 2mm\ (g))}{(\boldsymbol{Weight\ Sample\ \&\ Bag\ (g)}) - (\boldsymbol{Weight\ Bag\ (g)})} * 100$$

Sample ID	Weight Sample & Bag (g)	Weight Bag (g)	Weight <2mm (g)	Weight > 2mm (g)	Gravel weight %
DU-S3-1	87.4	9.6	77.8	0.6	0.8%
DU-S3-2	290.2	7.3	198.6	82.4	29.1%
DU-S3-3	310.5	8.5	297.2	11.2	3.7%
DU-S3-4	253.7	7.9	201.5	0.2	0.1%
DU-S3-5	251.5	9.7	241.3	0.8	0.3%
DU-S3-6	233.5	7.8	224.5	0.0	0.0%
DU-S3-7	303.9	8.3	302.2	0.0	0.0%
DU-S3-8	255.4	8.2	221.9	19.5	7.9%
DU-S3-9	244.1	8	233.3	0.6	0.3%
DU-S3-10	592.5	3.4	308.4	0.0	0.0%
DU-S4-1	210.9	8.7	182.8	0.0	0.0%
DU-S4-2	203.8	9.8	189.7	0.0	0.0%
DU-S4-3	200.5	8.7	173.4	2.0	1.0%
DU-S4-4	206.4	8.5	189.7	5.2	2.6%
DU-S4-5a	156.5	8.5	135.3	7.0	4.7%
DU-S4-5b	210.0	8.5	165.4	1.7	0.8%
DU-S4-5c	256.1	8.3	222.2	5.8	2.3%
DU-S4-6	211.5	8.3	181.6	6.7	3.3%
DU-S4-7	265.6	8.7	251.9	4.9	1.9%
DU-S4-8	191.6	8.2	150.5	3.7	2.0%
DU-S4-9	270.4	9.1	236.5	10.9	4.2%
DU-S5-1	150.8	9.1	141.3	0.0	0.0%
DU-S5-2	263.6	8.4	153.8	101.4	39.7%
DU-S5-3	253.3	8.2	230.9	7.4	3.0%
DU-S5-4	193.8	8.2	191.8	2.9	1.6%
DU-S5-5	168.6	8.2	160.2	0.2	0.1%
DU-S5-6	197.8	8.2	188.1	0.0	0.0%
DU-S5-7	228.6	8.3	216.9	0.0	0.0%
DU-S5-8	233.9	8.6	217.8	0.4	0.2%
DU-S5-9	151.9	8.8	140.7	0.0	0.0%
DU-S6-1	114.3	9.2	89.1	10.1	9.6%
DU-S6-2	129.2	8.6	107.0	6.2	5.1%
DU-S6-3	168.8	8.5	127.2	34.0	21.2%
DU-S6-4	166.4	8.7	150.9	4.2	2.7%
DU-S6-5	227.7	8.1	215.2	0.6	0.3%
DU-S6-6	177.7	8.5	167.0	0.7	0.4%
DU-S7-1	185.4	9.6	165.0	7.3	4.2%
DU-S7-2	223.6	8.7	185.7	26.1	12.1%
DU-S7-3	301.7	8.4	291.6	1.7	0.6%
DU-S7-4	345.5	8.6	329.3	0.1	0.0%
DU-S7-5	148.5	8.2	137.6	0.0	0.0%
DU-S7-6	209.4	8	199.6	0.0	0.0%
DU-S7-7	154.5	8.1	146.6	0.0	0.0%
DU-S7-8	148.4	8.2	138.7	0.0	0.0%
DU-S8-1	182.5	8.7	153.9	10.3	5.9%
DU-S8-2	222.8	8.1	201.0	4.1	1.9%
DU-S8-3	134.6	8.4	119.3	3.0	2.4%
DU-S8-4	186.3	8.2	180.7	1.0	0.6%
DU-S8-5	164.2	8.1	158.8	0.6	0.4%
DU-S8-6	211.5	8	207.7	0.5	0.2%
DU-S8-7	244.4	8.3	173.6	0.0	0.0%

Sample ID	Weight Sample & Bag (g)	Weight Bag (g)	Weight <2mm (g)	Weight > 2mm (g)	Gravel weight %
NR-S4-1	143.5	8.9	130.6	0.0	0.0%
NR-S4-2	203.7	8.1	194.3	0.0	0.0%
NR-S4-3	313.2	8.1	301.7	0.9	0.3%
NR-S4-4	336.7	8	311.7	9.2	2.8%
NR-S4-4b	534.4	10.7	413.8	105.8	20.2%
NR-S4-5	353.5	8.1	339.4	4.1	1.2%
NR-S4-6	323.5	8	312.5	0.3	0.1%
NR-S4-7	258.6	8.1	254.0	0.0	0.0%
NR-S4-8	493.1	8.1	482.2	0.0	0.0%
NR-S4-9	331.3	8	316.8	0.0	0.0%
NR-S13-1	78.2	8.2	67.7	0.7	1.0%
NR-S13-2	458.2	8.2	384.2	61.2	13.6%
NR-S13-3	480.4	8.1	270.5	199.5	42.2%
NR-S13-4	278.5	8.2	259.3	9.9	3.7%
NR-S13-5	343.3	8.2	330.7	1.2	0.4%
NR-S13-6	318.4	8.2	305.4	2.2	0.7%
NR-S13-7	293.8	8.2	283.2	0.8	0.3%
NR-S10-1	181.9	9.2	172.0	0.5	0.3%
NR-S10-2	330.9	8.3	316.4	10.5	3.3%
NR-S10-3	272.8	8.2	269.5	0.8	0.3%
NR-S10-4	202.0	8.6	198.9	2.7	1.4%
NR-S10-5	394.6	7.8	388.6	0.2	0.1%
NR-S10-6	292.2	8.1	283.1	0.5	0.2%
NR-S10-7	117.8	8.4	114.4	0.3	0.3%
NR-S9-1	152.3	10.3	131.6	8.7	6.1%
NR-S9-2	296.7	9.3	281.9	2.9	1.0%
NR-S9-3	442.8	8.3	425.2	4.3	1.0%
NR-S9-4	381.9	8.4	331.1	37.8	10.1%
NR-S9-5	281.3	8.1	263.5	7.1	2.6%
NR-S9-6	271.2	8.1	253.0	4.6	1.7%
NR-S9-7	180.1	8	169.4	0.0	0.0%
NR-S5b-1	256.7	9.3	241.9	0.0	0.0%
NR-S5b-2	225.1	8.1	204.3	11.4	5.3%
NR-S5b-3	284.1	8.2	273.0	1.8	0.7%
NR-S5b-4	323.0	8.2	312.9	0.4	0.1%
NR-S5-1	217.7	8.2	192.0	17.2	8.2%
NR-S5-2	311.6	8.3	281.3	21.0	6.9%
NR-S5-3	323.2	8.2	285.1	27.8	8.8%
NR-S5-4	257.0	8.3	223.4	24.0	9.7%
NR-S5-5	289.1	8.4	252.4	26.1	9.3%
NR-S5-6	375.8	8.6	339.4	23.5	6.4%
NR-S5-7	403.9	8.2	366.0	26.2	6.6%
NR-S1-1	239.4	9.2	229.5	0.5	0.2%
NR-S1-2	456.2	16.4	455.5	11.8	2.7%
NR-S1-3	468.4	8.2	459.2	5.9	1.3%
NR-S1-4	363.5	7.9	345.9	7.9	2.2%
NR-S1-5	342	8.2	323.7	5	1.5%
NR-S1-6	315	8.1	317.8	0.9	0.3%
NR-S1-7	409.4	9.3	409.6	5.4	1.3%
NR-S1-8	546.9	8.4	546.9	0	0.0%
NR-S1-9	450.5	8.5	449.3	3.7	0.8%
NR-S1-10	459.7	8.6	497.7	1.9	0.4%

Sample ID	Weight Sample & Bag (g)	Weight Bag (g)	Weight <2mm (g)	Weight > 2mm (g)	Gravel weight %
NR-S8-1	191.6	9.6	159.7	20.7	11.4%
NR-S8-2	316.7	8.5	257.8	48.8	15.8%
NR-S8-3	479.1	8.1	452.1	16.7	3.5%
NR-S8-4	336.5	8.3	302.3	15.7	4.8%
NR-S8-5	427.7	8.1	328.2	80.7	19.2%
NR-S8-6	463.6	8	387.9	55.0	12.1%
NR-S8-7	405.1	8.3	374.4	9.1	2.3%
NR-S6-1	154.5	9.7	115.5	26.5	18.3%
NR-S6-2	192.0	8.9	169.0	12.8	7.0%
NR-S6-3	268.5	8.3	252.4	5.3	2.0%
NR-S6-4	305.8	8	282.2	13.1	4.4%
NR-S6-5	268.2	8	256.0	4.8	1.8%
NR-S6-6	338.9	8	329.4	0.0	0.0%
NR-S7-1	189.7	9.5	173.9	4.7	2.6%
NR-S7-2	223.8	8.5	207.2	7.5	3.5%
NR-S7-3	264.1	8.6	244.4	9.4	3.7%
NR-S7-4	354.7	8.6	323.4	19.8	5.7%
NR-S7-5	293.6	8.2	283.0	0.0	0.0%
NR-S7-6	531.9	8.1	518.6	2.1	0.4%
NR-S7-7	389.0	7.8	378.1	0.8	0.2%
NR-S11-1	164.7	9.2	147.5	3.1	2.0%
NR-S11-2	316.9	9.5	301.8	3.6	1.2%
NR-S11-3	279.1	7.9	269.0	0.2	0.1%
NR-S11-4	421.4	8.3	408.9	0.0	0.0%
NR-S11-5	300.0	8.5	288.9	0.0	0.0%
NR-S12-1	142.1	8.3	127.6	3.3	2.5%
NR-S12-2	197.2	8.7	165.6	20.2	10.7%
NR-S12-3	237.3	8.2	227.5	0.6	0.3%
NR-S12-4	204.0	8.2	187.0	7.1	3.6%
NR-S12-5	162.2	8.2	152.4	0.4	0.3%
NR-S12-6	250.8	8.2	239.2	0.7	0.3%

Appendix F: Particle Size Analysis Methods and Raw Data

The following data was collected by Robert Griffin, Alec Wells, and Nora Vaughan following instructions in Soils Laboratory Manual Spring 2021, seen here:

PARTICLE SIZE ANALYSIS – Laser Diffraction Particle Analyzer Sample Preparation
(Modified from Day, 1965, and Jackson 1969). Last Modified 9/1/2017

The particle size analysis procedure is used to determine the percentage of different size fractions of your sample using the Beckman Coulter LS 13 320 Laser Diffraction Particle Analyzer with an Aqueous Liquid Module (ALM) autosampler introduction system.

Prior to the actual particle size procedure, any significant organic matter or carbonate must be removed from the sample (see procedures for small sample digestion). All horizons from most desert soils require carbonate removal (digestion) prior to analysis. If the soil fizzes in acid, you should digest the carbonate. All 'O' horizons require organic matter removal. Most other horizons from temperate-climate soils do not require organic matter digestion. When in doubt, show your soil to Eppes or someone else in the lab with experience.

EQUIPMENT
Balance (analytical), weighing paper, beakers, sonic bath,Squirt bottle containing dispersant solution, Water bottle (deionized)

REAGENTS
Dispersing agent: 10% Sodium Pyrophosphate
To make: Dissolve 53.520 ± 0.003 g of Sodium Pyrophosphate (Na4P2O7) and 4.240 g ± 0.003 of SodiumBicarbonate (Na2CO310H20) into one (1) liter of "super" deionized water to prepare the dispersant solution. It is recommended that you gently heat the dispersant solution and stir.

PROCEDURE
1. If sample contains abundant organic matter or carbonate it must be removed before proceeding with this procedure (see above explanation).
2. The particle size of the dispersant must be known. For every 40 samples or so, and each time that you change dispersants, prepare a dispersant 'blank'. i.e. follow all of the procedures starting below, but this 'sample' will not have any dirt in it only dispersant. Any values produced will ultimately be subtracted from your data at the end. Carefully keep track of which of your soil samples goes with which dispersant blank in the lab notebook. Label the blank dispersant "Blank 1_date", "Blank 2_date" etc. with the date the dispersant was made.
3. Shake up your baggie of <2mm sediment well to mix all particles before spooning out onto a weighing paper. Weigh out and record 0.2-0.4 ± 0.05 (finer soil or sediments) to 1.0-1.4 ±0.1 g (coarser soil or sediments) grams of the fine fraction (< 2mm) and place in a 13 ml autosampler tube.
4. Pipet 5 mL of 10% sodium pyrophosphate (aka dispersant) solution into the tube.
5. Place autosampler tubes in a beaker and place the beaker in a sonic bath. Add water to the beaker to the same height as the dispersant solution in the tube. Run the sonic bath for 30 minutes.
6. Clean walls of the autosampler tube with another 5 ml of dispersant solution and let sit overnight.
7. Sonic mix sample again 10 minutes prior to placing in the autosampler for the LS 13 320 Laser Diffraction Particle Analyzer.
8.The LS 13 320 will automatically dilute the sample to the appropriate obscuration (7-12%) before running the sample in triplicate. You must make sure you are in this range. If not, you will need to start over with less or more sample.
9. See manual for operating the LS 13 320 in order to analyze grain size distributions.

Sample ID	% gravel	% clay (<4um)	% sand	% silt
DU_S1-1	4	14.2	20.2	65.6
DU_S1-2	9.2	22.8	18.4	58.8
DU_S1-3	14.1	23.8	19.2	57.0
DU_S1-4	41.1	22.7	21.7	55.6
DU_S1-5	13.9	22.9	20.5	56.6
DU_S2-1	13.1	9.8	30.5	59.8
DU_S2-2	29.3	16.9	18.8	64.3
DU_S2-3	4.7	22.8	10.2	67.0
DU_S2-4	7.3	22.8	12.0	65.2
DU_S2-4_DUP	7.3	22.0	11.9	66.1
DU_S3_1	0.8	4.6	59.3	36.1
DU_S3_10	0	14.7	15.2	70.1
DU_S3_2	29.1	19.2	18.0	62.8
DU_S3_3	3.7	28.9	11.6	59.5
DU_S3_4	0	31.8	5.9	62.3
DU_S3_5	0.3	33.0	4.5	62.5
DU_S3_6	0	27.2	9.1	63.7
DU_S3_7	0	24.2	13.5	62.3
DU_S3_8	7.9	24.5	10.8	64.7
DU_S3_9	0.3	16.8	11.5	71.7
DU_S4_1	0	7.0	29.5	63.5
DU_S4_2	0	21.7	15.0	63.3
DU_S4_3	1	28.9	13.8	57.3
DU_S4_4	2.6	29.5	14.3	56.2
DU_S4_5A	4.7	21.1	49.9	29.0
DU_S4_5B	0.8	26.7	18.3	55.0
DU_S4_5C	2.3	23.2	21.3	55.5
DU_S4_6	3.3	16.8	23.1	60.1
DU_S4_7	1.9	23.8	21.8	54.4
DU_S4_8	2	27.0	23.5	49.5
DU_S4_9	4.2	24.3	27.9	47.8
DU_S5_1	0	10.1	24.6	65.3
DU_S5_2	39.7	31.1	8.2	60.7
DU_S5_3	3	30.9	6.1	63.1
DU_S5_4	1.6	31.6	4.3	64.1
DU_S5_5	0.1	28.4	3.8	67.8
DU_S5_6	0	27.3	3.7	69.0
DU_S5_7	0	24.9	5.2	69.9
DU_S5_8	0.2	23.5	6.7	69.8
DU_S5_9	0	17.4	14.7	67.9
DU_S6_1	9.6	12.6	29.1	58.3
DU_S6_2	5.1	29.3	17.7	53.0
DU_S6_3	21.2	48.0	0.0	52.0
DU_S6_4	2.7	46.4	0.0	53.6
DU_S6_5	0.3	35.3	1.2	63.5
DU_S6_6	0.4	22.5	5.6	71.9

Sample ID	% gravel	% clay (<4um)	% sand	% silt
DU_S7_1	4.2	8.5	32.0	59.5
DU_S7_2	12.1	26.2	8.3	65.5
DU_S7_3	0.6	30.3	6.3	63.4
DU_S7_4	0	27.9	11.5	60.6
DU_S7_5	0	23.0	15.2	61.8
DU_S7_6	0	23.4	7.5	69.1
DU_S7_7	0	20.1	14.8	65.1
DU_S7_8	0	14.2	23.6	62.2
DU_S8_1	5.9	12.5	21.7	65.8
DU_S8_2	1.9	29.6	8.7	61.7
DU_S8_3	2.4	32.2	7.9	59.9
DU_S8_4	0.6	31.0	12.5	56.5
DU_S8_5	0.4	29.5	11.3	59.2
DU_S8_6	0.2	26.4	16.1	57.5
DU_S8_7	0	21.1	23.4	55.5
DU_S8_8	5.2	22.8	33.7	43.5

Sample ID	% gravel	% clay (<4um)	% sand	% silt
NR_S1_1	0.2	9.0	48.8	42.2
NR_S1_10	0.4	19.9	15.4	64.7
NR_S1_2	2.7	11.8	38.4	49.8
NR_S1_3	1.3	10.8	39.6	49.6
NR_S1_4	2.2	10.3	52.3	37.4
NR_S1_5	1.5	15.8	28.1	56.1
NR_S1_6	0.3	17.8	17.6	64.6
NR_S1_7	1.3	16.8	16.3	66.9
NR_S1_8	0	17.7	11.3	71.0
NR_S1_9	0.8	19.5	12.8	67.7
NR_S10_1	0.3	5.3	53.5	41.2
NR_S10_2	3.3	15.1	23.1	61.8
NR_S10_3	0.3	15.7	26.1	58.2
NR_S10_4	1.4	15.3	20.1	64.6
NR_S10_5	0.1	16.8	18.4	64.8
NR_S10_6	0.2	12.7	18.9	68.4
NR_S10_7	0.3	8.1	39.3	52.6
NR_S11_1	3.1	5.6	55.5	39.0
NR_S11_2	1.2	15.4	21.6	63.0
NR_S11_3	0.1	19.0	15.0	66.0
NR_S11_4	0	16.7	15.4	67.9
NR_S11_5	0	13.3	25.6	61.1
NR_S12_1	2.5	17.3	30.4	52.3
NR_S12_2	10.7	11.6	37.4	51.0
NR_S12_3	0.3	22.9	14.4	62.7
NR_S12_4	3.6	20.9	14.1	65.0
NR_S12_5	0.3	20.7	14.9	64.4
NR_S12_6	0.3	22.2	11.0	66.8
NR_S13_2	13.6	13.9	20.9	65.2
NR_S13_3	42.2	15.8	20.6	63.6
NR_S13_5	3.7	19.5	9.5	71.0
NR_S13_6	0.4	18.6	10.3	71.1
NR_S13_7	0.7	12.8	20.7	66.5
NR_S13_7DUP	0.3	12.8	20.7	66.5
NR_S1_1	0.2	9.0	48.8	42.2
NR_S1_10	0.4	19.9	15.4	64.7
NR_S1_2	2.7	11.8	38.4	49.8
NR_S1_3	1.3	10.8	39.6	49.6
NR_S1_4	2.2	10.3	52.3	37.4
NR_S1_5	1.5	15.8	28.1	56.1
NR_S1_6	0.3	17.8	17.6	64.6
NR_S1_7	1.3	16.8	16.3	66.9
NR_S1_8	0	17.7	11.3	71.0
NR_S1_9	0.8	19.5	12.8	67.7
NR_S10_1	0.3	5.3	53.5	41.2
NR_S10_2	3.3	15.1	23.1	61.8
NR_S10_3	0.3	15.7	26.1	58.2
NR_S10_4	1.4	15.3	20.1	64.6
NR_S10_5	0.1	16.8	18.4	64.8
NR_S10_6	0.2	12.7	18.9	68.4
NR_S10_7	0.3	8.1	39.3	52.6

Sample ID	% gravel	% clay (<4um)	% sand	% silt
NR_S11_1	3.1	5.6	55.5	39.0
NR_S11_2	1.2	15.4	21.6	63.0
NR_S11_3	0.1	19.0	15.0	66.0
NR_S11_4	0	16.7	15.4	67.9
NR_S11_5	0	13.3	25.6	61.1
NR_S12_1	2.5	17.3	30.4	52.3
NR_S12_2	10.7	11.6	37.4	51.0
NR_S12_3	0.3	22.9	14.4	62.7
NR_S12_4	3.6	20.9	14.1	65.0
NR_S12_5	0.3	20.7	14.9	64.4
NR_S12_6	0.3	22.2	11.0	66.8
NR_S13_2	13.6	13.9	20.9	65.2
NR_S13_3	42.2	15.8	20.6	63.6
NR_S13_5	3.7	19.5	9.5	71.0
NR_S13_6	0.4	18.6	10.3	71.1
NR_S13_7	0.7	12.8	20.7	66.5
NR_S13_7DUP	0.3	12.8	20.7	66.5
NR_S4_1	0	3.8	70.3	25.9
NR_S4_2	0	13.0	20.1	66.9
NR_S4_3	0.3	15.3	11.0	73.7
NR_S4_4	2.8	18.5	16.5	65.0
NR_S4_5	1.2	20.3	10.3	69.4
NR_S4_6	0.1	20.1	9.1	70.8
NR_S4_7	0	17.7	14.1	68.2
NR_S4_8	0	10.5	35.2	54.3
NR_S5_1	8.2	8.1	47.2	44.7
NR_S5_2	6.9	10.3	46.0	43.7
NR_S5_3	8.8	15.6	21.7	62.7
NR_S5_4	9.7	16.9	15.9	67.2
NR_S5_5	9.3	15.4	19.6	65.0
NR_S5_6	6.4	16.3	18.6	65.1
NR_S5_7	6.6	15.8	19.8	64.4
NR_S5b_1	0	9.0	34.4	56.6
NR_S5b_2	5.3	11.9	33.8	54.3
NR_S5b_3	0.7	16.7	23.2	60.1
NR_S5b_4	0.1	14.1	36.1	49.8
NR_S5b_4dup	0.1	13.2	36.4	50.4
NR_S6_1	18.3	8.2	39.2	52.6
NR_S6_2	7	13.7	26.3	60.0
NR_S6_3	2	14.9	28.0	57.1
NR_S6_4	4.4	9.8	36.7	53.5
NR_S6_5	1.8	9.0	40.1	50.9
NR_S6_6	0	4.1	67.6	28.3
NR_S7_1	2.6	5.7	55.4	38.9
NR_S7_2	3.5	12.1	48.5	39.4
NR_S7_3	3.7	24.3	10.0	65.7
NR_S7_4	5.7	22.2	13.5	64.3
NR_S7_5	0	17.4	21.5	61.1
NR_S7_6	0.4	14.4	27.0	58.6
NR_S7_7	0.2	9.9	38.7	51.4

Sample ID	% gravel	% clay (<4um)	% sand	% silt
NR_S8_1	11.4	4.6	53.4	42.0
NR_S8_2	15.8	11.8	37.6	50.6
NR_S8_3	3.5	18.4	19.1	62.5
NR_S8_3dup	3.5	14.6	35.3	50.1
NR_S8_4	4.8	18.2	34.6	47.2
NR_S8_5	19.2	18.7	35.9	45.4
NR_S8_6	12.1	18.2	34.7	47.1
NR_S8_7	2.3	14.7	42.0	43.3
NR_S9_1	6.1	6.3	45.6	48.1
NR_S9_2	1	18.8	14.7	66.5
NR_S9_2dup	1	19.1	14.8	66.1
NR_S9_3	1	19.9	13.0	67.1
NR_S9_4	10.1	19.5	13.0	67.5
NR_S9_5	2.6	20.1	12.5	67.4
NR_S9_6	1.7	18.0	33.4	48.6
NR_S9_7	0	11.1	51.2	37.7

Appendix F: Particle Size Analysis Methods and Raw Data

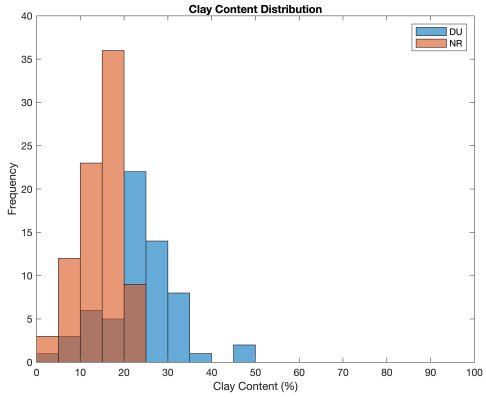

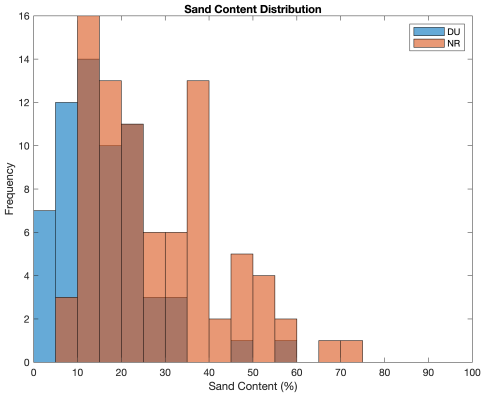

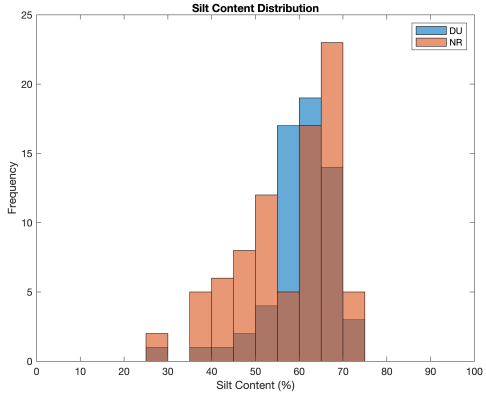

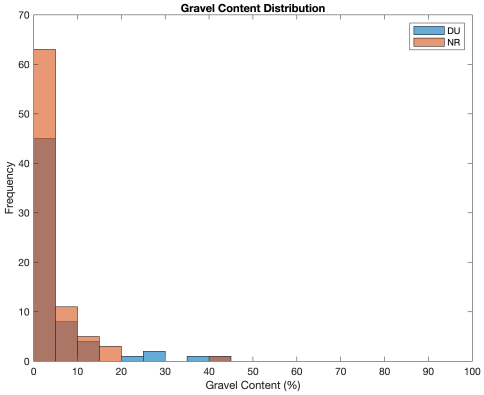

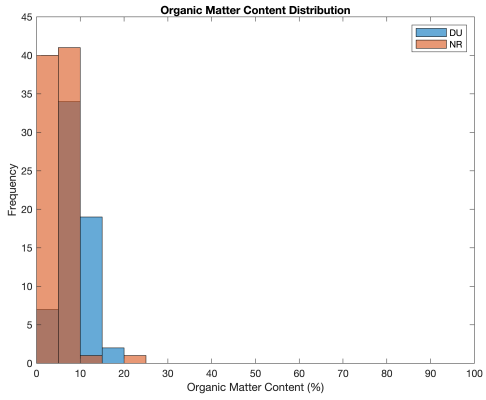

Histograms show distribution of clay, sand, silt, gravel, and organic carbon measured as loss-on-ignition in Duffey (blue) and North Rhyne (orange) watersheds.

Appendix F: Particle Size Analysis Methods and Raw Data

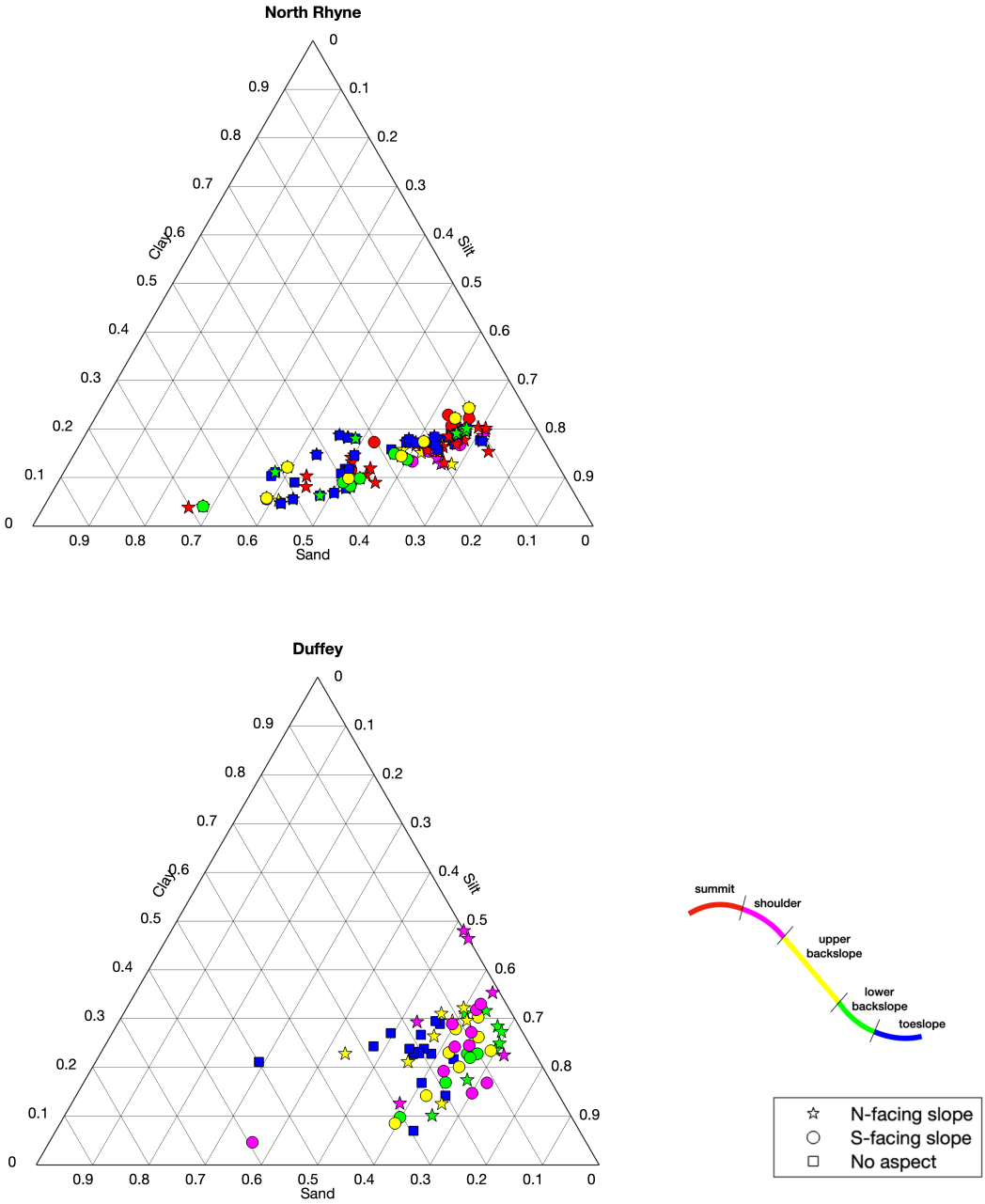

Ternary diagram of sand silt and clay. Samples from north-facing hillslopes are plotted as stars, samples from south-facing hillslopes are plotted as circles, and samples from toeslope positions with no hillslope aspect are plotted as squares. The hillslope position of each sample is represented by the color of each marker. Summit hillslope positions are in red, shoulder positions in magenta, upper backslope in yellow, lower backslope in green, and toeslope in blue.

Appendix F: Particle Size Analysis Methods and Raw Data

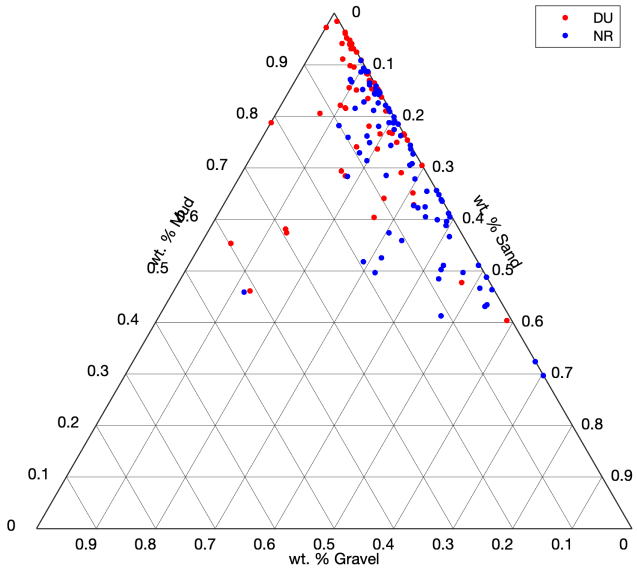

Ternary diagram of gravel, mud, and sand normalized to the gravel content. Samples from Duffey reported in red, and North Rhyne samples are reported in blue.

Appendix G: Loss on ignition methods and raw data

The following data was collected by Robert Griffin, and Nora Vaughan following instructions in Soils Laboratory Manual Spring 2021, seen here:

ORGANIC CARBON CONTENT BY LOSS ON IGNITION

This procedure is used for the routine measurement of soil organic matter by the loss of weight in a sample heated to a temperature high enough to burn organic matter but not so high as to decompose carbonates.

Materials and Apparatus

Oven or muffle furnace capable of operating up to 600 C
Ceramic crucibles
Mortar and pestle
Heat resistant gloves & tongs
Desiccator with fresh desiccant
Acetone

Procedures

1. Label crucibles with permanent marker (side) and pencil (bottom). These are likely to burn off in the furnace so always keep them arranged in a way whereby you can keep track of them in the oven and in the desiccator.
2. Heat crucibles in an ordinary drying oven at 110°C for longer than 1 hour (can be left overnight).
3. Place the crucibles in a desiccator to cool. Leave them in the desiccator until you use them to prevent them from absorbing moisture.
4. Weigh dry, cool crucibles and record the weight to the nearest 0.000 g.
5. Grind ~ 2 – 5 g of air-dried sample with mortar and pestle to a fine powder. Mortar and pestle should be washed between samples using acetone and Kimwipes which will dry quickly and keep samples dry.
6. Place sample in crucible and dry for 2 hours or longer in a 105° C oven.
7. Remove from oven and place in desiccator to cool.
8. When cool, weigh samples in the crucibles, recording the weight to 0.000 g. Make sure that you note which sample is in each specific crucible. This will be your 'oven dried sample weight'.
9. Using heat resistant gloves and appropriate (extra long) tongs, place crucibles in the furnace at 550 C. Remember, the labels are going to burn off so place them in a known and consistent order.
10. Heat for 1.5 hours until all dark, organic material is gone. Note: Flames will die down when you close the door.
11. Take crucibles out and place them in a heat resistant desiccator in a known and consistent order.
12. Weigh and record weight to 0.000 g when cool. This will be your 'incinerated sample weight'.
13. Note: If many samples are being run, the dry crucibles do not need to be reweighed after each batch as long as the numbers are always kept the same. Thus, it is critical to always keep the crucibles in a known order and re-label them after each use. Reweigh crucibles after every 4 uses to ensure that they have not chipped.

Organic content is calculated as a percent. (Original Sample weight – incinerated sample weight) (g)/original sample weight (g) *100

Sample ID	Crucible #	Weight crucible (g)	Oven dried sample weight	Incinerated sample weight	Organic content
DU-S3-1	1	12.3284	14.537	14.2453	13.21%
DU-S3-2	2	16.1503	19.4292	19.3517	2.36%
DU-S3-3	3	13.2893	16.7936	16.4938	8.56%
DU-S3-4	4	10.153	13.0096	12.7678	8.46%
DU-S3-5	5	11.9225	15.4558	15.1009	10.04%
DU-S3-6	6	12.4807	15.8116	15.5328	8.37%
DU-S3-7	7	17.7346	20.6541	20.3434	10.64%
DU-S3-8	1	12.2578	15.6603	15.3788	8.27%
DU-S3-9	9	13.1985	16.2218	15.8913	10.93%
DU-S3-10	10	10.5477	13.7763	13.5778	6.15%
DU-S4-1	11	11.8588	15.0319	14.5791	14.27%
DU-S4-2	12	9.8864	12.7699	12.5171	8.77%
DU-S4-3	13	12.799	16.236	15.7174	15.09%
DU-S4-4	14	12.2736	15.4962	15.2635	7.22%
DU-S4-5a	15	12.2581	15.5606	15.387	5.26%
DU-S4-5b	16	14.2827	17.5042	17.3898	3.55%
DU-S4-5c	17	10.8258	13.9605	13.7654	6.22%
DU-S4-6	18	12.051	15.3635	15.1944	5.10%
DU-S4-7	19	17.3044	20.6932	20.4208	8.04%
DU-S4-8	20	17.4102	20.4349	20.3872	1.58%
DU-S4-9	21	17.1038	20.2282	20.1852	1.38%
DU-S5-1	22	9.503	12.5684	12.1934	12.23%
DU-S5-2	23	11.7598	14.8751	14.629	7.90%
DU-S5-3	24	9.3445	12.5241	12.2628	8.22%
DU-S5-4	25	12.2201	15.314	14.9218	12.68%
DU-S5-5	26	13.5903	17.7826	17.3477	10.37%
DU-S5-6	27	10.1229	13.6697	13.2717	11.22%
DU-S5-7	28	9.5366	12.6096	12.2721	10.98%
DU-S5-8	29	14.3266	17.9081	17.4049	14.05%
DU-S5-9	30	10.9005	14.3164	13.9997	9.27%
DU-S6-1	2	12.3933	15.5965	15.3697	7.08%
DU-S6-2	32	11.3639	14.8839	14.664	6.25%
DU-S6-3	33	11.1011	14.4477	14.1085	10.14%
DU-S6-4	34	11.8061	15.7214	15.361	9.20%
DU-S6-5	35	12.5199	15.7111	15.4546	8.04%
DU-S6-6	22	14.3255	18.2708	17.9811	7.34%
DU-S7-1	3	10.8027	13.9638	13.6171	10.97%
DU-S7-2	4	11.9798	15.5445	15.2548	8.13%
DU-S7-3	5	11.0244	14.2294	13.9312	9.30%
DU-S7-4	6	13.0767	16.5833	16.2739	8.82%
DU-S7-5	7	13.4208	16.9589	16.662	8.39%
DU-S7-6	8	11.6488	15.0414	14.77	8.00%
DU-S7-7	9	12.7249	15.9262	15.67	8.00%
DU-S7-8	10	9.2284	12.7303	12.4632	7.63%
DU-S8-1	11	12.4176	15.8188	15.4912	9.63%
DU-S8-2	12	17.5862	20.7915	20.5966	6.08%
DU-S8-3	13	14.1114	17.6362	17.3842	7.15%
DU-S8-4	14	9.7844	12.9574	12.6804	8.73%
DU-S8-5	16	17.2103	20.2861	20.0217	8.60%
DU-S8-6	17	11.2339	14.4801	14.2162	8.13%
DU-S8-7	18	10.0056	13.3803	13.1142	7.89%
DU-S8-8	19	11.8788	15.2213	14.9742	7.39%

Sample ID	Crucible #	Weight crucible (g)	Oven dried sample weight	Incinerated sample weight	Organic content
NR-S8-1	19	11.7626	14.9335	14.6946	7.53%
NR-S8-2	20	12.4787	15.9339	15.8073	3.66%
NR-S8-3	30	9.4303	12.9149	12.7944	3.46%
NR-S8-4	31	16.7932	20.7007	20.6065	2.41%
NR-S8-5	32	10.6753	14.091	13.9958	2.79%
NR-S8-6	33	13.0702	16.4389	16.3385	2.98%
NR-S8-7	21	11.9227	15.4634	15.3262	3.87%
NR-S6-1	21	9.2822	13.6143	13.2884	7.52%
NR-S6-2	22	15.9807	20.1671	19.9324	5.61%
NR-S6-3	23	11.815	15.8587	15.6119	6.10%
NR-S6-4	24	14.1227	17.8816	17.7232	4.21%
NR-S6-5	25	10.9396	14.8349	14.6705	4.22%
NR-S6-6	26	12.0133	16.4129	16.2862	2.88%
NR-S7-1	1	12.344	15.432	15.198	7.58%
NR-S7-2	2	12.547	16.738	16.559	4.27%
NR-S7-3	3	10.899	13.925	13.68	8.10%
NR-S7-4	4	12.219	15.609	15.448	4.75%
NR-S7-5	5	11.122	14.845	14.638	5.56%
NR-S7-6	6	13.293	17.393	17.18	5.20%
NR-S7-7	7	13.593	17.823	17.681	3.36%
NR-S11-1	1	12.485	15.5826	15.2882	9.50%
NR-S11-2	15	12.251	15.817	15.654	4.57%
NR-S11-3	19	12.053	15.562	15.29	7.75%
NR-S11-4	20	12.477	15.756	15.524	7.08%
NR-S11-5	21	9.505	12.905	12.703	5.94%
NR-S12-1	22	16.148	20.309	19.995	7.55%
NR-S12-2	23	11.924	15.15	14.998	4.71%
NR-S12-3	24	14.326	17.807	17.555	7.24%
NR-S12-4	26	12.272	15.63	15.376	7.56%
NR-S12-5	29	11.763	15.25	14.982	7.69%
NR-S12-6	33	13.198	16.251	16.021	7.53%

Sample ID	Crucible #	Weight crucible (g)	Oven dried sample weight	Incinerated sample weight	Organic content
NR-S4-1	20	12.3125	15.3766	14.6379	24.11%
NR-S4-2	21	9.2822	12.6967	12.4918	6.00%
NR-S4-3	22	15.9807	19.3048	19.1321	5.20%
NR-S4-4	1	12.2578	16.1023	15.9792	3.20%
NR-S4-4b	24	14.1227	17.6054	17.5059	2.86%
NR-S4-5	25	10.9396	14.3849	14.2125	5.00%
NR-S4-6	26	12.0133	15.3805	15.1386	7.18%
NR-S4-7	27	10.4484	13.6984	13.4603	7.33%
NR-S4-8	28	10.0712	13.3365	13.1563	5.52%
NR-S4-9	2	12.3933	16.9468	16.7744	3.79%
NR-S13-1	3	10.8027	14.8504	14.2251	15.45%
NR-S13-2	4	11.9798	16.5141	16.3377	3.89%
NR-S13-3	5	11.0244	15.394	15.2481	3.34%
NR-S13-4	6	13.0767	17.5143	17.329	4.18%
NR-S13-5	7	13.4208	17.9512	17.6595	6.44%
NR-S13-6	8	11.6488	16.5602	16.2058	7.22%
NR-S13-7	9	12.7249	16.5531	16.312	6.30%
NR-S10-1	2	13.6292	16.3288	15.9726	13.19%
NR-S10-2	3	14.3777	17.2138	17.0592	5.45%
NR-S10-3	4	11.9451	14.8069	14.6726	4.69%
NR-S10-4	5	11.0885	14.8147	14.6052	5.62%
NR-S10-5	6	12.5207	15.2204	15.0391	6.72%
NR-S10-6	7	9.3472	12.1593	12.0007	5.64%
NR-S10-7	8	9.8857	12.8784	12.7583	4.01%
NR-S9-1	8	11.86	16.42	16.016	8.86%
NR-S9-2	9	12.799	16.937	16.708	5.53%
NR-S9-3	10	9.331	13.723	13.476	5.62%
NR-S9-4	11	12.522	15.971	15.781	5.51%
NR-S9-5	12	17.725	21.645	21.52	3.19%
NR-S9-6	13	14.284	18.231	17.998	5.90%
NR-S9-7	14	9.889	14.063	13.865	4.74%
NR-S5b-1	10	9.2284	13.9218	13.4709	9.61%
NR-S5b-2	11	12.4176	16.9968	16.8055	4.18%
NR-S5b-3	12	17.5862	21.9286	21.7581	3.93%
NR-S5b-4	13	14.1114	18.3995	18.2427	3.66%
NR-S5-1	14	9.7844	13.9569	13.8353	2.91%
NR-S5-2	15	12.1836	16.1904	16.0733	2.92%
NR-S5-3	16	17.2103	21.7745	21.5384	5.17%
NR-S5-4	17	11.2339	15.2169	15.0863	3.28%
NR-S5-5	18	10.0056	14.7463	14.6139	2.79%
NR-S5-6	19	11.8788	16.4804	16.3406	3.04%
NR-S5-7	20	12.3125	16.2018	16.0869	2.95%
NR-S1-1	9	11.1182	14.1947	13.9919	6.59%
NR-S1-2	10	10.9014	13.9579	13.8473	3.62%
NR-S1-3	11	13.2902	16.3373	16.2308	3.50%
NR-S1-4	12	12.8002	15.8716	15.779	3.01%
NR-S1-5	13	14.3279	17.2946	17.1861	3.66%
NR-S1-6	14	12.2572	15.15	15.0246	4.33%
NR-S1-7	15	11.9231	14.708	14.5776	4.68%
NR-S1-8	16	12.4809	15.4631	15.3052	5.29%
NR-S1-9	17	12.2223	15.072	14.9705	3.56%
NR-S1-10	18	12.3291	15.1529	15.0505	3.63%

Appendix H: Bulk density methods and raw data

BULK DENSITY-PARAFFIN CLOD METHOD
(Blake, 1965 and modified by Singer, 1986)

PRINCIPLE
In this method, an intact clod is removed from the soil for volume and weight measurement. Soils with coarse fragments present a special problem. Clod size must be increased proportionately as gravel size and soil volume occupied by gravel increases. For some soils with very high gravel content, a visual estimate of volumetric gravel content may be used. For nongravelly soils, a 200-250 g sample is convenient. The paraffin becomes a significant part of the total weight of smaller samples.

An undisturbed soil sample (ped) is weighed and its volume calculated by determining the volume of water it displaces after the sample is coated with a water proof material. Bulk density is calculated as the weight per unit volume, normally on an oven dry basis.

EQUIPMENT
Beam balance
String
Paraffin
Warming container for the paraffin
Oven
Balance (two decimal)

PROCEDURE
(1) Tie each ped by fine thread, oven dry for 24 hours at ~100 C, weigh and record the weight to the nearest 0.000 grams. A fine thread of twine or sewing thread works well for all but the weakest clods.
(2) Briefly immerse the clod in 48 °C paraffin. A brief immersion at the temperature slightly above the paraffin melting point helps to retard paraffin penetration into soil pores. One coating should be sufficient to waterproof the clod.
(3) Dip coated ped in beaker of cold water to check for leaks and to help cool the sample. If you notice bubbles coming from the ped, dry and re-dip.
(4) After the paraffin is solid, weigh the coated clod in air and in water by tying the string to the beam balance.
(5) If gravel free bulk density is desired, remove wax from ped, soak in water overnight and wash through a 2mm sieve. The gravel-free weight of the ped is calculated using the weight and volume of the gravel as a correction factor.
(6) WASTE DISPOSAL: Collect the coarse material from the washing in a water bath set beneath the sieve. Allow the water to evaporate and put the dry soil in the trash.

CALCULATION

<2mm BD = (Oven Dry Ped Weight - >2mm weight)/[Ped + Wax Weight – (Ped + Wax Weight in H2O) – (Wax Weight/.9) – (>2mm Weight/2.65)]

Where 2.65 = average density of rock
0.9 = density of paraffin

Appendix H: Bulk density methods and raw data

sample	oven dry ped weight	gravel weight %	gravel weight	ped+wax air weight	wax weight	ped+wax h2o weight	wax weight /.9	(>2mm Weight/ 2.65	<2mm BD (g/ ml)
DU-S3-2	20.6983	0.291	6.0232053	21.509	0.8107	11.1732	0.9007777778	2.27290766	2.048989104
DU-S5-6	19.1018	0	0	20.0638	0.962	6.9162	1.068888889	0	1.581443568
NR-S11-1	11.2144	0.02	0.224288	12.1919	0.9775	2.4056	1.086111111	0.08463698113	1.27561323
NR-S6-6	3.1661	0	0	3.5789	0.4128	1.3003	0.4586666667	0	1.739679109
NR-S4-9	17.9269	0	0	19.0499	1.123	6.7923	1.247777778	0	1.628264257
NR-S8-5	31.3561	0.19	5.957659	32.6567	1.3006	17.6805	1.445111111	2.248173208	2.251052983
NR-S11-3	14.116	0.01	0.14116	14.9981	0.8821	5.5572	0.9801111111	0.05326792453	1.662183188
DU-S5-9	12.7634	0	0	13.6037	0.8403	3.1662	0.9336666667	0	1.342973888
DU-S3-5	3.1233	0.03	0.093699	3.4442	0.3209	1.2581	0.3565555556	0.03535811321	1.688565422
NR-S9-3	15.6265	0.01	0.156265	16.4863	0.8598	6.0586	0.9553333333	0.05896792453	1.643427143
NR-S8-7	28.0436	0.02	0.560872	29.2192	1.1756	12.2193	1.306222222	0.2116498113	1.775137473
DU-S5-1	16.8618	0.15	2.52927	18.0108	1.149	4.9987	1.276666667	0.9544415094	1.329425922
DU-S5-2	14.0161	0.2	2.80322	15.0542	1.0381	5.1231	1.153444444	1.057818868	1.452476322
DU-S3-10	2.8642	0	0	3.2657	0.4015	1.0792	0.4461111111	0	1.645724136
NR-S4-6	38.996	0.01	0.38996	40.312	1.316	14.1624	1.462222222	0.147154717	1.573173964
NR-S4-1	27.4451	0	0	29.0411	1.596	8.3346	1.773333333	0	1.449577901

Appendix I: Radiocarbon dating

Date of Report	LAB SAMPLE #	Project Sample name	Other ID	Landform	Lattidtude DD	Longitude DD	Depth/ Soil Horizon	fraction	±	^{14}C age	±	Calibrated
4/28/23	D-AMS 049246	NR1-14C-3	North Rhyne	Alluvial fan, buried soil	N 35.2978641	W 81.0829493	82, Abg2	97.85	0.23	175	19	289-256 (18.9%); 225-138 (55.8%); 34-…(20.7%)
4/28/23	D-AMS 049247	NR7-14C-4	North Rhyne	upper backslope, Bt	N 35.2987352	W 81.0947244	86-93, 2BtCr	80.06	0.22	1786	22	1673-1613 (62.8%); 1730-1690 (30%)
4/28/23	D-AMS 049248	NR8-14C-1	North Rhyne	toeslope, 4Cr	N 35.2986882	W 81.0944457	149, 4Cr	insufficient material following pretreatment				
4/28/23	D-AMS 049249	NR4-14C-20	North Rhyne	summit, 2Eb	N 35.2975904	W 81.0943850	90-94, 2Eb	insufficient material following pretreatment				
4/28/23	D-AMS 049250	DU4-14C-4	Duffey	toeslope, CBw	N 35.2978101	W 81.0826572	57, CBw	99.68	0.27	modern		
4/28/23	D-AMS 049251	DU4-14C-5	Duffey	toeslope, BBg	N 35.2978101	W 81.0826572	82, BBg	98.62	0.26	112	21	140-25(70.8%); 263-220 (24.7%)
4/28/23	D-AMS 049252	DU7-14C-6	Duffey	backslope, Bt	N 35.2983054	W 81.0831859	32, Bt	82.07	0.3	1587	29	1531-1402 (95.4%)
4/28/23	D-AMS 049253	NR5-14C-8	North Rhyne	north face toeslope/ check dam, 4Bb	N 35.2978641	W 81.0829493	195, 4Bb	58.45	0.2	4313	27	4960-4836 (95.4%)
4/28/23	D-AMS 049254	NR13-14C-7	North Rhyne	shoulder, 2Eb	N 35.2976776	W 81.0941992	43, 2Eb	97.63	0.27	193	22	220-143 (58.5%) ; 294-263 (22.5%)
4/28/23	D-AMS 050867	NR8-14C-9	North Rhyne	south facing toeslope, 3BCb, 4Cr boundary?	N 35.2986882	W 81.0944457	105, 3BCb /4Cr boundary	47.09	0.18	6050	31	6985-6795 (95%)
4/28/23	D-AMS 050868	NR4-14C-10	North Rhyne	north facing summit, 2Eb	N 35.2975904	W 81.0943850	30, 2Eb	no charcoal present in matrix				
4/28/23	D-AMS 050869	NR1-14C-11	North Rhyne	alluvial fan	N 35.2978641	W 81.0829493	62, CB	98.83	0.3	95	24	259-222(25.8%); 142-30(69.7%)
4/28/23	D-AMS 050870	NR5-14C-13	North Rhyne	north face toeslope, check dam, 3Ab	N 35.2978641	W 81.0829493	120, 3Ab	81.4	0.28	1653	28	1605-1510 (71.2%); 1456-1415(13.1%) 1500-1471 (7.4%); 1689-1674(3.8%)

Charcoal samples were processed by DirectAMS.

OxCal v4.4.4 Bronk Ramsey (2021); Atmospheric data from Reimer et al (2020).

Appendix J: FeD and FeH methods and raw data

The following data was collected by Alec Wells and Nora Vaughan following instructions in Soils Laboratory Manual Spring 2021, seen here:

(FeD) EXTRACTION OF FE dOXYHYDROXIDES USING THE CITRATE-DITHIONITE BICARBONATE METHOD
(Hendricks, written communication, McKeague and Day, 1966, Mehra and Jackson, 1960)

Dithionite-citrate treatment is thought to remove the total free iron that is not included in silicate minerals; these are the crystalline oxides (geothite and hematite), amorphous hydrous oxides, and organic-bound iron.

EQUIPMENT
Crushed (<100 mesh) sample (see Crushing Instructions)
Centrifuge that will hold 50 mL plastic tubes.
Hot plate
30 ml pipette
190 x 100 mm pyrex dish
Centrifuge tube rack to fit pyrex dish
Thermometer
Stir rods
Spatula
50 ml centrifuge tubes with rack
100 ml or 150 ml volumetric flasks (250 ml flasks necessary for samples with >2% iron); these are the round-bottom flasks that are more accurate than standard Earlymeyer flasks. Note, these must be used for accuracy!

REAGENTS
Sodium Citrate - Bicarbonate buffer
For 100mL, add 90 ml 0.3 M Na Citrate Dihydrate $Na_3C_6H_5O_7 \cdot 2H_2O$ (88.23 g/l) to 10 ml 1M $NaHCO_3$ (84.01 g/l).
For 2250 mL, add 178.67 g of Na Citrate Dihydrate to 2025 ml DI water. In a separate beaker, add 18.9 g of $NaHCO_3$ to 225 ml of DI water. Mix the two solutions together. Both need to be heated slightly and stirred well so that all grains are dissolved. Shake or stir for several minutes.

Sodium dithionite ($Na_2S_2O_4$) Fe-standards (see below)

Note: All water in this procedure should be “Super DI”.

PROCEDURE – Note: important to use precise measurements for all liquids.

1. NOTE YOU MUST FIRST CRUSH YOUR SAMPLE FIRST. See CRUSHING INSTRUCTIONS.
2. Weigh 0.5 ± .002 g crushed (100-mesh) soil into 50 ml centrifuge tubes labeled with the Sample ID. Prep 1 duplicate for every 7-10 samples. Duplicates must be prepped from start to finish. NOT just run twice!
3. Record the sample ID and weight (to 0.000) in the lab-book.

NOTE: These weighed, dry samples can sit indefinitely in the closed tubes.

Appendix J: FeD and FeH methods and raw data

4. When you are ready to run your samples on the AA, within one week prior to doing that, prepare your reagent, and complete the following on a batch of ~25-50 samples.
5. Start a warm-water bath with the tube rack inserted in the pan, filling the pan up about ½ way with tap water and placing it on the hot plates under the hood. Keep an eye on the temperature. Bring to 80C ± 5C . While temps are coming up, you can do the following:
6. Add 30 ml citrate-bicarbonate buffer to each centrifuge tube—Place tubes in H_20 bath (that has reached about 80°C) for at least 10 minutes. Tubes can stay longer, but you must make sure that the water in the pan does not evaporate too low, or get too hot.
7. Remove tubes from bath and add 0.2 g ± 0.05 g $Na_2S_20_4$ (sodium dithionate) to each centrifuge tube. NOTE: This is a caustic agent. Wear eye protection and gloves. Stir or shake gently for 1 minute. Place back in the bath and shake gently 3-4 times over the next 15 minutes, returning the tube to the bath each time.
8. Remove from bath. Pipette 15 ml room-temperature distilled H_20 to each centrifuge tube.
9. Centrifuge samples at 1500-2000 RPM for 10 minutes. (If you don't have a full load, add tubes filled with tap water for balance).
10. Transfer supernatant (the liquid portion without the sediment) to a 100 ml volumetric flask (See above definition) that is labeled with the sample ID.
11. Repeat steps 6 through 10 again using the remaining sediment in the bottom of the centrifuge tube, being careful that the resulting supernatant goes in the same volumetric flask as before.
12. Fill volumetric flask containing the supernatant perfectly up to the 100 mL mark (bottom meniscus) with 'super' DI water. Carefully transfer the diluted supernatant to a labeled 100mL nalgene bottle. **Make sure to label the bottle with BOTH the sample ID and "FeD".**
13. Dilute (see below) and analyze within ~1 week.

Standard Preparation

You must create standards in the 100mL Nalgenes prior to analysis on the AA. You make these starting in the same way as the soil samples above, but with no dirt. In that way, you have the same chemicals, and but with a known amount of iron.

To make Standards:
1. Complete steps 5 through 13 above with **the prescribed amount of Fe Stock Solution**. In other words go through all of the steps but with no dirt in the tube, just Fe stock. Ex: the 0 concentration receives 0 stock solution. The 20 ppm concentration receives 2 mL of 1000 ppm Fe stock solution. **Make sure to measure accurately using an appropriate vessel or pipette.**
2. Note: you will need to use 100 mL nalgenes instead of 50mL tubes for the 100, 200 & 300 concentrations. Put those on the shaker table any time it says to centrifuge them.
3. When decanting into volumetric flasks, decant everything. Thus, for step 11, you will dissolve 0.2 g ± 0.05 g $Na_2S_20_4$ in 30 mL of reagent in a 50 mL tube in the hot water bath, and then add it to the volumetric flask rather than putting the entire thing through a bath again. Top off with Super DI. If the 2nd 15 mL of water doesn't fit in the volumetric flask, that is ok.
4. This will result in 7 of the same thing. In this case, however, the 100mL Volumetric flasks that you decant into will be labeled with the 7 different concentrations in ppm listed in the table below (0 to 300).
5. Top off each volumetric flask containing up to the 100 mL mark with DI water.
6. Transfer Standard solution to a 100 mL nalgene bottle. You have now made 7 standards.

Appendix J: FeD and FeH methods and raw data

mL of 1000ppm Fe Stock Solution	Standard Concentration ppm (µg/ml)	Conc. **After** 20X dilution (step 18a below)
0 (Blank)	0 (Blank)	0 (Blank)
1	10	0.5
2	20	1
5	50	2.5
10	100	5
20	200	10
30	300	15

Dilution

You must dilute all of your samples AND the standards to 20X prior to analyses.

To prepare a 20 x Dilution:
1) Use the samples and standards from the 100 mL nalgene bottles prepared as above. **Both the samples and standards are diluted in the same way:**
2) Shake the nalgene containing the undiluted sample vigorously for ~30 seconds. Then, using an **automated pipette** extract 5mL of sample or standard from the 100 mL Nalgene and transfer to a 100mL **volumetric** flask labeled with sample ID or standard concentration. **Use a clean pipette tube for each sample.**
3) Carefully, fill the flask up to the 100mL mark with 'super' DI water. This will result in a 20X dilution (concentration is now 1/20th of what it was prior to dilution).
4) Transfer the entire contents into a new, clean 100 mL nalgene labeled with the sample ID or standard concentration AND THE WORDS "FeD" AND '20X'. This is the solution that will be run on the AA. Save the rest of the other until you are 100% sure that things came out correctly on the AA.
5) Run the sample within ~1 week.

How to Set-up and run the AA

7. SEE BELOW – Note, you must have training from Jon Watkins prior to running the AA.

CALCULATIONS
1. The AA will give you the concentration (ug/mL) of Fe in your sample.
2. To calculate weight percent FeD use the measured AA Fe concentration in the following equation:_

Wt % Fe = ((mg/L Fe /Sample Weight (g))* 100mL* 10^{-4} * 20 (the dilution factor)

3. To calculate weight percent Fe2O3 use the calculated concentration in the following equation:_

Wt % Fe2O3 = ((μg/ml Fe * 1.4297)/Sample Weight (g))* 100mL* 10^{-4} * 20 (the dilution factor)

NOTE: If samples and standards were diluted, you must multiply this result by the dilution factor (for a dilution factor of 20X, multiply by 20 as shown in the formula; make sure to use the raw ug/ml and not one already corrected for the dilution).

Appendix J: FeD and FeH methods and raw data

The following data was collected by Alec Wells and Nora Vaughan following instructions in Soils Laboratory Manual Spring 2021, seen here:
(FeH) Iron Extraction (Hydroxalimine Method)
Acid hydroxylamine extraction is used for removing noncrystaline material from crystalline iron oxides. Results for Fe extraction by hydroxylamine solution were similar to those extracted with the oxalate solution. Hydroxylamine extractions are generally more advantageous for this laboratory because they are more easily analyzed by atomic absorption, and do not require removal of magnetics.

Equipment:

2 L volumetric flask	50 ml centrifuge tubes
Centrifuge	shaker
100 mL volumetric flasks	Analytical balance
100 mL Nalgenes	Scoopula

Reagent:
WARNING: Must be made in the hood with the vacuum on. Wear protective eye, hand and body (lab coat) covering.
Hydroxylamine hydrochloride-hydrochloric acid solution:
In a 2 L volumetric flask add 34.74 g $NH_2OH \cdot HCl$
Then add 41.3 mL concentrate HCl (12.1 *M*)
Dilute to fill line (2 L) and invert 20 times to mix

1.1 Procedure
1) Label dry 50 mL centrifuge tubes with sample ID
2) Weigh out 0.10 ± 0.02 g of crushed (<100 mesh) soil into 50 mL centrifuge tube.
3) Record sample ID and sample mass on data sheet
4) Add 25 ml of hydroxylamine solution to each centrifuge tube
5) Screw lids on tightly
6) Place tubes in shaker for 16 hours
7) Centrifuge at 2000 rpm for 10 minutes
8) Decant all the supernatant to 100 mL Nalgenes for later, OR carefully pipette out the correct amount of supernatant for dilution into a 100 mL Nalgene, making sure no sediment gets into the pipette.
9) Dilute samples (see below).
10) Analyze standards and samples by atomic absorption within no more than a week.
Standard Preparation

You must create standards in the 100mL Nalgenes prior to analysis on the AA. You make these starting in the same way as the soil samples above, but with no dirt. In that way, you have the same chemicals, but with a known amount of iron.

To make Standards:
1. **Complete steps 1 through 4** (**ONLY**) above with **7 empty 50mL tubes**. In other words, go through all of the steps but with no dirt in the tube and only hydroxylamine.
2. To each 50mL tube as prepped and labeled in #1, add the appropriate amount (mL) of Fe Stock Solution as indicated in the table below. Ex: the 0 concentration receives 0 solution. The 20 ppm concentration receives 2 mL of 1000 ppm Fe stock solution. **Make sure to measure accurately using an appropriate vessel or pipette.**

Appendix J: FeD and FeH methods and raw data

mL of 1000ppm Fe Stock Solution	Standard Concentration ppm (µg/ml)	Conc. **After** 20X dilution (step 18a below)
0 (Blank)	0 (Blank)	0 (Blank)
1	10	0.5
2	20	1
5	50	2.5
10	100	5
20	200	10
30	300	15

3. Shake for 16 hours.
4. Carefully decant each 50 mL tube into a labeled 100 mL volumetric flask. Fill each flask to the 100 mL mark with 'super' DI water.
5. Transfer Standard solution to a 100 mL nalgene bottle.
6. You have now made 7 FeH standards.

Dilution
You must dilute all of your samples AND the standards to 20X prior to analyses.

To prepare a 20 x Dilution:
1) Use the samples and standards from the 100 mL nalgene bottles prepared as above. **Both the samples and standards are diluted in the same way:**
2) If you transferred the supernatant to a 100 mL nalgene, shake the container the undiluted sample for ~30 seconds. If pipetting directly from the 50 mL tube, do not shake. Using an automated pipette extract 5mL of sample or standard from the 100 mL Nalgene or 50 mL tube and transfer to a 100mL **volumetric** flask labeled with sample ID or standard concentration. **Use a clean pipette tube for each sample.**
3) Carefully, fill the flask up to the 100mL mark with 'super' DI water. This will result in a 20X dilution (concentration is now 1/20th of what it was prior to dilution).
4) Transfer the entire contents into a 100 mL nalgene labeled with the sample ID or standard concentration AND THE WORDS 'FeH' and '20X'. This is the solution that will be run on the AA. Save the rest of the other until you are 100% sure that things came out correctly on the AA.
5) Run the sample within ~1 week.

CALCULATIONS
1. The AA will give you the concentration (ug/mL) of FeH in your sample.
2. To calculate weight percent FeH use the measured AA Fe concentration in the following equation:_

Wt % Fe = ((μg/ml Fe /Sample Weight)* 100mL* 10^{-4} * 20 (the dilution factor)

3. To calculate weight percent Fe2O3 use the calculated concentration in the following equation:_

Wt % Fe2O3 = ((μg/ml Fe * 1.4297)/Sample Weight)* 100mL* 10^{-4} * 20 (the dilution factor)

NOTE: If samples and standards were diluted, you must multiply this result by the dilution factor (for a dilution factor of 20X, multiply by 20 as shown in the formula; make sure to use the raw ug/ml and not one already corrected for the dilution).

Appendix J: FeD and FeH methods and raw data

Atomic Absorption Spectrometer Operation
NOTE: You must get training to run this machine. See your advisor.

1) Ensure lab exhaust system is operational (air should be drawn into exhaust manifolds and fume hoods)
2) Open compressed breathing air tank valve (This should be set at 30psi)
3) Turn on auto-sampler and attach pump tubing on peristaltic pump (ensure enough DI rinse water is available in beaker)
4) Turn on the main AAS power switch
5) Turn on the computer (there is no Windows 2000 administrator password)
6) Open the compressed acetylene tank valve (This should be set at 9psi)
7) Open the SolaarM program on the computer (program password is "solaar")
8) Close any wizard program windows that may appear
9) Click on lamps icon and turn on any required lamps and switch on the Deuterium lamp
a. Spectrometer can hold up to 6 lamps in the carousel, ensure required lamp is present
b. Lamp can be rotated into position using software (do not rotate turret by hand)
10) Click on probe wash (auto-sampler probe should lower into wash and pump starts)
11) Light the flame by pressing and holding the white flashing button on the main unit. If flame fails to light try again. Once the flame is lit, allow the machine to warm up for 15-20 minutes.
12) Open/load the appropriate method file
13) Work through methods file tabs, filling in appropriate information when required.
a. Sequence Tab - sequence starts with auto zero, calibration then followed by samples
b. Sequence Tab - Samples Details button is where dilution ratio is entered for auto calculated concentrations for diluted samples
c. Spectrometer tab - settings include 3 fast resamples of at least 3 seconds each
d. Spectrometer settings tab includes "Cook Book" button to access spectrometer/flame details
e. Spectrometer tab - background correction is "D2 quadline"
f. Flame tab - nebulizer uptake time should be 18 seconds minimum
g. Calibrations tab - enter number of calibration standards (do not include blank) and enter appropriate values in table (lowest to highest)
    i. Blank and calibration standards required to be contained in 50ml centrifuge tubes
h. Calibrations tab - curves are typically: Normal: Linear Least Squares Fit or Normal: Quadratic Least Squares Fit
i. Sampling Tab - Wash frequency is "Between Solutions" with a Wash Time of at least 4 seconds
j. QC tab - typically no changes
k. Save/Load method
14) Click on "Setup Optics" icon (ensure proper lamp is in analysis position)
15) Load auto-sampler with blank and standards in large rack locations. Samples should be in test tubes loaded in 60 position sample racks.
16) Click on pull down File icon and set up new results file
17) Once system is warmed up and optics aligned, click on Analyse to start analysis. Enter appropriate information when required
18) During analysis watch rsd values, the lower the better. Meanings of red "Results flags" that may show up during analysis are included at the end of this procedure.
19) At end of analysis, Export results as csv file
20) When all analyses are complete, turn off the flame by pushing the red button on the main unit, close SolaarM program, shut down computer, shut off main AAS unit, turn auto-sampler off then on to stop pump, unhook pump tubing and close valves on acetylene and breathing air tanks. Put standards away and dispose of sample tubes.

Appendix J: FeD and FeH methods and raw data

Results Flags

One or more single character flags may be appended to the displayed and printed results, to indicate that a special function has been used, or that an error occurred during the measurement. The flags are:

On resample results

O the resample measurement is under or over range.

F the resample result has been identified as a flier.

On mean results

O the mean is under or over range.

F all the resamples have been identified as fliers.

D the Intelligent Sample Dilution facility has been used, and the sample has been diluted.

C the concentration value calculated is outside the calibration range.

X the measured calibration graph curvature is outside the limits set.

U the measured calibration fit parameter is outside the limits set.

R the measured calibration graph curvature is outside the limits set (Zeeman systems only).

T a QC Test has failed.

Appendix J: FeD and FeH methods and raw data

FeD

Sample ID	Sample Wt. (g)	Concentration (mg/L)	Weight % Fe	Weight % Fe2O3
NR-S1-4	0.5007	1.9735236	3.7201	5.3187
NR-S1-10	0.5015	-0.1096904	-0.0437	-0.0625
NR-S1-10D	0.5003	0.6710772	0.2683	0.3835
NR-S4-2	0.5009	2.7402864	1.0941	1.5643
NR-S4-4	0.5002	1.3082956	0.5231	0.7479
NR-S4-6	0.5004	4.1267616	1.6494	2.3581
NR-S4-7	0.5012	5.2156348	2.0813	2.9756
NR-S5-2	0.4994	1.5848904	0.6347	0.9075
NR-S5-2d	0.5016	1.4483436	0.5775	0.8256
NR-S5-7	0.5003	1.5148664	0.6056	0.8658
NR-S5b-3	0.5001	2.9153464	1.1659	1.6669
NR-S5-4	0.501	1.2522764	0.4999	0.7147
NR-S6-2	0.4994	2.9713656	1.1900	1.7013
NR-S6-4	0.5002	2.5897348	1.0355	1.4804
NR-S7-2	0.5001	1.0947224	0.4378	0.6259
NR-S7-2d	0.4993	0.9266648	0.3712	0.5307
NR-S7-4	0.4992	5.219136	2.0910	2.9895
NR-S8-5	0.5009	2.085562	0.8327	1.1905
NR-S8-6	0.5018	1.8684876	0.7447	1.0647
NR-S9-2	0.5006	3.2899748	1.3144	1.8792
NR-S9-4	0.5014	4.5749152	1.8249	2.6090
NR-S9-5	0.501	3.8221572	1.5258	2.1815
NR-S9-6	0.4983	3.8921812	1.5622	2.2335
NR-S10-2	0.5016	1.9840272	0.7911	1.1310
NR-S10-2d	0.4998	1.9665212	0.7869	1.1251
NR-S10-5	0.4984	3.328488	1.3357	1.9096
NR-S10-6	0.5	3.8781764	1.5513	2.2179
NR-S11-2	0.4998	1.7984636	0.7197	1.0289
NR-S11-3	0.501	5.0475772	2.0150	2.8808
NR-S11-4	0.4989	4.221294	1.6922	2.4194
NR-S12-4	0.5009	9.0774584	3.6245	5.1819
NR-S13-3	0.4995	1.7599504	0.7047	1.0075
NR-S13-4	0.5008	2.243116	0.8958	1.2807
NR-S13-4d	0.4999	2.1940992	0.8778	1.2550
NR-S13-6	0.5006	4.2633084	1.7033	2.4352
DU-S3-3	0.5009	8.4192328	3.3616	4.8061
DU-S3-3d	0.5011	8.7413432	3.4889	4.9880
DU-S3-4	0.5019	11.573814	4.6120	6.5938
DU-S3-8	0.4993	15.4321364	6.1815	8.8377
DU-S4-4	0.501	9.8337176	3.9256	5.6125
DU-S4-8	0.502	4.5854188	1.8269	2.6119
DU-S4-4d	0.5002	9.4660916	3.7849	5.4113
DU-S5-1	0.4999	7.2428296	2.8977	4.1429
DU-S5-4	0.5	12.2950612	4.9180	7.0313
DU-S5-7	0.5	16.5665252	6.6266	9.4741
DU-S5-7d	0.5015	17.8339596	7.1122	10.1684
DU-S5-9	0.5013	17.3122808	6.9070	9.8749
DU-S6-3	0.4995	13.2158768	5.2916	7.5655
DU-S6-5	0.4997	14.4763088	5.7940	8.2837
DU-S7-6	0.502	14.199714	5.6573	8.0882
DU-S8-5	0.5003	13.1878672	5.2720	7.5374
DU-S8-5d	0.4997	12.239042	4.8986	7.0035
DU-S8-4	0.5003	7.2638368	2.9038	4.1516
blank	0	-0.1096904	#DIV/0!	#DIV/0!
blank	0	-0.1271964	#DIV/0!	#DIV/0!

FeH

Sample ID	Sample Wt. (g)	Concentration (mg/L) - not corrected aka *20 yet	Weight % Fe	Weight % Fe2O3
NR-S1-4	0.1061	0.0803	0.1514	0.2164
NR-S1-10	0.1095	0.325	0.5936	0.8487
NR-S4-2	0.1011	0.0806	0.1594	0.2280
NR-S4-4	0.1137	0.2633	0.4631	0.6622
NR-S4-6	0.122	0.1573	0.2579	0.3687
NR-S4-7	0.1015	0.1585	0.3123	0.4465
NR-S5-2	0.1089	0.4313	0.7921	1.1325
NR-S5-2d	0.105	0.3098	0.5901	0.8437
NR-S5-7	0.1041	0.2015	0.3871	0.5535
NR-S5b-3	0.1008	0.2622	0.5202	0.7438
NR-S5-4	0.1111	0.2506	0.4511	0.6450
NR-S6-2	0.1176	0.19	0.3231	0.4620
NR-S6-4	0.1041	0.1624	0.3120	0.4461
NR-S7-2	0.1002	0.1592	0.3178	0.4543
NR-S7-2d	0.1158	0.2773	0.4789	0.6847
NR-S7-4	0.1188	0.2189	0.3685	0.5269
NR-S8-5	0.1069	0.1524	0.2851	0.4076
NR-S8-6	0.1067	0.1751	0.3282	0.4692
NR-S9-2	0.105	0.2576	0.4907	0.7015
NR-S9-4	0.1001	0.1821	0.3638	0.5202
NR-S9-5	0.1172	0.2119	0.3616	0.5170
NR-S9-5	0.1172	0.2075	0.3541	0.5063
NR-S10-2	0.1189	0.293	0.4929	0.7046
NR-S10-2d	0.0998	0.4158	0.8333	1.1913
NR-S10-5	0.1003	0.1423	0.2837	0.4057
NR-S10-6	0.1094	0.1266	0.2314	0.3309
NR-S11-2	0.1165	0.5143	0.8829	1.2623
NR-S11-3	0.0998	0.1755	0.3517	0.5028
NR-S11-4	0.1	0.192	0.3840	0.5490
NR-S12-4	0.1053	0.2651	0.5035	0.7199
NR-S13-3	0.1071	0.2139	0.3994	0.5711
NR-S13-4	0.1056	0.1344	0.2545	0.3639
NR-S13-4d	0.1034	0.2126	0.4112	0.5879
NR-S13-6	0.1001	0.1587	0.3171	0.4533
DU-S3-3	0.1085	0.2922	0.5386	0.7701
DU-S3-3d	0.1012	0.2498	0.4937	0.7058
DU-S3-4	0.101	0.2562	0.5073	0.7253
DU-S3-8	0.1032	0.2406	0.4663	0.6666
DU-S4-4	0.1105	0.5721	1.0355	1.4804
DU-S4-8	0.1112	0.3888	0.6993	0.9998
DU-S4-4d	0.1105	0.5606	1.0147	1.4507
DU-S5-1	0.0982	0.4681	0.9534	1.3630
DU-S5-4	0.111	0.2537	0.4571	0.6535
DU-S5-7	0.1079	0.33	0.6117	0.8745
DU-S5-7d	0.1076	0.3865	0.7184	1.0271
DU-S5-9	0.106	0.4035	0.7613	1.0885
DU-S6-3	0.1019	0.2014	0.3953	0.5651
DU-S6-5	0.1095	0.2517	0.4597	0.6573
DU-S7-6	0.10541	0.4151	0.7876	1.1260
DU-S8-5	0.10524	0.2307	0.4384	0.6268
DU-S8-5d	0.1194	0.2465	0.4129	0.5903
DU-S8-4	0.1078	0.2143	0.3976	0.5684
blank	0	0.0683	#DIV/0!	#DIV/0!

Appendix K: Bulk elemental data methods and raw data using Olympus Vanta XRF

The following data was collected by Steven Porson, David Crews, Monica Rasmussen, Patricia Fall, Steven Falconer, Missy Eppes, and Nora Vaughan following instructions in the Delta Operation Manual.

Sample ID	Al	Si	Fe	Sr	Zr	Mg	K	Ca	Mn
NR-S11-1	6912	43967	18979	40	164	<LOD	20913.75	1143.27	<LOD
NR-S11-2	50087	143686	32129	42	215	11169.3	12852.96	<LOD	<LOD
NR-S11-3	57569		36328	15	101	<LOD	2888.89	3994.85	<LOD
NR-S11-4	96312	142889	44290	12	142	44718.36	<LOD	<LOD	<LOD
NR-S11-5	55936	101021	37556	14	148	<LOD	14830.3	<LOD	<LOD
NR-S13-1	<LOD	33390	14009	24	141	<LOD	8829.36	2642.21	<LOD
NR-S13-2	75979	284418	29847	24	267	59920.71	<LOD	<LOD	<LOD
NR-S13-3	20345	107002	19992	19	221	<LOD	23899.57	<LOD	<LOD
NR-S13-4	21876	82114	25862	25	189	<LOD	33759.72	<LOD	<LOD
NR-S13-5	73969	139958	37816	23	155	20075.19	5927.14	<LOD	<LOD
NR-S13-6	66857	105032	49039	29	178	<LOD	13460.74	<LOD	<LOD
NR-S13-7	48331	81895	45041	37	177	<LOD	41715.6	<LOD	<LOD
NR-S4-1	13013	37923	18198	21	58	<LOD	15619.62	21224.97	<LOD
NR-S4-2	7432	45124	23676	15	139	<LOD	18261.37	930.71	<LOD
NR-S4-3	55563	178470	34486	24	237	27802.49	16700.49	<LOD	<LOD
NR-S4-4a	26243	118063	19532	15	198	<LOD	10709.85	9896.8	<LOD
NR-S4-4b	23085	34404	2649	24	15	<LOD	15457.65	81911.65	<LOD
NR-S4-5	75915	168242	41610	20	214	34258.55	<LOD	<LOD	<LOD
NR-S4-6	75996	125199	52797	17	161	18774.25	<LOD	<LOD	<LOD
NR-S4-7	55472	86448	41874	15	110	<LOD	<LOD	18877.93	<LOD
NR-S4-8	89517	182854	46857	16	178	48719.21	<LOD	<LOD	<LOD
NR-S4-9	40375	136702	28762	15	151	<LOD	24983.07	<LOD	<LOD
NR-S9-1	5936	59535	19258	19	221	<LOD	21473.47	581.97	<LOD
NR-S9-2	22830	80000	32762	18	169	<LOD	23537.38	704.1	<LOD
NR-S9-3	57649	122149	50687	25	180	13096.91	13264.49	<LOD	<LOD
NR-S9-4	37784	88366	38065	16	180	<LOD	15548.54	<LOD	<LOD
NR-S9-5	28331	69089	34091	17	159	<LOD	17948.31	993.17	<LOD
NR-S9-6	67299	129847	46516	35	174	26672.84	10705.74	<LOD	<LOD
NR-S9-7	21451	55066	32439	25	133	<LOD	24836.22	7664.87	<LOD
NR-S10-4 2Bb	26352	72830	28338	21	146	<LOD	30767.58	<LOD	<LOD
NR-S10-5 2Btb	74293	145768	38532	16	134	26640.49	<LOD	<LOD	<LOD
NR-S10-6 3Btb	21024	64767	31175	14	126	<LOD	24709.86	<LOD	<LOD
NR-S10-7 3Cr	7265	34610	12094	11	84	<LOD	19363.73	2184.07	<LOD
DU-S3-1	6093	21945	3180	12	39	<LOD	15529.2	5354.39	<LOD
DU-S3-2	6622	41472	27779	<LOD	251	<LOD	<LOD	592.91	<LOD
DU-S3-3	27019	75750	49382	11	230	<LOD	<LOD	<LOD	<LOD
DU-S3-4	15374	43774	60463	10	184	<LOD	<LOD	192.37	<LOD
DU-S3-5	32186	50140	69190	8	132	<LOD	<LOD	197.17	<LOD
DU-S3-6	17953	33651	66848	7	82	<LOD	<LOD	610.15	<LOD
DU-S3-7	26779	45100	71599	6	118	<LOD	<LOD	382.62	<LOD
DU-S3-8	15369	34479	71027	<LOD	103	<LOD	<LOD	<LOD	<LOD
DU-S3-9	6577	18134	36008	7	55	<LOD	17809.53	1466.38	<LOD
DU-S3-10	21256	50124	59654	5	141	<LOD	35470.83	178.05	<LOD
DU-S5-1	14276	50502	41932	38	176	<LOD	<LOD	2437.13	960.73
DU-S5-2	23769	68249	48491	12	204	<LOD	<LOD	221.64	814.3
DU-S5-3	8446	31769	39348	8	152	<LOD	<LOD	361.19	<LOD
DU-S5-4	15679	32182	49468	6	121	<LOD	<LOD	421.77	<LOD
DU-S5-5	5987	13932	42006	7	72	<LOD	<LOD	1829.91	<LOD
DU-S5-6	51650	76076	105151	10	87	<LOD	<LOD	<LOD	651.48
DU-S5-7	61505	83887	105023	9	74	<LOD	<LOD	<LOD	<LOD
DU-S5-8	10471	22787	74278	<LOD	58	<LOD	<LOD	636.78	<LOD
DU-S5-9	14036	30592	89508	<LOD	60	<LOD	<LOD	289.6	<LOD
DU-S6-1	44808	187027	44591	19	277	23236.52	<LOD	<LOD	953.85
DU-S6-2	28493	104788	40703	9	252	<LOD	<LOD	<LOD	<LOD
DU-S6-3	37865	64057	65792	7	161	<LOD	<LOD	<LOD	<LOD
DU-S6-4	92050	117529	107311	6	212	41679	<LOD	<LOD	303.65
DU-S6-5	91067	115718	113348	8	131	42513.71	<LOD	<LOD	<LOD
DU-S6-6	65971	119620	71542	4	183	19050.46	<LOD	<LOD	<LOD
DU-S4_1	25140	85444	47247	26	211	<LOD	<LOD	2283.94	662.48
DU-S4_2	37899	111605	47746	13	295	<LOD	<LOD	<LOD	751.25
DU-S4_3	8506	46997	39391	7	234	<LOD	<LOD	170.54	<LOD
DU-S4_4	19364	57976	51606	<LOD	324	<LOD	<LOD	<LOD	<LOD
DU-S4_5a	11477	58321	43586	7	181	<LOD	<LOD	<LOD	<LOD
DU-S4_5b	15287	76525	30988	9	308	<LOD	<LOD	<LOD	<LOD
DU-S4_5c	30735	112850	50388	9	329	<LOD	<LOD	<LOD	<LOD
DU-S4_6	9572	54798	32256	17	272	<LOD	<LOD	723.15	<LOD
DU-S4_7	42591	152431	38938	50	361	<LOD	<LOD	766.42	1126.4
DU-S4_8	11597	60661	26760	31	330	<LOD	<LOD	1293.7	<LOD
DU-S4_9	50759	183184	40174	59	371	23745.76	<LOD	808.67	740.64
DU-S7-1	37940	101148	55521	23	265	<LOD	<LOD	436.07	972.55
DU-S7-2	73306	120435	80480	11	173	22014.68	<LOD	<LOD	<LOD
DU-S7-3	71731	93854	95263	10	113	15249.07	<LOD	<LOD	<LOD
DU-S7-4	63781	76934	99392	14	51	24216.52	<LOD	<LOD	466.08
DU-S7-5	48957	75099	104208	6	54	<LOD	<LOD	<LOD	<LOD
DU-S7-6	10853	25557	55332	8	33	<LOD	<LOD	160.91	<LOD
DU-S7-7	8096	25094	70503	<LOD	42	<LOD	<LOD	<LOD	<LOD
DU-S7-8	8268	22841	73457	<LOD	38	<LOD	<LOD	<LOD	<LOD
DU-S8-1	28545	90939	46238	14	294	<LOD	<LOD	<LOD	473.62
DU-S8-2	72083	155473	61779	10	269	32857.3	<LOD	<LOD	<LOD
DU-S8-3	41016	83189	64724	<LOD	190	<LOD	<LOD	<LOD	<LOD
DU-S8-4	73163	102073	85857	5	125	17183.83	<LOD	<LOD	<LOD
DU-S8-5	91430	127973	98859	7	194	45802.2	<LOD	<LOD	497.59
DU-S8-6	86499	114409	95970	6	141	35921.84	<LOD	<LOD	589.81
DU-S8-7	95205	125307	92856	4	216	37840.67	<LOD	<LOD	481.18
DU-S8-8	115580	151334	113670	<LOD	165	59915.9	<LOD	<LOD	1733.5
NR-S6-1	44103	104685	30207	46	212	<LOD	33329.3	893.49	<LOD
NR-S6-2	126392	216859	44544	49	201	71166.47	<LOD	<LOD	<LOD
NR-S6-3	95112	152664	41328	32	123	37801.53	<LOD	<LOD	<LOD
NR-S6-4	124097	224860	40076	47	147	71819.99	<LOD	<LOD	<LOD
NR-S6-5	80738	196076	30000	41	171	42728.42	<LOD	<LOD	<LOD
NR-S6-6	113950	329158	23781	72	190	77953.98	<LOD	<LOD	<LOD
NR-S7-1	95968	246351	31003	56	204	64608.68	<LOD	<LOD	<LOD
NR-S7-2	100256	298602	23562	55	229	71006.02	<LOD	<LOD	<LOD
NR-S7-3	115604	181890	53023	30	205	63263.2	<LOD	<LOD	<LOD
NR-S7-4	159267	206844	56348	23	158	81915.36	<LOD	<LOD	<LOD
NR-S7-5	149734	204528	52009	37	174	79200.22	<LOD	<LOD	<LOD
NR-S7-6	150852	236027	43524	39	150	81945.34	<LOD	<LOD	<LOD
NR-S7-7	126750	218296	42402	46	173	72639.38	<LOD	<LOD	<LOD
NR-S5b-1	79374	202703	37976	28	207	42851.49	2037.58	<LOD	<LOD
NR-S5b-2	41700	129806	29033	16	187	<LOD	19564.24	<LOD	<LOD
NR-S5b-3	90546	231536	36566	24	199	57373.12	<LOD	<LOD	<LOD
NR-S5b-4	93751	251348	34582	24	218	64431.95	<LOD	<LOD	<LOD
NR-S5-1	60482	153112	29260	26	162	26519.91	34320.43	<LOD	<LOD

Table 1: Raw XRF data for elements that are used in calculating enrichment/depletion ratios. Unit is ppm for all.

Table 1 continued: Raw XRF data for elements that are used in calculating enrichment/depletion ratios. Unit is ppm for all.

Sample ID	Al	Si	Fe	Sr	Zr	Mg	K	Ca	Mn
NR-S5-2	99737	253323	31426	26	217	67979.96	<LOD	<LOD	482.43
NR-S5-3	105013	232539	34554	39	199	67543.43	4746.04	<LOD	510.42
NR-S5-4	100091	222733	30814	42	199	60574.7	3726.84	<LOD	<LOD
NR-S5-5	63104	168420	29382	37	200	29292.86	33420.54	<LOD	<LOD
NR-S5-6	112681	261067	34829	43	209	73442.36	<LOD	<LOD	<LOD
NR-S5-7	114291	256019	35889	42	217	73915.49	<LOD	<LOD	<LOD
NR-S8-1	30233	94819	26773	25	224	<LOD	25388.23	351.32	<LOD
NR-S8-2	109432	263887	33590	34	268	73044.52	<LOD	<LOD	<LOD
NR-S8-3	116992	282652	27955	29	281	77961.94	<LOD	<LOD	467.86
NR-S8-4	107180	272867	27873	24	310	70144.99	<LOD	<LOD	<LOD
NR-S8-5	91563	228377	30448	21	303	55569.41	<LOD	<LOD	<LOD
NR-S8-6	117810	264158	31533	23	276	74487.98	<LOD	<LOD	<LOD
NR-S8-7	130975	250743	37229	49	206	77435.23	<LOD	<LOD	<LOD
NR-S12-1	26905	109263	29197	53	202	<LOD	10786.39	1533.94	567.86
NR-S12-2	43083	141793	36864	50	235	<LOD	4999.95	235.61	<LOD
NR-S12-3	113303	173222	53610	29	170	58544.43	<LOD	<LOD	<LOD
NR-S12-4	72557	110184	55406	22	148	22793.68	<LOD	<LOD	<LOD
NR-S12-5	87407	117728	58526	17	125	29965.27	<LOD	<LOD	<LOD
NR-S12-6	139561	180978	63432	26	167	71941.8	<LOD	<LOD	<LOD
NR-S1-1	69263	244525	29963	52	244	48327.81	<LOD	<LOD	<LOD
NR-S1-2	94697	273003	33681	52	244	67364.47	<LOD	<LOD	367.62
NR-S1-3	106773	295784	34798	51	233	75400.42	<LOD	<LOD	359.63
NR-S1-4	105470	314534	27337	54	225	75009.86	<LOD	<LOD	313.96
NR-S1-5	87306	282203	26790	64	285	63249.03	<LOD	<LOD	<LOD
NR-S1-6	65982	229280	29096	69	258	43536.47	<LOD	<LOD	<LOD
NR-S1-7	97646	288740	31109	63	303	70573.8	<LOD	<LOD	749.47
NR-S1-8	109911	286499	32725	59	309	75501.92	<LOD	<LOD	655.28
NR-S1-9	107471	297620	31015	49	326	73926.25	<LOD	<LOD	<LOD
NR-S1-10	107911	266295	33022	46	318	72395.15	<LOD	<LOD	<LOD
NR-S1-10 (dupe)	111177	268253	33449	45	312	72892.78	<LOD	<LOD	<LOD
DU-W4 20 ft bs	27283	120164	29873	212	115	<LOD	<LOD	42243.25	<LOD
DU-W4 20 ft bs	33976	123710	27604	216	131	<LOD	<LOD	27029.69	<LOD
DU-W4 20 ft bs	24103	105597	128113	233	44	33057.79	<LOD	12433.57	630.4
NR-W4 21 ft bs	25285	364583	10631	129	52	57264.65	<LOD	25427.84	<LOD
NR-W4 21 ft bs	23118	317294	29768	203	61	52607.51	<LOD	47258.55	442.48
DU-W1 80 ft bs	66974	202621	60149	372	113	57566.06	<LOD	22971.57	486.97
DU-W1 80 ft bs	66493	195107	62448	373	111	59386.3	<LOD	22912.02	870.59
DU-W1 80 ft bs	66165	186343	61752	392	107	51036.5	<LOD	25024.68	371.43
SR-W2 50 ft bs	60684	160935	62616	438	112	42672.08	<LOD	22706.88	1423
SR-W2 50 ft bs	81630	184873	73232	492	151	60594.7	<LOD	30447.81	1106.1
SR-W2 50 ft bs	50112	130084	57775	345	113	22612.74	<LOD	19365.52	786.97
SR-W3 60 ft bs	29195	78447	58672	416	80	<LOD	66086.98	14007.9	852.67
SR-W3 60 ft bs	20197	57064	80841	409	74	<LOD	76074.12	12619.56	1792.1
NR-DE W1 58 ft bs	68530	120793	27660	231	106	46834.38	147925.4	3983.69	<LOD
NR-DE W1 58 ft bs	70888	119616	28594	232	100	46119.07	160022.57	7419.09	<LOD
NR-DE W1 58 ft bs	70650	135495	25791	185	148	53803.53	129543.69	38650.19	<LOD
NR-DE W1 58 ft bs	64996	170263	59349	1233	67	60111.43	<LOD	41512.55	2230.5
DE-W2 69 ft bs	74888	199834	55146	1130	79	69985.82	<LOD	43801.15	1976.9
DE-SR W1 70 ft bs	76881	188955	64794	512	79	59057.93	<LOD	41866.27	905.91
DE-SR W1 70 ft bs	77483	205155	79635	506	105	58362.96	<LOD	46657.52	837.15
NR-S10 Ap (no field samples from this horizon)	27137.68	119482.54	27377.13	56.88	199.53	<LOD	24182.12	3984.71	604.43
NR-S10 Bp	26927.19	99265.69	27461.52	17.82	189.12	<LOD	22963.6	<LOD	<LOD
NR-S10 2Eb	44578.88	126837.89	32522.18	19.42	195.89	<LOD	28371.84	<LOD	<LOD
NR-S10-4 2Bb	26351.84	72829.68	28337.96	21.27	145.96	<LOD	30767.58	<LOD	<LOD
NR-S10-5 2Btb	74292.9	145767.76	38531.91	16.31	133.72	26640.49	<LOD	<LOD	<LOD
NR-S10-6 3Btb	21024.37	64766.5	31175.13	13.64	125.56	<LOD	24709.86	<LOD	<LOD
NR-S10-7 3Cr	7265.33	34610.1	12093.91	10.96	84.1	<LOD	19363.73	2184.07	<LOD
NR-S5 82-90 cmbs saprolite from auger test	27638.07	48757.13	16262.22	24.36	121.31	<LOD	21605	<LOD	<LOD
NR-S5 82-90 cmbs saprolite from auger test	46219.77	136637.7	25299.44	33.35	178.24	11753.45	35123.21	<LOD	<LOD
NR-S5 BOP+93 cmbs saprolite from auger test	40750.21	122705.08	21543.9	38.07	180.89	<LOD	51563.17	<LOD	<LOD
NR-S5 BOP+93 cmbs saprolite from auger test	40415.87	129324.53	18511.33	32.07	175.22	<LOD	43450.83	<LOD	<LOD
NR-S5 BOP+75 cmbs saprolite from auger test	29016.68	64009.95	21811.3	26.1	190.16	<LOD	27415.21	<LOD	<LOD
NR-S5 BOP+75 cmbs saprolite from auger test	104376.26	269565.63	29529.03	40.48	256.72	74160.55	<LOD	<LOD	<LOD
DU-S4 BOP+62 cmbs saprolite from auger test	59130.99	205181.1	29785.49	111.04	572.59	38611.79	<LOD	5443.19	586.5
DU-S4 BOP+62 cmbs saprolite from auger test	41410.74	132471.17	25615.06	81.76	214.65	<LOD	<LOD	4498.88	<LOD
DU-S4 BOP+62 cmbs saprolite from auger test	50270.865	168826.135	27700.275	96.4	393.62	38611.79	#DIV/0!	4971.035	586.5
NR-S5 BOP+75 cmbs saprolite from auger test	48069.4767	128500.003	22159.5367	32.405	183.756667	42957	35831.484	#DIV/0!	######
DU-w1 average	66733.45	198864.265	61298.435	372.46	112.045	58476.18	#DIV/0!	22941.795	678.78
sr-w3 average	24696.105	67755.51	69756.345	412.445	77.1	#DIV/0!	71080.55	13313.73	1322.4
DE-SR W1 70 ft bs	77182.155	197054.84	72214.6	509.11	92.125	58710.445	#DIV/0!	44261.895	871.53
DE-W2 69 ft bs	74887.84	199833.8	55145.97	1129.58	79.45	69985.82	<LOD	43801.15	1976.9
NR-DE W1 58 ft bs	68766.0075	136541.523	35348.665	470.28	105.0825	51717.1025	145830.553	22891.38	2230.5
SR-W2 50 ft bs	64142.2367	158630.447	64541.0933	425.026667	125.323333	41959.84	#DIV/0!	24173.4033	1105.3
NR-W4 21 ft bs	24201.585	340938.265	20199.55	166.2	56.5	54936.08	#DIV/0!	36343.195	442.48
DU-W4 20 ft bs	28454.0233	116490.383	61863.4467	220.006667	96.4066667	33057.79	#DIV/0!	27235.5033	630.4
NR-S4-9	40375	136702.4	28762.33	15.42	150.8	<LOD	24983.07	<LOD	<LOD
MVF average (DU-W1, DE-SR W1, SR-W2)	208057.842	554549.552	198054.128	1306.59667	329.493333	159146.465	#DIV/0!	91377.0933	2655.7

Appendix K: Bulk elemental data methods and raw data using Olympus Vanta XRF

DELTA Handheld XRF

Limits of Detection (LODs) for Geochemical Analyzers



Olympus recommends four DELTA X-ray Fluorescence (XRF) analyzer configurations for the mineral exploration, geochemistry and mining industry. These are the:

- DELTA Premium (DP-6000) – Highest sensitivity with superior light element (Ag, Al, Si) performance.
- DELTA Professional (DPO-2000) – Mid-range XRF analyzer with good light element performance and excellent all-around capabilities.
- DELTA Classic (DCC-6000) – Value-leading XRF analyzer when light element detection is not required.
- DELTA Premium-50 (DP-4050) – 50 kV XRF analyzer for improved performance in heavy metals (Ag, Cd, Sn, Sb, Te and Ba) and rare earth elements (REE: Y, La, Ce, Pr and Nd).

LODs for Soil and GeoChem Modes (PPM)

	DP-6000	DPO-2000	DCC-6000	DP-4050
X-ray Tube	Rh	Rh	Ta / Au	Ta / Au
Mg*	3000-10000	5000-16500	-	-
Al*	450-1400	650-2200	-	1800-5500
Si*	250-800	300-1000	-	830-2500
P*	40-120	50-175	10000-50000	120-375
S*	50-150	60-200	1000-5000	100-350
Cl	-	-	500-1000	40-100
K	20-50	35-70	150-250	25-80
Ca	10-35	30-50	150-250	15-45
Ti	5-10	5-10	20-50	4-10
V	4-10	4-10	10-30	4-10
Cr	2-9	3-10	10-30	4-10
Mn	3-7	5-8	10-30	4-10
Fe	5-20	10-20	10-30	5-15
Ni	4-10	5-10	20-40	5-15
Cu	2-6	5-8	15-30	4-8
Zn	1-3	3-5	10-15	1-3
W	4-10	5-10	15-30	3-9
Hg	2-5	2-4	10-15	1-4
Au	2-4	3-5	8-15	2-4
As	1-3	2-4	4-8	1-3
Se	1-2	1-2	4-8	1-2
Pb	1-4	3-5	5-10	2-4
Rb	1-2	1-2	3-5	1-2
U	1-6	3-7	5-15	1-6
Sr	1-2	1-2	3-5	1-2
Y	1-2	1-2	5-10	1-2
Zr	1-2	2-4	3-5	1-2
Nb	1	2-4	3-5	1-2
Th	2-6	4-8	7-15	1-4
Mo	1-2	2-4	3-5	1-2
Ag	5-12	7-12	20-30	3-5
Cd	5-9	12-15	20-30	2-3
Sn	9-14	15-25	30-40	5-8
Sb	10-13	17-25	30-40	5-7
Ba	-	-	40-60	20-25
La	-	-	-	30-50
Ce	-	-	-	45-60
Pr	-	-	-	65-100
Nd	-	-	-	75-350

*GeoChem Mode

The Limits of Detection (LODs) Table (reverse) gives an indication of the performance of each DELTA model across a consistent element suite and set of Certified Standards. Notes on these LOD values:

- LODs were developed testing a variety of certified reference materials or standards.
- LODs are dependent on testing time, sample heterogeneity, the presence/absence of interfering elements (causing spectral overlaps), level of statistical confidence (99.7%) and the XRF beam conditions used (kV, µA, and filter settings of the X-ray tube).
- The lower number in the range of the LODs is the lowest quantity of an element that can be distinguished in an interference-free silica blank.
- The upper end of the range represents samples with more challenging compositions and likely to be more representative of real-world conditions. These values can be used as a guide, but LODs could be higher than those listed here in other sample types.
- Real-world samples may contain interfering elements There are many commonly known inter-element interferences (e.g. Fe on Cr, Ti on Ba, Pb on As). Please contact your nearest Olympus representative for more information.
- All values are determined using Soil Mode except where Geochem Mode is noted, using multiple beam conditions (optimized voltage, current and filter).
- Analysis time is 120 seconds per beam condition.
- Only the common elements are listed – many other elements are possible but need to be examined for interferences before being added.
- Additional information regarding Gold (Au) analysis:
  - Gold naturally forms clumps or "nuggets" and is not evenly distributed in the sample. Reported values will be high when a nugget is in the X-ray beam and low if the nugget is missed.
  - Au has multiple inter-element interferences including As, Zn, W and Se. Subsequently, Au results can often be either over-reported (false-positives) or under-reported (not-detected) when these elements are present.
  - The use of pathfinder elements is recommended for gold exploration when these elements are present.

Figure 1: Limits of detection for Olympus Santa pXRF DP-6000, highlighted in yellow

Appendix K: Bulk elemental data methods and raw data using Olympus Vanta XRF

The Olympus Delta Premium 50kV GeoChem Analyzer can analyze concentrations (in ppm or % depending on the element) of Al, Si, Ca, S, P, Ti, V, Cr, Mn, Fe, Co, Ni, Cu, W, Zn, Hg, As, Pb, Bi, Se, Th, U, Rb, Sr, Y, Zr, Mo, Ag, Cd, Sn, Sb, Mg, Sc, Ba, Ga, Au, K, and REE Elements La, Ce, Nd, Pr, Nb.

The limits of detection (LOD) indicate the performance of the pXRF. Since the LOD is dependent on testing time and sample heterogeneity, each analysis was set to run for 120 seconds per beam, and all soil analyses were performed on sieved and homogenized samples. When scanning rock, the average of three 120 second per beam analyses was used instead of a single value.

Zirconium, strontium, iron, silicon, and aluminum values were reported for almost every sample with no <LOD values. All values were significantly above the limit of detection. Most samples reported as less than the limit of detection for Mn (3-7 ppm), but any measured value was reported between around 400 to 1000 ppm. Most samples that were reported came from Duffey watershed. Calcium had many samples reported as less than the limit of detection (10-35 ppm), but measured values range from about 200 to 80000 ppm across both watersheds. Most samples with <LOD (20-50 ppm) for K were in Duffey watershed, most of the samples from North Rhyne had potassium values around 15,000 ppm. Magnesium values were also often reported as <LOD, but measured values for this element typically fall between 15,000 and 80,000 ppm.

In the protolith, the averaged concentrations for each element were significantly above the LOD for every element except for potassium. Each of the three samples that were averaged for the protolith had values <LOD for potassium. This suggests that there is less than 20 ppm K in the protolith. A value of 11.11 was arbitrarily used for the concentration of potassium in the protolith so that the data from the soils could be assessed.

Appendix L: XRF sample locations from NR-S10 in North Rhyne watershed, Redlair Observatory, NC





NR-S10 Field sampling method using Olympus pXRF



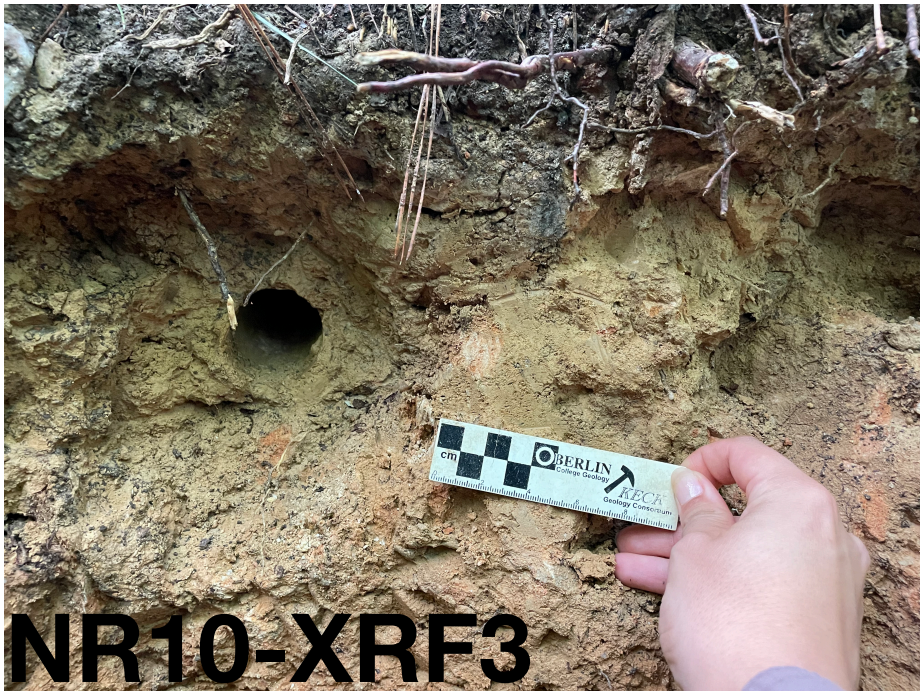
NR10-XRF3
cm
BERLIN
College Geology
KECK
Geology Consortium

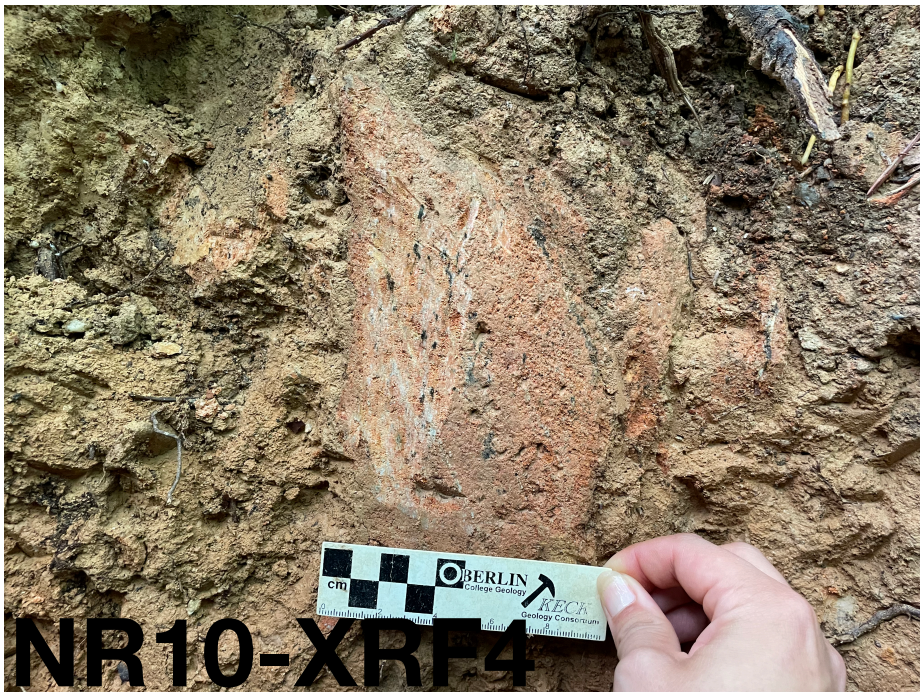
NR10-XRF4
cm
BERLIN
College Geology
KECK
Geology Consortium


cm
BERLIN
College Geology
KECK
Geology Consortium
NR10-XRF5

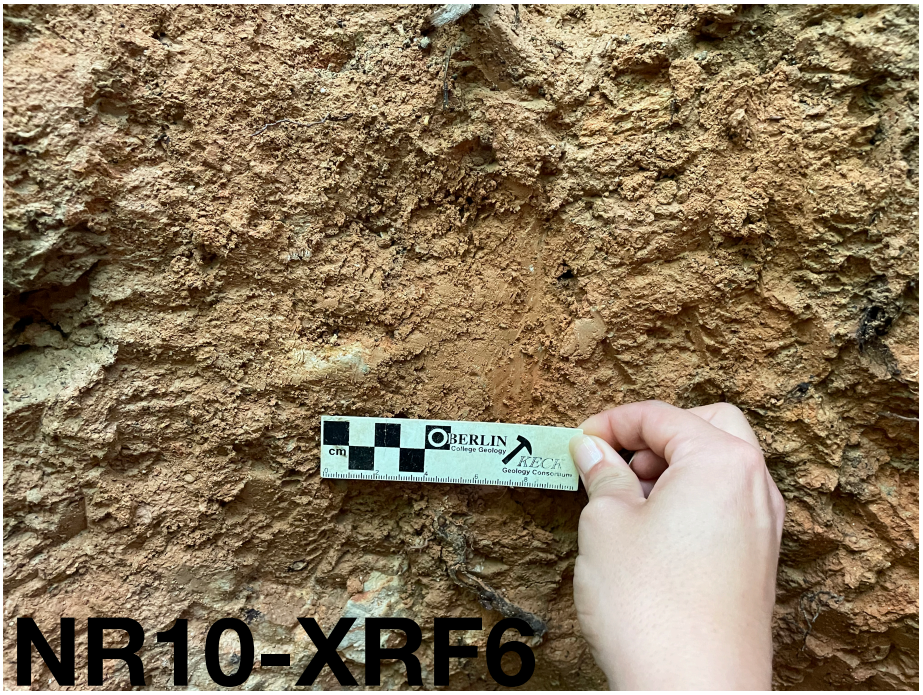
cm
BERLIN
College Geology
KECK
Geology Consortium
NR10-XRF6


BERLIN
KECK
NR10-XRF7

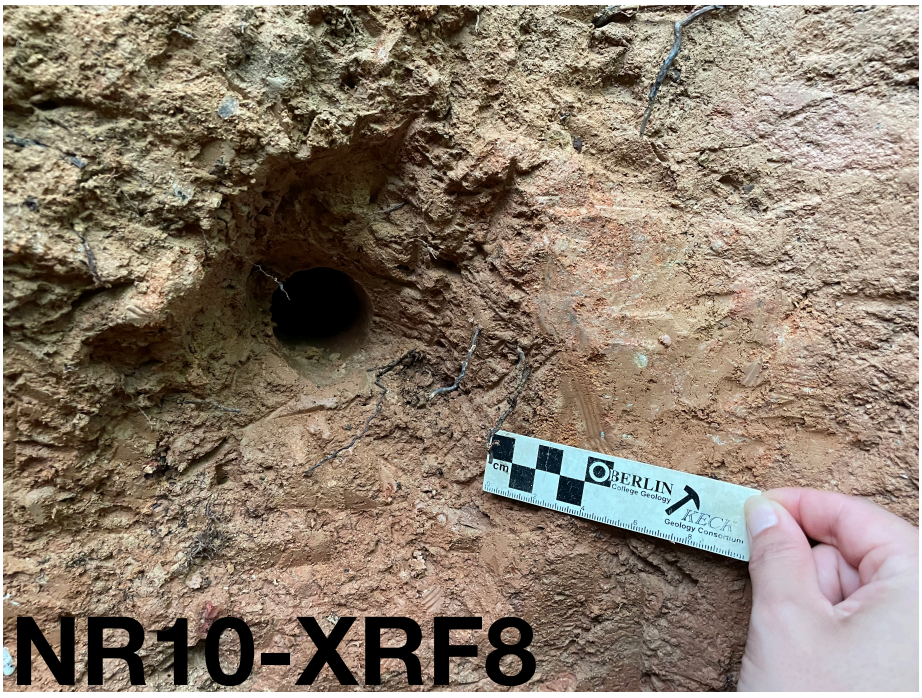
cm
BERLIN
KECK
NR10-XRF8


NR10-XRF9
BERLIN
College Geology
cm


NR10-XRF10
BERLIN
College Geology
cm


BERLIN
College Geology
NR10-XRF11

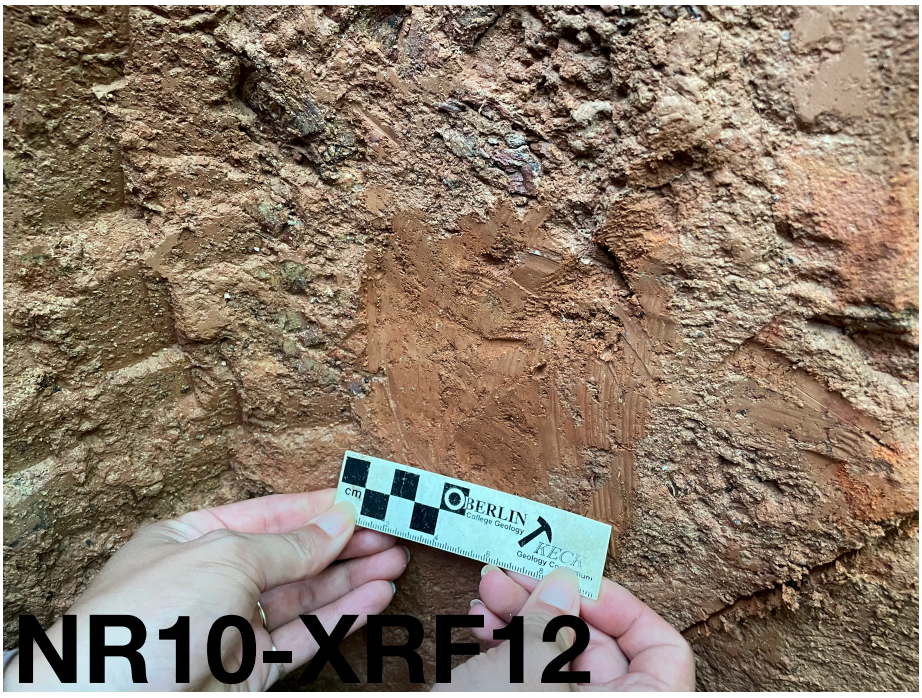
BERLIN
College Geology
NR10-XRF12


BERLIN
College Geology
KECK
Geology Consortium
NR10-XRF13


BERLIN
College Geology
KECK
Geology Consortium
NR10-XRF14


cm
BERLIN
College Geology
NR10-XRF15

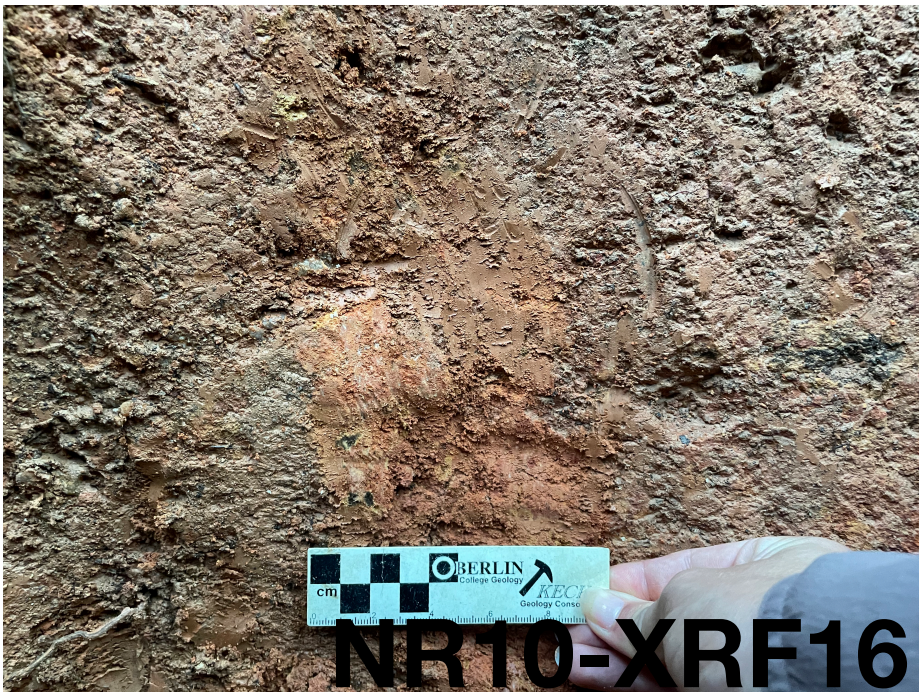
cm
BERLIN
College Geology
NR10-XRF16


NR10-XRF17
BERLIN
College Geology

Appendix M: Protolith Determination

In order to determine the protolith for the field area, data from geologic field maps (Goldsmith et al., 1988), field surveys by Price (2009), and XRF data collected by Nora Vaughan, Steven Porson, and David Crews (Appendix E).

The following map includes relevant lithological descriptions surrounding Redlair Observatory (white star). The scale of this map is not fine enough to confidently determine a protolith for the field area, but it provides useful information about the surrounding lithologies.

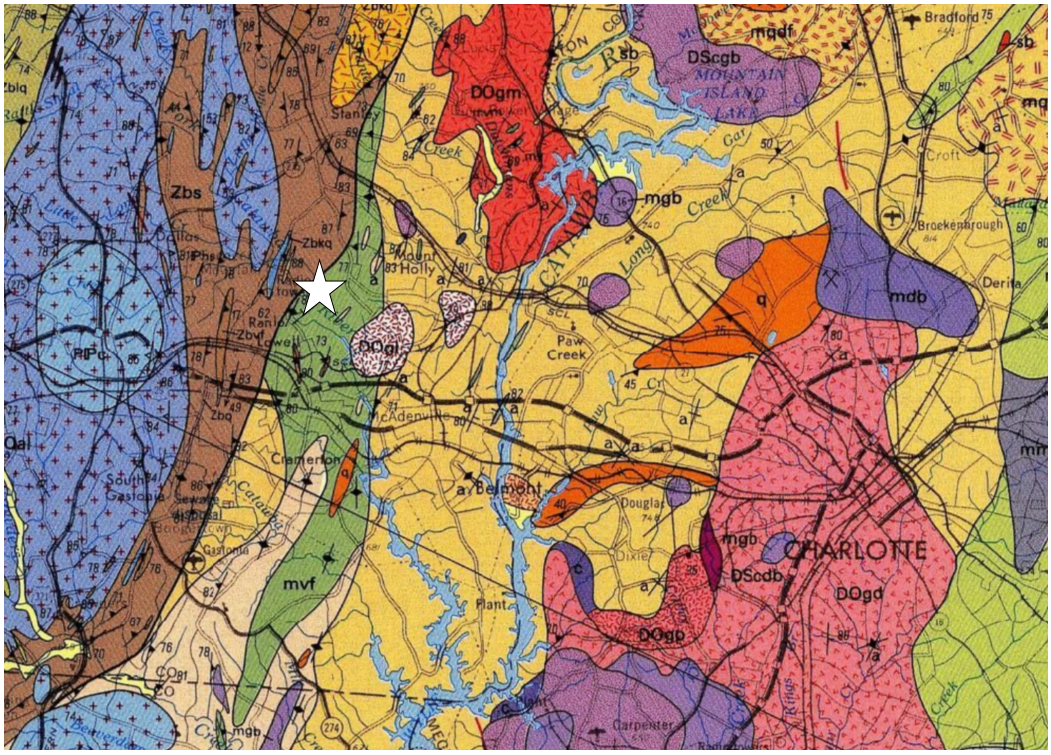

mvf — Felsic Metavolcanic Rocks—Fine- to medium-grained, locally coarse-grained or agglomeratic rhyolitic and rhyodacitic metatuffs. May include some hypabyssal intrusives. Contains minor intermediate and mafic metavolcanic rocks. Probably correlative, at least in part, with felsic metavolcanic rocks of the Battleground Formation (Zbvf)

Battleground Formation (Late Proterozoic)

Zbs — Quartz-sericite schist—Very fine to medium-grained quartz-sericite schist and phyllite. Very light gray, light-bluish-gray, light-brown, or yellowish-gray. Composed largely of quartz (typically >50%) and sericitic white mica (muscovite and paragonite). Accessory minerals may include chloritoid, biotite, pyrite, hematite, kyanite, andalusite, sillimanite, staurolite, garnet, oligoclase or albite, chlorite, tourmaline, zircon, and graphite

DOgt — **Biotite monzogranite and leucogranite**—Very light to light- to yellowish-gray, medium- to coarse-grained, massive-to very weakly foliated biotite monzogranite and leucogranite southwest of Mt. Holly, N.C. Plagioclase variably saussuritized; grains fractured and strained. May be related to Salisbury Plutonic Suite

Appendix M: Protolith Determination

Price (2009) worked to identify the location of the Boogertown Shear Zone and other rock units previously mapped at a larger scale (1:250,000) by Goldsmith et al. (1988) at Redlair Observatory based on outcroppings on the property (of which there are few). The shear zone is an important landscape feature that not only separates different lithologies, but is also the contact between different metamorphic facies. It separates the felsic metavolcanics (Mvf) on the east from the quartz-sericite schist (Zbs) of the Battleground formation to the west (Late Proterozoic), which is part of the Kings Mountain Belt. The shear zone bisects Redlair Observatory laterally, but evidence of sericite schist in the bedrock of a soil pit on the eastern side of the shear zone suggests further investigation is needed to find its exact location. Many Piedmont shear zones have multiple phases of deformation: early ductile deformation followed by a later semi-ductile to brittle deformation.

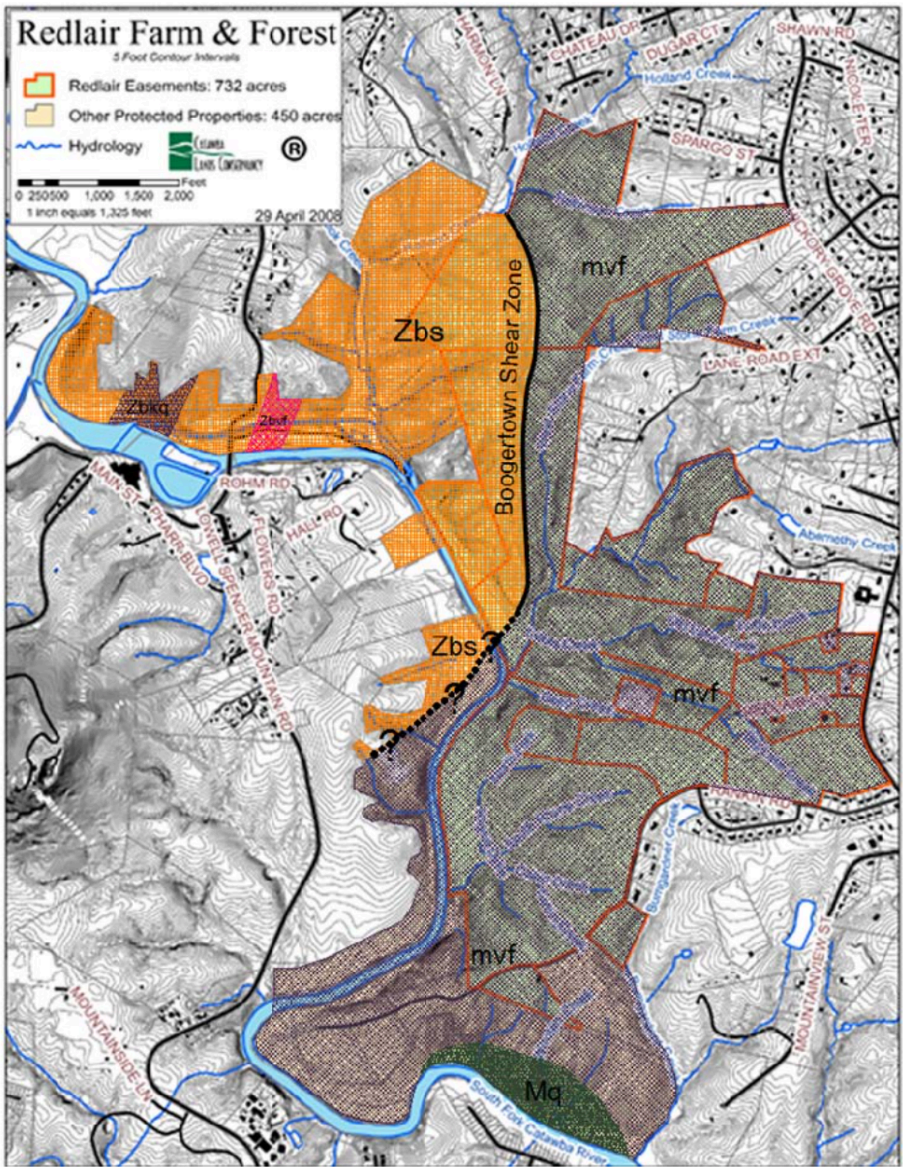

Figure 1. Geologic map of the Redlair property, Gastonia, North Carolina. Portion of Boogertown Shear Zone that is dashed with question marks is an approximate location.

Price (2009)

Appendix M: Protolith Determination

Seventeen bedrock cores were collected via sonic well boring by Geologic Exploration, Inc in April, 2019 at 17 different locations in Redlair Observatory. Material from the cores has been archived at UNCC. The coordinates, depth, and name of each web boring can be found in the table below:

Name	Type	Type of level logger	Latitude	Longitude	Top of screen (ft BLS)	Bottom of screen (ft BLS)
DU-W4-S	Well	Hobo	35.298926	-81.084404	9	14
DU-W4-D	Well	Hobo	35.298926	-81.084404	17	20
DU-W1-S	Well	Hydros - 15m	35.298878	-81.081755	48	53
SR-W-2-S	Well	Hobo	35.297879	-81.089785	45	50
SR-W-2-D	Well	Hobo	35.297879	-81.089785	27	32
DE-SR-W1-S	Well	None (dry)	35.298664	-81.089741	34	39
DE-SR-W1-D	Well	Hobo	35.298664	-81.089741	65	70
DU-W1-Int	Well	Hydros - 20m	35.298878	-81.081755	64	69
DU-W1-D	Well	Hydros - 20m	35.298878	-81.081755	75	80
SR-W3-S	Well	Hydros - 10m	35.297540	-81.090048	20	25
SR-W3-D	Well	Hydros - 10m	35.297540	-81.090048	64	69
NR-DE-W1-S	Well	None (dry)	35.298612	-81.092895	41	46
NR-DE-W1-D	Well	Hobo - 25m	35.298612	-81.092895	51	56
DE-W2-S	Well	None	35.299303	-81.089517		
DE-W2-D	Well	Hobo	35.299303	-81.089517		
NR-W4-S	Well	Hobo	35.297940	-81.095592	10	15
NR-W4-D	Well	Hydros - 10m	35.297940	-81.095592	18	21

Hard rock samples from well borings surrounding Duffey and North Rhyne watersheds were photographed and scanned with the pXRF to determine bulk elemental composition of the rocks. Saprolite samples from toeslope positions were collected with a hand auger by Alec Wells and Nora Vaughan. Hard rock outcrops from Duffey and North Rhyne were also collected and photographed. This map shows the location of the well mornings (in pink) alongside some photos of the hard rock from the bottom of the cores.

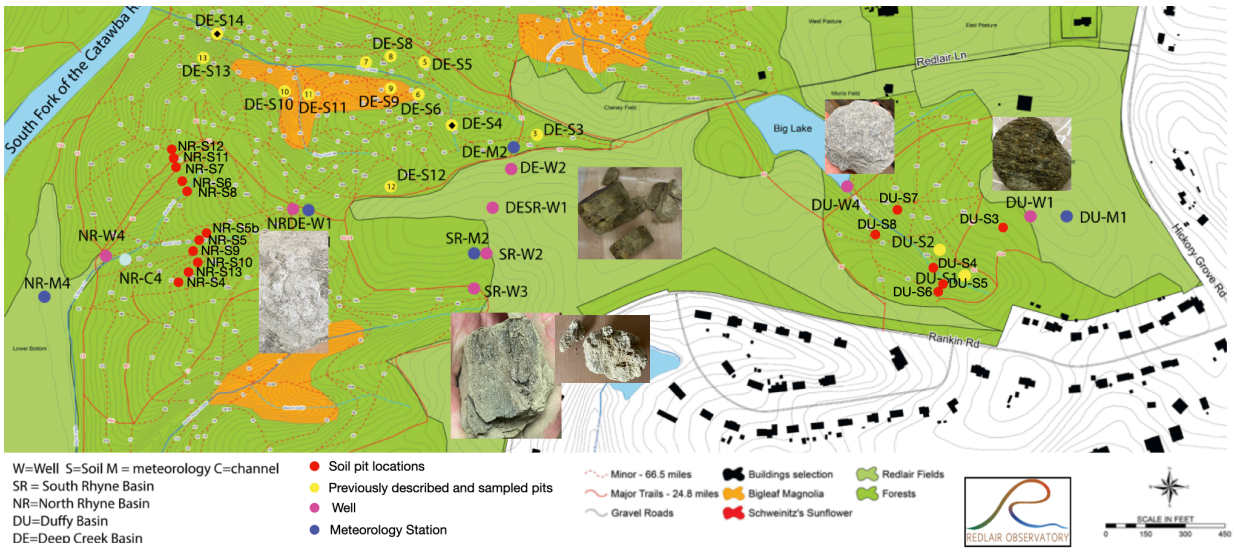

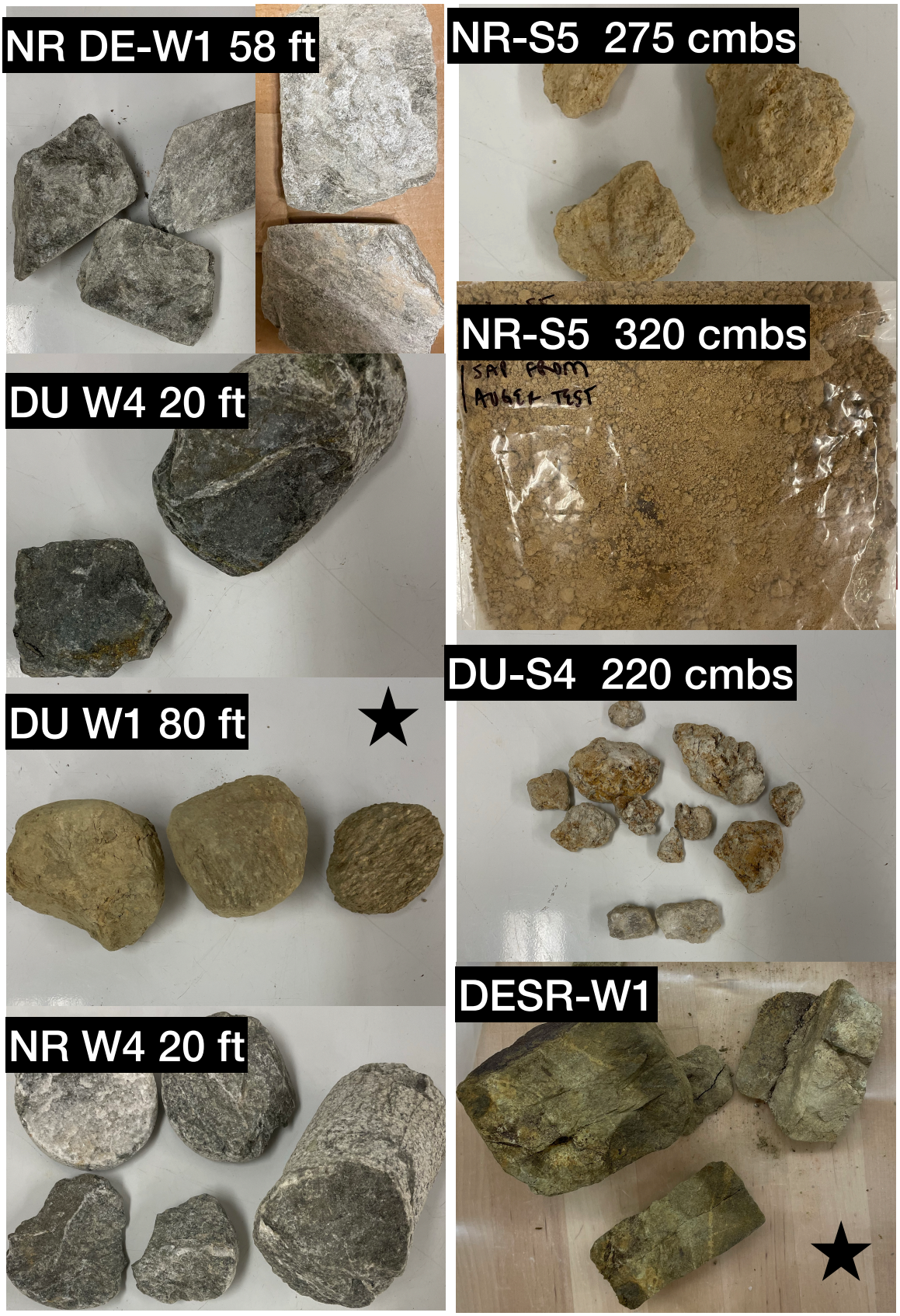
NR DE-W1 58 ft
NR-S5 275 cmbs
NR-S5 320 cmbs
SAT FROM
AUGER TEST
DU W4 20 ft
DU-S4 220 cmbs
DU W1 80 ft
DESR-W1
NR W4 20 ft


NR-S9
SR-W2
NR-S10
DE-W2
Duffey stream outcrop
SR-W3

Appendix M: Protolith Determination

The elemental composition of potential protolith samples is represented by the stacked bar graph. The table at the bottom shows concentrations of each major element for each sample that are plotted in the bar graph.

Map unit descriptions in combination with the physical properties of the samples, their bulk elemental composition, and the location of the samples in the field were all factors used to determine an average elemental composition for the felsic metavolcanic (MvF map unit) protolith in both North Rhyne and Duffey Watersheds (black stars).

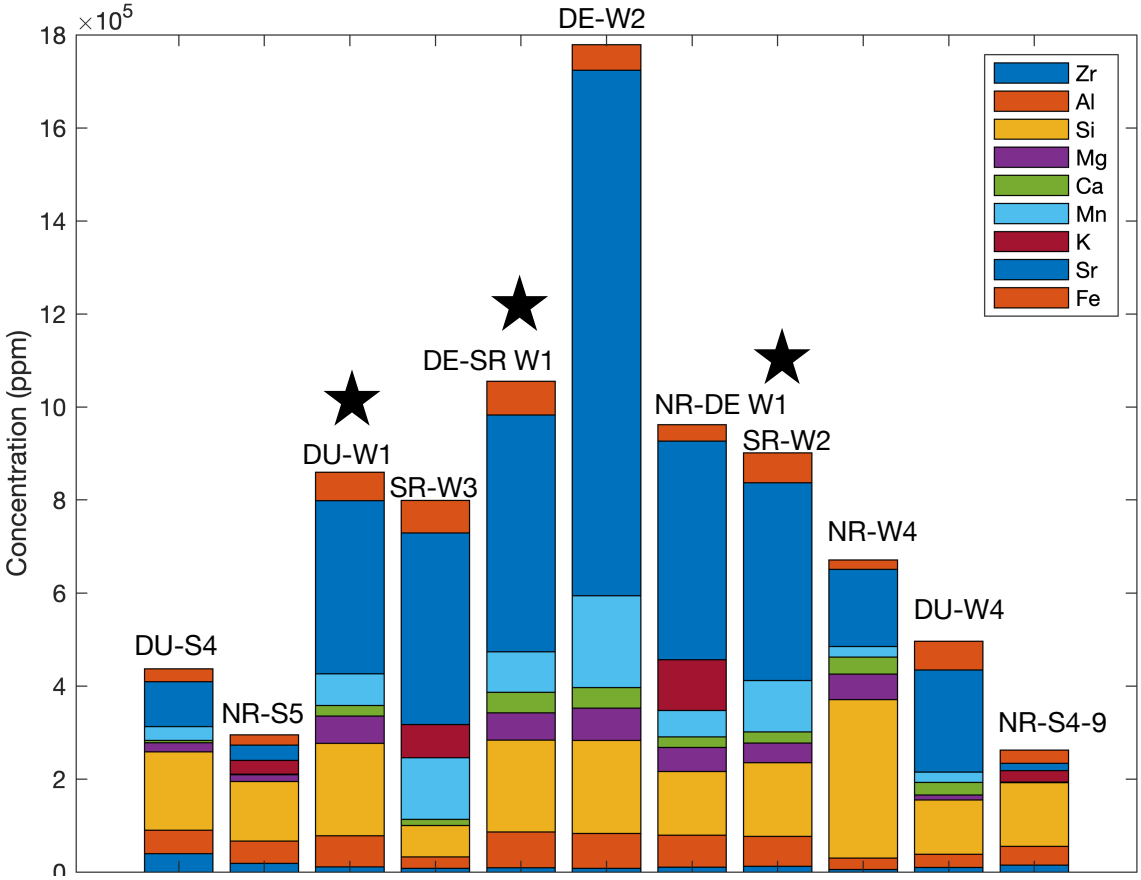

Sample ID	Al (ppm)	Si (ppm)	Fe (ppm)	Sr (ppm)	Zr (ppm)	Mg (ppm)	K (ppm)	Ca (ppm)	Mn (ppm)
DU-S4 BOP+62 cmbs saprolite from auger	50270.865	168826.135	27700.275	96.4	393.62	38611.79	#DIV/0!	4971.035	586.5
NR-S5 BOP+75 cmbs saprolite from auger	48069.4767	128500.003	22159.5367	32.405	183.756667	42957	35831.484	#DIV/0!	######
DU-W1 average	66733.45	198864.265	61298.435	372.46	112.045	58476.18	#DIV/0!	22941.795	678.78
SR-W3 average	24696.105	67755.51	69756.345	412.445	77.1	#DIV/0!	71080.55	13313.73	1322.4
DE-SR W1 70 ft bs	77182.155	197054.84	72214.6	509.11	92.125	58710.445	#DIV/0!	44261.895	871.53
DE-W2 69 ft bs	74887.84	199833.8	55145.97	1129.58	79.45	69985.82	<LOD	43801.15	1976.9
NR-DE W1 58 ft bs	68766.0075	136541.523	35348.665	470.28	105.0825	51717.1025	145830.553	22891.38	2230.5
SR-W2 50 ft bs	64142.2367	158630.447	64541.0933	425.026667	125.323333	41959.84	#DIV/0!	24173.4033	1105.3
NR-W4 21 ft bs	24201.585	340938.265	20199.55	166.2	56.5	54936.08	#DIV/0!	36343.195	442.48
DU-W4 20 ft bs	28454.0233	116490.383	61863.4467	220.006667	96.4066667	33057.79	#DIV/0!	27235.5033	630.4
NR-S4-9	40375	136702.4	28762.33	15.42	150.8	<LOD	24983.07	<LOD	<LOD

Appendix N: Soil geochemistry and mass balance calculations

To estimate chemical enrichment and depletion (tau) values, we compare changes in the concentrations of 9 major elements (Al, Si, Fe, Sr, Zr, Mg, K, Ca, Mn) in the soil to the concentrations of that of the protolith. Tau values for soils were calculated using zirconium and aluminum as the immobile
elements, following Brimhall and Dietrich (1987), Chadwick et al. (1990), and Holbrook (2019) in equation 1:

$$\tau_{i,j} = \frac{C_{j,w} C_{i,p}}{C_{j,p} C_{i,w}} - 1$$

Equation 1 is used to calculate the mass transfer coefficient ($\mathfrak{t}_{i,j}$,), which is the fractional loss or gain of an element (subscript *j*) with respect to the immobile element (subscript *i*) in the protolith (subscript *p)*. *C* is concentration, subscript *w* denotes the weathered material, respectively. If an element is neither lost nor gained with respect to the immobile element then $\mathfrak{t}_{i,j} = 0$. Negative and positive $\mathfrak{t}_{i,j}$ values imply loss and gain, respectively.

Here, we are using Al and Zr as our immobile reference elements, based on the assumption that they are relatively insoluble in felsic metavolcanic rocks. Hodson (2002) found that in granitic podzol soils, Zr and Al showed the lowest percent loss (0.0002% and 0.008%, respectively) compared to all other trace and major elements. Differences in the tau value between Zr and Al are expected because Zr is slightly less mobile than Al.

The protolith was defined based on the averaged compositions of three hard rock samples (DU-W1, DE-SR W1, and SR-W2) from 66, 70, and 50 feet below surface at Redlair (Appendix H). If the parent material was chosen correctly, and there are no additional inputs to the system (i.e. aeolian sediment), tau values comparing Zr/Al would be 0. In Duffey watershed, the tau values are often enriched greater than 100%, suggesting there are likely differences in the underlying geology within and between watersheds. This result aligns with findings from geologic maps of the area from Goldsmith et al. (1988) and Price (2009).

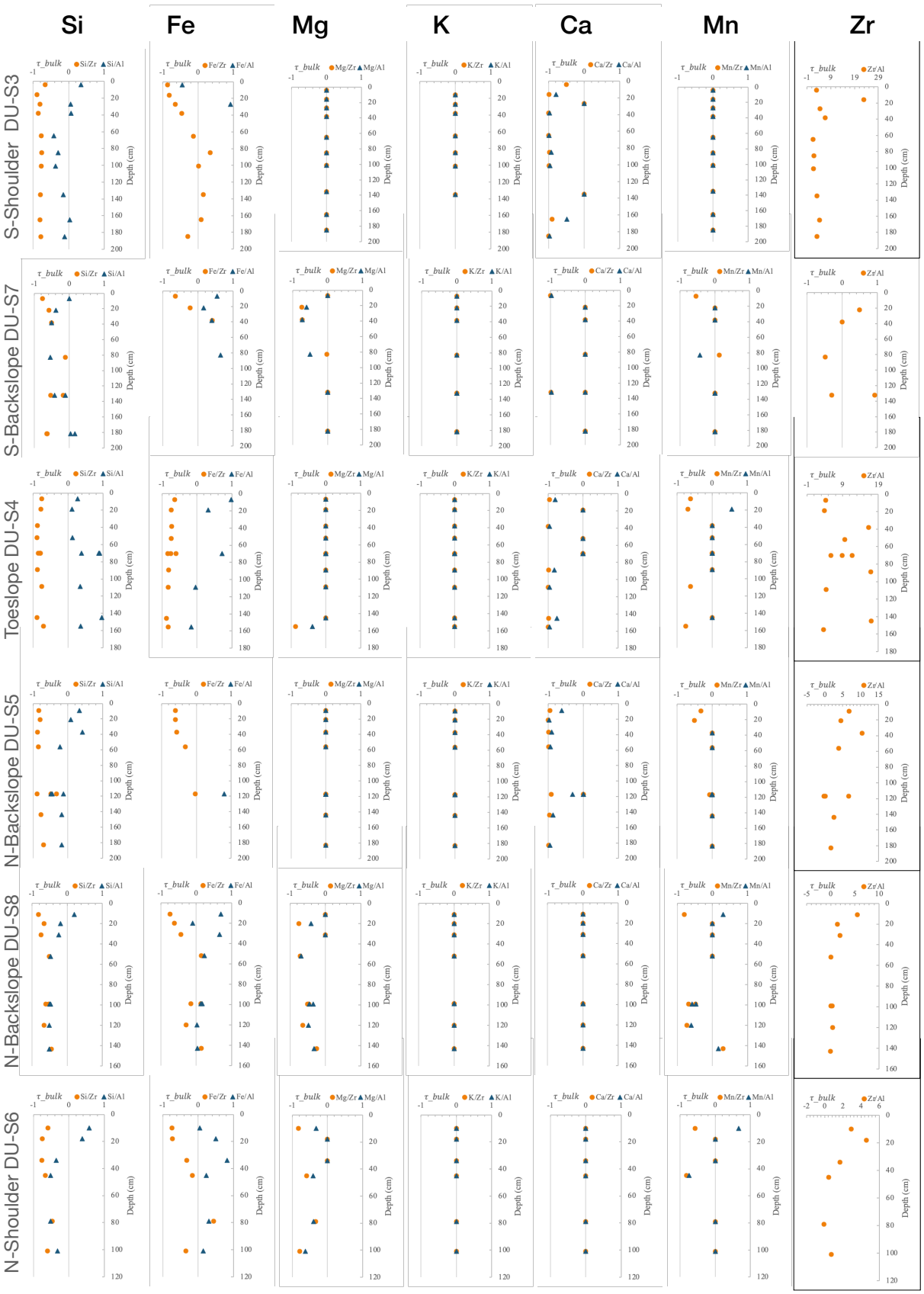
Si
Fe
Mg
K
Ca
Mn
Zr
S-Shoulder DU-S3
S-Backslope DU-S7
Toeslope DU-S4
N-Backslope DU-S5
N-Backslope DU-S8
N-Shoulder DU-S6
τ_bulk
Si/Zr
Si/Al
Fe/Zr
Fe/Al
Mg/Zr
Mg/Al
K/Zr
K/Al
Ca/Zr
Ca/Al
Mn/Zr
Mn/Al
Zr/Al
Depth (cm)

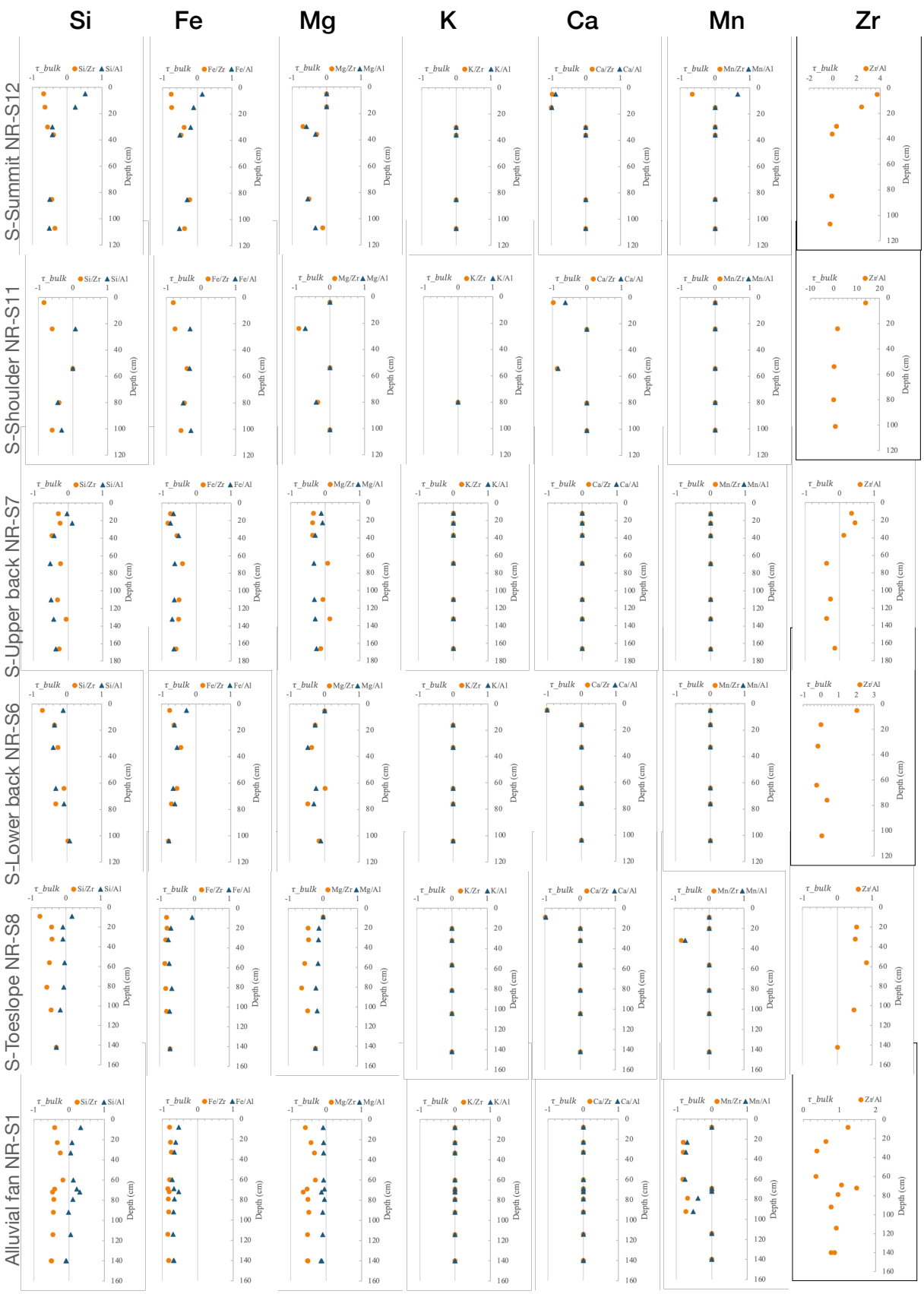
Si
Fe
Mg
K
Ca
Mn
Zr
S-Summit NR-S12
S-Shoulder NR-S11
S-Upper back NR-S7
S-Lower back NR-S6
S-Toeslope NR-S8
Alluvial fan NR-S1
τ_bulk
Si/Zr
Si/Al
Fe/Zr
Fe/Al
Mg/Zr
Mg/Al
K/Zr
K/Al
Ca/Zr
Ca/Al
Mn/Zr
Mn/Al
Zr/Al
Depth (cm)

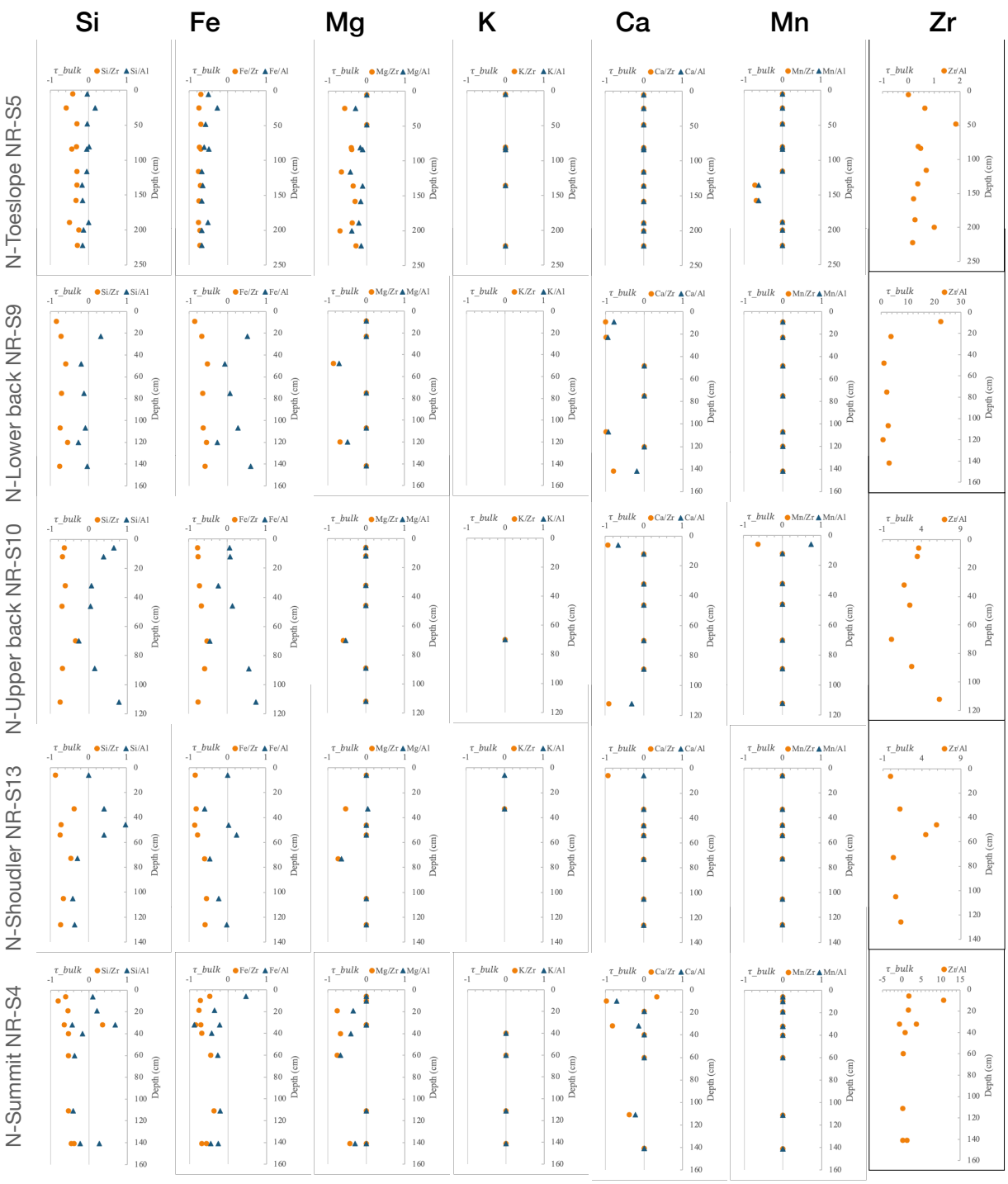
Si
Fe
Mg
K
Ca
Mn
Zr
N-Toeslope NR-S5
N-Lower back NR-S9
N-Upper back NR-S10
N-Shoulder NR-S13
N-Summit NR-S4
τ_bulk
Si/Zr
Si/Al
Fe/Zr
Fe/Al
Mg/Zr
Mg/Al
K/Zr
K/Al
Ca/Zr
Ca/Al
Mn/Zr
Mn/Al
Zr/Al
Depth (cm)

Appendix O: OSL sample locations from North Rhyne and Duffey watersheds, Redlair Observatory, NC

The following samples were collected by Michelle Nelson, Missy Eppes, and Nora Vaughan.



NR-S5-OSL-1 collected from C horizon, 57 cmbs
NR-S5-OSL-2 collected from 3BCb horizon, 187 cmbs



NR-S10-OSL-3collected from 2BEb horizon, 18 cmbs
NR-S10-OSL-4 collected from 2Btb horizon, 57 cmbs



NR-S13-OSL-5 collected from 2BEb horizon, 43cmbs



NR-S4-OSL-6 collected from 2BEb horizon, 30 cmbs



NR-S9-OSL-7 collected from 2Btb horizon, 48 cmbs
NR-S9-OSL-8 collected from 3Btb horizon, 107 cmbs



DU-S3-OSL-9 collected from B2B horizon, 25 cmbs



DU-S4-OSL-10 collected from CBw horizon, 54 cmbs
DU-S4-OSL-11 collected from Bb horizon, 85 cmbs



DU-S5-OSL-12 collected from B horizon, 21 cmbs
DU-S5-OSL-13 collected from Bt2 horizon, 45 cmbs



DU-S6-OSL-14 collected from Bt horizon, 33 cmbs
DU-S6-OSL-15 collected from 2Bt2 horizon, 55 cmbs



DU-S8-OSL-16 collected from AB horizon, 18 cmbs
DU-S8-OSL-17 collected from Bt horizon, 44 cmbs, see second photo for charcoal



DU-S7-OSL-18 collected from Bt horizon, 31 cmbs